Simulation and control of a multi-axes pneumatically actuated animated figure

Uebing, Matthias

Award date:
1999

Awarding institution:
University of Bath

SIMULATION AND CONTROL OF A MULTI-AXES PNEUMATICALLY ACTUATED ANIMATED FIGURE

submitted by Matthias Uebing

for the degree of PhD

of the University of Bath

1999

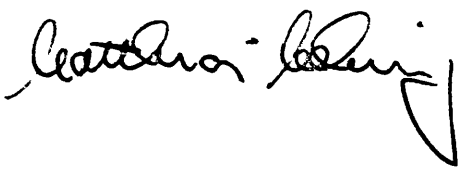

ProQuest LLC
789 East Eisenhower Parkway
P.O. Box 1346
Ann Arbor, MI 48106-1346

SUMMARY

The following thesis deals with the problem of simulation and control of a multi-axes pneumatically actuated animated figure. This problem can be viewed as a specific case of the general problem of modelling and control of multi-degree-of-freedom pneumatically actuated manipulators or robots.

Developing a non-linear and a linear dynamic model of the pneumatic actuation system it was found that the dynamic characteristics were not only actuator position dependent as reported in literature but also direction of valve opening and hence direction of actuator motion dependent. This is due to the unequal quiescent actuator chamber pressures. As a result, an advanced linear model had to be derived in order to identify the dynamically worst conditions required for controller design. Furthermore, it was found that precisely calibrating the valve model of the non-linear simulation model was crucial in order to obtain a good agreement between simulation of the dynamic response of the pneumatic servo and experimental results. To calibrate the valve model a calibration routine based on the idea of charging and discharging a known dead volume under the assumption of a constant polytropic index was employed rather than using a gas mass flow meter. The obtained results were excellent.

Due to the complexity and the highly non-linear nature of the overall system dynamics it was decided to adopt an individual single-axis controller approach rather than an overall controller for the whole figure. This approach also supported the modular structure of the animated figure and allows for the addition or omission of individual axes without the need of a controller redesign. In order to provide the superior disturbance rejection capabilities and robustness to system parameter changes required by the highly non-linear system dynamics and the individual axis control approach it was decided to employ a Continuous Sliding Mode Controller (CSLMC). The design of the CSLM controller consisted of three steps: a basic design using the reachability condition for a chosen sliding surface defining the desired closed-loop system dynamics, the determination of occurring limit cycles based on the extended Nyquist criterion and the evaluation of possible digital, hybrid and analogue implementation approaches. It was found that an analogue CSLM

controller was the ideal solution for the control problem under consideration. The resulting controller is based on a novel analogue CSLM control card providing double differentiation of the measured displacement feedback signal, definition of the sliding surface by means of state gains and a boundary layer neighbouring the sliding surface to minimise chattering. The analogue controller provides the required closed-loop system dynamics, disturbances rejection capabilities and robustness to system parameter changes.

CONTENT

TABLES

CHAPTER 3

CHAPTER 4

CHAPTER 5

CHAPTER 8

CHAPTER 9

APPENDIX A1

LIST OF FIGURES

CHAPTER 3

CHAPTER 4

CHAPTER 5

CHAPTER 6

CHAPTER 7

CHAPTER 8

CHAPTER 9

APPENDIX A1

NOTATION

a_i	transfer function parameter
A	cross section area of actuator chamber
$\boldsymbol{A}$	state-space plant matrix
$\boldsymbol{A}_n^m$	sub-matrix of state-space matrix $\boldsymbol{A}$
A_v	valve flow area
b_i	transfer function parameter
$\boldsymbol{B}$	state-space plant input matrix
$\boldsymbol{B}_n^m$	sub-matrix of state-space matrix $\boldsymbol{B}$
c_f	viscous friction coefficient
c_i	state gain of sliding surface
$\boldsymbol{C}$	state-space output matrix
C_d	discharge coefficient
C_m	flow coefficient
C_P	specific heat capacity at constant pressure
C_V	specific heat capacity at constant volume
d	external disturbance
e_i	displacement error of link i
e_{1i}	filtered displacement error of link i
E	error cost function
E	servo error
$\boldsymbol{E}$	transfer matrix of arbitrary disturbance
E_1	filtered error
f	vector containing the transient non-linearities of the system dynamics
$f_{i\max}$	maximum bound of ith manipulator parameter
$f_{i\min}$	minimum bound of ith manipulator parameter
f_0	break frequency of analogue filter
F	unknown manipulator parameter vector
$F(s)$	open-loop transfer function
$F(t)$	arbitrary disturbance vector
$F(\dot{\Theta})$	vector representing friction torques

$\hat{F}$	estimates/bounds of manipulator parameters
F_C	Coulomb friction force
F_{Cd}	dynamic Coulomb friction force
F_{Cs}	static Coulomb friction force
F_{ext}	external force
F_{fric}	total friction force
g	gravitational acceleration
g_g	vector containing the steady-state non-linearities of the system dynamics
$G(s)$	closed-loop transfer function
$G(\Theta)$	vector representing gravity caused torques
G_{pi}	transfer function of link i
h	discrete time interval
h'	specific enthalpy
h'_{in}	specific enthalpy of mass flow into control volume
h'_{out}	specific enthalpy of mass flow out of control volume
H_{in}	heat input
J_i	moment of inertia of link i
k	spring stiffness
k_{Di}	velocity feedback gain for link i
k_i	friction coefficient of joint i
k_v	valve gain
k_1	partial derivative with respect to control signal of gas mass flow
k_2	partial derivative with respect to upstream pressure of gas mass flow
k_3	partial derivative with respect to downstream pressure of gas mass flow
k_4	partial derivative with respect to upstream temperature of gas mass flow
K	controller feedback gain
K_a	acceleration feedback gain
K_{eq}	equivalent control gain
K_p	proportional feedback gain

K_{ult}	ultimate gain at stability border
K_v	velocity feedback gain
$\boldsymbol{K}$	compliance matrix
$\boldsymbol{K_p}$	diagonal feedback gain matrix
$\boldsymbol{K_v}$	diagonal feedback gain matrix
l	actuator stroke
l_{ci}	location of *i*th centre of gravity
l_i	length of manipulator link *i*
L	Lyapunov function
m	mass to be moved
$\dot{m}$	gas mass flow rate
m_i	mass of link *i*
M_p	percentage overshoot
$\boldsymbol{M}$	inertia matrix
$\boldsymbol{M}(\Theta)$	position dependent mass matrix
$\hat{\boldsymbol{M}}(\Theta)$	estimated/bounds of manipulator inertia matrix
n	polytropic index
N	number of samples
$N(\Theta,\dot{\Theta})$	Coriolis, centrifugal, gravitational and frictional torque vector
$\hat{N}(\Theta,\dot{\Theta})$	vector of estimates/bounds of Coriolis, centrifugal, gravitational and frictional torque
$N(\hat{\sigma})$	describing function
p^N	vector of unknown parameters
P	pressure
P_r	pressure ratio (upstream/downstream)
q_i	generalised co-ordinates of *i*th degree of freedom
Q_i	generalised forces and torques applied to each generalised co-ordinate
r	vector of reference signals
R	gas constant
s	Laplace operator
t	time
T	temperature

T_{samp}	sampling time
T_{sett}	settling time
u	control signal
u_{eq}	equivalent control signal
u_{switch}	switching control signal
U	potential energy of system
$U_{\max}$	maximum available control signal
v	velocity
V	volume
$V(\Theta,\dot{\Theta})$	vector representing torques caused by centrifugal and Coriolis effects
W_{out}	work output
x	actuator displacement
x_v	valve stroke

GREEKS

α_i	upper switched gain
β_i	lower switched gain
γ	specific hear ratio (=1.4 for air)
δ	width of sliding surface boundary layer
ε_i	tolerance bandwidth for link i
ζ_{valve}	damping ratio of valve
ϑ_i	angle of displacement of link i
Θ	manipulator displacement vector
Θ_d	demanded manipulator displacement vector
Θ^*	feedback control signal
λ	sliding surface tuning parameter
ρ	density of gas
σ	sliding surface
σ_{BL}	sliding surface boundary layer
τ	vector of control torques

τ_d	vector of unknown signals due to unmodelled dynamics and external disturbances
φ	actuator mounting angle
φ_{del}	phase shift due to system time delay
Ψ	sliding surface constant matrix
Ψ_i	switched gain
ω_{BL}	cut-off frequency of boundary layer
ω_n	natural frequency
ω_{valve}	natural frequency of valve

SUBSCRIPTS

a	actuator chamber A
ae	from chamber A to return
as	from supply to chamber A
b	actuator chamber B
be	from chamber B to return
bs	from supply to chamber B
d	downstream
exp	experimental
ext	extending
f	in vena contracta
i	initial
in	input
max	maximum
meas	measured
min	minimum
nom	nominal
out	output
par	parameter
ret	retracting
s	supply
sim	simulation

stag	stagnation
stat	static
sur	of surrounding
u	upstream

ABBREVIATIONS

CSLMC	Continuos Sliding Mode Control
DOF	Degree Of Freedom
DSLMC	Discrete Sliding Mode Control
GA	Genetic Algorithm
ID	Intelligent Dither
LSB	Least Significant Bit
LVDT	Linear Variable Differential Transformer
MIMO	Multiple-Input Multiple-Output
MRAC	Model Reference Adaptive Control
PAA	Parameter Adaptation Algorithm
PVA	Position, Velocity, Acceleration (= state-feedback)
SISO	Single-Input Single-Output
SLMC	Sliding Mode Control
VSAC	Variable Structure Adaptive Control
VSC	Variable Structure Control
ZOH	Zero Order Hold

ACKNOWLEDGEMENTS

I would like to express my thanks to Dr. Nicholas Vaughan, my supervisor, for all his invaluable help and support. Many times, the discussions with him brought me back to the real problems that had to be tackled during the research for this thesis.

I also would like to thank the Tussauds Studios, London for giving me the opportunity to work on such an interesting problem and for all their financial support, making this work possible. Furthermore, I cannot forget the DAAD (Deutscher Akademischer Austauschdienst) which supported me during my lectureship in *Engineering with German* and therefore making it possible for me to combine my teaching and research interests. Both have been invaluable experiences.

Further thanks to Prof. Brian Surgenor at Queen's University, Kingston, Canada. The time I could spent in his laboratory as a visiting student and the many enlightening discussions on pneumatics and control gave my research many important impulses.

Thanks to Esti, Bénédicte, Rainer, John, Ricardo, Carlitos, Torsten and many others for their friendship and for looking after my mental health. The last years I spent with them in Bath showed me that there are other things to life than research and work.

Thanks to my parents and family. The strong principles they taught me made me who I am.

1 INTRODUCTION

1.1 MODELLING AND CONTROL OF A PNEUMATICALLY ANIMATED FIGURE

This thesis deals with the general problem of modelling and control of multi-degree-of-freedom (*n*DOF) pneumatically actuated manipulators or robots. In particular, the case of a pneumatically actuated animated figure for the entertainment industry is considered.

In a first attempt, most manipulators can be mathematically modelled assuming a chain of rigid links connected via rigid joints. To activate the axes of these manipulators usually electrical, hydraulic or pneumatic actuators provide the required torques or forces at the joints. These actuators introduce additional dynamics into the system which in case of electrical actuators are often neglected, because of their mainly first-order dynamic behaviour and their response time which is in general much shorter than the response time of the mechanical structure. The higher-order dynamic characteristics of hydraulic and pneumatic actuators though can have a significant influence on the overall manipulator dynamics and can therefore not be neglected. In particular, pneumatic systems are known to have a very slow response time and also exhibit a significant lack of stiffness due to the compressibility of air which makes them very sensitive to external disturbances.

Hence, when confronted with the task of designing a controller for a *n*DOF pneumatically actuated manipulator not only the kinematic and dynamic interactions of the various members of the manipulator but also the dynamic properties of the pneumatic actuators have to be taken into account.

In general, all linear and non-linear control design methods are based on a dynamic model of the system to be controlled. Therefore, the first step when designing a controller is to decide on a system model to be used as a design basis. The plant under consideration for this thesis is a highly non-linear coupled multi-degree-of-freedom (*n*DOF) system. Although it is theoretically possible to use an

inherently non-linear control method based on a non-linear plant model, in general the plant dynamics have to be precisely known to successfully apply these methods. The results of a preliminary study which illustrate this fact are presented in Appendix A1. If this is not the case, it can be generally recommended to apply a control method based on a linearised model of the non-linear systems.

In order to adopt the linearised model approach, the *n*DOF manipulator can be modelled as a linearised multi-input multi-output (MIMO) system. Due to the non-linear nature of the physical plant though the dynamic parameters of this linear model are subject to changes depending on the system state and its position relative to the linearisation point. Another way of describing the system dynamics is to treat each member of the manipulator as a separate system and therefore to model the plant as n independent linear single-input single-output (SISO) systems. In the case of designing the controller based on the full linear MIMO model the linear parts of the kinematic and dynamic coupling of the members are an integral part of the resulting controller while in the case of treating each member separately the coupling torques and forces are seen as external disturbances by the single axis controller. Hence, if a full model of the plant to be controlled is available and the resulting MIMO controller can be realised with the available controller hardware, the first approach is preferable avoiding the necessity of treating linear coupling effects as external disturbances. In case the whole plant cannot be fully mathematically described or the burden of this task on the controller hardware proves to be too demanding, it is necessary to design n single-axis controllers which provide stability and a satisfactory dynamic behaviour of the closed-loop system in the presence of system parameter changes and external disturbances.

As mentioned at the beginning, the system that is to be investigated as part of this thesis is a pneumatically animated figure for the entertainment industry performing human like movements. This figure is of a modular structure that means it can, depending on its application, consist of between 2 and 14 axes to be controlled. Furthermore, the figure can exhibit different dynamic properties due to the fact that it can be covered with different body shells and costumes resulting in varying inertial and friction properties.

The extreme complexity of this system and the related difficulty of modelling the system as a whole makes the single-axis approach mentioned above the favourable choice. This choice is further justified by the modular structure of the animated figure. Due to the fact that the superposition principle is not valid for non-linear systems this modular structure of the animated figure results in the necessity of providing a completely new linearised system model for every axes configuration and hence a new MIMO controller structure. Thus, when adding a further axis to the figure the system model cannot be simply upgraded by adding a further axis model to it.

From the above reflections the following conclusions can be drawn:

- The controller for the pneumatically animated figure has to be based on a linearised SISO model of a single-axis pneumatic servomechanism resulting in n independent single-axis controllers.
- The closed-loop system has to be robust to changes in the system parameters and guarantee stability and satisfactory dynamic behaviour over the whole working space of the figure.
- The controller has to provide the closed-loop system with excellent disturbance rejection capabilities due to the fact that kinematic and dynamic coupling effects between the members of the manipulator are not modelled and hence treated as external disturbances by the controller.
- Because of the fact that the axes of the animated figure are only fitted with displacement transducers measuring the actuator piston displacement this piston displacement is the only feedback signal available to the chosen controller.

It follows from above specifications that either a robust or an adaptive feedback control scheme has to be employed in order to guarantee robustness of the closed-loop system to severe parameter changes. Furthermore, the control algorithm should ideally enable the use of high feedback gains to ensure sufficient disturbance rejection capabilities of the single-axis system. If this conflicts with the obvious stability criteria an additional disturbance cancellation term has to be included in the controller structure. Moreover, since a significant number of pneumatic servo-mechanisms have to be controlled in parallel the control algorithm should be as simple as possible in terms of computational demands in order to limit the hardware

costs and ideally allow for implementation on a standard personal computer or on an analogue control card. Since the animated figure is only equipped with potentiometer displacement transducers, the only information on the dynamic state of the system directly available to the controller is the displacement of the pneumatic cylinders actuating the members of the figure. Therefore, numerical differentiation and filtering, a system state observation technique or analogue differentiation filters have to be employed in order to obtain the additional information on the system state which cannot be obtained by means of measurement but are in general required for feedback control.

1.2 STRUCTURE OF THESIS

This thesis is structured as follows:

Chapter 2 gives a general overview of positioning control of pneumatic servo mechanisms. The main linear, non-linear, adaptive and robust control approaches reported in literature are described, compared and evaluated in terms of their applicability to the control problem under consideration in this thesis. The conclusion that can be drawn from this analysis is that Variable Structure Control (VSC) and in particular Continuous Sliding Mode Control (CSLMC) seems theoretically to be most appropriate despite the fact that previous attempts of applying it to pneumatic servo control failed.

In Chapter 3 the pneumatically animated figure to be controlled and the specific experimental test rig set-ups used in this investigation are described in detail. The rigs are a single-axis pneumatic servo system with variable gravity load and a vertically mounted unequal area linear actuator and the arm of the animated figure consisting of two pneumatically actuated members. In terms of the influence of system non-linearities and parameter changes the single-axis test rig represents the dynamically worst case which can occur on the animated figure. Therefore, the results concerning robustness to system non-linearities and parameter changes that were obtained with this simple test rig are also valid for the more complex animated figure. Only the external disturbance rejection capabilities of the system had to be

determined directly using the 2 DOF arm of the animated figure. Furthermore, in this chapter the control and data acquisition system is described.

Chapters 4 and 5 present respectively a non-linear and a new linearised model of a pneumatic servo mechanism used to activate the manipulator axes. These chapters highlight the difficulties when modelling pneumatic systems. As will be shown, the key to successfully modelling a pneumatic servo is the highly non-linear servo valve model. A method to validate the simulation results by experimentally determining mass flow rates by charging and discharging dead volumes will be presented. Using this heuristic method the strongly non-linear relationship between mass flow rate and valve displacement, pressure ratio and heat exchange can be determined. Based on the non-linear simulation model a new linearised model of the servo-mechanism is then derived which predicts not only a position dependency of the dynamic behaviour of the servo but also a direction of valve opening dependency. This new linearised model proves to be ideally suited for determining the dynamic worst case conditions for which the resulting controller has to be optimised in order to guarantee stability over the whole workspace. Furthermore, by comparison of the response of the linearised and the non-linear system model, it can be demonstrated that the changing actuator chamber pressures, which are the only parameters assumed to be constant when linearising the system dynamics, have a stabilising effect on the system dynamics. This result gives further justification to the use of the chosen linearised model as a control design basis. The dynamic characteristics of pneumatic servo mechanisms under linear closed-loop control will be illustrated by means of simulation and experimental step response results. Using the new linear model to design the state-feedback controller results in improved dynamic performance of the servo system. Nevertheless, the presented results show the limitations of linear state-feedback control when applied to the highly non-linear pneumatic servo.

In Chapter 6 the Variable Structure Control (VSC) approach is introduced in detail. VSC is a particular type of robust control. The interesting feature of VS control is that in so called sliding mode, VS control theoretically offers maximum robustness to the action of external disturbances, system non-linearities and system parameter changes. This type of controller is also called Sliding Mode Control (SLMC). The switching characteristic of this control method lends itself to

discontinuously dynamically changing systems (e.g. position of valve opening dependency) like the pneumatic servo as shown in Chapters 3 and 4. Sliding Mode is reviewed against the background of relay control, Variable Structure Control (VSC) and Model Reference Adaptive Control (MRAC). It will be shown that Sliding Mode is a particular type of Variable Structure control and can also be seen as a MRAC algorithm without integral action. The interpretation of the sliding surface as the reference model describing the desired dynamic performance of the system results in greater freedom when designing this surface and also results in natural limits on the system demand. The problems with the implementation of Sliding Mode control and in particular the problems with its digital realisation and with numerical differentiation at low sampling rates offered by a conventional personal computer are discussed.

Chapter 7 concentrates on the basic design procedure for a Continuous Sliding Mode Controller (CSLMC) for the pneumatic servo under consideration. Since in sliding mode the dynamics of the control system are determined by the dynamics of the switching surface, this surface can be seen as a reference model of the desired system response. Therefore, by designing the switching surface the closed-loop dynamics can easily be determined. Reachability of the chosen second-order switching surface is discussed. In this context, the effects of supply pressure and valve size are investigated. As a result, the presented basic design procedure can also be used to determine parameters like supply pressure and valve size in order to achieve a given dynamic performance of the closed-loop control system.

Since unmodelled dynamics significantly reduce the infinite switching frequency theoretically required by the control system, the effects of valve bandwidth and digital implementation are thoroughly investigated in Chapter 8. The switching frequency of the control system in quasi- or pseudo-sliding mode is estimated using the extended Nyquist criterion. Amplitude and frequency of the resulting limit cycles occurring in quasi-sliding mode are compared with simulation results.

Finally in Chapter 9 the synthesised CSLM control is implemented on the single-axis test rig and two members of the arm of the animated figure. As predicted by theory a purely digital implementation using numerical double differentiation of the measured displacement signal does not yield satisfying results for the maximum

sampling frequency of 1 kHz achievable with the controller hard- and software. By introducing an additional accelerometer an excellent dynamic performance of the pneumatic servo can be obtained. Since the use of an accelerometer is outside the scope of this project, analogue differentiation filters are implemented as alternative ways of generating the required unmeasureable system states. Differentiating the measured displacement signal by means of these analogue differentiation filters improves the system response significantly in comparison to numerical differentiation. Yet, discrete-time switching, in combination with the phenomenon that high-frequency noise is amplified by the differentiation filter, still leads to a rather jerky system response even in the presence of a boundary layer around the switching surface. This fact prompted the development of a novel purely analogue CSLM control card offering double differentiation of the measured displacement signal, definition of the switching surface using state gain potentiometers and relay-like switching by means of a saturated operational amplifier. Omitting the control PC as a closed-loop system element, reducing the switching frequency and introducing this purely analogue CSLM card yields the desired system response. As shown by experimental step and frequency response tests the novel analogue CSLM card offers excellent dynamic performance and robustness to system parameter changes (in particular the mass to be moved). Since no control PC is needed for implementation and the CSLM card only requires displacement as an input the hardware costs are minimised. The superior disturbance rejection capabilities allow the application of the analogue CSLM card to *n*DOF systems without the need of an overall coupling compensation algorithm as demonstrated experimentally. Therefore, it is ideally suited for the application to the animated figure allowing for freedom in the figure set-up. Adding or omitting axes, body shells or costumes does not result in complex retuning procedures or a redesign of the controller structure.

2 CONTROL OF PNEUMATIC SERVO MECHANISMS

Servo position and/or velocity control for robots and other industrial machines is usually achieved through the use of hydraulic or electric actuators. In general, pneumatic actuation systems are only used for motion control to mechanical end-stops (e.g. for pick and place handling equipment or to open and close robot grippers). This situation can be attributed mainly to three reasons:

- Firstly, the compressibility of low pressure gas used as the working medium affects the steady-state and dynamic behaviour of the pneumatic servo resulting in a low natural frequency, significant time lag and high load sensitivity.
- Secondly, the highly non-linear equations describing compressible gas flow and the thermodynamics during charging and discharging of a control volume are more difficult to handle than those describing a hydraulic or electrical system. Therefore, in general, advanced control algorithms have to be applied in order to enable a servo controller to compensate for the inherent system non-linearities. To digitally realise these control algorithms in real time generally powerful control computer equipment is required. Using conventional linear control does usually not yield a satisfactory system performance.
- Thirdly, servo control is usually achieved through the use of high-performance proportional control valves which only recently have become available at competitive prices for pneumatics. Most commonly, cheap on/off-valves and analogue controllers have been and still are in use for pneumatic drives lending themselves mainly to motion control to end-stops.

2.1 CHARACTERISTICS OF PNEUMATIC SERVO MECHANISMS

The fact that pneumatic servos use a very compressible working fluid accounts for the two main system characteristics: a comparatively low natural frequency and a lack of stiffness. These two characteristics distinguish pneumatic drives from hydraulic and electric ones.

Pneumatics always exhibit a significant time delay whereas hydraulic systems have a rapid initial response. If for example an actuator chamber is charged with air,

a sufficient amount must flow into the cylinder volume to increase the pressure and build up enough force to overcome static Coulomb friction. In hydraulic systems a small mass flow into the actuator chamber causes a rapid pressure rise and hence an almost immediate system response. In this context Shearer and Lee (1956) showed in an example that the hydraulic system responds approximately 50 times faster than the pneumatic system for the same supply pressure and load mass. In other words, gas mass flow into a pneumatic actuator results in an increase in pressure **and** an increase in fluid density while oil mass flow into a hydraulic actuator results principally in an increase in pressure. That is the reason why conventionally in an analysis (as being performed in Chapters 4 and 5) it is pneumatic mass flow that is considered whereas hydraulic volumetric flow.

The other main difference between pneumatics and hydraulics, the lack of stiffness of pneumatic systems due to the compressibility of air results in a very high sensitivity to changes in external load and external disturbances. It has been shown by Burrows (1972) that a hydraulic system has a stiffness of approximately 400 times that of the equivalent pneumatic system. Therefore to achieve a sufficient stiffness of pneumatic systems, either the actuators must be large enough to counteract any load variations with relatively small changes in pressure or the servo valves must provide a flow rate large enough to rapidly add or remove gas to the actuator chambers. Especially in robotic systems with various kinematically and dynamically linked axes the actuation system is permanently subject to external disturbances due to the coupling effects. It is therefore very difficult to control such systems in a satisfactory manner if they are actuated pneumatically.

Another problem with pneumatic systems is the low overall efficiency of valve-controlled drives as stated by Shearer and Lee (1956). This is mainly due to energy losses caused by throttling. These losses are more serious with air than with oil, because more work is required to compress air between given pressure limits than is required to pump oil between the same limits. Furthermore, pneumatic servo mechanisms do not offer the possibility of pump control of the mass flow. This method is often used for hydraulic applications requiring large power output. There is no variable-displacement compressor commercially available, so the control of

pneumatic servo mechanisms is always achieved by means of a servo valve throttling the flow and hence dissipating energy.

However, pneumatic servo mechanisms also provide advantages over hydraulic servos. Pneumatic systems in general are lighter than hydraulic systems due to the low weight of the gas in the lines and the lighter components designed only to withstand much lower system pressures. In pneumatic systems there is also no need to provide a return line since the relatively low pressure air from the motor can be exhausted to the atmosphere. An exhaust diffuser is often recommended to reduce excessive exhaust noise. Furthermore, pneumatic systems can work at temperatures above 500°C where electrical and hydraulic systems usually fail. For example in aircraft and missile applications products of combustion at temperatures ranging from 500°C to 2000°C are available as sources of energy. Drives used in these fields are called *hot-gas servo mechanisms*. Since temperature has only a second-order effect on the properties of gas like viscosity and bulk modulus the response of pneumatic servo mechanisms is little affected by changes in temperature. Also the power supply for pneumatic systems is cheap in comparison to hydraulic power units. Most industrial plants are equipped with an air supply of 5 to 10 bar. Moreover, there are no problems with leakage and pneumatics are also very environmentally friendly and clean.

To conclude the above reflections, pneumatic systems are particularly useful and possess inherent advantages in applications where the dynamic response requirements are not too demanding and where the system is not subjected to significantly varying external disturbance forces. Yet, in the context of this thesis it will be shown that with new high-performance servo valves and analogue control solutions the area of application of pneumatic servo control can be significantly extended to systems with fast dynamic responses, high positioning accuracy and varying external disturbances.

2.2 Review of Recent Contributions in Pneumatic Servo Control

Despite the fact that in contrast to the study of hydraulic servos relatively little attention has been paid in the past to the analysis of the highly non-linear pneumatic servo systems some research studies as early as 1950 (e.g. Shearer (1956)) have demonstrated the feasibility of producing relatively low cost pneumatic servo drives. Following the introduction of reasonably priced pneumatic servo valves and the sharp decrease in the price of computing hardware in recent years, a variety of approaches have been used in deriving computer controls for pneumatic servos, leading to commercially available integrated drive system elements that have begun to be accepted by system designers and engineers in the manufacturing industry. In the following some of the most important contributions to pneumatic servo control reported in literature are described and their advantages and disadvantages are highlighted in brief. The fact that all the contributions mentioned in the following are generally only suitable for one specific control problem or application and not applicable to a wide range of pneumatic systems and in particular not applicable to the *n*DOF pneumatically actuated animated figured under consideration prompted the research work being presented in this thesis.

2.2.1 Linear Feedback Control

As will be demonstrated in Section 5.3 of this thesis, due to the highly non-linear dynamic characteristics of the pneumatic servo linear canonical state-feedback control utilising position, velocity and acceleration signals (also called PVA-control) is in general not capable of providing the required dynamic response of the closed-loop control system especially if the actuator chamber pressures are unequal due to unequal piston areas or an external load being applied. No matter whether pole placement (e.g. Burrows and Webb (1969), Taha and Nor (1989), Uebing *et al* (1997)), linear quadratic optimisation (Liu and Bobrow (1988)) or similar techniques are used to tune the controller, asymptotic stability can only be guaranteed in the neighbourhood of the linearisation point. Outside this neighbourhood the closed-loop dynamics can deviate significantly from the desired behaviour. Also a control system

designer has to be aware of the fact that, since the bandwidth of the pneumatic servo is limited by the limited valve opening non-linearity and the choked flow effect, the closed-loop poles of the transfer function can only be shifted a certain distance to the left of the complex plane even with large feedback gains.

Large steady-state position errors due to Coulomb friction and leakage effects are an inherent part of the closed-loop state-feedback system dynamics. In order to reduce these errors integral action is often included into the control law. PI (proportional and integral action) and PID (proportional, integral and differential action) control schemes are very common and can reduce steady-state errors effectively. Yet, integral action has an adverse effect on closed-loop stability. It can therefore only be recommended when steady-state errors are a more important issue than speed of response.

2.2.2 Extensions of Linear State-feedback Control and Other Linear Techniques

In order to adopt the linear canonical state-feedback approach to the control of pneumatic servo mechanisms various extensions to the basic method have been proposed. One way of dealing with the problem of position dependent servo dynamics for instance is to use different gains for different regions within the operating space as demonstrated by Virvalo (1995). This method, called *gain scheduling* can be implemented by means of an on-line lookup table of the optimal gains. Although by varying the feedback gains the dynamic performance of the control system can theoretically be improved, gain scheduling controllers are difficult to tune and also, in general, do not take account of discontinously changing system dynamics like the direction of valve opening dependency of the servo dynamics. For systems with unequal area actuators this effect is more significant than the position dependency as will be shown in Section 5.3.1 and would require a discontinuous switching of feedback gains with all the problems involved. Switching of control signals will be discussed in more detail in the context of Sliding Mode Control (SLMC) in Chapter 6.

As mentioned before, a serious problem with linear canonical state-feedback control without integral action is its inability to compensate for the effects of stiction which can have a significant influence on the dynamics of a pneumatic servo. The stiction effect in combination with the compressibility of air often results in the so-called *stick slip* effect when the actuator piston is moving slowly. Abou-Fayssal and Surgenor (1997) clearly demonstrated the shortcomings of linear state-feedback control in the presence of stiction and investigated the application of friction model based compensators. Although their proposed algorithms do not yield the expected results the investigation highlights the seriousness of the problem. Another way of dealing with high Coulomb friction is to use a dither signal as reported by Surgenor and Wijesuriya (1992). A common problem with conventional dither signals is the constant demand for air due to the actuator piston constantly moving with a fixed dither frequency. Also, the high control action of the servo valve being constantly excited may result in excessive wear of its moving parts. The *Intelligent Dither* (ID) introduced by Surgenor and Wijesuriya is therefore only activated in the case that the actuator piston is stuck. Although the additional ID signal reduces the steady-state error effectively the system response is very jerky since the dither action is only activated once the piston stops moving.

If state-feedback control is used for path tracking as opposed to set point positioning of pneumatic servo systems large path tracking errors usually occur. By means of feedforward compensators in combination with state-feedback path tracking controllers as proposed by Moore *et al* (1985) and Pu *et al* (1991) these large position following errors can be reduced significantly but only if the actuator piston is moving. If the piston motion comes to a halt stiction causes a delay in the system response and increases the tracking error until the piston starts moving again and the compensator reduces the tracking error.

Cascaded or hierarchical feedback loops including additional pressure feedback as proposed by Noritsugu and Takaiwa (1995) and Kawamura *et al* (1989) theoretically add additional features like robustness to load changes while also compensating for stiction. It has been pointed out by Mannetje (1981) that the performance of pneumatic servo systems can be improved considerably by using embedded pressure feedback loops. Cotsaftis *et al* (1995) showed that in theory when

applying a control law only using displacement and pressure feedback there exists a domain for the control gains where the closed-loop response is stable and not impaired by an oscillatory behaviour even without considering the dissipative effects of friction and leakage. By feeding back measured differential actuator chamber pressure load changes can be sensed and compensated for. Friction effects can be compensated for in a similar manner since differential pressure in combination with measured acceleration allows for the identification of the friction force. Although the experimental results presented by Noritsugu and Takaiwa show a clear improvement when compared to simple P and PI controller results they are overall not satisfying. Tuning of the inner and outer feedback loops is quite an involved task and even additional disturbance observers in the inner pressure feedback loop are necessary to provide acceptable dynamic performance of the control system under changing load conditions. Another disadvantage of an inner pressure feedback loop is the additional cost of pressure transducers.

An alternative way of improving the dynamic response of pneumatic actuation systems under closed-loop control is to choose appropriate demand signals into the system which do not exceed its dynamic limits. In this context a profile planning strategy has been proposed by Pu *et al* (1992) which represent an alternative way of optimising and tuning the system response. By means of cosine-, sine- , circular- and trapezoidally-shaped demand profiles a desired system response can be achieved by directly influencing load acceleration and deceleration and initial time delay. Therefore, profile planning represents an additional tool to improving the system dynamics and can complement controller optimisation.

2.2.3 NON-LINEAR CONTROL

To fully account for the non-linearities of pneumatic servos a non-linear controller based on a precise non-linear system model can be employed. Usually, non-linear control algorithms consist of an inner linearisation loop which transforms the non-linear system state into an equivalent linear state. Outside this inner loop spans an outer linear feedback loop which can be tuned similarly to plain linear feedback control loops. In general, one of the main problems with the inner feedback linearisation loops is that apart from the transformation being mathematically

involved it also might introduce local singularities where the transformation is impossible and hence the control concept breaks down. Kimura *et al* (1995) showed though that any SISO pneumatic system with an input-state feedback linearisable load and an isothermal pneumatic actuator is linearizable by state-feedback. He demonstrated by means of experimental results using a system with a rubber artificial muscle (RAM) actuator that feedback linearisation can improve the performance of a linear feedback controller. Further examples of controllers for electro-pneumatic servos based on input-output linearisation can be found in Richard and Scavarda (1989) and Lin *et al* (1993).

In general it can be said, that providing that the non-linear system model of the plant to be controlled is linearisable and no singularities occur within the operating space, the model has to be a precise description of the plant because any deviation of the model from the plant might cause an unpredictable dynamic behaviour due to the non-linear nature of the system. Discrepancies between non-linear model and plant, for instance due to parametric uncertainties, might have a more serious effect on the closed-loop dynamics than discrepancies between a linear model and the plant as is demonstrated in Appendix A1 where linear and non-linear control methods are compared by means of simulation step response results of a 2DOF system with ideal actuators.

2.2.4 ADAPTIVE CONTROL

Especially in France many attempts have been made to use adaptive control algorithms to control pneumatic actuation systems. Guihard *et al* (1994, 1995) use two different model reference adaptive controllers (MRAC) to control a 2DOF pneumatically actuated robotic leg. The first control algorithm is based on a full non-linear 2DOF dynamic model of the system derived by means of the Lagrangian energy equation resulting in the required torques for a given trajectory. The control task is decomposed in two objectives: the computation of the optimal torque and the tracking of the desired trajectory. The time-varying system parameters are adapted on-line by an integral type parameter adaptation algorithm (PAA). The stability is guaranteed by applying Lyapunov's stability theory. The second algorithm applied by Guihard is based on a single-axis decentralised approach proposed by Seraji (1989).

Each axis of the pneumatic leg is treated as a separate subsystem being controlled by an independent controller. In this case coupling effects are treated as external disturbances. Therefore, again by means of an integral type parameter adaptation algorithm, the single-axis dynamic system model and an additional error model have to be adapted. Guihard concludes that the 2DOF controller is highly complex and difficult to compute in real time even for only a 2DOF system. It is therefore only applicable for systems with a small number of actuated axes. The decentralised controller on the other hand can only be used within a limited system velocity range due to fact that a large number of controller gains have to be adjusted on-line. High velocities lead to instability.

Bobrow and Jabbari (1989, 1991) compared a model reference adaptive controller (MRAC) with a parameter identification type adaptive algorithm by means of experimental results obtained with a single-axis pneumatic servo with a linear actuator. Like Guihard, the authors also conclude that MRAC only yields satisfying results for small system velocities. Although the results with the parameter identification controller, based on a least-square identification method in combination with pole placement, was generally preferable, distinct and highly undesirable position dependent high-frequency components in the system response occurred. Increasing the order of the dynamic model underlying the controller in order to account for these high-frequency oscillations resulted in instability which was according to Bobrow due to the limited displacement sensor resolution.

Keller and Isermann (1993) also used an adaptive control algorithm based on least-square parameter identification. In their system they included an additional inner pressure feedback loop and a model based friction compensator. The reported experimental results look very promising. The system is robust to load changes and is perfectly able to cope with stiction. Yet, the high costs of the additional pressure transducers are a drawback which has to be taken into account.

McDonell and Bobrow (1993) also used an identification algorithm to update the adaptive controller parameters on-line by means of solving a discrete-time Riccati equation. The system state used to synthesise the control signal includes the differential actuator chamber pressure. Again, the results of the parameter identification adaptive control approach were satisfactory.

Generalising the results above it can be said that MRAC is always limited by the adaptation speed of the algorithm. This limitation restricts its use to systems with reasonably slow changes in the dynamic state relative to the adaptation speed. Li and Cheng (1994) and Fok *et al* (1995) give further examples demonstrating this fact.

Parameter identification adaptive control algorithms on the other hand are prone to high-frequency disturbances due to unmodelled dynamics and in general only allow for reasonable parameter identification if the system is sufficiently and constantly excited (Goodwin and Sin (1984)).

It should be mentioned that none of the algorithms discussed above provide exceptional disturbance rejection capabilities exceeding those of linear feedback controllers.

2.2.5 VARIABLE STRUCTURE AND SLIDING MODE CONTROL

The Variable Structure or Sliding Mode approach to pneumatic servo position control is the most promising attempt reported in literature in particular due its robustness to system parameter changes and the excellent capabilities to linearise the system dynamics and to reject external disturbances.

A first attempt by Tang and Walker (1995) to apply a continuous (as opposed to discrete) sliding mode controller to a pneumatic servo failed due to the fact that a first-order sliding surface was used for a system whose predominant dynamics are of third-order (see Section 5.1).

Surgenor *et al* (1995) then successfully used a second-order surface and an additional phase compensator to compensate for the phase lag introduced by the numerical differentiation routines used to generate velocity and acceleration signals. The reported results were very satisfactory.

Drakunov *et al* (1997) showed that sliding mode control with a second-order sliding surface (including differential pressure feedback) is also able to cope with one of the most serious problems for pneumatic servos: stiction.

Thomasset *et al* (1993), Bouri *et al* (1994) and Bouri *et al* (1996) used sliding mode control with additional system state linearisation. Although the experimental results with the nominal system were good, the linearising state transformation decreased the systems robustness to parameter changes significantly which, as mentioned above, is one of the main features of sliding mode control. Furthermore, the resulting control algorithm is highly complex and lacks the simplicity of conventional sliding mode algorithms. It is the authors opinion that, although some of the results reported by Thomasset and Bouri were extremely good, the additional state transformation contradicts the basic philosophy of sliding mode control and diminishes the benefits of its most distinguished characteristics.

2.3 CLOSURE

Reviewing the control approaches reported in literature and presented above and first experimental results obtained in collaboration with the control laboratory of Queen's University, Kingston, Canada lead to the conclusion that Variable Structure Control (VSC) is probably the most promising control method for pneumatic servo positioning systems. Therefore, this approach will be discussed in detail in Chapter 6 and applied to the *n*DOF pneumatically animated figure which is the subject of this thesis.

3 DESCRIPTION OF EXPERIMENTAL RIGS

In the course of the investigation two experimental rigs have been used:

- the pneumatically actuated animated figure to be controlled and
- a single-axis pneumatic servo test rig.

Both systems and their hardware are described in this chapter.

3.1 ANIMATED FIGURE

The animated figure for the entertainment industry for which a controller is to be designed as part of this thesis consists of seven axes actuated by linear and rotary pneumatic servo mechanisms. All actuated axes are manufactured of aluminium and are kinematically and dynamically coupled as can be seen in Figure 3.1. The moving members of the animated figure are mounted on low-friction roller bearings while the whole figure is mounted on a steel frame. The displacement of each individual member of the figure can be measured by means of linear or rotary displacement transducers. Further measurement equipment is not incorporated.

During the investigation mainly the arm providing 2 degrees of freedom as shown in Figure 3.1 was used in order to test the disturbance rejection capabilities of the proposed controller.

3.1.1 PNEUMATIC SERVO MECHANISM

The pneumatic servo mechanisms employed to actuate the axes of the animated figure consist of a pneumatic actuator (linear or rotary), a pneumatic servo control valve and a potentiometer-type displacement transducer. The valves and actuators are connected via rubber pipes with an internal diameter of 2 mm and an average length of about 1 m. The pressure drop in the connecting pipes was measured to be less than 0.3 bar. A schematic of the linear and the rotary servo is depicted in Figure 3.2.

To provide the required air supply pressure for the pneumatic actuators the supply port of each servo control valve is connected to the main air supply of the University. It was found during experimental testing that the air supply pressure varied between P_s = 6.5 bar and P_s = 7.7 bar depending on the total load on the main air supply.

3.1.1.1 Pneumatic Actuators

The following two actuator types are used to actuate the axes of the animated figure:

- the linear double acting piston actuator JPA produced by Kyoto, Japan and
- the miniature rotary vane actuator comp-act 042-121 by Turn-Act, USA.

The technical data for both actuators can be found in Tables 3.1 and 3.2, respectively.

3.1.1.2 Pneumatic Servo Valve

The valves used on all axes of the animated figure are servo valves DDV 27A1 produced by HR Textron, USA. It is a straightforward direct drive design as can be seen in Figure 3.3. A limited angle, rotary torque motor drives a sliding spool directly through an eccentric which is built into the motor shaft. Rotary operation of the motor results in linear spool motion, which modulates the flow from the pressure port S through the cylinder ports A and B of the valve. Flow is then ported to the system return R.

The direct drive servo valve (DDV) requires an electronic controller also depicted in Figure 3.3. This controller compares the command input signal with the actual spool position which is monitored by an electric device within the torque motor and compensates for the non-linear relationship between input voltage and flow area.

Technical data provided by the manufacturer can be seen in Table 3.3. The spool displacement-flow area characteristic is depicted in Figure 3.4. As mentioned above the non-linear nature of this characteristic is compensated by means of the valve driver module including the spool position controller.

The frequency response provided by the manufacturer is shown in Figure 3.5. As can be seen, depending on the spool opening amplitude the bandwidth (-3 dB point) of the control valve varies between 500 Hz for a spool opening of 2.5% and 135 Hz for a valve opening of 100%. When measuring the frequency response of the valve spool displacement under no-flow condition it was found that the bandwidth only varied between 290 Hz and 200 Hz. The damping ratio was found to be between 0.68 and 0.71. Furthermore, the average valve spool delay under no-flow condition could be measured to be less than 1 ms.

The various pressure losses in the servo valve have been experimentally determined as shown for the example of the pressure loss in the flow path supply port S - port A in Figure 3.6. The resulting pressure loss coefficients are listed in Table 3.4.

3.1.1.3 Displacement Transducers

To measure the displacement of the pistons of the linear actuators the potentiometer-type displacement transducer HLP 095 150 12 K by Penny & Giles is used while the displacement of the rotary actuator is measured by means of the rotary potentiometer-type displacement transducer 89 44 0006 by the same manufacturer. The specification for both transducers are listed in Tables 3.5 and 3.6, respectively. The calibration results can be found in Figure 3.7. The relative measuring error depicted in Figure 3.7b relates the measured absolute displacement error to the displacement to be measured.

3.2 SINGLE-AXIS TEST RIG

In order to validate the simulation models of the pneumatic components and also to test and compare the performance of the controllers investigated a simple single-axis test rig as depicted in Figure 3.8 was designed. The system consists of a vertical linear actuator with variable gravity load and the HR Textron DDV 27A1 proportional control valve connected via 100 mm of rubber hose (internal diameter of 2 mm).

Again the supply port of the servo valve was connected to the main air supply of the University and therefore the supply pressure varied between P_s = 6.5 bar and P_s = 7.7 bar in experiment. This fact did not prove to be a problem in the context of validating the simulation models since the supply pressure could be measured and its variations could be accounted for in simulation.

The dimensions of the linear actuator chosen can be found in Table 3.7. In addition to one of the displacement transducers used on the animated figure, the single-axis test rig was fitted with chamber pressure transducers and an accelerometer.

Due to the vertical orientation of the linear actuator and the fact that the gravity load acts on the smaller actuator piston area the single-axis test rig represents the dynamically worst case in terms of controllability. Resulting from the large pressure difference in the actuator chambers, system non-linearities and parameter changes are more severe on the test rig than in the case of the animated figure. These phenomena will be discussed in more detail in Chapter 5. Therefore, results obtained with the single-axis test rig concerning controller robustness to system non-linearities and parameter changes could be directly evaluated and interpreted for the animated figure. Only the disturbance rejection capabilities of the proposed controller had to be tested directly on the animated figure as mentioned above.

3.2.1 PRESSURE TRANSDUCERS

To enable the measurement of the actuator chamber pressures two miniature piezo-resistive pressure transducers EPK-125-300 were used which were mounted in the inlet and outlet pipes outside the actuator chambers as shown in Figure 3.9. The measured pressure signals were only used for the simulation model validation and not as inputs to the controller.

Due to the way the transducers were incorporated into the pipes they measured static pressure in the pipe instead of total pressure in the actuator chambers. This difference could be easily compensated for in simulation by adding the dynamic pressure (being a function of the gas flow velocity) to the measured static pressure in order to obtain the total pressure. The specifications of the pressure

transducers can be found in Table 3.8. The calibration results are depicted in Figures 3.10 and 3.11. The relative measuring error depicted in Figures 3.10b and 3.11b relates the measured absolute pressure error to the absolute pressure to be measured.

3.2.2 ACCELEROMETER

In order to obtain reliable actuator piston acceleration data the accelerometer 4383 by Brüel & Kjær, Denmark was fitted to the single-axis test rig. Its technical data can be found in Table 3.9.

Measuring actuator piston acceleration was important during the simulation model validation phase of the project. Furthermore, the measured acceleration signal could by used for control purposes and to determine the quality of acceleration signals obtained numerically and by means of analogue differentiation filters.

3.3 DATA ACQUISITION AND CONTROLLER HARDWARE

To implement the various control algorithms digitally a commercially available PC with a 166 MHz Pentium processor was used. The D/A- and A/D-conversion was realised by means of a DT2812A I/O board by Data Translation as shown in Figure 3.8. The technical data concerning the I/O board can be found in Table 3.10.

Tables

Table 3.1 - Data for linear double acting piston actuator JPA produced by Kyoto

stroke	30-50 mm
piston diameter	25-32 mm
piston rod diameter	10-12 mm

Table 3.2 - Data for miniature rotary vane actuator comp-act 042-121 produced by Turn-Act

maximum nominal rotation	90°, double vane
output torque	60 in-lbs at 100 psi
shaft	double ended
shaft load capacity	max. side load 250 lbs max. end load 10 lbs
air leak rate	less than 4 cfh at 100 psi

Table 3.3 - Data for direct drive servo valve DDV 27A1 produced by HR Textron

rated flow	2 SCFM at 100 psi
electrical power	0.1 Watts max for full pneumatic flow
null bias	± 1 %
hysteresis	1.0 %
linearity	5.0 %
amplitude ratio	-3 dB at 200 Hz
phase angle	-90°± at 150 Hz
linearity	5.0 %
power	23 Watts (RMS) at 150 Hz

Table 3.4 - Empirical leakage coefficients of pneumatic servo valve

flow path	**valve position**	**ports**	**leakage coefficient [(l/s)/bar]*10^{-7}**
S-A	0	blocked	7.42
	0	open	5.46
	-1	blocked	7.67
	-1	open	2.48
S-B	0	blocked	7.91
	0	open	5.04
	1	blocked	9.71
	1	open	2.79
A-B	0	blocked	7.11
	0	open	0
	1	blocked	8.40
	1	open	3.10
B-A	0	blocked	7.39
	0	open	0
	-1	blocked	8.38
	-1	open	4.81
A-E	0	blocked	9.28
	0	open	10.05
	1	blocked	8.73
	1	open	4.47
B-E	0	blocked	8.03
	0	open	8.75
	-1	blocked	9.22
	-1	open	3.35
S-E	0	blocked	6.93
	0	open	0
	1	blocked	11.36
	1	open	3.76
	-1	blocked	9.28
	-1	open	3.59

Table 3.5 - Data for translational potentiometer-type displacement transducer HLP 095 150 12 K produced by Penny & Giles

stroke	30 mm
range	0-10 V

Table 3.6 - Data for rotary potentiometer-type displacement transducer 89 44 0006 produced by Penny & Giles

stroke	180°
range	0-10 V
resistance	10 kΩ ± 20%
linearity	± 0.5%

Table 3.7 - Dimensions of linear actuator on single-axis test rig

stroke	30 mm
rod diameter	10 mm
internal cylinder diameter	25 mm
linearity	± 0.5%

Table 3.8 - Data for miniature pressure transducer EPK-125-300

range	300 psig (20.7 bar)
excitation	6 V
output	0.421 mV/psig
input impedance	551 Ω
output impedance	328 Ω

Table 3.9 - Data for accelerometer 4383 produced by Brüel & Kjær

charge sensitivity	3.1 pC/ms^{-2}
voltage sensitivity	2.44 mV/ms^{-2}
capacitance (include. cable)	1271 pF
maximum transverse sensitivity	2.5 % at 30 Hz, 100 ms^{-2}
typical undamped natural frequency	51 kHz
typical transverse resonance frequency	10 kHz

Table 3.10 - Data for DT 2812A I/O-board produced by Data Translation

analogue inputs	
resolution	12 bits (0.024 % FSR)
throughput	100 kHz
input channels	16SE / 8DI
gain	1, 2, 4, 8
range	0-10 V
system error	± 0.03 % of FSR for G = 1, ± 0.05 % of FSR for G = 8
conversion time	8 µs
CMRR	> 70 dB at 60 Hz
S/H aperture uncertainty	0.3 ns
analogue outputs	
DACs:	2
resolution:	12 bits (0.024 % FSR)
throughput:	100 kHz / DAC
range:	± 5 V at ± 5 mA
settling time:	10 µs
slew rate:	1.5 V/µs
error:	± 0.2 % of FSR
drift zero:	±3 ppm of FSR/°C
drift gain:	±30 ppm of FSR/°C

FIGURES

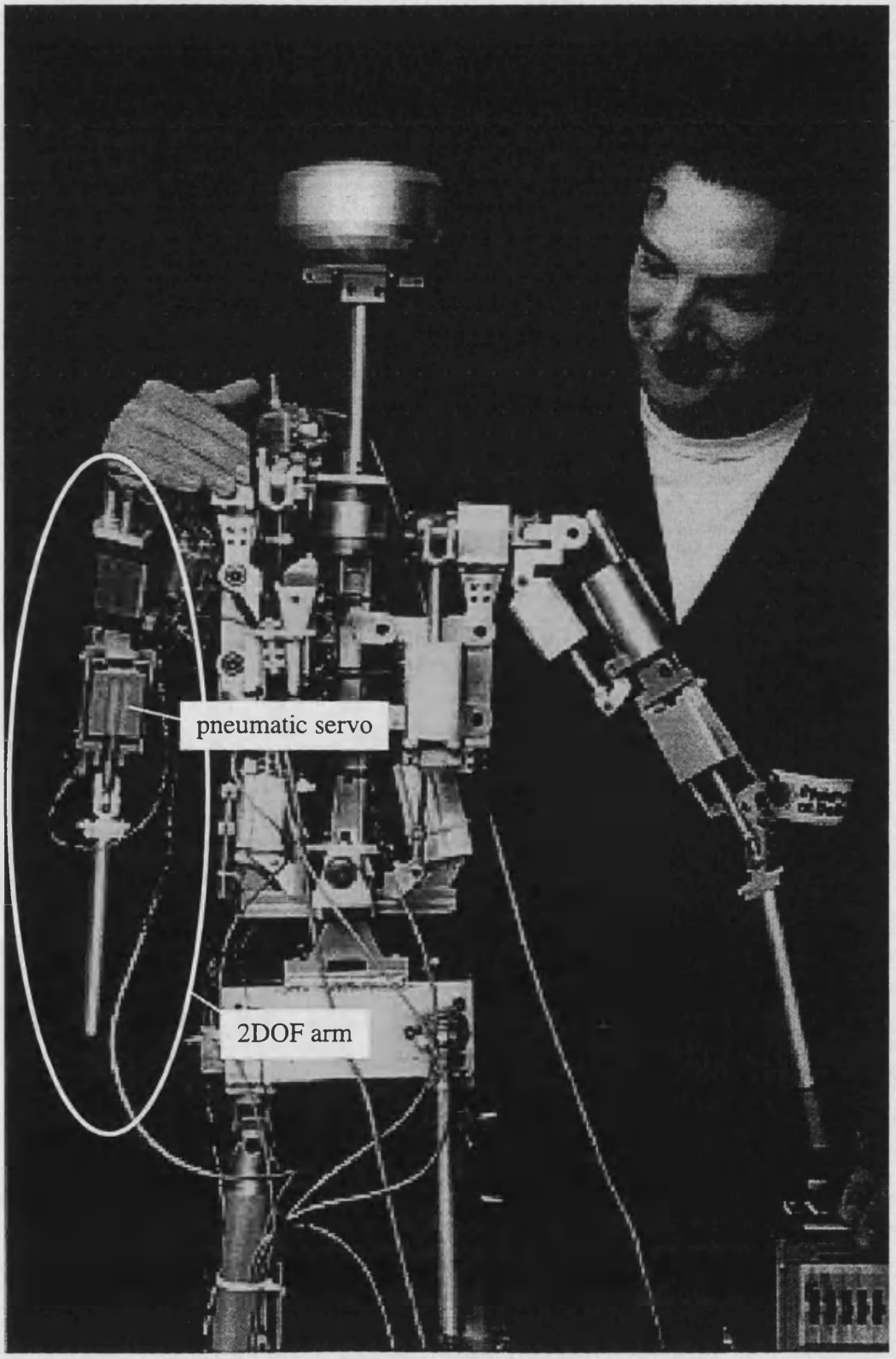

Figure 3.1 - Pneumatically actuated animated figure

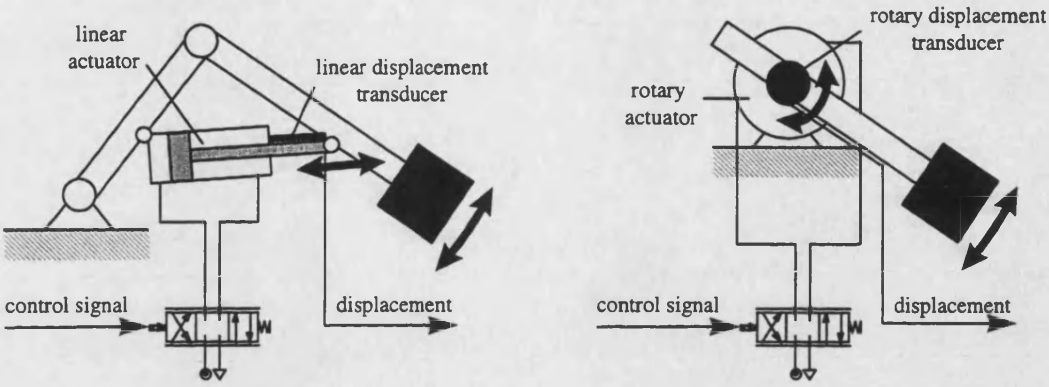

Figure 3.2 - Schematic of pneumatic servo mechanisms

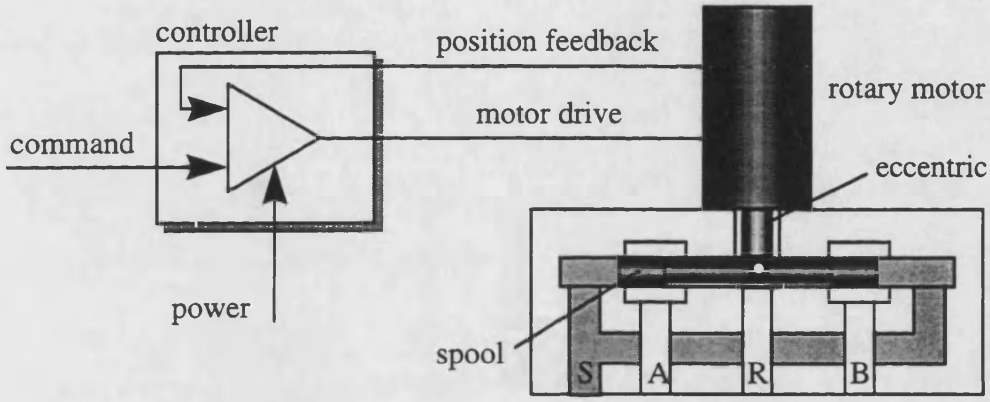

Figure 3.3 - Direct drive servo valve DDV 27A1 produced by HR Textron

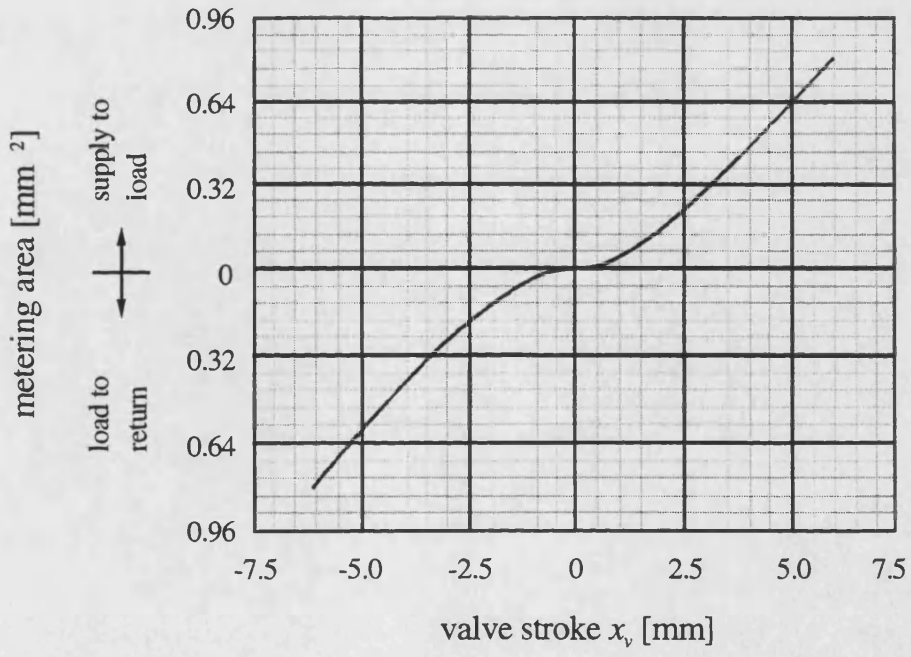

Figure 3.4 - Spool displacement - flow area characteristic (manufacturers data)

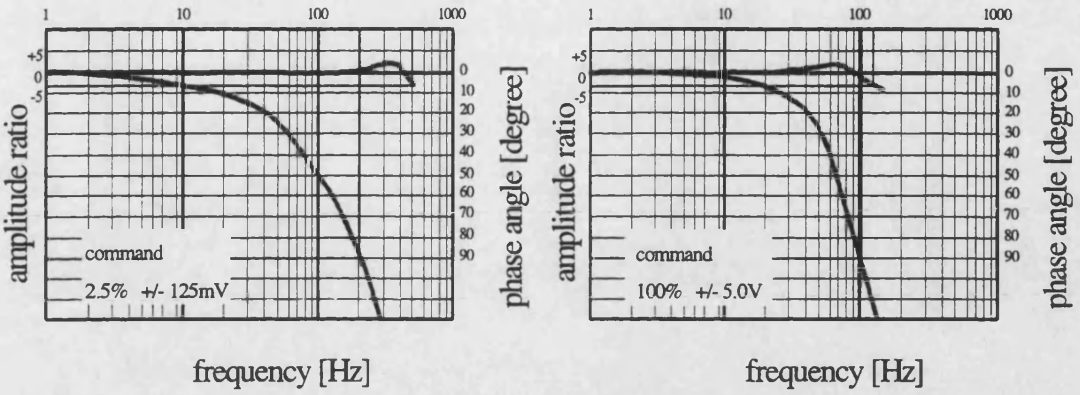

Figure 3.5 - Frequency response of pneumatic servo valve (manufacturers data)

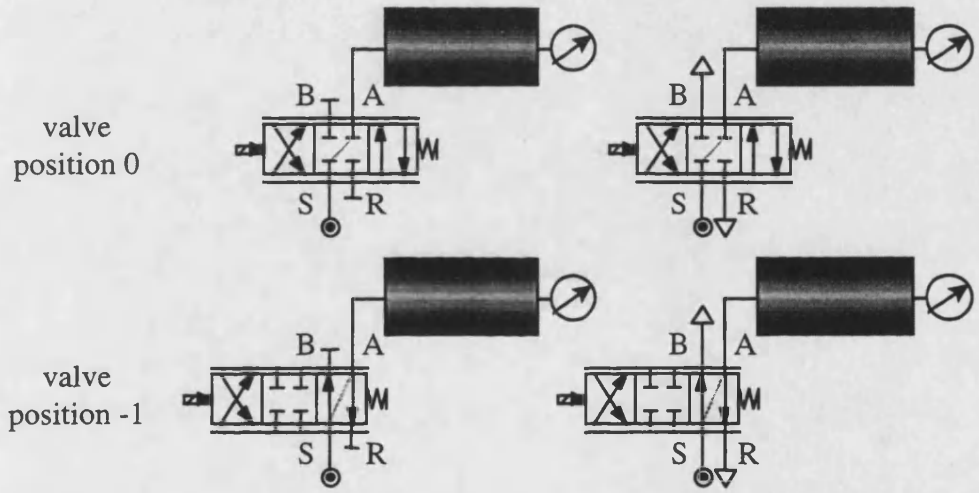

Figure 3.6 - Determination of pressure loss in flow path S-A

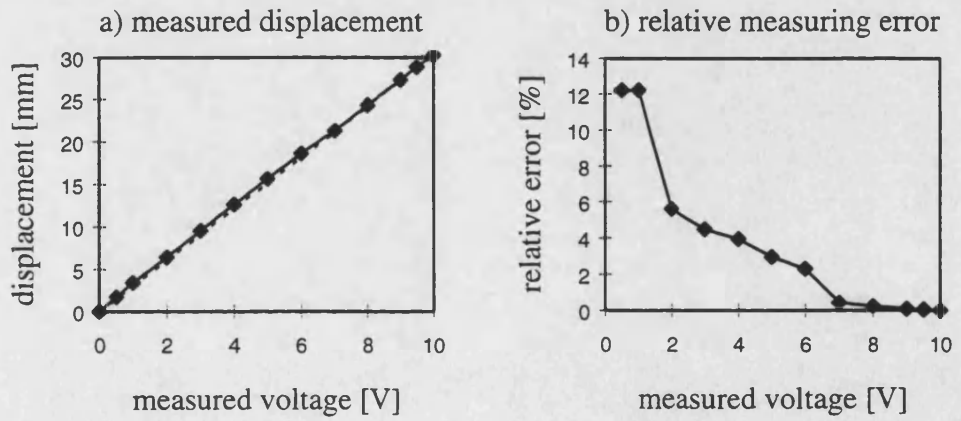

Figure 3.7 - Calibration of displacement transducer

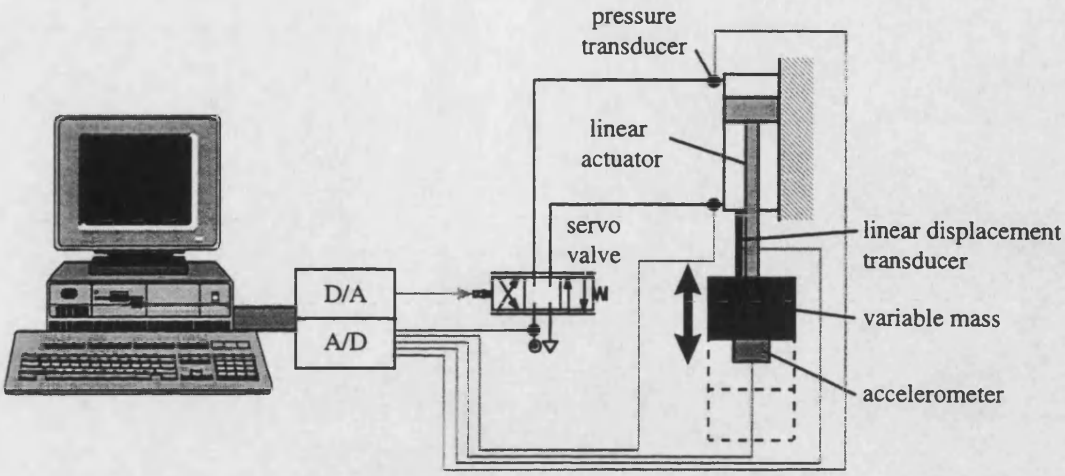

Figure 3.8 - Schematic of single-axis test rig

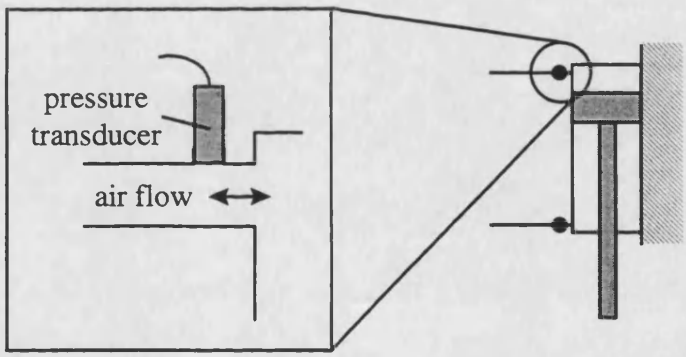

Figure 3.9 - Placement of actuator chamber pressure transducers

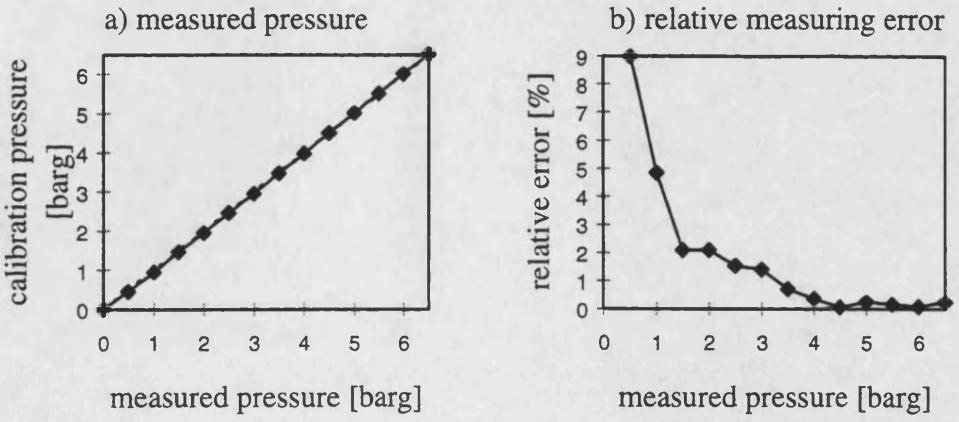

Figure 3.10 - Calibration of pressure transducer for chamber pressure P_a

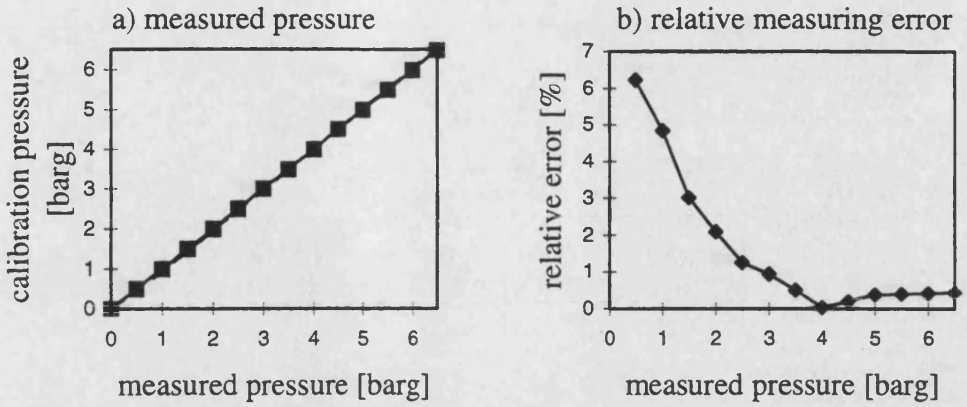

Figure 3.11 - Calibration of pressure transducer for chamber pressure P_b

4 NON-LINEAR MODEL OF A PNEUMATIC SERVO MECHANISM

In this chapter, the mathematical models describing the dynamics of the components of the pneumatic servo actuation system are derived in detail. This section basically summarises well known modelling approaches, discusses their validity and in some respects slightly extends their interpretation horizon. The presented mathematical relationships are used as the basis for the dynamic valve and actuator simulation models developed within the Bath*fp* simulation environment (Lo and Tilley (1993)) described briefly in Appendix A1.

In order to validate the proposed valve model a simple yet effective experimental calibration procedure will be presented. Instead of utilising expensive mass flow meters the calibration procedure is based on the idea of measuring the rate of change of pressure in a known volume while charging and discharging. The dynamic parameters of the pneumatic actuator model are obtained by means of least-square and genetic algorithm (GA) identification routines.

To illustrate the successful modelling of the highly non-linear dynamic behaviour of the pneumatic servo actuation system a comparison between simulation and experimental step response results will be presented to conclude this chapter. The excellent agreement between simulation and experiment allows the use of the pneumatic simulation models as a tool for controller design and testing.

4.1 BASIC ELEMENTS OF PNEUMATIC COMPONENT MODELS

Apart from the dynamics of the actuator piston the dynamic behaviour of pneumatic servo systems is governed by two main physical processes:

- charging and discharging of a control volume and
- compressible gas flow through an orifice.

In the mathematical model of the servo mechanism these processes are represented by capacitive and restrictive elements respectively. Both processes also include heat exchange phenomena.

4.1.1 CAPACITIVE ELEMENT

4.1.1.1 Charging and Discharging of a Control Volume

Considering an infinitely small volume of gas with fixed boundaries as shown in Figure 4.1 across which mass and energy transfer may occur, the change in energy in the gas volume equates the net energy input through air flow, heat exchange and work:

$$\dot{E} = \sum \dot{m}_{in} h_{in}^{'} - \sum \dot{m}_{out} h_{out}^{'} + \dot{H}_{in} - \dot{W}_{out} \tag{4.1}$$

In order to obtain the expressions of $\dot{E}$ and h' in terms of gas properties the thermodynamic definitions and laws are to be used. The procedure is fully described by Harris (1990) and leads to the following expressions:

$$h' = u + \frac{P}{\rho} + \frac{v^2}{\rho} + gz = C_P T + \frac{v^2}{2} + gz \tag{4.2}$$

$$\dot{E} = \frac{d}{dt}(C_V \rho V T) \tag{4.3}$$

For pneumatic systems it is reasonable to expect the kinetic and potential energy terms to be small. These terms are certainly negligible when compared to the specific enthalpy and specific internal energy terms (Lo and Tilley (1993)). The change in kinetic or potential energy between inflow and outflow will be even less significant (except for nozzles and diffusers which have a large difference between the inlet and outlet flow areas). For pneumatic systems, the work done on or by the gas is considered to be related to the change of gas volume:

$$\dot{W}_{out} = P\dot{V} \tag{4.4}$$

where negative $\dot{V}$ represents the decrease of gas volume and therefore, work is done on the gas. Using the ideal gas law:

$$\frac{P}{\rho} = RT \tag{4.5}$$

gives:

$$\begin{aligned} C_P\left(\sum \dot{m}_{in} T_{in} - \sum \dot{m}_{out} T_{out}\right) - PV + \dot{H}_{in} &= \frac{C_V}{R}\frac{d}{dt}(PV) \\ &= \frac{C_V}{R}\left(\dot{P}V + P\dot{V}\right) \end{aligned} \tag{4.6}$$

The rate of heat transfer $\dot{H}_{in}$ can be represented by the general expression:

$$\dot{H}_{in} = \alpha A\left(T_{sur} - T\right) \tag{4.7}$$

α represents the overall heat transfer coefficient between the gas and the surroundings taking into account convection, conduction and radiation. This linearised approximation is considered reasonable over the relatively limited temperature range of pneumatic actuation systems.

Differentiating the equation of state given by the ideal gas law (Equation (4.5)) the rate of change of pressure is:

$$\dot{P} = \frac{RT}{V}\dot{m} - \frac{P}{V}\dot{V} + \frac{mR}{V}\dot{T} \tag{4.8}$$

Using the relationships of gas properties:

$$C_P - C_V = R \quad \text{and} \quad \gamma = \frac{C_P}{C_V} \tag{4.9}$$

Equation (4.8) can be written as:

$$\dot{P} = \frac{\gamma}{V}\left[R\left(\Sigma \dot{m}_{in}T_{in} - \Sigma \dot{m}_{out}T_{out}\right) - P\dot{V} + \frac{(\gamma - 1)}{\gamma}UA\left(T_{sur} - T\right)\right] \tag{4.10}$$

Since the heat transfer is strongly dependent on the geometry of the area over which the heat transfer occurs and also on the flow conditions of the gas (laminar or turbulent) the analysis is very complicated and experimental data are often desirable (Scholz (1990)). Hence, the determination of pressure variation related to the heat transfer may be regarded as being approximately polytropic in form (Rogers and Mayhew (1973), Andersen (1985)):

$$P\left(\frac{1}{\rho}\right)^n = const \tag{4.11}$$

It follows that:

$$\dot{P} = \frac{n}{V}\left[R\left(\dot{m}_{in}T_{in} - \Sigma \dot{m}_{out}T_{out}\right) - P\dot{V}\right] \tag{4.12}$$

It is generally assumed that n lies between 1 (isothermal process) and γ (adiabatic process). For slow movement of gas, heat may transfer through the boundary maintaining a constant gas temperature inside the volume resulting in a thermodynamic equilibrium and a polytropic index n equal to 1 (isothermal). For

rapid change or a well insulated pneumatic component, little heat is assumed to flow into or out of the control volume and n will be equal to γ(adiabatic).

Assuming that no gas flows out of the control volume the mass flow going into the control volume can be expressed as:

$$\dot{m}_{in} = \frac{1}{RT_{in}}\left(P\dot{V} + \frac{1}{n}V\dot{P}\right) \tag{4.13}$$

Note, that for pneumatic systems the mass flow rate is determined and not the volumetric flow rate as for hydraulic systems. It can be seen in Equation (4.13) that the mass flow causes a change in volume and a change in pressure. The ratio of these two changes is quantified by the polytropic index n.

4.1.1.2 Temperature Changes in Control Volume

Once the rate of change of pressure has been determined, the rate of change of gas temperature inside the gas volume can be obtained by rearranging Equation (4.8) into the following form:

$$\dot{T} = \frac{T}{PV}\left(P\dot{V} + V\dot{P} - \dot{m}RT\right) \tag{4.14}$$

Note, that $\dot{m}$ is the net mass flow rate in the gas volume ($= \sum \dot{m}_{in} - \sum \dot{m}_{out}$).

The theoretical analysis described above is based on the assumption of an infinitely small gas volume with uniform pressure and temperature throughout the volume. The extension of the results to a volume with realistic dimensions is called *lumped parameter*-approach.

Summarising, when deriving the capacity model the following assumptions were made:

- The change in condition of the gas is polytropic in form.
- Air behaves like an ideal gas (γ= 1.4).
- Pressure and temperature are constant throughout the volume.
- Potential and kinetic energy of the gas flow are negligible.

4.1.2 RESTRICTIVE ELEMENT

4.1.2.1 Gas Flow through an Orifice

Restrictive elements as depicted in Figure 4.2 are those components requiring a sizeable local pressure drop to cause gas to flow. Fixed restrictions which have constant flow area are usually called *orifices*. Variable restrictions which have variable flow areas are called *valves*. Neglecting heat transfer and assuming that no work crosses the boundary the flow through an orifice can be fairly accurately predicted by (Backé (1986), McCloy and Martin (1980)):

$$\dot{m} = C_d C_m A_v \frac{P_u}{\sqrt{T_u}} \tag{4.15}$$

The value of the mass flow coefficient C_m depends upon whether the flow is sonic or subsonic. The flow is subsonic, if:

$$P_r = \frac{P_d}{P_u} \geq \left(\frac{2}{\gamma - 1}\right)^{\frac{\gamma}{\gamma-1}} \quad (= 0.528 \quad \text{for air}) \tag{4.16}$$

and the flow coefficient C_m is given by (see Figure 4.3):

$$C_m = \sqrt{\frac{2\gamma}{R(\gamma - 1)}\left[(P_r)^{2/\gamma} - (P_r)^{(\gamma+1)/\gamma}\right]} \tag{4.17}$$

Note, that the pressure ratio P_r is defined as the ratio of downstream static pressure P_d in the minimum cross section flow area (*vena contracta*) to upstream stagnation pressure P_u.

Otherwise, if $P_r < 0.528$ the flow is sonic and said to be *choked*. In this case C_m can be calculated as:

$$C_m = \left(\frac{2}{\gamma + 1}\right)^{\frac{1}{\gamma-1}} \sqrt{\frac{2\gamma}{R(\gamma + 1)}} \quad (= 0.0404 \quad \text{for air}) \tag{4.18}$$

For the choked condition C_m has reached its maximum and is now only dependent on the upstream temperature T_u (Backé (1986)). When the flow is choked the fluid is moving at the speed of sound through the vena contracta of the flow path. Assuming a constant upstream pressure (charging with constant supply pressure) a further reduction in the downstream pressure will not result in a higher mass flow rate as can be seen in Figure 4.4a. The reduction in pressure will not propagate back to the

nozzle since pressure waves travel with the speed of sound. When assuming a constant downstream pressure (exhaustion to atmosphere) the relation between upstream pressure and mass flow rate becomes linear after a small initial curved portion as can be seen in Figure 4.4b.

It has to be mentioned that a super sonic flow speed can be achieved by gradually increasing the flow area behind the smallest cross section and expanding the gas adiabatically. In this case C_m can be calculated using Equation (4.17) for the whole pressure range. This means the flow coefficient drops again after reaching the maximum at $P_r = 0.528$ for air (see grey line in Figure 4.3). Although the flow velocity now becomes super sonic as pressure ratio P_r drops below the critical pressure ratio the mass flow decreases because the density of the gas decreases more than the velocity increases.

Nevertheless, the mass flow rate can only be calculated as shown above (Equation (4.15)) provided that the upstream total pressure P_u, upstream total temperature T_u and static pressure in the vena contracta P_d are known and the velocities across these sections are constant. In the usual situation, however, none of these provisions is satisfied. The discharge coefficient C_d is introduced as a correction factor mainly to take account of the jet contraction. As mentioned above, this contraction results in an effective flow area (vena contracta) which is smaller than the orifice area A_v (see Equation (4.15)). Also reduction in mass flow due to friction and heat losses and velocity profile effects are included in the discharge coefficient. Andersen (1985) reported on the following range of values for C_d:

- nozzles 0.95
- squared edged orifices 0.82
- sharp edged orifices 0.61 to 0.84
- poppets: conical 0.72 to 0.87
  spherical 0.75 to 0.88

He recommends calibration tests for any *unusual* configurations or mountings. If this is impractical, the square edged orifice value of 0.82 is considered within +/- 10% for nearly all types of restrictions. It should be noted that in recent studies Ye *et al* (1992) used a value of 0.68 for a poppet type valve, whereas Lai *et al* (1990) used a value of 0.95 for a dissimilar poppet type valve. Thus, it appears that calibration tests

are in order regardless of the configuration being used. Furthermore, Grace and Lapple (1951) published results (see Figure 4.5a) which indicate a drop off in C_d for subsonic flow through a square edged orifice (pressure ratios above the critical pressure ratio of 0.528). Perry (1949) also reported a drop off in C_d with increasing pressure ratios for gas flow through a sharp edged orifice. This results can be seen in Figure 4.5b. The decrease in C_d with increasing pressure ratio P_r implies a decreasing throat area (vena contracta). Moreover, Stenning (1955) found by investigating 'two-dimensional' gas flow through spool valve orifices that the discharge coefficient was greater for reattached flow than for jet flow. Also, for pressure ratios near unity the flow will be laminar which results in a further reduction of C_d. Nevertheless, when gas is flowing through an orifice the Reynolds number due to the low kinematic viscosity is in general sufficiently high to neglect this Reynolds number effect (McCloy and Martin (1980)).

As will be shown in Section 4.3.1, all of the effects described above have a measurable influence on the flow characteristics of a pneumatic valve and hence have to be considered when modelling its dynamic behaviour.

4.1.2.2 Thermodynamic Behaviour of Gas Flow through an Orifice

The analysis of the thermodynamic behaviour of gas flow through an orifice and valve can be carried out using the steady-state energy balance equation. For a given streamline the energy equation is expressed as:

$$C_P T + \frac{v^2}{2} = const \tag{4.19}$$

This is the form of equation for steady adiabatic gas flow in which the gas neither does work on its surrounding nor has work done on itself. In the case of flow through an orifice or valve, the heat transfer across the boundary can be neglected as the surface area over which the heat transfer might occur is very small. Since in general the inlet and outlet chambers are large in comparison to the flow area (i.e. $v_u \approx v_d << v_f$) the kinetic energy in these chambers can be neglected. The energy equation can now be written as:

$$C_P T_u = C_P T_f + \frac{v_f^2}{2} = C_P T_d \tag{4.20}$$

Hence, for a flow of gas passed through an orifice or valve, the outflow gas temperature T_d is assumed to be equal to the inflow gas temperature T_u as the recovery of the gas temperature occurs while the temperature in the vena contracta T_f can be significantly lower. As a matter of fact, it was found in various applications that the decrease of temperature in the vena contracta can cause valves to freeze if the air used in the system is humid (Lo (1995)).

If an attempt is made to determine the gas temperature T_f at the flow area, the isentropic relationship (Backé (1986)) can be used. Subsonic flow yields:

$$T_f = T_u \left(\frac{P_d}{P_u} \right)^{\frac{\gamma-1}{\gamma}} \tag{4.21}$$

Sonic flow gives:

$$T_f = T_u \frac{2}{\gamma+1} \tag{4.22}$$

Summarising, when deriving the restriction model the following assumptions were made:

- No heat is exchanged with the surroundings due to a small surface area.
- The upstream stagnation pressure and stagnation temperature are known.
- The static pressure in the vena contracta is known.
- The velocity is constant across the cross sections where the pressures are determined.
- No work is done by the gas nor is done on the gas.
- Air behaves like an ideal gas (γ= 1.4).
- Kinetic energy in the inlet and outlet chambers can be neglected.

4.2 PNEUMATIC COMPONENT MODELS

In order to simulate the dynamic behaviour of the pneumatic actuation system two component models have been developed within the Bath*fp* simulation environment described briefly in Appendix A1: a model of linear pneumatic actuator and servo control valve model. The dynamic influence of the connecting pipes has been incorporated into these two models: the capacity effect of the pipes has been

considered by adding the pipe volume to the actuator chamber volume and the restriction effect has been incorporated into the valve restriction by means of calibrating the discharge coefficient C_d.

4.2.1 LINEAR PNEUMATIC ACTUATOR

Linear actuators are used to convert gas pressure or flow into force or motion of the piston. The motion of the piston is obtained by taking into account the forces acting on the piston as shown in Figure 4.6. These are:

- net pressure force ($P_a A_a - P_b A_b$)
- weight of the piston and mass to be moved ($mg \sin \varphi$)
- viscous friction force ($c_f \dot{x}$)
- Coulomb friction force ($F_C \ \mathrm{sgn}(\dot{x})$)
- spring compression force ($k(x - x_{max})$)
- external disturbance force (F_{ext})

Using Newton's law the equation of motion of the cylinder piston is given by:

$$m\ddot{x} = A_a P_a - A_b P_b - mg \sin\varphi - c_f \dot{x} - F_C \ \mathrm{sgn}(\dot{x}) - k(x - x_{max}) - F_{ext} \qquad (4.23)$$

It is assumed that the spring is fully extended for a fully extended actuator. Furthermore, it has to be noted that the net force acting on the piston has to exceed the stiction force F_{Cs} before the piston can move. Neglecting Coulomb friction and external forces and differentiating Equation (4.23) gives:

$$m\dddot{x} + c_f \ddot{x} + k\dot{x} = A_a \dot{P}_a - A_b \dot{P}_b \qquad (4.24)$$

Substituting Equation (4.12) for $\dot{P}_a$ and $\dot{P}_b$ results in:

$$\begin{aligned} m\dddot{x} + c_f \ddot{x} + k\dot{x} = {} & n\frac{A_a}{V_a}\left[R(\dot{m}_{as} T_s - \dot{m}_{ae} T_a) - P_a \dot{V}_a\right] \\ & -n\frac{A_b}{V_b}\left[R(\dot{m}_{bs} T_s - \dot{m}_{be} T_b) - P_b \dot{V}_b\right] \end{aligned} \qquad (4.25)$$

Tl $V_a = A_a \dot{x} + \dot{V}_{min}$ and $V_b = A_b(l - x) + V_{min}$

Hence, the rate of change of volumes is: (4.26)

Hence, the rate of change of volumes is:

$$\dot{V}_a = A_a\dot{x} \quad \text{and} \quad \dot{V}_b = -A_b\dot{x} \tag{4.27}$$

Inserting Equation (4.27) into Equation (4.25) yields:

$$\begin{aligned} m\ddot{x} + c_f\ddot{x} + \left[k + n\left(\frac{P_a A_a^2}{V_a} + \frac{P_b A_b^2}{V_b}\right)\right]\dot{x} &= n\frac{A_a}{V_a}\left[R(\dot{m}_{as}T_s - \dot{m}_{ae}T_a)\right] \\ &\quad -n\frac{A_b}{V_b}\left[R(\dot{m}_{bs}T_s - \dot{m}_{be}T_b)\right] \end{aligned} \tag{4.28}$$

For ease of analysis it is now assumed that $T_a = T_b = T_s = T$ and that no external spring is attached to the actuator ($k = 0$). Considering a piston motion in the positive x-direction (extension of actuator piston) that means chamber A is charged while chamber B is discharged ($\dot{m}_{ae} = 0, \dot{m}_{bs} = 0$) yields:

$$m\ddot{x} + c_f\ddot{x} + \left[n\left(\frac{P_a A_a^2}{V_a} + \frac{P_b A_b^2}{V_b}\right)\right]\dot{x} = nRT\left[\frac{A_a\dot{m}_{as}}{V_a} + \frac{A_b\dot{m}_{be}}{V_b}\right] \tag{4.29}$$

For motion in the negative x-direction (retraction of actuator piston) the differential equation of the system dynamics is:

$$m\ddot{x} + c_f\ddot{x} + \left[n\left(\frac{P_a A_a^2}{V_a} + \frac{P_b A_b^2}{V_b}\right)\right]\dot{x} = -nRT\left[\frac{A_a\dot{m}_{ae}}{V_a} + \frac{A_b\dot{m}_{bs}}{V_b}\right] \tag{4.30}$$

These differential equations are of third order with coefficients depending on displacement x, chamber pressures P_a and P_b and temperature T. The system is excited by the mass flow rates $\dot{m}_a$ and $\dot{m}_b$ being the external inputs.

4.2.2 Pneumatic Servo Valve

The valve model consists of two distinct operations. Firstly, the spool motion is carried out by various forces acting on it. The spool opens and closes the gas flow area and hence increases and decreases the gas flow rate. Secondly, due to a pressure drop across the valve air flows through the valve opening.

The mass flow rate through the opening of the valve is determined using a similar approach to that for the orifice described above (Equation (4.15)) where the effective flow area is related to the spool displacement x_v and the maximum flow area A_v:

$$\dot{m} = C_d C_m A_v \frac{P_u}{\sqrt{T_u}} x_v \tag{4.31}$$

The spool motion is modelled using a second-order transfer function between the applied voltage u and the spool displacement x_v:

$$m_s \ddot{x}_v + c_s \dot{x}_v + k_s x_v = u \tag{4.32}$$

In general, in order to simplify the analysis it is possible to neglect the spool dynamics since for pneumatic systems the natural frequency of the valve is usually more than a magnitude higher than the natural frequency of the pneumatic actuation system. The equation relating the gas mass flow rate to the input voltage would hence be:

$$\dot{m} = C_d C_m A_v \frac{P_u}{\sqrt{T_u}} k_v u \tag{4.33}$$

Yet, within this investigation the natural frequency of the valve spool is taken into account in the simulation model as its influence on the closed-loop system dynamics in sliding mode control is of major importance as will be demonstrated in Chapter 8.

Leakage is not included in the valve model although it has been measured in a similar manner to the mass flow rate through the valve as described in Section 3.3.1. It was found that the leakage coefficients vary with valve opening and pressure difference across the valve and between the actuator chambers as can be seen in Table 3.4. Since the leakage flow rates are almost negligible though and mainly result in steady-state errors which are of no concern in the context of the research work presented it has been decided not to include an additional leakage model into the valve model.

4.3 VALIDATION OF PNEUMATIC SERVO MODEL

In order to use the previously presented component models for simulating the dynamic behaviour of the pneumatic actuation system, each model had to be validated and calibrated. An initial simulation study revealed that the simulation results are most sensitive to the flow characteristics of the pneumatic control valve. Therefore, most effort has been spent on calibrating in particular this component

model. The calibration of the models of the pneumatic actuator and the connecting pipes was found to be fairly straight forward.

4.3.1 VALIDATION OF VALVE MODEL

As described in Section 3.1.1.2, the valve to be modelled in this investigation is the 4 port servo valve HR Textron 27A1. From the rated mass flow the nominal discharge coefficient can be determined to be $C_d = 0.8$ for a pressure ratio of $P_r = 0.15$. This compares well with values given by other researchers as listed in Section 3.1.2. Nevertheless, as will be demonstrated by the results presented in this chapter the discharge coefficient is strongly dependent on the pressure ratio and the geometry of the orifice. To determine the discharge coefficient as a function of pressure ratio P_r and input voltage (valve opening) the steady-state mass flow rate was measured at 10 different spool displacements across the spool stroke for all four flow paths: supply to port A (S-A), supply to port B (S-B), port A to return (A-R) and port B to return (B-R).

In order to avoid the use of expensive mass flow meters the mass flow rate through the control valve was determined indirectly by measuring the rate of change of pressure in a dead volume of known size. The experimental set-up used can be seen in Figure 4.7. This indirect way of measuring the mass flow proved to be advantageous in many respects. For instance, using this method it was possible to measure the mass flow for a fixed input voltage (valve opening) and a varying pressure ratio P_r (due to the build-up of downstream pressure P_d for charging and the decrease of upstream pressure P_u for discharging). Using Equation (4.12) the mass flow rate can be derived from the measured rate of change of pressure:

$$\dot{m} = \frac{\dot{P}_{meas} V}{n R T_u} = C_d C_m A_v \frac{P_u}{\sqrt{T_u}} \tag{4.34}$$

The problem is that the polytropic index n for the change in condition in the dead volume is unknown and there are no precise guidelines available on how to choose its value. Nevertheless, in the course of the research work presented here this was found to be an irrelevant problem. A simulation study done by Lo and Tilley (1993) showed that although the polytropic index n has a significant influence on the simulated temperature, the influence on the actuator chamber pressures is much

smaller and the influence on actuator piston displacement is almost negligible. Since actuator piston displacement is the most important entity in the context of position controller design (without pressure feedback) the choice of the polytropic index appears to be mainly of academic interest as long as the discharge coefficient C_d is calibrated under the assumption of the chosen fixed numerical value.

As explained in Section 4.1.1 in general it is assumed that n lies between 1 (isothermal change in condition) and 1.4 (adiabatic change in condition). In the following n is set to 1.4 (adiabatic flow). This assumption is based on the idea that the charging and discharging of the dead volume is so rapid that no heat exchange with the surrounding can occur. For large valve openings where the charging time is less than 1 s it seems to be a reasonable assumption. Yet, for smaller valve openings of for example 2% of the full spool stroke the charging time can increase to more than 3 minutes. In this case, the change in condition in the dead volume is closer to being isothermal than to being adiabatic. Therefore, assuming a polytropic index of 1.4 (adiabatic) results in the fact that the mass flow through the valve predicted from the rate of change of pressure in the dead volume is assumed to be lower than it is in reality. As a consequence, for small valve openings the discharge coefficient C_d is predicted to be lower than its real value by a factor of up to 70%. Yet, using the above approach and calibrating C_d accordingly it is not necessary to determine the polytropic index n for the actuator model as a function of e.g. process time. Therefore, by calibrating the valve model assuming a constant polytropic index n the same index can be used for all component models in the simulation routine. The variations in n are in this case taken into account by means of the variations in the calibrated discharge coefficient C_d.

As a results of the chosen calibration method, one has to be aware of the fact that although the simulated system displacement results agree well with experiment only for fast changes in condition all simulated variables are modelled physically correct while for slower changes in condition temperatures and pressures might deviate from measured values.

If it is of interest to exactly measure the mass flow rate through the valve by means of charging or discharging a dead volume without using a mass flow meter the technique above can be slightly modified. In a recent publication Kawashima *et al*

(1997) describe the use of approximately isothermal chambers which were filled with steel wool. The use of these chambers justified the assumption of isothermal changes of condition. Hence, the polytropic index n can be set to unity.

When determining the mass flow through the valve as described above it was found that the maximum flow areas were different for each flow path and also up to 8% different to the value given by the manufacturer. Furthermore, it was found that the return port areas were smaller than the supply port areas. The results can be seen in Table 4.1. Also, despite the fact that the input voltage-flow area characteristic depicted in Figure 3.4 is linearised by means of a linearisation circuit on the valve control card, the actual characteristic was found to be far from being linear. Especially for valve openings of less than 20%, the valve's steady-state characteristics become significantly non-linear. The deviation from the linear behaviour can become up to 70% in the worst case. It is suspected that the overlap compensation circuit on the valve control module and a change in flow path are the reason for this observed behaviour. In the valve simulation model an additional position dependent spool displacement-flow area gain for all four flow paths as depicted in Figure 4.8 had to be introduced to compensate for this non-linearity.

The numerical values of the discharge coefficient C_d resulting from the calibration procedure described above and used in the simulation model can be found in Tables 4.2 to 4.5. The valve model uses linear interpolation to predict the flow rates for the pressure and spool displacement regions not exactly measured. The resulting discharge coefficient-pressure ratio relationship can be seen in Figure 4.9.

The most important results from the valve calibration procedure are the following:

- The C_d value of 0.8 obtained by using the rated mass flow represents the flow condition fairly accurately for choked flow ($P_r < 0.528$) and large valve openings.
- For larger pressure ratios a drop off in C_d can be observed. This implies a decreasing throat flow area (vena contracta).
- In some cases a further drop-off in C_d occurs for very large pressure ratios near unity. This is due to a change from turbulent to laminar flow causing an increase in flow friction.

- For smaller valve openings an increase in C_d with pressure ratio after an initial drop off was found. This implies a reattachment of the flow jet to the walls of the orifice as described by Stenning (1995).
- For very small valve openings the discharge coefficient for the flow paths A-E and B-E decreases significantly already at relatively small pressure ratios. This can be explained by the long discharging times and hence the occurrence of heat exchange with the surrounding.
- For the flow path B-E the discharge coefficient decreases to 0 for an input voltage of 2% of the maximum voltage. Although a pressure drop exists across the valve orifice no gas flow can be observed. This effect is not due to spool movement in the valve since the valve spool position remains constant throughout the discharging.

It can be derived from the experimental results that also the choking point varies from P_r = 0.49 to 0.33 depending on the valve opening. Since air chokes theoretically for P_r = 0.528 the different choking point is reflected in a further drop in C_d in the model. The choking at pressure ratios less than the critical pressure ratio is caused by the fact that air does not behave like an ideal gas (McCloy and Martin (1980)) which is assumed in the theoretical derivation of the mass flow in Section 4.1.2. Furthermore, the choking point seems to be dependent on the orifice geometry. Due to the length of the flow path through the orifice the flow can theoretically choke at varying points along the path. This affects the pressures measured outside the valve. Hence the measured pressures can be closer to or further away from the pressures theoretically assumed. It follows, that the prediction of the choking point can be more or less accurate depending on the geometry.

Altogether, the above results highlight again the importance of calibration tests as suggested by Andersen (1985).

As mentioned already in Section 3.1.1.2, by means of frequency response tests the natural frequency of the valve spool for maximum valve opening was determined to be about 200 Hz. This corresponds to the natural frequency given by the manufacturer for a valve opening of 2.5% (see Figure 3.5).

4.3.1.1 Comparison between Simulation and Experimental Charging and Discharging Results

A comparison of simulated and measured pressures in the measuring volumes for charging and discharging can be seen in Figures 4.10 to 4.13. In Figure 4.10 the results obtained with an uncalibrated simulation model using the nominal discharge coefficient of $C_d = 0.8$ are shown. It can be seen that the simulation results deviate significantly from the experimental ones. Using the calibrated valve model with a valve opening and pressure ratio dependent discharge coefficient yields a good agreement between simulation and experiment as can be seen in Figure 4.11. Obviously, the gas flow effects described above have a significant influence on the mass flow rate through the valve and calibration is of major importance in order to achieve good simulation results. Nevertheless, despite the fact that all the above described effects on the steady-state mass flow characteristic have been modelled there are still small observable differences between simulation and experiment. These differences are mainly due to the following factors:

- the influence of measuring errors and limited transducer accuracy on the experimental data
- the measurable flow area deadband of 0.03V (0.6% of maximum input voltage)
- manufacturing accuracy of the valve

In particular, when discharging the measuring volumes slight discrepancies between simulation and experiment are visible. This can be explained by the influence of the linearisation circuit of the valve control card described in Section 3.1.1.2: for small valve openings the linearisation circuit opens the charging port overproportionally in order to successfully linearise the charging side as the experimental results imply. Yet, this also results in an overproportional reduction in flow area on the discharging side and hence an overproportional reduction in the discharging air flow. A further effect which reduces the gas flow near the spool centre position and which has not been modelled is a deadband of about 0.6% of the maximum voltage of 5 V.

The effects of the manufacturing tolerance of the valve are illustrated in Figure 4.12. The simulation results are compared to experimental results taken with a

different valve of the same make. Differences between simulation and experiment are up to about 0.2 bar.

Even when using a calibrated valve simulation model one has to be aware of the sensitivity of the gas flow to changes in the environmental conditions as depicted in Figures 4.13. Here, the simulation results are compared to experimental results obtained on a different day than the ones used to calibrate the valve model. As can be seen, slight changes in the air temperature and pressure of the surroundings have a visible influence on the flow rate through the valve.

4.3.2 VALIDATION OF ACTUATOR AND LOAD MODEL

Having calibrated the valve model as described in the previous chapter the last step of synthesising the pneumatic servo simulation model is to validate the actuator and the load model. The main parameters of the pneumatic actuator and load that had to be identified were:

- effective mass to be moved m
- viscous friction coefficient c_f
- dynamic Coulomb force F_{Cd} and stiction force F_{Cs}
- actuator geometry

The geometric sizes of the actuator and connecting pipes were derived from data provided by the manufacturer. It should be mentioned again that the capacitive effects of the pipes were taken into account by adding their volume to the actuator chamber volumes. The accuracy of these parameters proved to be sufficient for this analysis. Therefore, only parameters remained to be identified which relate the net pressure force to the motion of the actuator piston. The relationship of all of these parameters is described in the force balance Equation (4.23).

One way of identifying the required parameters from experimentally measured data is to use the least-square method. Since this is in general the simplest method to be used it has been chosen for this investigation. Other methods to identify the dynamic system parameters are based on for example neural network approaches or genetic algorithm (GA) search engines. In the following these alternative methods

are also presented briefly and their advantages and disadvantages are discussed. Moreover, due to the importance of gaining a precise knowledge of the required system parameters the results obtained with the least-square method are compared with the results from the GA parameter search.

Having determined the numerical values of the required system parameters these parameters are then used in simulation and experimental and simulation results are compared.

4.3.2.1 Least-Square Method for Parameter Identification

In this section, the least-square approach to parameter identification is presented, its limitations are discussed and it is applied to the specific identification problem. The algorithm is tested and validated using simulation data obtained by means of the developed non-linear simulation model described in Section 3.2. The algorithm is then used to determine the required system parameters mass m, viscous friction coefficient c_f and dynamic Coulomb friction force F_{Cd} of the single-axis test rig.

The stiction force F_{Cs} is neglected in this investigation although usually when investigating pneumatic systems, stiction is a serious problem which strongly effects the dynamic behaviour of these systems and also their controllability. In this context, the so-called stick-slip effect is often mentioned (see for instance Abou-Fayssal and Surgenor (1997)). Nevertheless, stiction proved to be of minor importance in this investigation due to the low friction properties of the actuators used and the fact that most joints on the animated figure were fitted with low friction roller bearings.

Using the same notation used by Lin and Kortüm (1992) and following their train of thoughts the dynamics of a mechanical system with non-linear components can always be written in the following form:

$$M\ddot{x}(t)+C\dot{x}(t)+Kx(t)+r\left(x,\dot{x},p^N\right)=u(t) \tag{4.35}$$

or in component notation:

$$\sum_{j=1}^{n} m_{ij}\ddot{x}_j(t)+\sum_{j=1}^{n} c_{ij}\dot{x}_j(t)+\sum_{j=1}^{n} k_{ij}x_j(t)+r_i\left(x,\dot{x},p^N\right)=u_i(t)\,,\quad i=1,2,\ldots,n \tag{4.36}$$

where $x(t)$ represents the system's state, $u(t)$ is the external excitation force vector and $\boldsymbol{M}$, $\boldsymbol{C}$ and $\boldsymbol{K}$ represent the linear part of the system dynamics that is the inertia, viscous friction and compliance. The last term on the left-hand side of Equation (4.36) is the vector containing all non-linear elements with respect to the measured system variables. As mentioned before, to identify the vector of unknown parameters p^N using the least-square method it is necessary that the non-linear elements of the system equation are *linear in the parameters* that means:

$$r_i\left(x,\dot{x},p^N\right)=\boldsymbol{p}_i{}^{N^T}g_i(x,\dot{x}) \tag{4.37}$$

where:

$$\boldsymbol{p}_i{}^{N^T}=\left[p_{i1}^N\ldots p_{ii_n}^N\right] \tag{4.38}$$

$$g_i^T(x,\dot{x})=\left[g_{i1}(x,\dot{x})\ldots g_{ii_n}(x,\dot{x})\right] \tag{4.39}$$

Assuming that piston displacement, velocity and acceleration and also the actuator chamber pressures can be measured or determined otherwise it can be seen that Equation (4.23) is *linear in the parameters* mass, viscous friction and Coulomb friction to be identified despite the fact that Coulomb friction is a non-linear term in the force balance. As a result, the chosen least-square approach is valid.

Since discrete experimental data is to be processed Equation (4.36) has to be converted into its discrete form. Furthermore, due to the fact that in this investigation only displacement is measured at a constant discrete time interval $h=t_q-t_{q-1}$ the following approximations are used for $\dot{x}^q$ and $\ddot{x}^q$:

$$\dot{x}^q=\frac{x^{q+1}-x^{q-1}}{2h},\quad \ddot{x}^q=\frac{x^{q+1}-2x^q+x^{q-1}}{h^2} \tag{4.40}$$

Please note, that these centre differencing schemes do not introduce an additional phase shift into the differentiated signals.

Error cost functions can be defined as follows:

$$\varphi_i=\sum_{q=1}^{N-1}\left(\Delta_i^q\right)^2;\quad (i=1,2,3) \tag{4.41}$$

with:

$$\Delta_i^q = m\left(x^{q+1} - 2x^q + x^{q-1}\right) + c_f \frac{h}{2}\left(x^{q+1} - x^{q-1}\right) + F_{cd} h^2 \operatorname{sgn}\left(\frac{x^{q+1} - x^{q-1}}{2}\right) - h^2\left(A_a P_a - A_b P_b\right) \tag{4.42}$$

Minimising these error cost functions yields the parameters to be identified $\hat{p}_i$:

$$\frac{\partial \varphi_i}{\partial p_i} = 0 \quad \Rightarrow \quad \hat{p}_i \tag{4.43}$$

As a result the following linear equation system is obtained:

$$\begin{pmatrix} \hat{p}_1 \\ \hat{p}_2 \\ \hat{p}_3 \end{pmatrix} = \begin{pmatrix} m \\ c_f \\ F_{Cd} \end{pmatrix} = \begin{pmatrix} A_{11} & A_{12} & A_{13} \\ A_{21} & A_{22} & A_{23} \\ A_{31} & A_{32} & A_{33} \end{pmatrix}^{-1} h^2 u_1^q \begin{pmatrix} \sum_{q=1}^{N-1}\left(x^{q+1} - 2x^q + x^{q-1}\right) \\ \sum_{q=1}^{N-1}\left(x^{q+1} - x^{q-1}\right) \\ \sum_{q=1}^{N-1}\operatorname{sgn}\left(x^{q+1} - x^{q-1}\right) \end{pmatrix} \tag{4.44}$$

with:

$$A_{11} = 2\sum_{q=1}^{N-1}\left(x^{q+1} - 2x^q + x^{q-1}\right)^2 \tag{4.45}$$

$$A_{12} = \frac{h}{2}\sum_{q=1}^{N-1}\left(x^{q+1} - x^{q-1}\right)\left(x^{q+1} - 2x^q + x^{q-1}\right) \tag{4.46}$$

$$A_{13} = h^2\sum_{q=1}^{N-1}\left(x^{q+1} - 2x^q + x^{q-1}\right)\operatorname{sgn}\left(x^{q+1} - x^{q-1}\right) \tag{4.47}$$

$$A_{22} = \frac{h^2}{4}\sum_{q=1}^{N-1}\left(x^{q+1} - x^{q-1}\right)^2 \tag{4.48}$$

$$A_{23} = \frac{h^3}{2}\sum_{q=1}^{N-1}\left(x^{q+1} - x^{q-1}\right)\operatorname{sgn}\left(x^{q+1} - x^{q-1}\right) \tag{4.49}$$

$$A_{33} = h^4\sum_{q=1}^{N-1} 1 \tag{4.50}$$

$$A_{ij} = A_{ji} \tag{4.51}$$

Using the above algorithm on data synthesised by means of the non-linear simulation model with known parameters and additional noise it was found that the following four measures were able to improve the identification results significantly:

- Filtering of the measured system data
- Introducing a velocity deadband
- Scaling of the force terms in the force balance Equation (4.23)
- Iterative identification of the individual terms

Filtering of the measured data was important to minimise the effects of noise in the measured signals on the identification results. Especially, the Coulomb force term was found to be very sensitive to noise due to it being a function of the sign of the differentiated displacement (see Equation (4.23)). In this investigation a second-order Butterworth filter with a cut-off frequency of f_{cut} = 50 Hz was used for experimental data acquired with a sampling frequency of f_{samp} = 500 Hz. The filter was used on all measured signals although the measured pressure signals were of very low noise in comparison to the displacement signal. Yet, filtering all measured signals like this, all force terms in the force equation to be identified maintained their relative phase angles.

In order to further reduce the influence of noise on the identified Coulomb friction force and also to prevent stiction effects to influence the identification results a low velocity deadband of v_{dead} = 0.005 m/s around zero velocity as depicted in Figure 4.14 was used within which no identification was performed.

Scaling the force terms in order to obtain equal maxima during the identification process resulted in the identification algorithm being theoretically almost equally sensitive to variations in all force terms in Equation (4.23) therefore allowing for all parameters to be identified with the same accuracy.

Despite the scaling of the force terms it was found though, that mass m and viscous friction c_f could be determined with a greater consistency than Coulomb friction F_{Cd} due to the discontinuous sign function characteristic of Coulomb friction. Therefore, above identification algorithm was implemented as an iterative scheme. In other words, in a first instance all three parameters were identified from a given data set. It was found that usually the identification of mass was the most reliable. During the second iteration, mass was then assumed to be known using the identified value resulting in the viscous friction to be identified with greater accuracy. In the third

iteration, also viscous friction was set to its identified value and only Coulomb friction was identified.

Another important factor of influence on the identification results is the demand signal exciting the pneumatic servo mechanism. In a noise-free environment it can be seen from the linear Equations (4.23) that three linearly independent state vectors are needed in order to solve the system for three unknown parameters. In the presence of noise the measured signals have to be significantly richer in information in order to compensate for the disturbing influence of noise. It was therefore decided to excite the pneumatic servo system under closed-loop proportional feedback control with a sinusoidal demand signal sweeping through frequencies from 0.5 Hz to 20 Hz over a time period of 60s. Since it was suspected that the friction properties of the actuator piston are position and also direction of motion dependent, the system was demanded to perform small amplitude oscillations around three different piston positions: 2/5 (12 mm), 1/2 (15 mm) and 3/5 (18 mm) of the piston stroke. Furthermore, two identical but independent identification routines were performed per data set, one for each direction of motion.

As already mentioned, the proposed identification routine was first tried on simulation data produced using the non-linear simulation model to be validated. Since in this case the friction effects are independent of piston position and direction of motion the system was only excited round the mid stroke. The results in Figure 4.15 demonstrate the capability of the proposed algorithm to identify a mass of $m = 7$ kg, a viscous friction coefficient of $c_f = 100$ N/(m/s) and a Coulomb force of $F_{Cd} = 15$ N. It was found that in general only 500 points are needed to successfully obtain the correct results in the presence of a maximum noise level of 0.3% of the maximum measured signals. This was about the noise level of the displacement transducer used for this investigation (about 0.09 mm with a stroke of 30 mm).

Using the validated identification algorithm on experimental data obtained on the single-axis test rig resulted in the values for mass, viscous friction and Coulomb friction listed in Table 4.6. (As a comparison, when dismantling the test rig and weighing the effective mass to be moved it was determined to be $m = 1.82$ kg as opposed to the identified value of $m = 1.81$-1.84 kg.)

It should be mentioned that although it was found that the friction effects were piston position and direction of motion dependent it was not possible to obtain a consistent relationship between friction and these variables due to the fact that repeatability of the experiments was rather low and friction effects changed constantly from experiment to experiment. Therefore, only average values are reported here which are used for the simulation model. One interesting result is the low value of the dynamic Coulomb force of only F_{Cd} = 1-3 N.

4.3.2.2 Alternative Identification Methods

As discussed in the previous section, the least-square identification method requires the system model to be linear in the parameters to be identified. Since this is not always the case or not known a priori another way of identifying system parameters is to use inherently non-linear neural networks which can be trained with simulation data obtained using a simulation model of the system to be identified and known system parameters. This method is discussed and successfully applied in the context of fault analysis and condition monitoring of fluid power systems by Pollmeier (1997) and therefore not further detailed here.

It is also possible to employ genetic algorithms (GA's) in combination with non-linear dynamic simulation models for parameter identification. The genetic algorithm in this application is used to minimise the error between experimental and simulation results by altering the unknown system parameters in the simulation model. The optimal solution for this problem yields the desired values of the parameters to be identified.

Although both techniques are able to cope with highly non-linear identification problems, they require powerful computers to deal with the time consuming training or optimisation procedure. Also, a detailed dynamic model of the system to be investigated representing all concerning dynamic influences on the system's behaviour is essential.

Due to the fact that for this investigation a detailed system simulation model is available and also to validate the least-square method results, it was tried to

identify the unknown dynamic parameters by means of the GA technique. The identification procedure can be described as follows:

- A generation of *individuals* (sets of parameters to be identified) is generated by randomly varying the numerical values of the parameters to be identified (mass, viscous friction, dynamic Coulomb friction and stiction).
- A simulation run is performed with each individual.
- The fitness of each individual is determined by evaluating the following error cost function representing a quantitative measure for the difference in response between simulation and experiment:

$$E = \int_{t=0}^{T_{exp}} \left(x_{meas} - x_{sim}\right)^2 \tag{4.52}$$

- The error cost function is minimised by crossing and modifying the *genetic* information stored in the individuals according to the rules of procreation of the genetic algorithm.
- The fittest individual minimising the error cost function E provides the set of system parameters which results in the best agreement between simulation and experiment.

As can be seen in Table 4.7 the optimised system parameters are within the range identified by the least-square algorithm and hence confirm the results found by using least-square identification.

Due to the random nature of the observed friction effects no significant improvements in identifying friction could be achieved with this method using the constant parameter friction model:

$$F_{fric} = c_f \dot{x} + F_{Cd}\,\mathrm{sgn}(\dot{x}) \tag{4.53}$$

Yet, using GA's is was possible to find a numerical value of F_{Cs} = 1 N for the stiction force which has to be exceeded before the actuator piston starts moving and which was not identified using the least-square method. Since as mentioned before and as the identification results confirm stiction effects are of minor importance for this investigation and are hence neglected in the following.

It was observed during experimental testing that friction is strongly position and direction of motion dependent. Perhaps, it would have been possible to fit

simulation and experimental results more closely by introducing a position and direction of motion dependent friction model such as:

$$F_{fric} = \begin{cases} c_f^+(x)\dot{x} + F_{Cd}^+(x)\mathrm{sgn}(\dot{x}) & \text{for} \quad \dot{x} > 0 \\ c_f^-(x)\dot{x} + F_{Cd}^-(x)\mathrm{sgn}(\dot{x}) & \text{for} \quad \dot{x} < 0 \end{cases} \tag{4.54}$$

It was decided though, that the simple model was sufficient for the requirements of this research work.

4.3.3 Comparison of Simulated and Experimental Step Response Results

Having identified all unknown system parameters the last and most crucial step of the validation of the non-linear model is a comparison between experimental and simulation data. For this purpose, the dynamics of the single-axis test rig under proportional displacement feedback control were simulated. In Figures 4.16 and 4.17 the simulated and experimentally measured step responses for a proportional feedback gain of K_p = 1 are compared. In order to obtain a close match between both responses the parameters in Tables 4.7 and 4.8 were used in the simulation model. It can be seen that the simulation model predicts the displacement of the physical system very accurately. Figure 4.17 reveals that even small oscillations of the actuator piston when approaching the set-point are modelled precisely. As expected, the steady-state errors of the physical system are slightly larger than the errors of the simulation model since stiction and also leakage effects are not modelled. Furthermore, the simulated actuator chamber pressures differ slightly from the ones obtained experimentally. This is as well due to unmodelled stiction effects especially in the case of a retracting actuator piston and also the assumption of a constant polytropic index n as explained in Section 4.3.1.

Increasing the proportional feedback gain to K_p = 3.4 results in a more oscillatory system response depicted in Figures 4.18 and 4.19. In this case the physical system falls into a mode of sustained oscillation in the mid position. When validating a simulation model it is of great importance to consider this oscillatory behaviour and to model the system oscillations correctly in order to be able to use the simulation model as a controller design tool. Looking at Figure 4.18 the first

impression is that now the discrepancies between simulation and experiment have increased significantly. Yet, examining the responses in more detail (see Figure 4.19) reveals that the actuator piston extending motion is modelled very accurately. Only when retracting the piston the simulated system response is more oscillatory than the experimental one.

Concentrating first on the extending motion of the actuator piston it can be seen in Figure 4.19 that the first step response from mid position (15 mm) to $4/5^{th}$ of the stroke (24 mm) is modelled very precisely. Also the step response from $1/5^{th}$ of the stroke (6 mm) to mid position is modelled precisely at the beginning. Yet, after this initial agreement between simulation and experiment the experimental oscillation amplitude and frequency increases while the simulated amplitude and frequency remains constant. This increase in experimental amplitude and frequency can be explained by the fact that the sustained vertical oscillation of the actuator piston excites also a horizontal oscillation which could clearly be observed in experiment and is not modelled. Even the second step response from 15 mm to 24 mm being performed right after the mid position test which has been modelled precisely before without the horizontal disturbance oscillations is now showing differences between simulation and experiment due to the fact that the horizontal oscillations have not vanished completely.

When retracting the actuator piston now from 24 mm to 15 mm and from 15 mm to 6 mm the simulated response is slightly more oscillatory than the response obtained experimentally. This is due to changing friction properties. Increasing the viscous friction coefficient c_f to the maximum value of 109 N/(m/s) as identified by the least-square method (see Table 4.6) a close match can be achieved. In this case though the simulated step responses for extending the actuator piston are more damped than the experimental ones. Hence, it was decided to use the lower damping properties in order to concentrate on the dynamic case more difficult to control.

4.4 CLOSURE

To summarise, the non-linear pneumatic servo simulation model using the constant polytropic index approach to represent the changes of gas condition and a

constant coefficient friction model is able to precisely predict the dynamic behaviour of the pneumatic actuation system under investigation. The developed model is therefore an ideal tool for further investigating the dynamic behaviour of the pneumatic actuation system. Moreover, it provides an ideal environment for controller development and testing.

Another interesting fact that can be concluded from the results presented in this chapter is that the servo dynamics are position and also direction of motion dependent. This phenomenon will be discussed in more detail in Chapter 5 where the linearised model of the pneumatic servo is introduced and investigated.

TABLES

Table 4.1 - Maximum flow area of the flow paths of servo valve HR Textron DDV 27A1

flow path	maximum flow area
S - A	$0.870 * 10^{-6}$ mm^2
B - E	$0.810 * 10^{-6}$ mm^2
S - B	$0.870 * 10^{-6}$ mm^2
A - E	$0.795 * 10^{-6}$ mm^2

Table 4.2 - Discharge coefficient C_d as a function of pressure ratio P_r as used in the valve simulation model for flow path S-A

input voltage	C_{d0} / P_{r0}	C_{d1} / P_{r1}	C_{d2} / P_{r2}	C_{d3} / P_{r3}	C_{d4} / P_{r4}
5 V	0.80 / 0	0.80 / 0.25	0.75 / 0.60	0.65 / 0.90	0.60 / 1
4 V	0.80 / 0	0.80 / 0.20	0.75 / 0.53	0.66 / 0.73	0.61 / 1
3 V	0.80 / 0	0.80 / 0.20	0.74 / 0.53	0.60 / 0.90	0.57 / 1
2 V	0.82 / 0	0.82 / 0.20	0.78 / 0.30	0.65 / 0.90	0.50 / 1
1 V	0.83 / 0	0.83 / 0.15	0.76 / 0.28	0.64 / 0.90	0.40 / 1
0.8 V	0.80 / 0	0.80 / 0.25	0.80 / 0.30	0.65 / 0.95	0.30 / 1
0.6 V	0.80 / 0	0.80 / 0.20	0.75 / 0.53	0.62 / 0.90	0.40 / 1
0.4 V	0.80 / 0	0.80 / 0.20	0.78 / 0.45	0.61 / 0.90	0.35 / 1
0.2 V	0.80 / 0	0.80 / 0.20	0.78 / 0.50	0.52 / 0.85	0.20 / 1
0.1 V	0.80 / 0	0.80 / 0.20	0.72 / 0.50	0.40 / 0.80	0.00 / 1

Table 4.3 - Discharge coefficient C_d as a function of pressure ratio P_r as used in the valve simulation model for flow path B-E

input voltage	C_{d0} / P_{r0}	C_{d1} / P_{r1}	C_{d2} / P_{r2}	C_{d3} / P_{r3}	C_{d4} / P_{r4}
5 V	0.90 / 0	0.90 / 0.15	0.55 / 0.65	0.45 / 0.90	0.30 / 1
4 V	0.85 / 0	0.85 / 0.15	0.60 / 0.50	0.44 / 0.80	0.32 / 1
3 V	0.83 / 0	0.82 / 0.15	0.67 / 0.30	0.42 / 0.90	0.32 / 1
2 V	0.84 / 0	0.84 / 0.14	0.59 / 0.40	0.46 / 0.80	0.33 / 1
1 V	0.80 / 0	0.80 / 0.15	0.53 / 0.29	0.50 / 0.80	0.37 / 1
0.8 V	0.80 / 0	0.80 / 0.15	0.50 / 0.30	0.52 / 0.80	0.32 / 1
0.6 V	0.80 / 0	0.80 / 0.15	0.51 / 0.25	0.54 / 0.70	0.40 / 1
0.4 V	0.80 / 0	0.80 / 0.15	0.57 / 0.20	0.30 / 0.80	0.00 / 1
0.2 V	0.80 / 0	0.80 / 0.15	0.48 / 0.20	0.31 / 0.30	0.00 / 1
0.1 V	0.81 / 0	0.70 / 0.15	0.18 / 0.20	0.00 / 0.25	0.00 / 1

Table 4.4 - Discharge coefficient C_d as a function of pressure ratio P_r as used in the valve simulation model for flow path S-B

input voltage	C_{d0} / P_{r0}	C_{d1} / P_{r1}	C_{d2} / P_{r2}	C_{d3} / P_{r3}	C_{d4} / P_{r4}
5 V	0.83 / 0	0.83 / 0.20	0.80 / 0.30	0.70 / 0.80	0.60 / 1
4 V	0.83 / 0	0.83 / 0.20	0.80 / 0.30	0.66 / 0.80	0.60 / 1
3 V	0.82 / 0	0.82 / 0.20	0.70 / 0.60	0.62 / 0.90	0.40 / 1
2 V	0.82 / 0	0.82 / 0.20	0.78 / 0.30	0.63 / 0.90	0.40 / 1
1 V	0.82 / 0	0.82 / 0.20	0.78 / 0.50	0.65 / 0.90	0.40 / 1
0.8 V	0.80 / 0	0.80 / 0.20	0.75 / 0.30	0.60 / 0.95	0.40 / 1
0.6 V	0.81 / 0	0.81 / 0.20	0.78 / 0.50	0.65 / 0.90	0.40 / 1
0.4 V	0.81 / 0	0.81 / 0.20	0.80 / 0.40	0.65 / 0.85	0.40 / 1
0.2 V	0.81 / 0	0.81 / 0.20	0.78 / 0.40	0.54 / 0.90	0.40 / 1
0.1 V	0.81 / 0	0.81 / 0.20	0.76 / 0.50	0.53 / 0.85	0.35 / 1

Table 4.5 - Discharge coefficient C_d as a function of pressure ratio P_r as used in the valve simulation model for flow path A-E

input voltage	C_{d0} / P_{r0}	C_{d1} / P_{r1}	C_{d2} / P_{r2}	C_{d3} / P_{r3}	C_{d4} / P_{r4}
5 V	0.82 / 0	0.82 / 0.16	0.68 / 0.33	0.50 / 0.74	0.33 / 1
4 V	0.82 / 0	0.82 / 0.15	0.60 / 0.40	0.56 / 0.70	0.25 / 1
3 V	0.82 / 0	0.82 / 0.15	0.58 / 0.35	0.45 / 0.90	0.20 / 1
2 V	0.82 / 0	0.82 / 0.14	0.58 / 0.35	0.44 / 0.80	0.30 / 1
1 V	0.82 / 0	0.80 / 0.13	0.53 / 0.32	0.48 / 0.80	0.30 / 1
0.8 V	0.80 / 0	0.75 / 0.15	0.46 / 0.32	0.48 / 0.80	0.48 / 1
0.6 V	0.80 / 0	0.73 / 0.14	0.46 / 0.25	0.47 / 0.83	0.20 / 1
0.4 V	0.82 / 0	0.70 / 0.15	0.45 / 0.25	0.46 / 0.45	0.10 / 1
0.2 V	0.82 / 0	0.81 / 0.14	0.48 / 0.19	0.10 / 0.85	0.00 / 1
0.1 V	0.82 / 0	0.82 / 0.14	0.41 / 0.16	0.05 / 0.42	0.00 / 1

Table 4.6 - Identified system parameters using least-square algorithm

parameter	**identified value**
mass to be moved: m [kg]	1.81 - 1.84
viscous friction coefficient: c_f [N/(m/s)]	97 - 109
Coulomb friction force: F_{Cd} [N]	1 - 3

Table 4.7 - Identified system parameters using genetic algorithms (GA's)

parameter	**identified value**
mass to be moved: m [kg]	1.825
viscous friction coefficient: c_f [N/(m/s)]	102.53
dynamic Coulomb friction force: F_{Cd} [N]	1.013
stiction force: F_{Cs} [N]	1.234

Table 4.8 - Simulation system parameters

parameter	**chosen value**
sampling time: T_{samp} [ms]	1
natural frequency of valve: ω_{valve} [Hz]	200
damping ratio of valve: ζ_{valve}	1

FIGURES

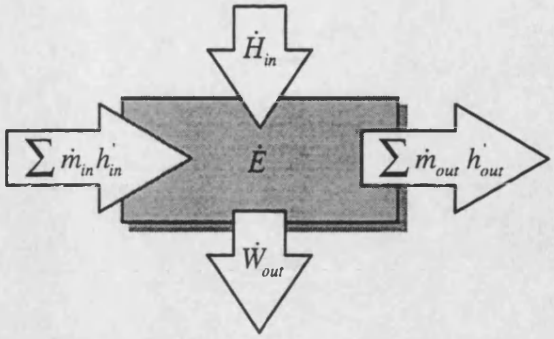

Figure 4.1 - Control volume

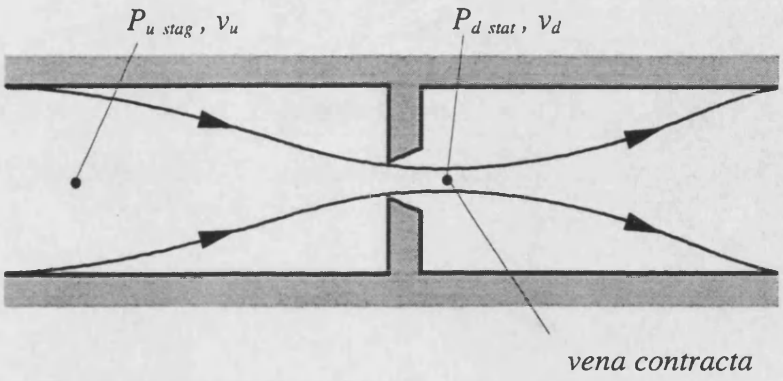

Figure 4.2 - Gas flow through a restriction

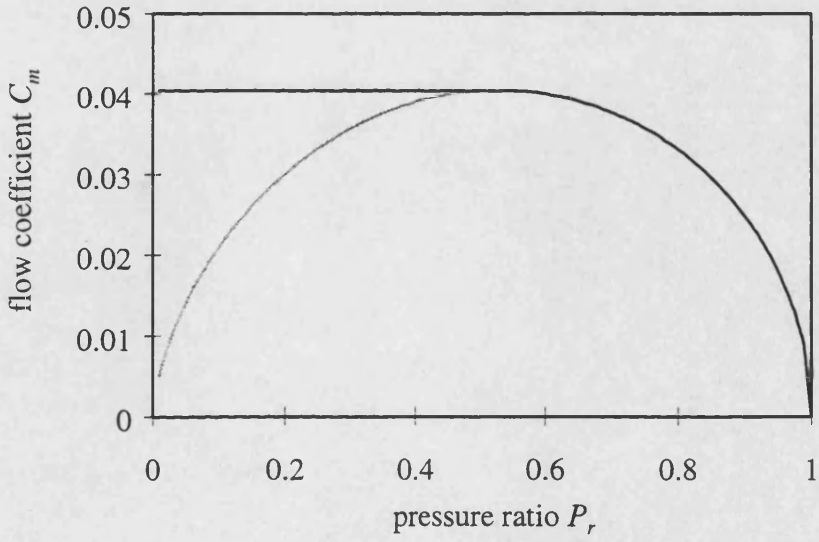

Figure 4.3 - Variation of flow coefficient C_m with pressure ratio P_r

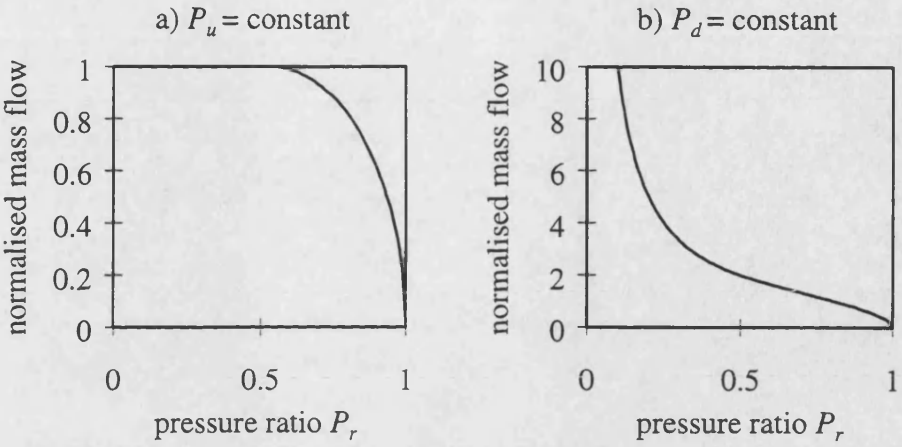

Figure 4.4 - Normalised mass flow versus pressure ratio P_r

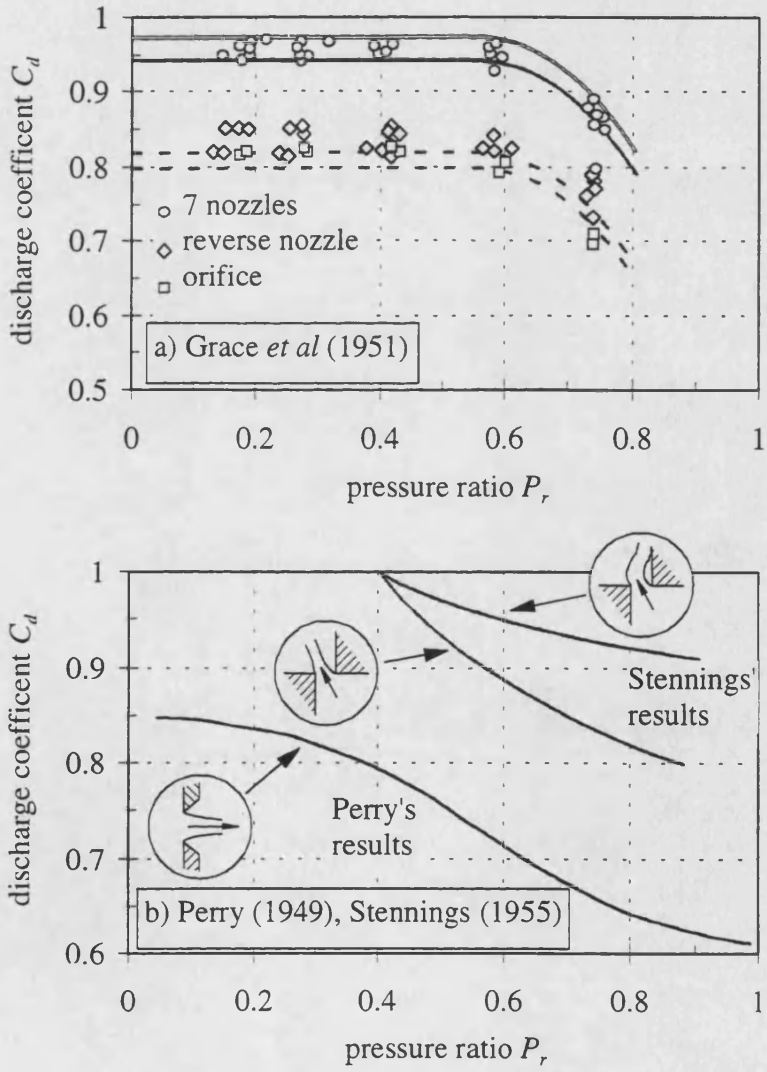

Figure 4.5 - Discharge coefficient C_d

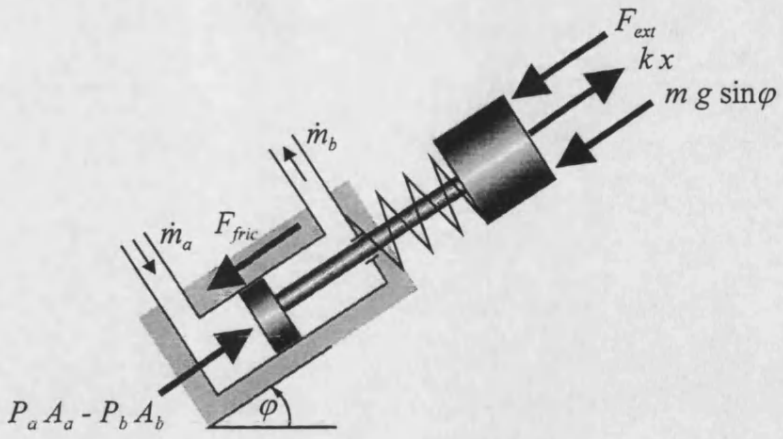

Figure 4.6 - Forces acting on a linear actuator

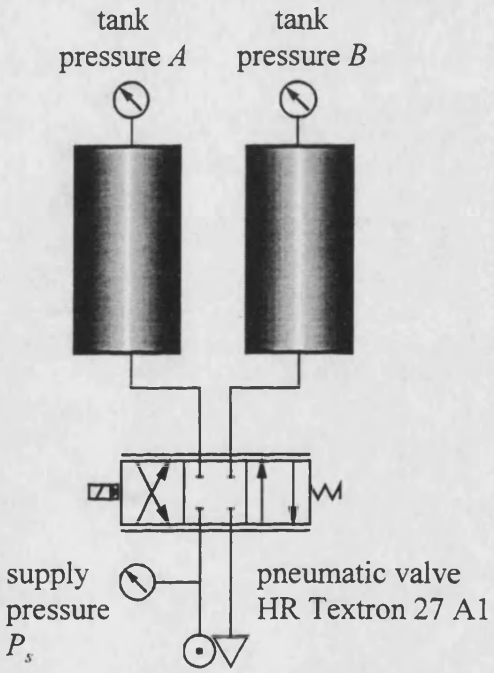

Figure 4.7 - Experimental set-up used to calibrate valve model

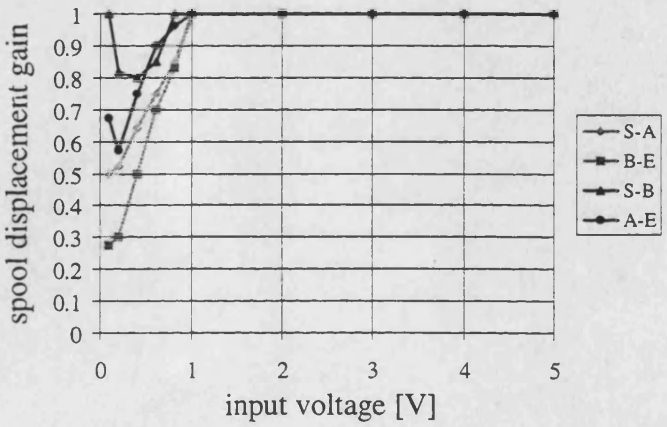

Figure 4.8 - Flow area gains used in simulation model of servovalve

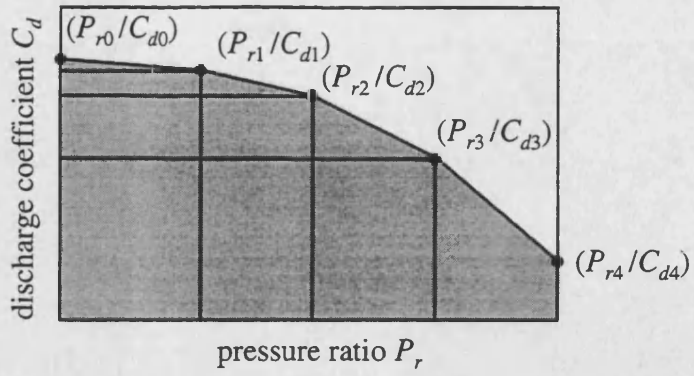

Figure 4.9 - Discharge coefficient model

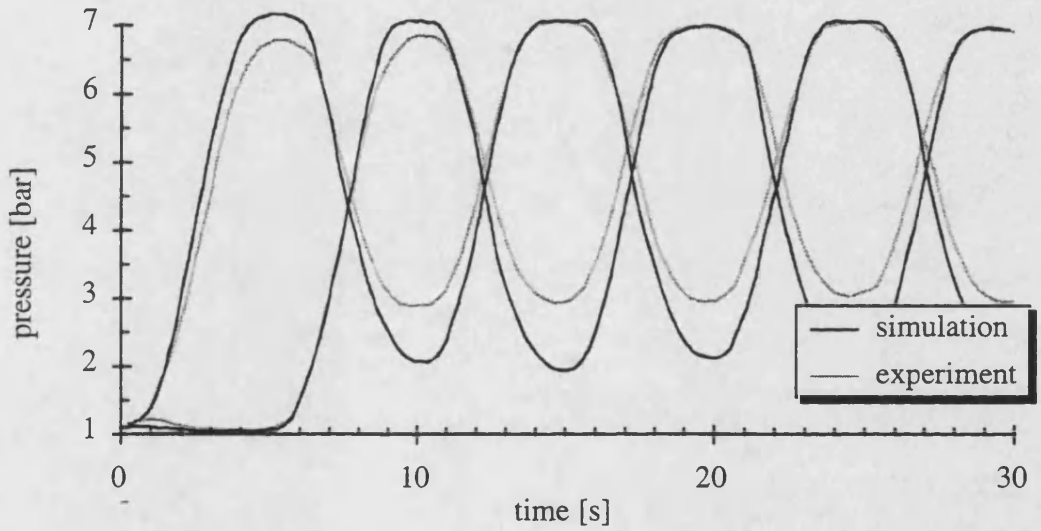

Figure 4.10 - Pressures in measuring chambers using nominal valve model

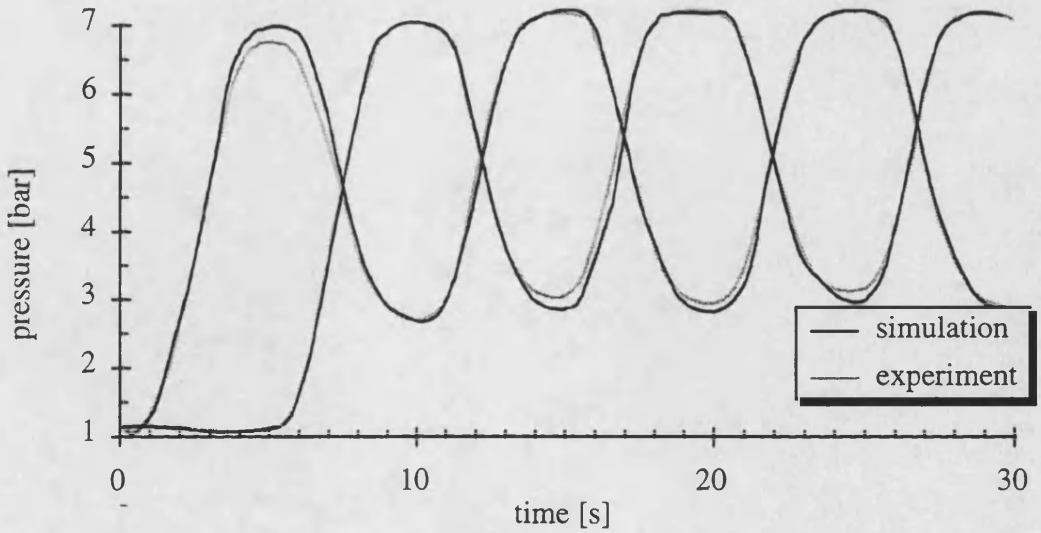

Figure 4.11 - Pressures in measuring chambers using calibrated valve model

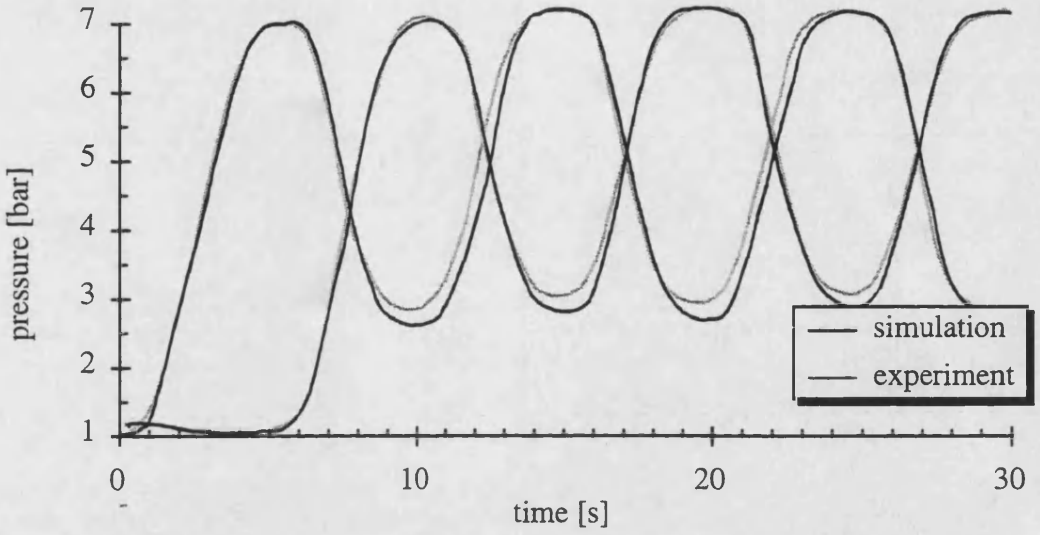

Figure 4.12 - Experimental results obtained with a different HR Textron DDV 27A1 valve

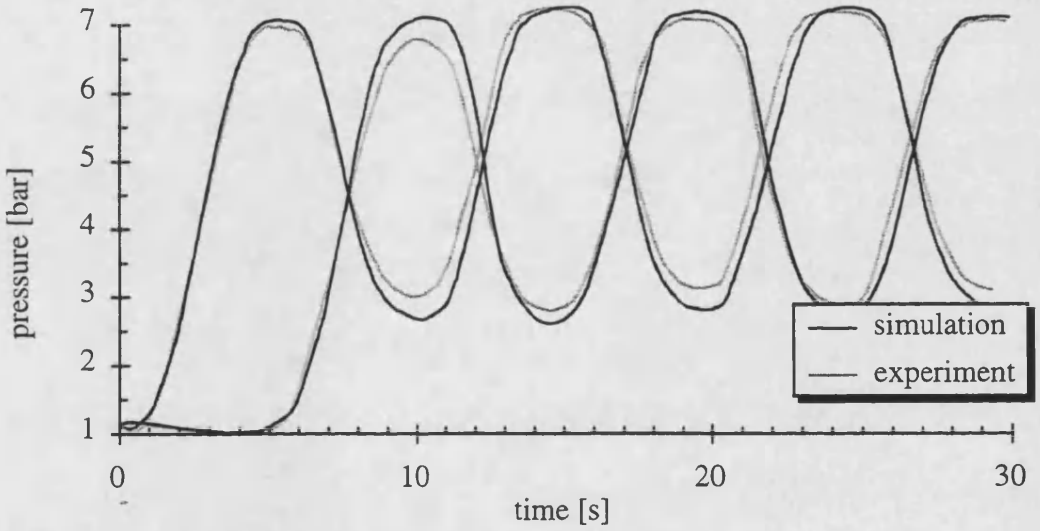

Figure 4.13 - Experimental results obtained on a different day

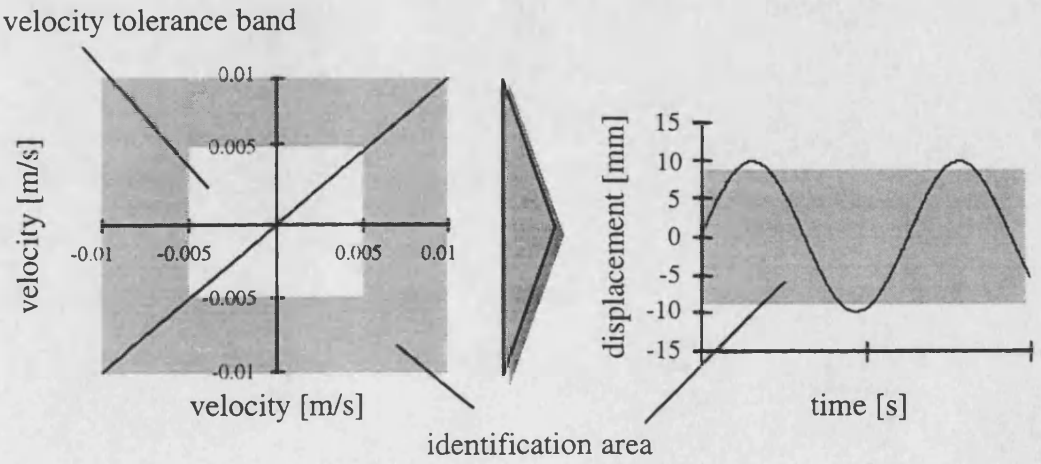

Figure 4.14 - Velocity dead-band used in identification routine

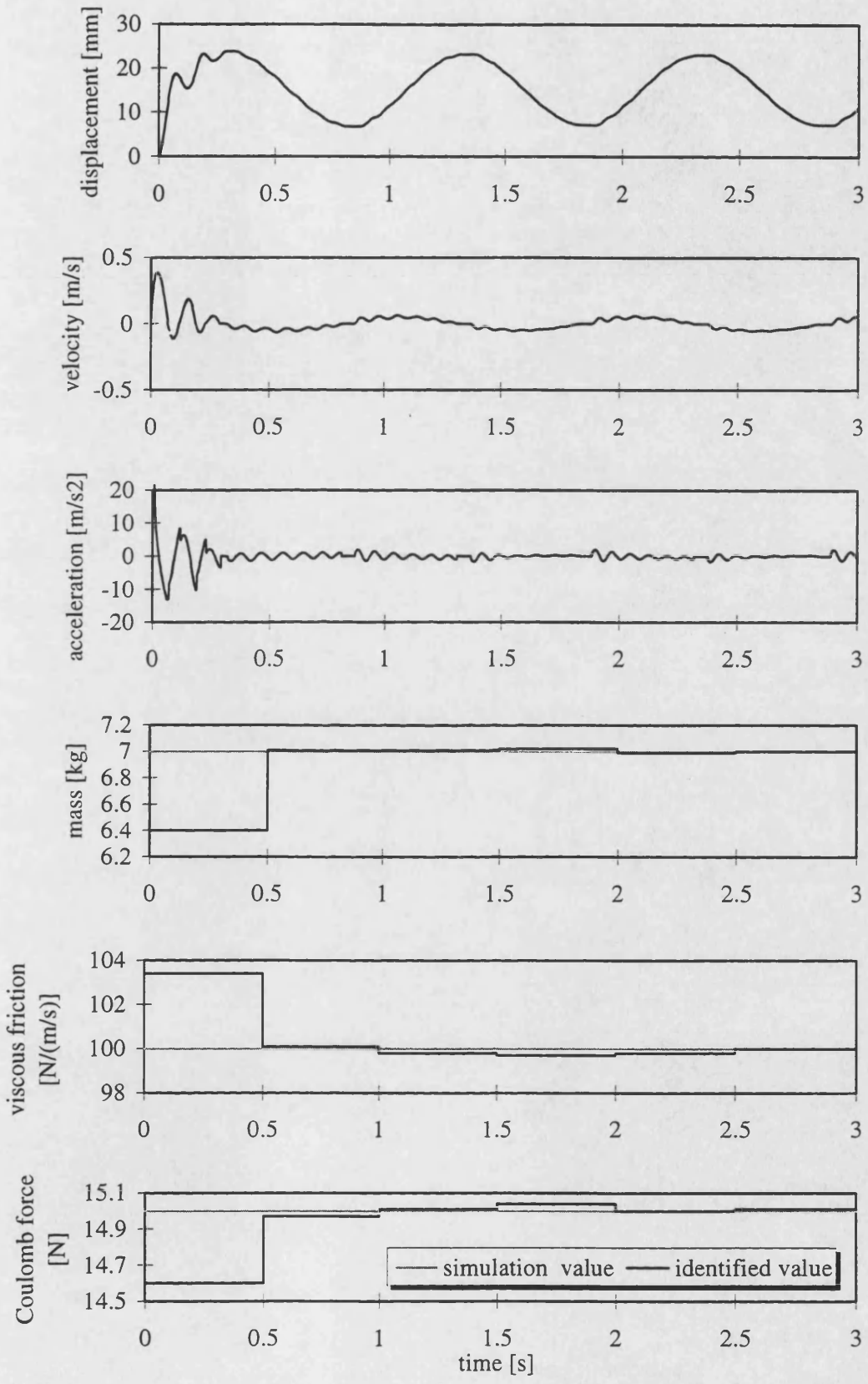

Figure 4.15 - Test of least-square parameter identification routine

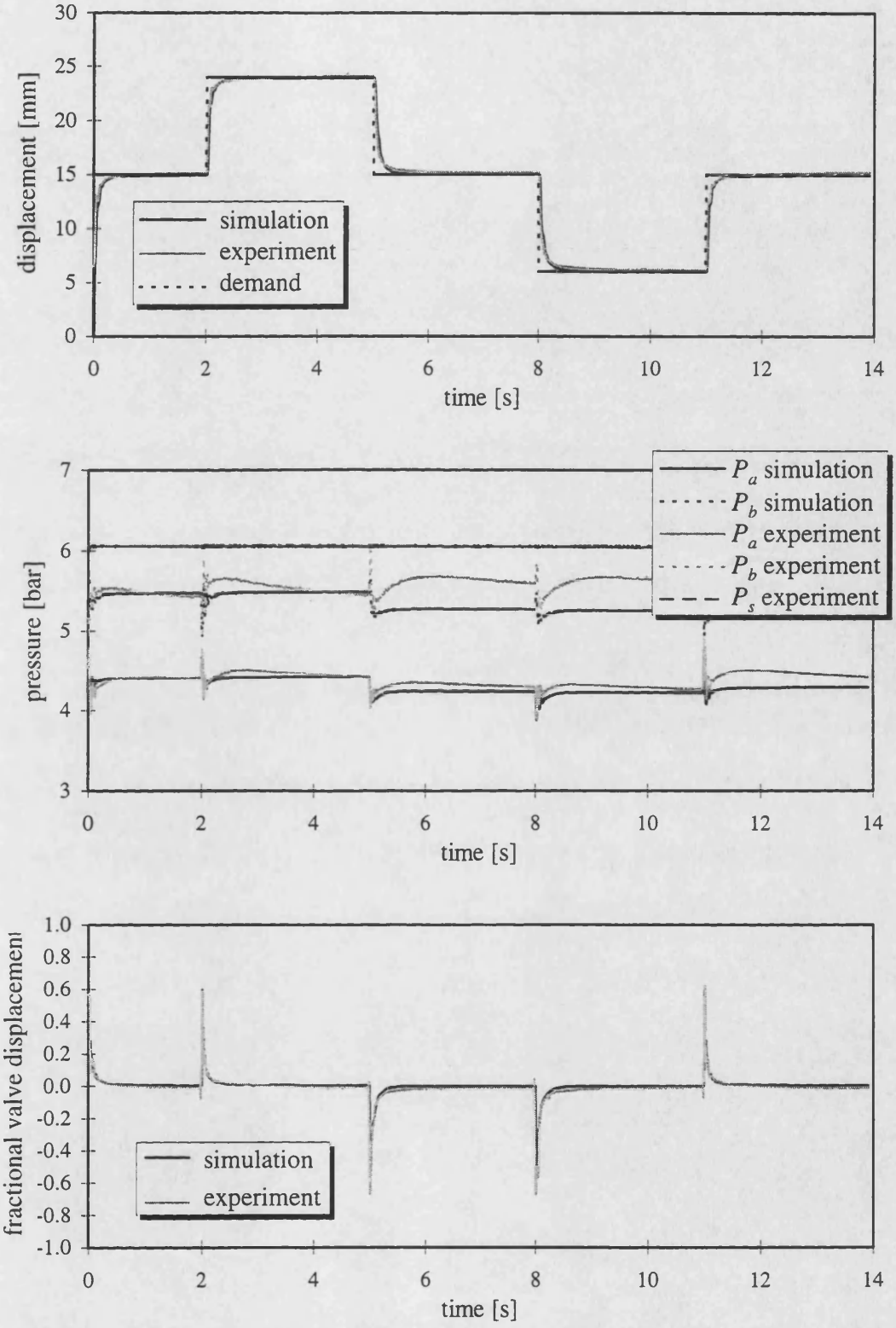

Figure 4.16 - Comparison between simulation and experimental results (K_p = 1)

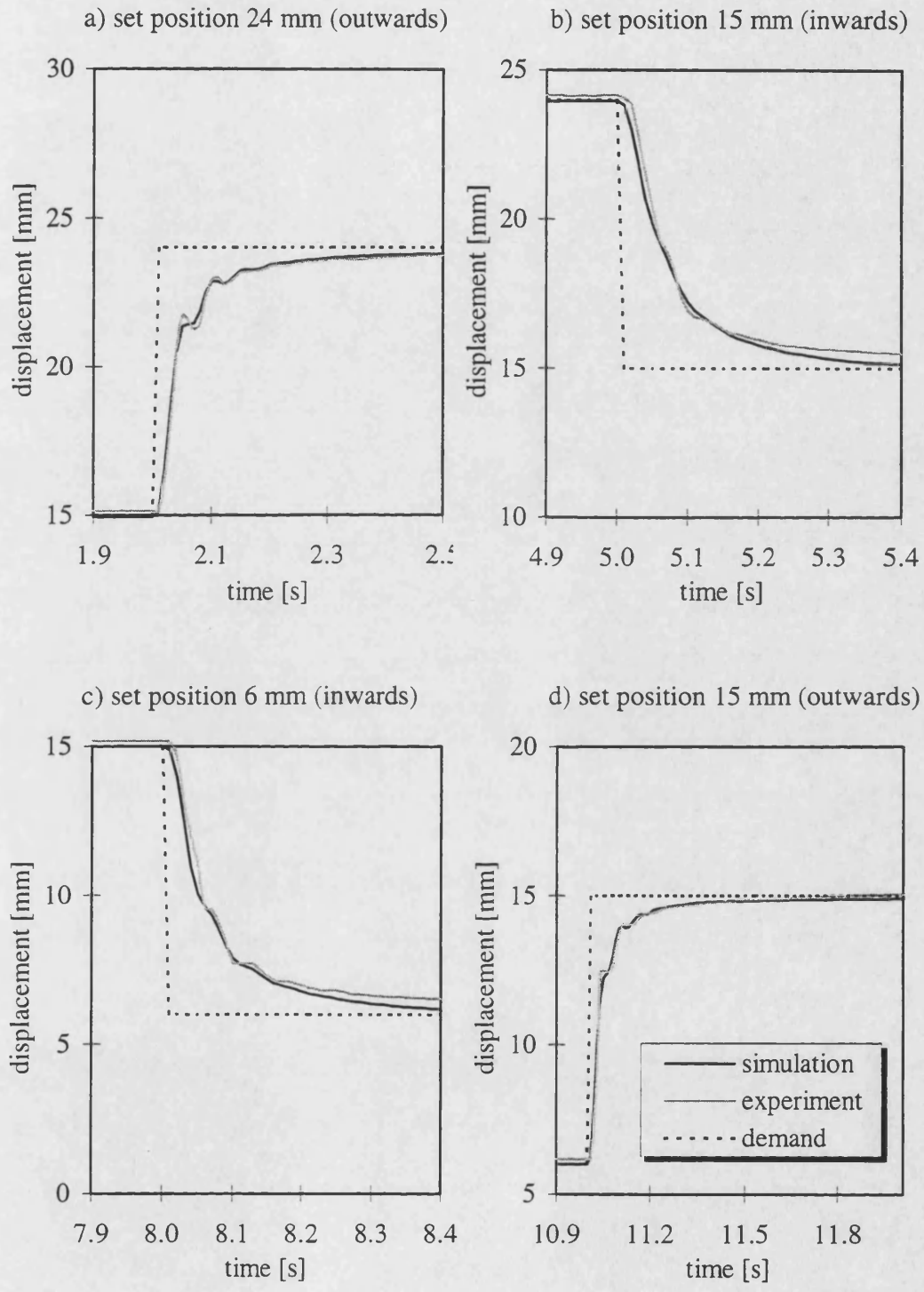

Figure 4.17 - Comparison between simulation and experimental results (K_p = 1)

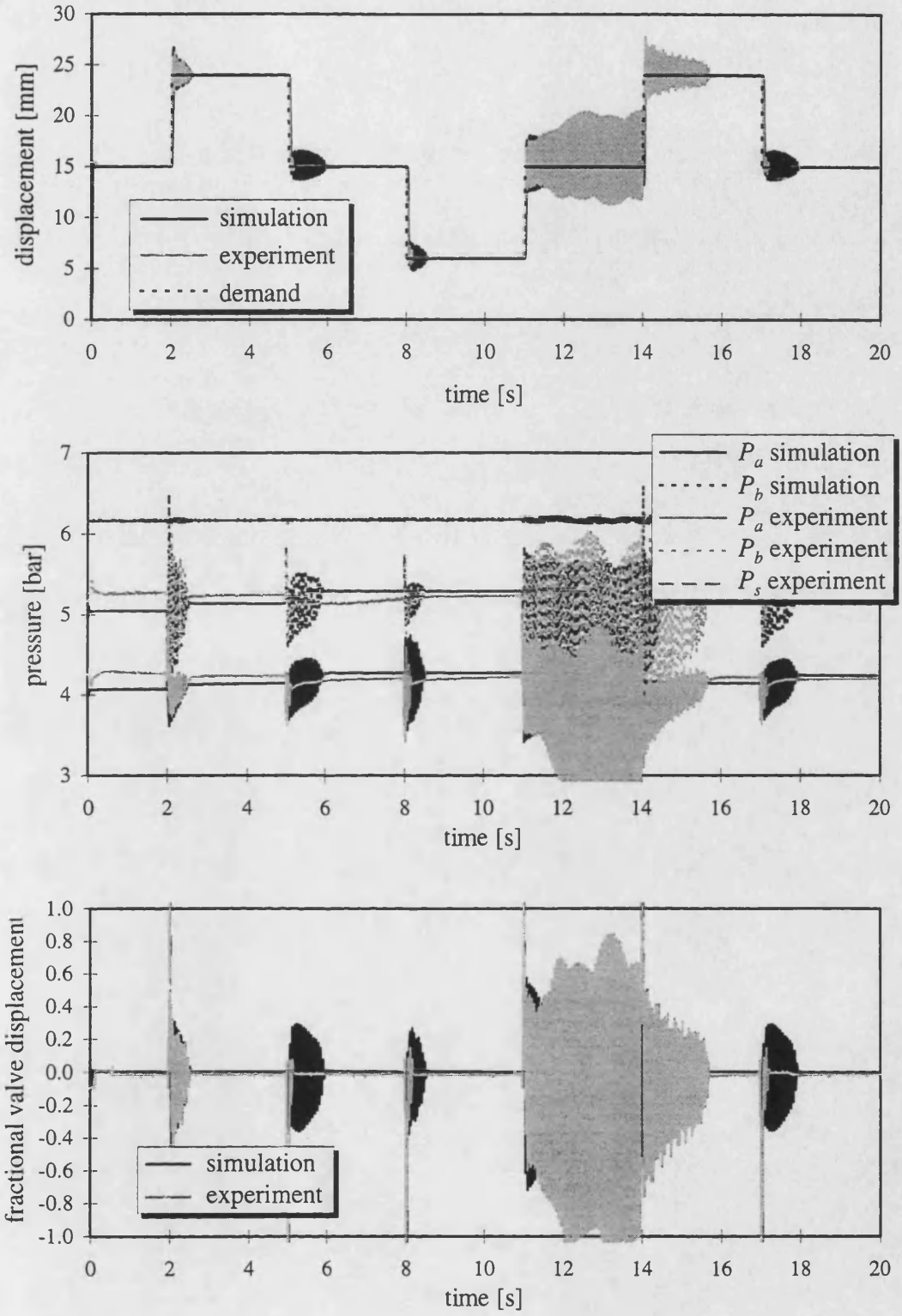

Figure 4.18 - Comparison between simulation and experimental results ($K_p = 3.4$)

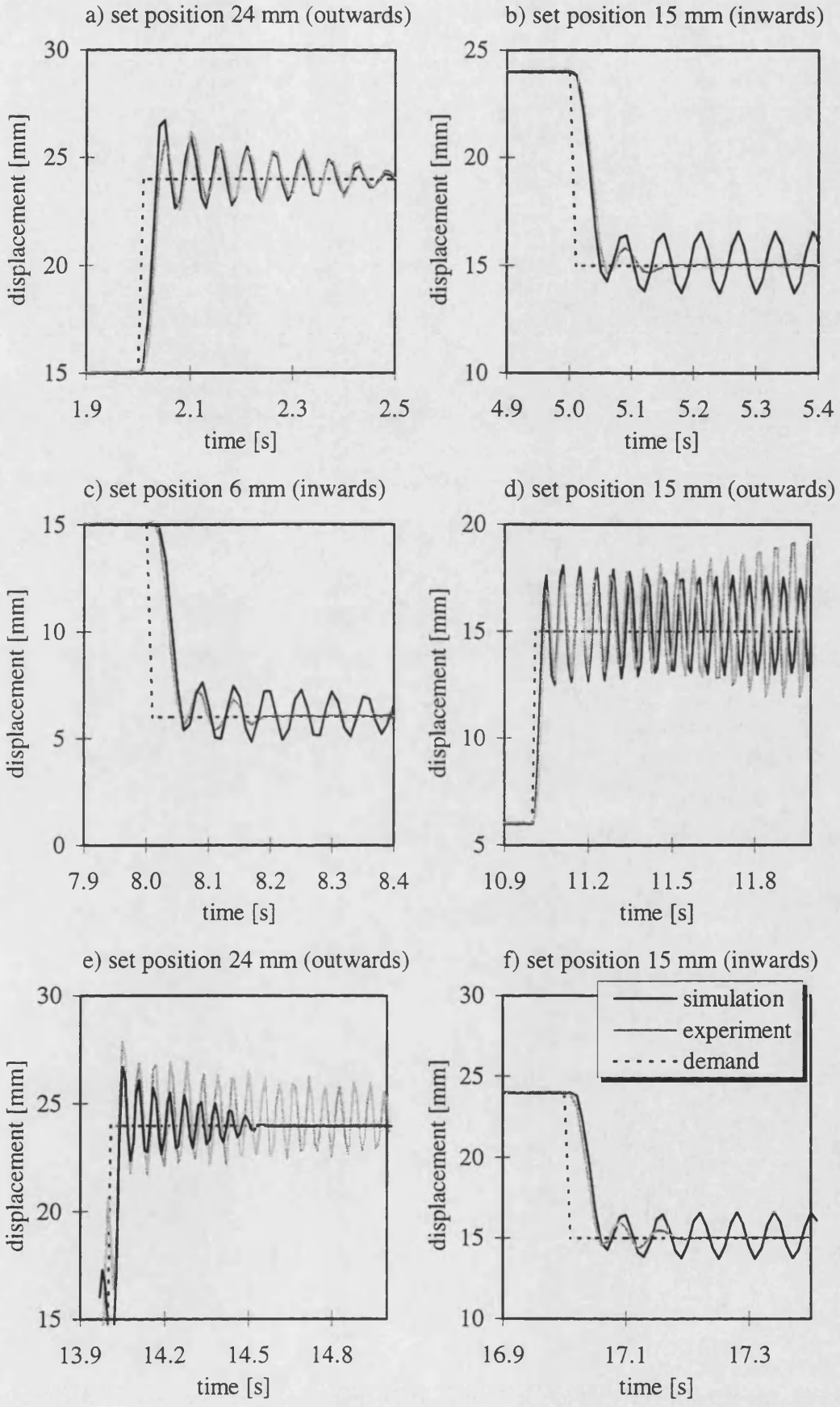

Figure 4.19 - Comparison between simulation and experimental results (K_p = 3.4)

5 LINEARISED ANALYSIS OF PNEUMATIC SERVO MECHANISM

In this chapter the characteristics of the linearised dynamic model of the pneumatic actuation system as depicted in Figure 5.1 are investigated. A new advanced linearised model is derived which represents an extension to the conventional linearised model commonly referred to in literature. The new advanced linearised model predicts accurately the piston position and direction of valve opening dependent dynamics of the pneumatic servo already envisaged during the experimental testing as reported in the Chapter 4. Using the advanced linear model therefore as a basis for linear feedback controller design improves the closed-loop system response significantly as demonstrated in this chapter.

5.1 CONVENTIONAL LINEARISED MODEL

Relatively little attention has been paid in literature to the linearised analysis of pneumatic servo systems. This is mostly due to the fact that the equations describing compressible gas flow are highly non-linear and difficult to handle. Furthermore, pneumatic servos are by far not as popular as hydraulic or electrical actuation systems.

Shearer (1956, 1957) first published a linear analysis of a pneumatic servo. depicted in Figure 5.1. He required the following assumptions to be made:

- Supply pressure P_s and supply temperature T_s are constant.
- Temperatures are uniform throughout the system: $T_a = T_b = T_s = T$.
- No heat is transferred between the gas and the surrounding: n = 1.4 (i.e. adiabatic).
- The cylinder is of equal areas: $A_a = A_b = A$.
- The central position is chosen as a linearisation point and the piston only moves small distances from this position:

$$V_{ai} = A\left(\frac{l}{2}+x\right)+V_{\min} = A\frac{l}{2}+V_{\min}, V_{bi} = A\left(\frac{l}{2}-x\right)+V_{\min} = A\frac{l}{2}+V_{\min} \quad \text{for } x=0.$$

- Cylinder chamber A is charged while chamber B is discharged.
- The cylinder pressures in chambers A and B are equal and vary only by small amounts from any initial steady value: $P_{ai} = P_{bi} = P_i$.

Following the approach presented by McCloy and Martin (1980) the valve characteristics (Equation (4.15)) can be expanded as a Taylor's series about some initial point *i*. Since only small changes are considered higher order terms can be neglected. It yields:

$$\dot{m} - \dot{m}_i = \delta\dot{m} = \left(\frac{\partial \dot{m}}{\partial u}\right)_i \delta u + \left(\frac{\partial \dot{m}}{\partial P_u}\right)_i \delta P_u + \left(\frac{\partial \dot{m}}{\partial P_d}\right)_i \delta P_d + \left(\frac{\partial \dot{m}}{\partial T_u}\right)_i \delta T_u \qquad (5.1)$$
$$= k_1 \delta u + k_1 \delta P_u + k_3 \delta P_d + k_4 \delta T_u$$

The partial derivatives are evaluated as follows:

$$\left(\frac{\partial \dot{m}}{\partial u}\right)_i = \left(C_d C_m A_v \frac{P_u}{\sqrt{T_u}} k_v\right)_i = k_1 \qquad (5.2)$$

$$\left(\frac{\partial \dot{m}}{\partial P_u}\right)_i = \left(C_d A_v \frac{k_v u}{\sqrt{T_u}}\left(C_m + \frac{\partial C_m}{\partial P_u} P_u\right)\right)_i = k_2 \qquad (5.3)$$

$$\left(\frac{\partial \dot{m}}{\partial P_d}\right)_i = \left(C_d A_v \frac{P_u}{\sqrt{T_u}} k_v u \frac{\partial C_m}{\partial P_d}\right)_i = k_3 \qquad (5.4)$$

$$\left(\frac{\partial \dot{m}}{\partial T_u}\right)_i = \left(-\frac{1}{2} C_d C_m A_v \frac{P_u}{\sqrt{T_u}} k_v u \frac{1}{T_u}\right)_i = k_4 \qquad (5.5)$$

Partial derivatives of C_m with respect to P_u and P_d are zero for choked (sonic) gas mass flow ($P_r < P_{rcrit} = 0.528$). For unchoked flow follows:

$$\left(\frac{\partial C_m}{\partial P_u}\right)_i = \left(\frac{1}{C_m R(\gamma - 1)}\left[(\gamma+1)P_r^{(\gamma+1)/\gamma} - 2P_r^{2/\gamma}\right]\frac{1}{P_u}\right)_i = \left(\zeta \frac{1}{P_u}\right)_i \qquad (5.6)$$

$$\left(\frac{\partial C_m}{\partial P_d}\right)_i = \left(\frac{1}{C_m R(\gamma - 1)}\left[(\gamma+1)P_r^{(\gamma+1)/\gamma} - 2P_r^{2/\gamma}\right]\left(-\frac{1}{P_r P_u}\right)\right)_i = \left(-\zeta \frac{1}{P_r P_u}\right)_i \qquad (5.7)$$

It has to be noted that:

$$\left(\frac{\partial C_m}{\partial P_u}\right)_i = -\frac{1}{P_r}\left(\frac{\partial C_m}{\partial P_d}\right)_i \qquad (5.8)$$

Using Equations (5.6) and (5.7) the partial derivatives k_2 and k_3 can be written as follows:

$$k_2 = \left(C_d A_v \frac{k_v u}{\sqrt{T_u}} (C_m + \zeta) \right)_i \tag{5.9}$$

$$k_3 = -\left(C_d A_v \frac{k_v u}{\sqrt{T_u}} \left(\zeta \frac{1}{P_r} \right) \right)_i \tag{5.10}$$

The variation of k_2 and k_3 with pressure ratio P_r can be seen in Figure 5.2.

Assuming that the piston is moving in the positive x-direction chamber A of the actuator is charged while chamber B is discharged. The linearised mass flow rates are:

$$\delta \dot{m}_{as} = k_{1a} \delta u + k_{2a} \delta P_s + k_{3a} \delta P_a + k_{4a} \delta T_s \tag{5.11}$$

$$\delta \dot{m}_{be} = k_{1b} \delta u + k_{2b} \delta P_b + k_{3b} \delta P_e + k_{4b} \delta T_b \tag{5.12}$$

Now $\delta P_s = \delta P_e = 0$ and $\delta T_s = \delta T_b = 0$. This results in:

$$\delta \dot{m}_{as} = k_{1a} \delta u + k_{3a} \delta P_a \tag{5.13}$$

$$\delta \dot{m}_{be} = k_{1b} \delta u + k_{2b} \delta P_b \tag{5.14}$$

The valve coefficient k_1 is often called *flow gain*, or *flow sensitivity*, the coefficients k_2 and k_3 *flow-pressure coefficient* (Burrows (1972)). Assuming now that the flow charging into chamber A is choked and the flow discharging from chamber B is unchoked the analysis can be further simplified by using $k_{2b} = -k_{3a}$ (see Figure 5.2). McCloy and Martin (1980) use the same simplification but he justifies it by assuming that the pressure ratios tend to unity which implies small pressure drops across the orifices. As can be seen in Figure 5.2, McCloy and Martin's strong assumption of small pressure drops is not necessary. Even for realistically large pressure drops with a pressure ratio of e.g. 0.8 the above simplification can be valid. Furthermore, using $k_{1b} = k_{1a}$ results in:

$$\delta \dot{m}_{as} = k_1 \delta u + k_2 \delta P_a \tag{5.15}$$

$$\delta \dot{m}_{be} = k_1 \delta u - k_2 \delta P_b \tag{5.16}$$

Linearising the equation for the rate of change of the pressures P_a and P_b (Equation (4.10)) for motion in the positive x-direction results in:

$$\delta\dot{P}_a = \left(\frac{\partial \dot{P}_a}{\partial V_a}\right)_i \delta V_a + \left(\frac{\partial \dot{P}_a}{\partial \dot{m}_{as}}\right)_i \delta\dot{m}_{as} + \left(\frac{\partial \dot{P}_a}{\partial \dot{V}_a}\right)_i \delta\dot{V}_a$$
$$-\frac{n}{V_{ai}^2}\left(RT_s\dot{m}_{asi} - P_{ai}\dot{V}_{ai}\right)\delta V_a + \frac{nRT_s}{V_{ai}}\delta\dot{m}_{as} - \frac{nP_{ai}}{V_{ai}}\delta\dot{V}_a \tag{5.17}$$

$$\delta\dot{P}_b = \left(\frac{\partial \dot{P}_b}{\partial V_b}\right)_i \delta V_b + \left(\frac{\partial \dot{P}_b}{\partial \dot{m}_{be}}\right)_i \delta\dot{m}_{be} + \left(\frac{\partial \dot{P}_b}{\partial \dot{V}_b}\right)_i \delta\dot{V}_b$$
$$-\frac{n}{V_{bi}^2}\left(-RT_b\dot{m}_{bei} - P_{bi}\dot{V}_{bi}\right)\delta V_b - \frac{nRT_b}{V_{bai}}\delta\dot{m}_{be} - \frac{nP_{bi}}{V_{bi}}\delta\dot{V}_b \tag{5.18}$$

At this stage it is necessary to linearise the load equation (Equation (4.23)). The linearised load equation is:

$$m\delta\dddot{x} + c_f\delta\ddot{x} = A_a\delta\dot{P}_a - A_b\delta\dot{P}_b \tag{5.19}$$

Inserting from Equations (5.17) and (5.18) gives:

$$\delta\dddot{x} + \frac{c_f}{m}\delta\ddot{x} + \frac{n}{m}\left(\frac{P_{ai}A_a^2}{V_{ai}} + \frac{P_{bi}A_b^2}{V_{bi}}\right)\delta\dot{x}$$
$$+\left(\frac{nA_a^2}{V_{ai}^2}\left[RT_s\dot{m}_{asi} - P_{ai}\dot{V}_{ai}\right] + \frac{nA_b^2}{V_{bi}^2}\left[-RT_b\dot{m}_{bei} - P_{bi}\dot{V}_{bi}\right]\right)\delta x \tag{5.20}$$
$$= nR\left(\frac{T_sA_ak_{1a}}{V_{ai}} + \frac{T_bA_bk_{1b}}{V_{bi}}\right)\delta u + nR\left(\frac{T_sA_a}{V_{ai}}\delta P_a - \frac{T_bA_b}{V_{bi}}\delta P_b\right)k_2$$

It can be shown for equal area actuators that the last term on the right-hand side increases the damping and the stiffness of the servo. It has been demonstrated by Burrows and Webb (1969) that the effects arising from the increase in downstream pressure for charging and the decrease of upstream pressure for discharging is negligible, especially for a closed-centre valve; that is, k_2 can be set to zero to simplify the linear analysis. To justify this simplification step response results of the system with constant and with varying actuator chamber pressures are shown in Section 5.3. The analysis is further simplified by $\dot{m}_{asi} = \dot{m}_{bei} = 0$, $\dot{V}_{ai} = \dot{V}_{bi} = 0$. For motion in the positive x-direction the following dynamic equation is obtained:

$$\delta\dddot{x} + \frac{c_f}{m}\delta\ddot{x} + \left[\frac{n}{m}\left(\frac{P_{ai}A_a^2}{V_{ai}} + \frac{P_{bi}A_b^2}{V_{bi}}\right)\right]\delta\dot{x} = \frac{nR}{m}\left(\frac{T_sA_ak_{1a}}{V_{ai}} + \frac{T_bA_bk_{1b}}{V_{bi}}\right)\delta u \tag{5.21}$$

A similar argument for motion in the negative x-direction yields:

$$\delta\dddot{x} + \frac{c_f}{m}\delta\ddot{x} + \left[\frac{n}{m}\left(\frac{P_{ai}A_a^2}{V_{ai}} + \frac{P_{bi}A_b^2}{V_{bi}}\right)\right]\delta\dot{x} = \frac{nR}{m}\left(\frac{T_aA_ak_{1a}}{V_{ai}} + \frac{T_sA_bk_{1b}}{V_{bi}}\right)\delta u \tag{5.22}$$

With the assumptions made at the beginning of this section it follows:

$$\delta\dddot{x}+\frac{c_f}{m}\delta\ddot{x}+\left[\frac{nP_iA}{m}\left(\frac{1}{\left(\frac{l}{2}+x\right)+\frac{V_{\min}}{A}}+\frac{1}{\left(\frac{l}{2}-x\right)+\frac{V_{\min}}{A}}\right)\right]\delta\dot{x}$$
$$=\frac{nR\sqrt{T}C_dC_mA_v}{m}\left(\frac{P_s}{\left(\frac{l}{2}+x\right)+\frac{V_{\min}}{A}}+\frac{P_i}{\left(\frac{l}{2}-x\right)+\frac{V_{\min}}{A}}\right)\delta u \tag{5.23}$$

Due to the fact that the actuator is assumed to be of equal area and in horizontal position so that no gravity load has to be supported the chamber pressures P_a and P_b are equal. Therefore, no distinction between the different direction of valve opening has to be made. The choice of the central piston position as a linearisation point (that is $x = 0$) yields:

$$\delta\dddot{x}+\frac{c_f}{m}\delta\ddot{x}+\left(\frac{4nP_iA}{ml+D_{\min}}\right)\delta\dot{x}=\frac{2nR\sqrt{T}C_dC_mA_v}{ml+D_{\min}}(P_s+P_i)\delta u \tag{5.24}$$

with: $D_{\min}=\frac{2mV_{\min}}{A}$

As stated by Pu and Weston (1990) the steady-state chamber pressures in equal area actuators are in general assumed to be approximately 80% of the supply pressure. This yields:

$$\delta\dddot{x}+\frac{c_f}{m}\delta\ddot{x}+\left(\frac{3.2nP_sA}{ml+D_{\min}}\right)\delta\dot{x}=\frac{3.6nR\sqrt{T}C_dC_mA_vP_s}{ml+D_{\min}}\delta u \tag{5.25}$$

Introducing the Laplace operator gives the open-loop transfer function of the pneumatic servo system:

$$G(s)=\frac{X(s)}{U(s)}=\frac{b_0}{s\left(s^2+a_2s+a_1\right)} \tag{5.26}$$

with:

$$a_1=\frac{3.2nP_sA}{ml+D_{\min}},\quad a_2=\frac{c_f}{m},\quad b_0=\frac{3.6nR\sqrt{T}C_dC_mA_vP_s}{ml+D_{\min}}. \tag{5.27}$$

As can be seen from Equation (5.26) the transfer function is of third-order consisting of a second-order system and an integrator. The frequency response of the linear model can be seen in Figures 5.3 and 5.4. Figure 5.3 shows a Bode plot of the frequency response for the three different actuator piston positions listed in

Table 5.1. It is assumed that the actuator piston is retracting. In Figure 5.4 the frequency response of the linear model is depicted for both directions of piston motion (retracting and extending) and the piston being in position 1. The system parameters used in the model can be found in Table 5.2. They represent the dynamic characteristics of the single-axis test rig described in Chapter 3. One can observe that the frequency response changes with piston position but not with its direction of motion since the coefficients of the linear transfer function (Equation (5.27)) are position but not direction dependent. To examine the implications of the position dependent dynamics on natural frequency ω_n and damping ratio ζ in detail the following explicit relationships describing these parameters can be used:

$$\omega_n = \sqrt{a_1} = \sqrt{\frac{3.2nP_sA}{ml + D_{\min}}}, \quad \zeta = \frac{a_2}{2\sqrt{a_1}} = \frac{c_f}{3.6}\sqrt{\frac{l + \frac{D_{\min}}{m}}{mnP_sA}} \tag{5.28}$$

Furthermore, using Routh-Hurwitz the ultimate gain at the stability border K_{ult} of the pneumatic servo system under closed-loop proportional feedback control can be calculated to be:

$$K_{ult} = \frac{a_1 a_2}{b_0} = \frac{0.89 c_f A}{mR\sqrt{T}C_d C_m A_v} \tag{5.29}$$

Using the above linearisation approach but varying the piston position x (measured from the mid position) shows that the stiffness and hence the natural frequency of the pneumatic servo reaches a minimum at the actuator mid point while the damping ratio reaches a maximum (see Figure 5.5).

The dependency of the ultimate gain on the piston position can be seen in Figure 5.6. Like the natural frequency the ultimate gain reaches its minimum when the actuator piston is in its mid position. The relationship between the ultimate gain and the piston position is linear unlike the relationship reported by Pu *et al* (1992) which is also depicted in Figure 5.6. The relationship presented by Pu *et al* can only be achieved assuming that the numerator of the open-loop transfer function b_0 is constant (i.e. not dependent on the linearisation point) which is clearly not the case (see right-hand side of Equation (5.23)). Yet, the above results justify the choice of the mid position as the linearisation point for a system with an equal area actuator and no gravity load. When designing a controller based on the linear mid position

model and tuning the controller in order to ensure stability for this position it can be assumed that the system is also stable for all other possible piston positions.

5.2 Advanced Linearised Model of a Pneumatic Servo

5.2.1 Underlying Assumptions

Considering now an unequal area actuator which is also supporting an additional gravity load (e.g. due to the fact that it is not aligned horizontally) a few assumptions and simplifications used in Section 5.1 when linearising the equations for an equal area horizontal actuator are no longer valid. First of all, the total actuator chamber volume of the unequal area actuator is not constant along the actuator stroke as was the case for the equal area actuator. The total chamber volume of the unequal area actuator increases when the piston moves outwards resulting in a lower overall stiffness of the system when the actuator is fully extended in comparison to the stiffness when the actuator is fully retracted. Furthermore, unlike for the equal area actuator the central piston position is not the position where both actuator chambers have the same volume and consequently the actuator exhibits the lowest stiffness. In addition, due to the unequal areas of the piston acted upon by the chamber pressures the steady-state pressures are not equal anymore. The pressure ratio across the piston now depends on the piston area ratio and also on the gravitational load to be supported. The different chamber pressures result in different charging and discharging conditions depending on whether the valve is open in the positive or the negative direction and hence charging or discharging the chamber with the higher steady-state pressure or the with the lower one.

As a result, the following assumptions are made now to linearise the equations for the pneumatic servo system with an unequal area vertical actuator and unequal chamber pressures:

- Supply pressure P_s and supply temperature T_s are constant.
- Temperatures are uniform throughout the system: $T_a = T_b = T_s = T$.
- No heat is transferred between the gas and the surrounding: $n = 1.4$.

- The cylinder pressures vary only by small amounts from any initial steady value.

5.2.2 OPEN-LOOP TRANSFER FUNCTION

As explained above, since there is no apparent reason anymore for choosing the piston mid position as the linearisation point, the actuator displacement is now measured from the fully retracted piston position that is $x = 0$ at this point. The chamber volumes are calculated to be:

$$V_{ai} = A_a x + V_{\min}, \quad V_{bi} = A_b(l-x) + V_{\min} \tag{5.30}$$

Inserting Equation (5.30) into Equation (5.21) and considering above assumptions yields:

$$\begin{aligned} \delta\ddot{x} + \frac{c_f}{m}\delta\ddot{x} + \left[\frac{n}{m}\left(\frac{P_{ai}A_a}{x+\frac{V_{\min}}{A_a}} + \frac{P_{bi}A_b}{(l-x)+\frac{V_{\min}}{A_b}}\right)\right]\delta\dot{x} \\ = \frac{nR\sqrt{T}C_d A_v}{m}\left(\frac{C_{ma}P_s}{x+\frac{V_{\min}}{A_a}} + \frac{C_{mb}P_b}{(l-x)+\frac{V_{\min}}{A_b}}\right)\delta u \end{aligned} \tag{5.31}$$

It follows for the parameters of the open-loop transfer function (Equation (5.26)):

$$a_1 = \frac{n}{m}\left(\frac{P_{ai}A_a}{x+\frac{V_{\min}}{A_a}} + \frac{P_{bi}A_b}{(l-x)+\frac{V_{\min}}{A_b}}\right), \quad a_2 = \frac{c_f}{m} \tag{5.32}$$

$$b_{0ext} = \frac{nR\sqrt{T}C_d A_v}{m}\left(\frac{C_{ma}P_s}{x+\frac{V_{\min}}{A_a}} + \frac{C_{mb}P_b}{(l-x)+\frac{V_{\min}}{A_b}}\right) \tag{5.33}$$

The above equation assumes that the valve opening is positive that means that chamber A of the actuator is charged while chamber B is discharged. A similar argument for negative valve opening yields a different denominator of the open-loop transfer function:

$$b_{0ret} = \frac{nR\sqrt{T}C_d A_v}{m}\left(\frac{C_{ma}P_a}{x+\frac{V_{\min}}{A_a}} + \frac{C_{mb}P_s}{(l-x)+\frac{V_{\min}}{A_b}}\right) \tag{5.34}$$

5.2.3 Quiescent Chamber Pressures

A further effect that has not been taken into account yet, is that the mass flow is generally choked when discharging (C_m = 0.0405) and unchoked when charging (C_m < 0.0405). In addition to that, due to the different chamber pressures in the unequal area actuator the flow coefficient C_m also depends on whether chamber A or chamber B is charged or discharged.

Extending the derivation presented by Pu and Weston (1990) to unequal area actuators to determine the quiescent chamber pressures in a pneumatic actuator it is assumed that the gas flow is always choked when discharging and unchoked when charging as is the case in most pneumatic systems. This results in the fact that the piston velocity only depends on the valve opening x_v and not on the chamber pressures. Charging chamber A and discharging chamber B (positive valve opening and hence positive direction of motion) yields:

$$v_{ext} = \frac{Q}{A_b} = \frac{\dot{m}_b R T_b}{A_b P_b} = \frac{C_{db}C_{mb}A_{va}\sqrt{T_b R}}{A_b}x_v \tag{5.35}$$

Determining the resulting mass flow rate into chamber A gives the pressure ratio from supply to chamber A:

$$P_{ra} = \frac{P_a}{P_s} = \frac{C_{da}C_{ma}A_{va}x_v T_a A_b}{C_{db}C_{mb}A_{vb}x_v\sqrt{T_b T_s}A_a} \tag{5.36}$$

The flow coefficient C_{mb} is constant for choked flow while the flow coefficient C_{ma} is a function of P_{ra}. Assuming now that the temperature is uniform throughout the system and that the discharge coefficients and flow areas for all valve ports are equal yields:

$$P_{ra} = \left(\sqrt{\left(\frac{D_a^2}{2}\right)^2 + D_a^2} - \frac{D_a^2}{2}\right)^{\frac{\gamma}{\gamma-1}} \tag{5.37}$$

with

$$D_a = \frac{A_b}{A_a}\sqrt{\frac{\gamma+1}{\gamma-1}}\left(\frac{\gamma+1}{2}\right)^{\frac{1}{\gamma-1}} = 3.864\frac{A_b}{A_a} \text{ (for air)} \tag{5.38}$$

A similar relationship is reported by Pu and Weston (1990). Charging now chamber B instead of chamber A results in a different piston velocity:

$$v_{ret} = \frac{Q}{A_a} = \frac{\dot{m}_a R T_a}{A_a P_a} = \frac{C_{da} C_{ma} A_{va} \sqrt{T_a R}}{A_a} x_v \tag{5.39}$$

and hence a different driving pressure ratio:

$$P_{rb} = \left(\sqrt{\left(\frac{D_b^2}{2}\right)^2 + D_b^2} - \frac{D_b^2}{2}\right)^{\frac{\gamma}{\gamma-1}} \tag{5.40}$$

with:

$$D_b = \frac{A_a}{A_b}\sqrt{\frac{\gamma+1}{\gamma-1}}\left(\frac{\gamma+1}{2}\right)^{\frac{1}{\gamma-1}} = 3.864\frac{A_a}{A_b} \text{ (for air)} \tag{5.41}$$

The above equations result in the steady-state driving pressures for the single-axis test rig model listed in Table 5.3. The pressures in the opposite chamber are determined assuming a zero resulting force acting on the actuator piston for motion with constant velocity. In this force balance the gravity load is taken into account.

It can be seen that the steady-state pressures depend on the direction of piston motion. Assuming now that during a representative working cycle the piston is moving back and forth with the same frequency it can be concluded that the steady-state pressures would tend to reach a level in-between the upper and lower bounds in Table 5.3. Using non-linear simulation models and experimental data it was found that due to the unequal charging and discharging conditions for the two actuator chambers the chamber pressures are closer to the lower bound (for a retracting actuator piston) and increase slightly when the piston is moving outwards. It has to be noted though that when the piston is mainly moving outwards the pressures approach the upper bound.

5.2.4 Dynamic Characteristics of Advanced Linearised Model

The frequency response of the advanced linear model for the pneumatic servo with an unequal area vertical actuator can be seen in Figures 5.7 and 5.8. Figure 5.7

shows the response for the three different piston positions listed in Table 5.1 and a retracting piston while Figure 5.8 shows the response for both directions of piston motion and piston position 1. The parameters of the dynamic model are similar to the ones used in the conventional linear model (see Table 5.2) corresponding to the dynamic characteristics of the single-axis test rig. It is clear that the response is dependent on the piston position and also on the direction of piston motion.

The equations for natural frequency ω_n, damping ratio ζ and ultimate gain K_{ult} of the open-loop pneumatic servo system resulting from the advanced linear model can easily be obtained by inserting Equations (5.32) to (5.34) into Equations (5.28) and (5.29) to give:

$$\omega_n = \sqrt{a_1} = \sqrt{\frac{n}{m}\left(\frac{P_{ai}A_a}{x+\frac{V_{\min}}{A_a}} + \frac{P_{bi}A_b}{(l-x)+\frac{V_{\min}}{A_b}}\right)} \tag{5.42}$$

$$\zeta = \frac{a_2}{2\sqrt{a_1}} = \frac{c_f\sqrt{n}}{2m^{3/2}}\left(\frac{P_{ai}A_a}{x+\frac{V_{\min}}{A_a}} + \frac{P_{bi}A_b}{(l-x)+\frac{V_{\min}}{A_b}}\right)^{-1/2} \tag{5.43}$$

$$K_{ult\,ext} = \frac{a_1 a_2}{b_{0ext}} = \frac{nc_f}{2mR\sqrt{T}C_d A_v}\frac{\left(\frac{P_{ai}A_a}{x+\frac{V_{\min}}{A_a}} + \frac{P_{bi}A_b}{(l-x)+\frac{V_{\min}}{A_b}}\right)}{\left(\frac{C_{ma}P_s}{x+\frac{V_{\min}}{A_a}} + \frac{C_{mb}P_b}{(l-x)+\frac{V_{\min}}{A_b}}\right)} \tag{5.44}$$

$$K_{ult\,ret} = \frac{a_1 a_2}{b_{0ret}} = \frac{nc_f}{2mR\sqrt{T}C_d A_v}\frac{\left(\frac{P_{ai}A_a}{x+\frac{V_{\min}}{A_a}} + \frac{P_{bi}A_b}{(l-x)+\frac{V_{\min}}{A_b}}\right)}{\left(\frac{C_{ma}P_a}{x+\frac{V_{\min}}{A_a}} + \frac{C_{mb}P_s}{(l-x)+\frac{V_{\min}}{A_b}}\right)} \tag{5.45}$$

As can be seen when looking at the natural frequency and the damping ratio as a function of piston position and direction of motion (Figure 5.9), these two parameters are still almost symmetrical with respect to the piston mid position. The lowest natural frequency and highest damping are still experienced in the middle of the stroke. At the end positions it has to be noted though that the natural frequency is slightly lower and the damping is slightly higher for a fully extended than for a fully retracted piston. This is due to the larger total volume at the fully extended position resulting in a slightly lower total stiffness. It has to be noted furthermore that both natural frequency and damping ratio are only position dependent as predicted by the conventional linear model. No direction dependency is envisaged.

The ultimate gain K_{ult} at the stability border though is position and direction dependent as can be seen in Figure 5.10. For positive valve opening (extension, that means charging chamber A and discharging chamber B) the ultimate gain is significantly lower than for negative valve opening (retraction, charging chamber B and discharging chamber A). Furthermore, for positive valve opening the ultimate gain increases with the actuator moving outwards while for negative valve opening the gain increases with the actuator moving inwards. The conclusion seems to be that the system can become unstable while moving outwards and becomes stable again when moving inwards. The difficulty with this interpretation of the results in Figure 5.10 is that when the system becomes unstable it starts oscillating in both directions with the control valve changing its direction of opening in quick succession hence switching between a stable and an unstable mode. Therefore, the only conclusion that can be drawn at this point is that the system is stable as long as the proportional feedback control gain is lower than the lowest ultimate gain (positive valve opening) and unstable when the proportional gain exceeds the highest ultimate gain (negative valve opening). That means that the system is most likely to become unstable when the piston is fully extended and not in the mid position as predicted by the conventional linear model.

Using the advanced linear model now to model again the equal area actuator with no gravity load yields the same natural frequency and damping ratio as the conventional linear model due to the fact that for this system the denominator of the open-loop transfer function which determines natural frequency and damping ratio is

the same in both models. The ultimate gain K_{ult} now becomes direction dependent as can be seen in Figure 5.11. This is caused by the numerator of the open-loop transfer function being a function of the flow conditions and the valve opening direction. The changes in gain with direction of piston motion are almost negligible though.

It is important to note that the advanced model predicts higher ultimate feedback gains than the conventional model so that the latter can still be safely recommended to be used when tuning a controller for a pneumatic servo with an equal area actuator and no gravity load. Using the conventional model as a design basis for such a system, stability can be guaranteed over the whole piston stroke and for both directions of motion. Yet, the full dynamic capabilities of the system cannot be exploited.

5.3 Design and Tuning of a State-Feedback Controller Based on the Linear Model

In the following the conventional and the advanced linear model will be used as a basis for controller design and tuning. A controller often used for positioning control of servo actuation systems is a linear state-feedback controller. Position, velocity and acceleration (the canonical system state) of the system to be controlled are measured or derived from measured data and used to compute the controller input. The closed-loop transfer function of a pneumatic servo system under state-feedback control (see Figure 5.12) is given by:

$$F(s)=\frac{X(s)}{U(s)}=\frac{K_p b_0}{s^3+(a_2+K_a b_0)s^2+(a_1+K_v b_0)s+K_p b_0} \tag{5.45}$$

When tuning the controller the poles of the closed-loop transfer function are placed in order to obtain the desired dynamic behaviour of the closed-loop system. The above transfer function is of third order, therefore three poles have to be placed. Choosing the settling time T_{sett} and damping ratio ζ of the closed-loop system the poles can be placed as follows:

$$s_{1/2}=-\omega_n\zeta\pm i\omega_n\sqrt{1-\zeta^2}\,,\quad s_3=-10\omega_n\zeta\quad\text{with }\omega_n=\frac{4}{T_{sett}\zeta} \tag{5.46}$$

This above choice of poles results in the following explicit relationships for the state-feedback gains:

$$K_p = \frac{10\omega_n^3\zeta}{b_{0(ext/ret)}} = \frac{640}{T_{sett}^3\zeta^2 b_{0(ext/ret)}} \tag{5.47}$$

$$K_v = \frac{\omega_n^2\left(1+20\zeta^2\right)-a_1}{b_{0(ext/ret)}} = \frac{\frac{16}{T_{sett}^2}\left(\frac{1}{\zeta^2}+20\right)-a_1}{b_{0(ext/ret)}} \tag{5.48}$$

$$K_a = \frac{12\omega_n\zeta - a_2}{b_{0(ext/ret)}} = \frac{48\frac{1}{T_{sett}} - a_2}{b_{0(ext/ret)}} \tag{5.49}$$

(Another easy way of synthesising the controller gains is to use the *place*-algorithm in MATLAB or similar software.) As can be seen from Equations (5.47) to (5.49) all feedback gains are a function of the open-loop transfer function numerator b_0 and hence not only position but also direction of piston motion dependent. Using the above relationships and the dynamic parameters of the single-axis test rig (see Table 5.2) a state-feedback controller for a pneumatic servo system with an unequal area vertical actuator has been tuned. The resulting state-feedback gains as a function of piston position and direction of motion can be found in Figure 5.13. As an example the response time is chosen to be T_{sett} = 0.4 s and the damping ratio is set to ζ = 0.4. It can be seen that the highest proportional, velocity and acceleration gains occur around the piston mid position. The negative values of the velocity gains indicate a decrease in damping due to velocity feedback. The direction of motion and piston position dependency of the controller gains needed to provide the desired system response can be clearly seen.

5.3.1 Step Response of the Linear Model

To further investigate the dynamic characteristics of the pneumatic servo system step response results have been performed. First, the advanced linear model of the servo with an equal area actuator and no gravity load was used to tune the state-feedback controller. The sets of controller gains tuned for positions 1 to 3 as defined in Table 5.1 can be found in Table 5.4. As in the previous examples, the dynamic parameters correspond to the ones of the single-axis test rig (Table 5.2).

Figure 5.14 to 5.16 show the step responses of the linear model at the piston positions 1 to 3 for all three sets of controller gains, respectively. The framed graphs show the step responses for which the controller is tuned. For comparison the ideal system response that means the response the control system is tuned for is plotted as well. It can be observed that the simulated step response at all three piston positions and with all three sets of controller gains is as required and in no case more oscillatory. A similar step response can be obtained using the conventional linear model to synthesise the controller gains. The step response results therefore confirm the findings from the analysis in Section 5.2. Thus, for a system with equal area actuator and no gravity load the conventional model is sufficient as a basis for controller design.

Performing the same tuning procedure now assuming a servo with an unequal area actuator and additional gravity load results in the feedback gains listed in Table 5.5. As can be seen the resulting feedback gains not only depend on the actuator piston position but also on its direction of motion. The simulated step response results using the advanced linear model and the feedback gains in Table 5.5 can be seen in Figures 5.17 and 5.18. Again the framed graphs depict the response of the linear model for which the controller is tuned.

It was found that all sets of controller gains in Table 5.5 obtained assuming **negative** valve opening (and hence retraction of the actuator piston) result in an unstable or highly oscillatory step response of the linear model assuming **positive** valve opening (extension of actuator piston) almost independent of the piston position as shown in Figures 5.17 and 5.19 for one set of controller gains. Interestingly, a similar oscillatory response of the control system can be observed using the controller gains based on the conventional linear model. In this case, the step response of the linear model is also unstable when extending the actuator.

For this specific servo configuration a step response of the linear model which is guaranteed stable for all piston positions and directions of motion can only be achieved with controller gains resulting from the advanced linearised model assuming positive valve opening (extension of actuator piston) as can be seen in Figures 5.18 and 5.20. In this case the system response is generally more damped than it is tuned for.

The conclusion that can be drawn from this investigation is that in the case of pneumatic servos with unequal quiescent chamber pressures the direction dependency can be more important to the system dynamics than the position dependency as it is the case for the servo system under consideration. Therefore, changing the direction of valve opening (piston motion) can result in a significant change in the system dynamics and has to be taken into account when designing a linear feedback controller. As a consequence, the conventional model might not be a sufficient basis for controller design and it can be necessary to employ the advanced linearised model in order to determine the dynamically worst conditions and tune the controller accordingly.

5.3.2 Step Response of the Non-Linear Model

The results and conclusions presented above are only based on a linearised analysis. The validity of these results depends on the ability of the advanced linearised model to predict the dynamic behaviour of the highly non-linear pneumatic servo and has to be determined separately.

Comparing therefore the step response of the linear with the step response of the non-linear model for all sets of controller gains listed in Table 5.5 yields that the non-linear model response does for none of the controller gains exhibit the highly oscillatory behaviour the linear model exhibits when controller gains for a retracting actuator piston are applied to a system with extending actuator piston. This fact is illustrated in Figure 5.21 for the set of controller gains tuned for position 1 and a retracting actuator piston.

Nevertheless, comparing the response of the non-linear model with the ideal system response (ideal refers to the response the control system is tuned for) it can be seen that when using controller gains determined for an retracting motion of the actuator piston the extension overshoots of the non-linear system are significantly larger than the ideal ones while the retraction overshoots are satisfactory. The explanation for this phenomenon can be found by looking at the characteristics of the advanced linear model. As a first approximation, the non-linear response for any specific set point can be interpreted as a superposition of the two related direction

dependent step responses of the advanced linear model as depicted in Figure 5.22. When the non-linear system moves outwards it follows the highly-oscillatory response of the linear model for extension. When the non-linear system moves inwards it follows the damped response of the linear system for retraction. Hence, the non-linear response exhibits large outwards overshoots and rather small inwards overshoots.

Therefore, the advanced linear model predicts the dominant non-linear characteristics of the pneumatic servo correctly despite the fact that two phenomena of the non-linear dynamics have not been included in the linearised analysis: the continuously with the piston position changing stiffness of the charged actuator chambers and also the changing chamber pressures. As can be seen though from a comparison between linear and non-linear response, these two effects add damping and are therefore not critical for the dynamic analysis and hence for controller design.

Thus, applying controller gains based on the advanced linear model yields a response of the non-linear system which in any case is more damped than the response the control system is tuned for. Therefore, any instability problem can be ruled out by analysing the relatively simple advanced linear model. Hence, this model represents a sufficient tool for feedback controller design for this highly non-linear system.

In Figure 5.23 a comparison between experimental and simulation step response results is presented. It confirms the validity of the non-linear simulation model presented in Chapter 4 and as expected proves the usefulness of the advanced linear model as a basis for controller synthesis. The most significant difference between simulation and experiment is a slightly larger steady-state error in the experimental results. The reason for this slight discrepancy is leakage in the pneumatic actuator and valve and also stiction. Both effects have not been included in the simulation model.

5.3.3 STEP RESPONSE OF THE *PARAMETER UPDATE* MODEL

As mentioned before, since the two effects of changing stiffness and changing actuator chambers pressures are not included in the advanced linearised model they are investigated in more detail in this section. In order to distinguish between these two effects an additional model has been developed which is called the *parameter update* model. It takes account of the changing stiffness of the actuator chambers without modelling the changing chamber pressures. Its transfer function is as follows:

$$F(x,dir,s)=\frac{X(s)}{U(s)}=\frac{b_0(x,dir)}{s\left(s^2+a_2 s+a_1(x)\right)} \tag{5.50}$$

The dynamic parameters in the transfer function F are updated during simulation depending on the current system state. Therefore, the only difference between the full non-linear model and the parameter update model is the effect of the changing actuator chamber pressures not taken into account by the update model. In Figure 5.24 step response results of the linear, the non-linear and the parameters update model are shown. As can be seen from a comparison between the response of the linear and the parameter update model the changing stiffness adds damping to the system dynamics. Additional damping is than added by the changing chamber pressures as a comparison between the responses of the non-linear and the parameter update model indicates. The latter observation corresponds to the results presented by Burrows and Webb (1969) who also states that the effects arising from the increase in downstream pressure for charging and the decrease in upstream pressure for discharging add damping to the dynamic response of the pneumatic servo. According to Burrows these effects are so small though that they can be neglected (see Section 5.1). This is also validated by the results in Figure 5.24. The main additional damping effects arise from the changing chamber stiffness and only a small part results from the changing chamber pressures.

To conclude the analysis conducted in this chapter, the advanced linear model describes all the significant dynamic phenomena of a pneumatic servo with unequal quiescent chamber pressures e.g. due to unequal area actuators or additional load. It is therefore sufficient to analyse the dynamics of such a system.

5.3.4 Guidelines on How to Choose the Right Linearisation Conditions for Servo Controller Design

It is worth mentioning that when using the results obtained in the above investigation, the specific conclusions about the dynamically worst conditions arising from the advanced linearised model are only valid for the specific servo system considered here. This includes the component sizes and the dynamic parameters. For other systems with unequal area actuators or unsymmetric load (e.g. gravity) it can be recommended to proceed as follows:

1. Determine the steady-state actuator chamber pressures by taking into account the actuator piston area ratio between chamber A and B and also possible external loads as demonstrated in Section 5.2.
2. Determine the dynamic parameters of the advanced linearised model as a function of piston position and valve opening over the whole piston position range space.
3. Determine the ultimate gain K_{ult} at the stability border as a function of piston displacement and direction of valve opening as described in Section 5.2 and choose the conditions with the lowest ultimate gain as a basis for controller design.

Following the above procedure one can always be sure that the dynamic response of the non-linear system will not be less damped than the response of the advanced linear system no matter whether direction of motion, piston displacement or actuator chamber pressures change. Stability of the highly non-linear pneumatic servo system can therefore be guaranteed by following this simple procedure.

TABLES

Table 5.1 - Actuator piston positions

piston position	displacement [mm]	fractional displacement [fraction of piston stroke]
1	6	1/5
2	15	1/2
3	24	4/5

Table 5.2 - Numerical data representing the single-axis pneumatic test rig

	equal area horizontal actuator	unequal area vertical actuator
A_a [m^2]	$412.3 * 10^{-6}$	$490.9 * 10^{-6}$
A_a [m^2]	$412.3 * 10^{-6}$	$412.3 * 10^{-6}$
P_a [bar]	5.25	5.49
P_b [bar]	5.25	5.57
P_s [bar]	6.5	6.5
C_d	0.70	0.70
A_v [m^2]	$0.81 * 10^{-6}$	$0.81 * 10^{-6}$
V_{min} [l]	$1.7 * 10^{-3}$	$1.7 * 10^{-3}$
n	1.4 (adiabatic)	1.4 (adiabatic)
k [N/(m/s)]	100	100
m [kg]	1.82	1.82

Table 5.3 - Steady-state chamber pressures for unequal area vertical actuator

	extension	retraction
P_a [bar]	6.50	6.50
P_b [bar]	5.85	5.49
P_s [bar]	6.00	5.57

Table 5.4 - State-feedback gains for pneumatic servo with equal area horizontal actuator (T_{sett} = 0.4 s, ζ = 0.4)

	position 1	position 2	position 3
K_p	0.2056	0.2743	0.2056
K_v	-0.0485	-0.0478	-0.0485
K_a	0.0002	0.0003	0.0002

Table 5.5 - State-feedback gains for pneumatic servo with unequal area vertical actuator (T_{sett} = 0.4 s, ζ = 0.4)

	retraction			extension		
	position 1	position 2	position 3	position 1	position 2	position 3
K_p	0.2341	0.2907	0.2151	0.1729	0.2407	0.1993
K_v	-0.0314	-0.0458	-0.0460	-0.0380	-0.0379	-0.0427
K_a	0.0002	0.0003	0.0002	0.0002	0.0002	0.0002

FIGURES

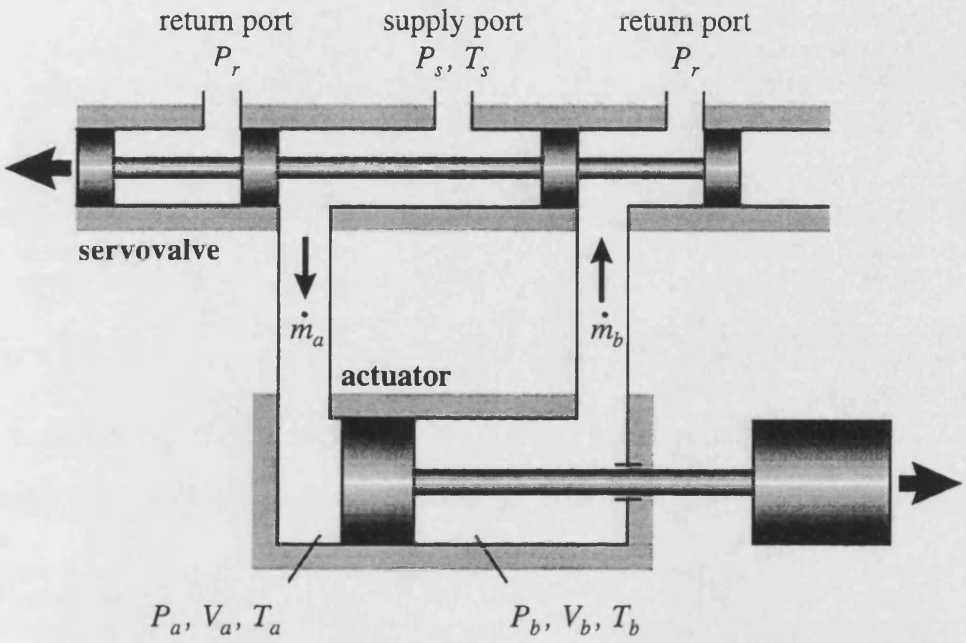

Figure 5.1 - Schematic of pneumatic servo mechanism

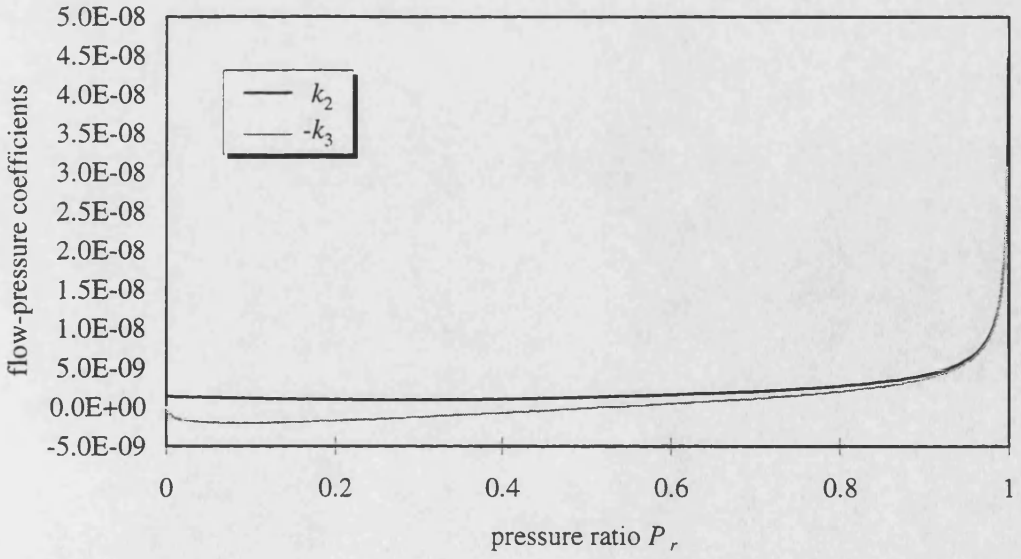

Figure 5.2 - Variations of flow-pressure coefficients k_2 and k_3 with pressure ratio P_r

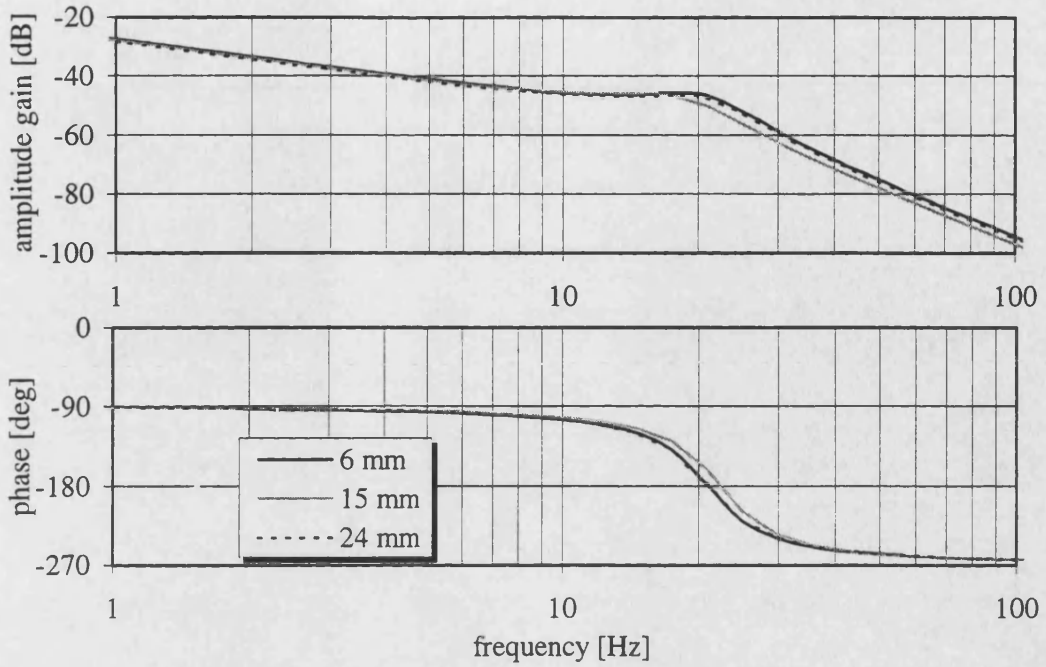

Figure 5.3 - Frequency response of linear model of pneumatic servo with equal area actuator and no gravity load (actuator piston rectracting)

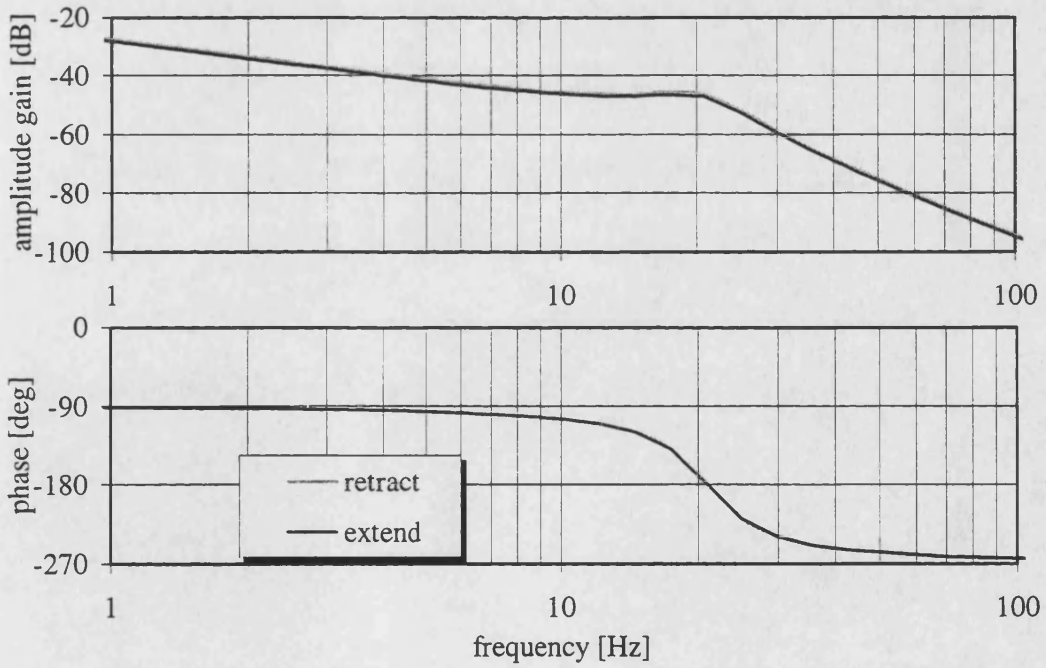

Figure 5.4 - Frequency response of linear model of pneumatic servo with equal area actuator and no gravity load (piston position 1 (6 mm))

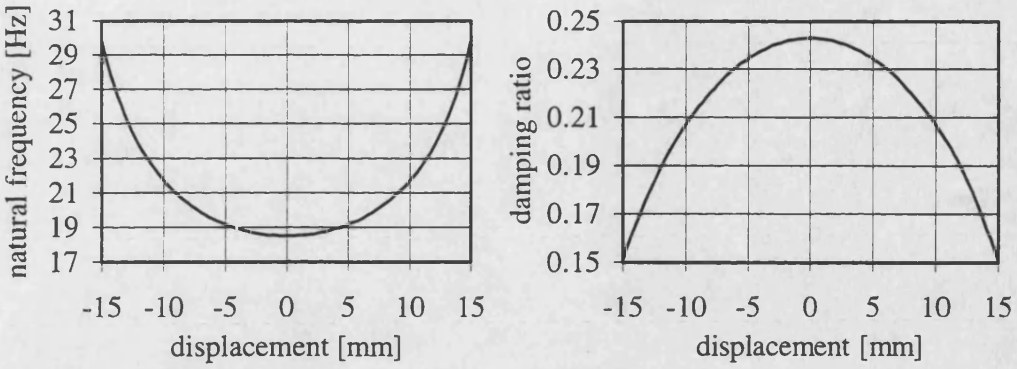

Figure 5.5 - Natural frequency and damping ratio of linear model of pneumatic servo with equal area actuator and no gravity load

Figure 5.6 - Ultimate proportional feedback gain K_{ult} of linear model of pneumatic servo with equal area actuator and no gravity load

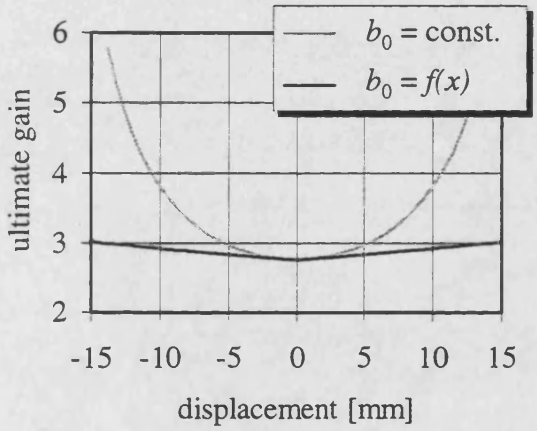

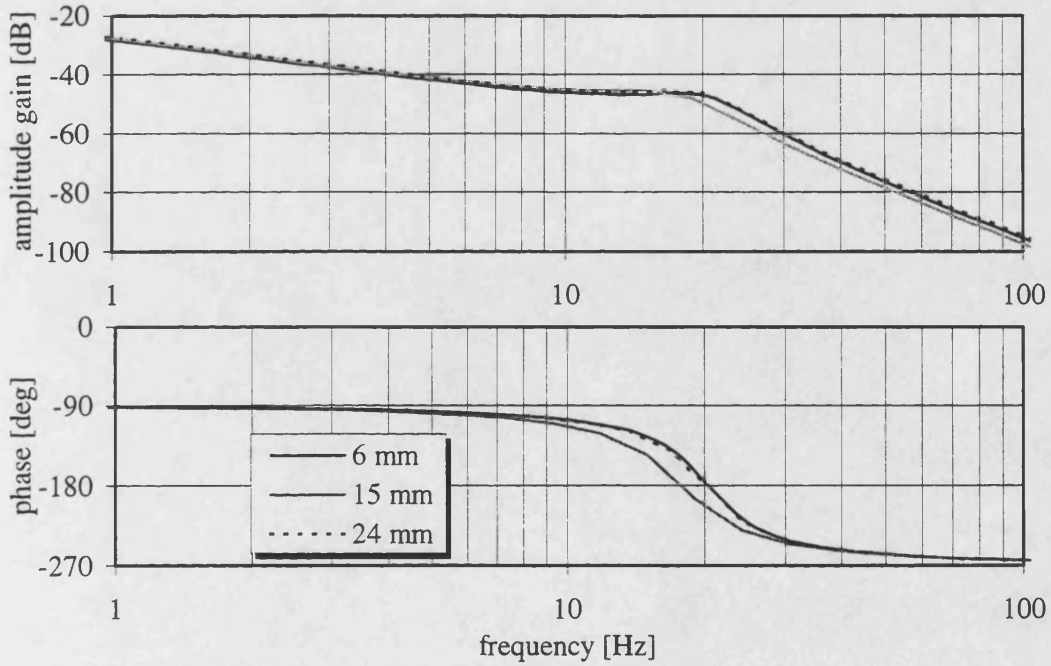

Figure 5.7 - Frequency response of linear model of pneumatic servo with unequal area actuator and gravity load (actuator piston rectracting)

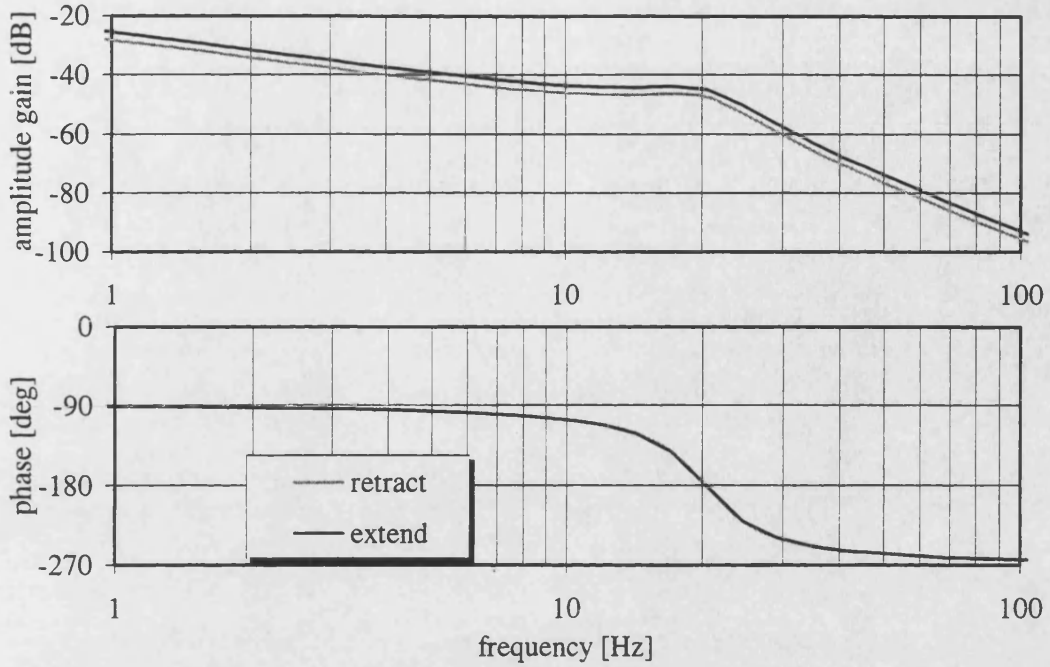

Figure 5.8 - Frequency response of linear model of pneumatic servo with unequal area actuator and gravity load (piston position 1 (6 mm))

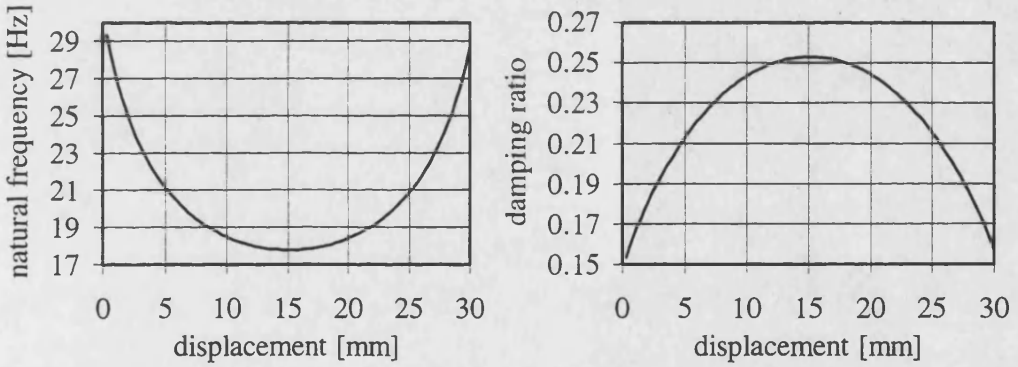

Figure 5.9 - Natural frequency and damping ratio of linear model of pneumatic servo with unequal area actuator and gravity load

Figure 5.10 - Ultimate proportional feedback gain K_{ult} of linear model of pneumatic servo with unequal area actuator and gravity load

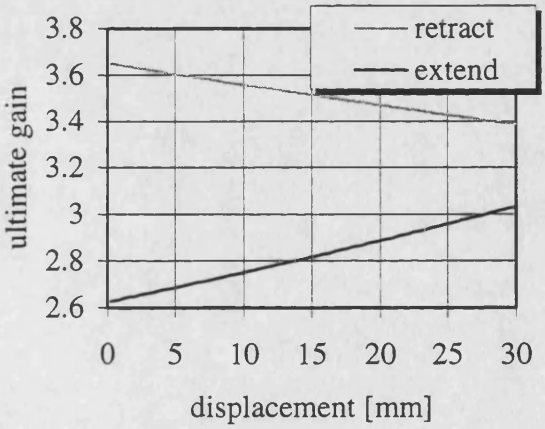

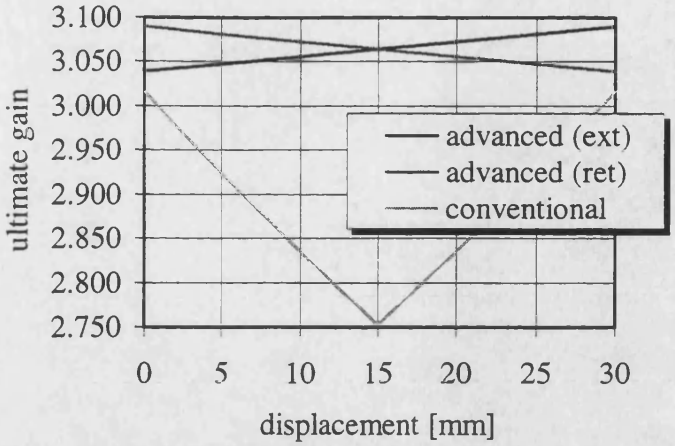

Figure 5.11 - Ultimate proportional feedback gain K_{ult} of linear model of pneumatic servo with equal area actuator and no gravity load

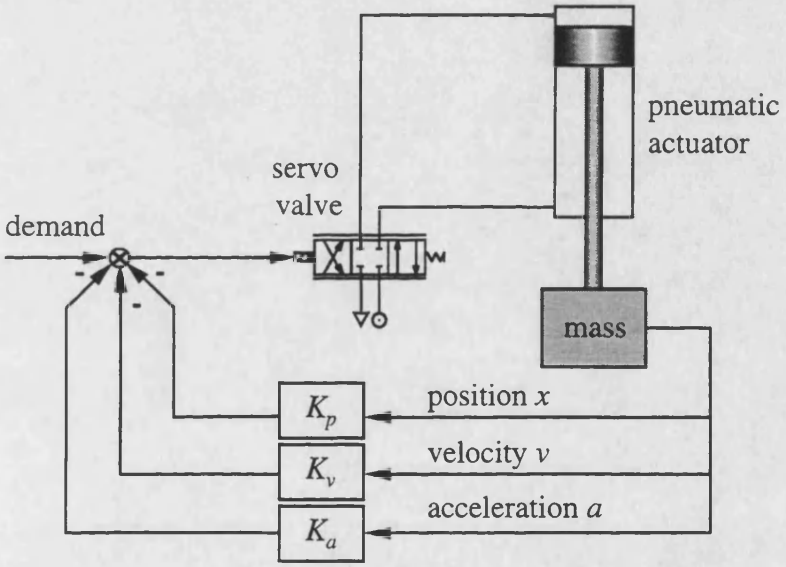

Figure 5.12 - State-feedback control system

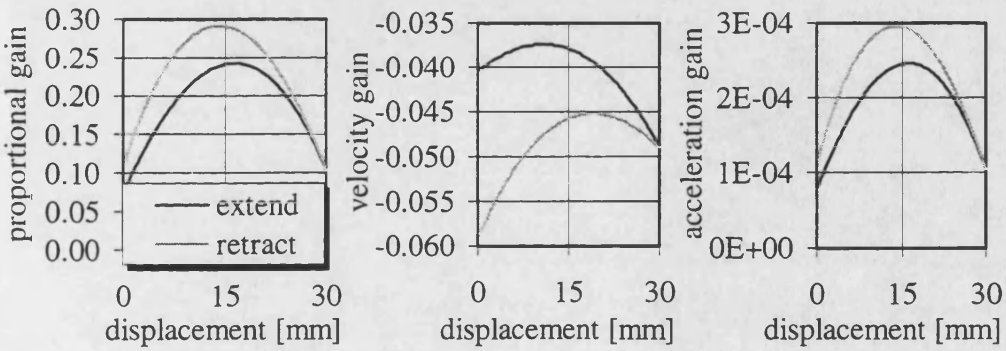

Figure 5.13 - State-feedback control gains as a function of actuator piston displacement and direction of piston motion

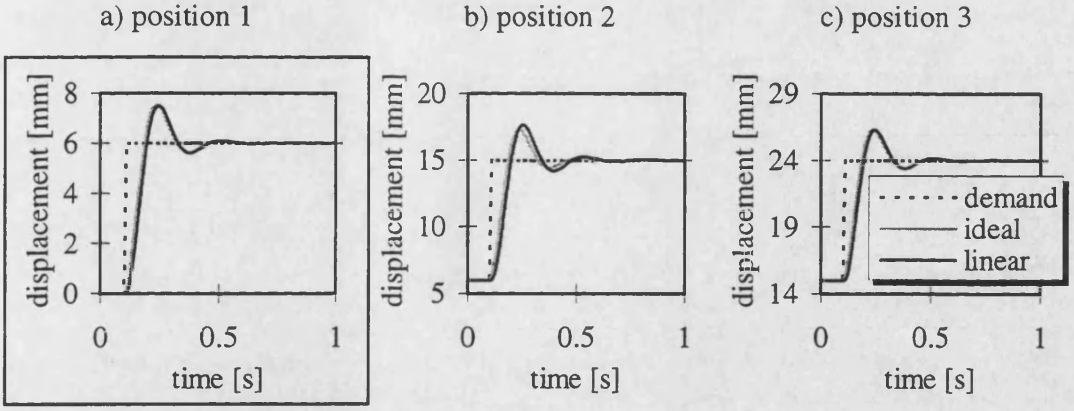

Figure 5.14 - Step response of linear model of pneumatic servo with equal area actuator and no gravity load (controller tuned for position 1 (6 mm))

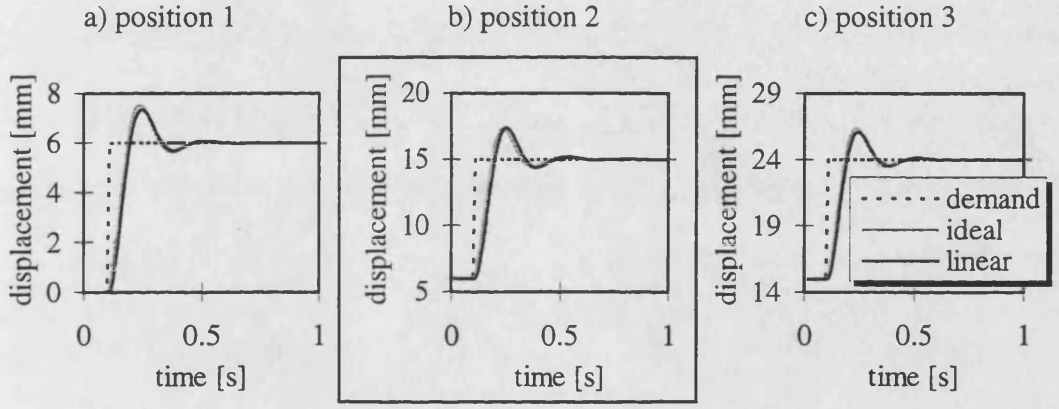

Figure 5.15 - Step response of linear model of pneumatic servo with equal area actuator and no gravity load (controller tuned for position 2 (15 mm))

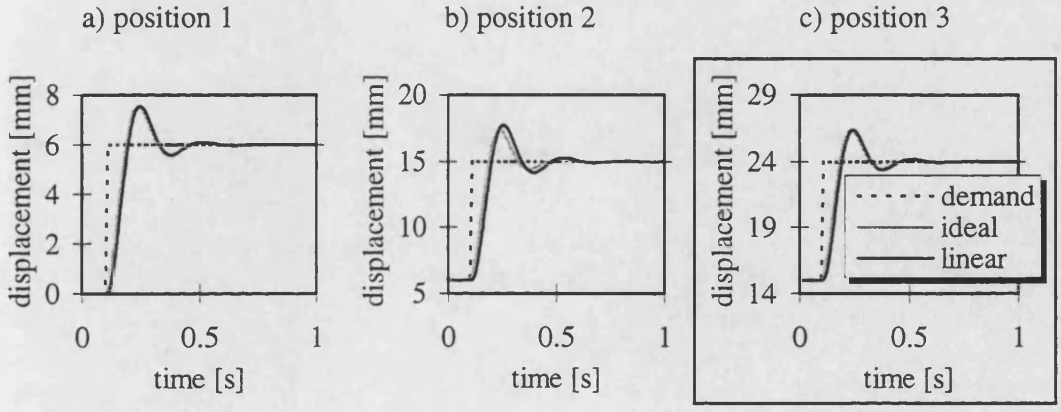

Figure 5.16 - Step response of linear model of pneumatic servo with equal area actuator and no gravity load (controller tuned for position 3 (24 mm))

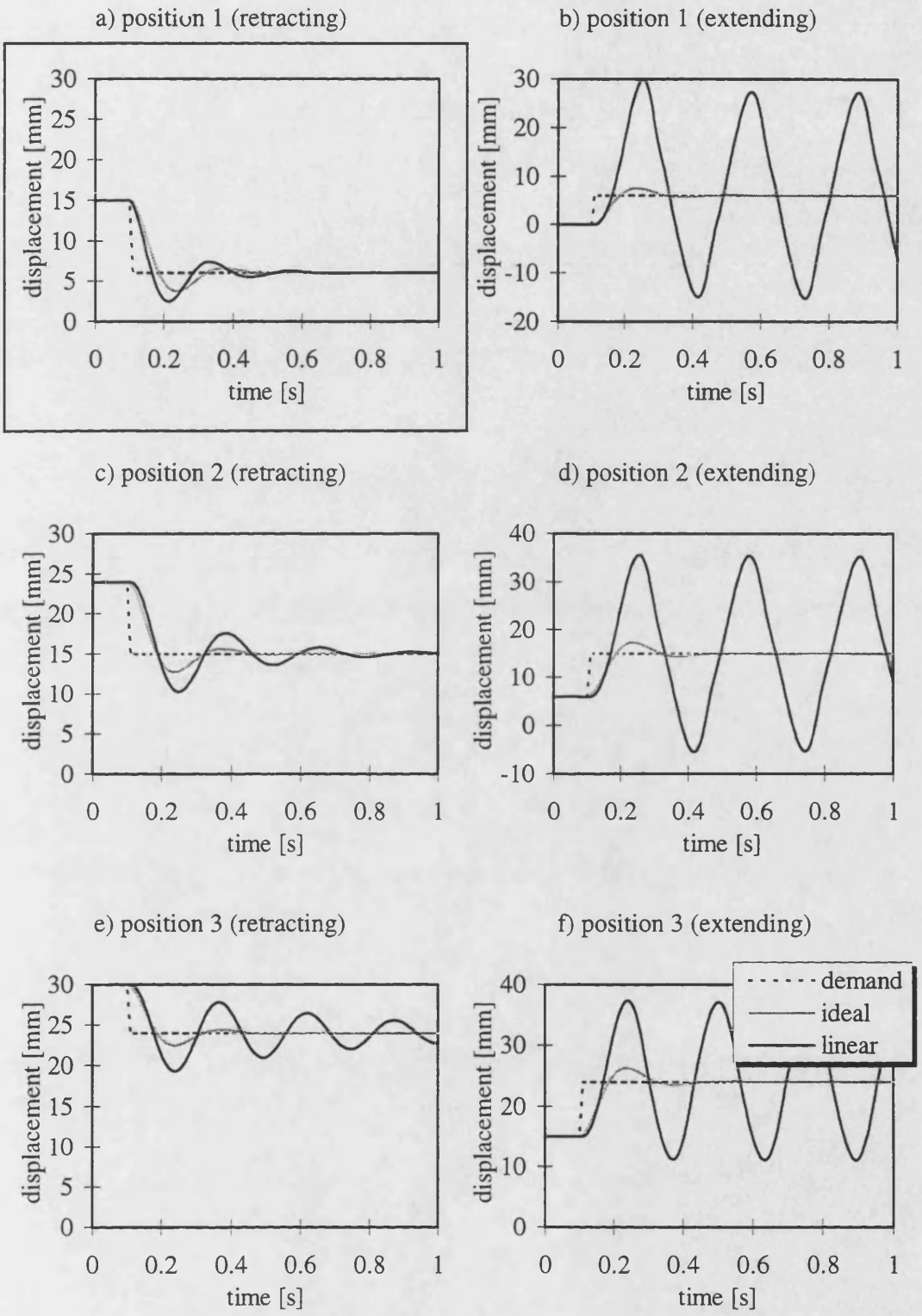

Figure 5.17 - Step response of linear model of pneumatic servo with unequal area actuator and gravity load (controller tuned for position 1 (6 mm), retraction)

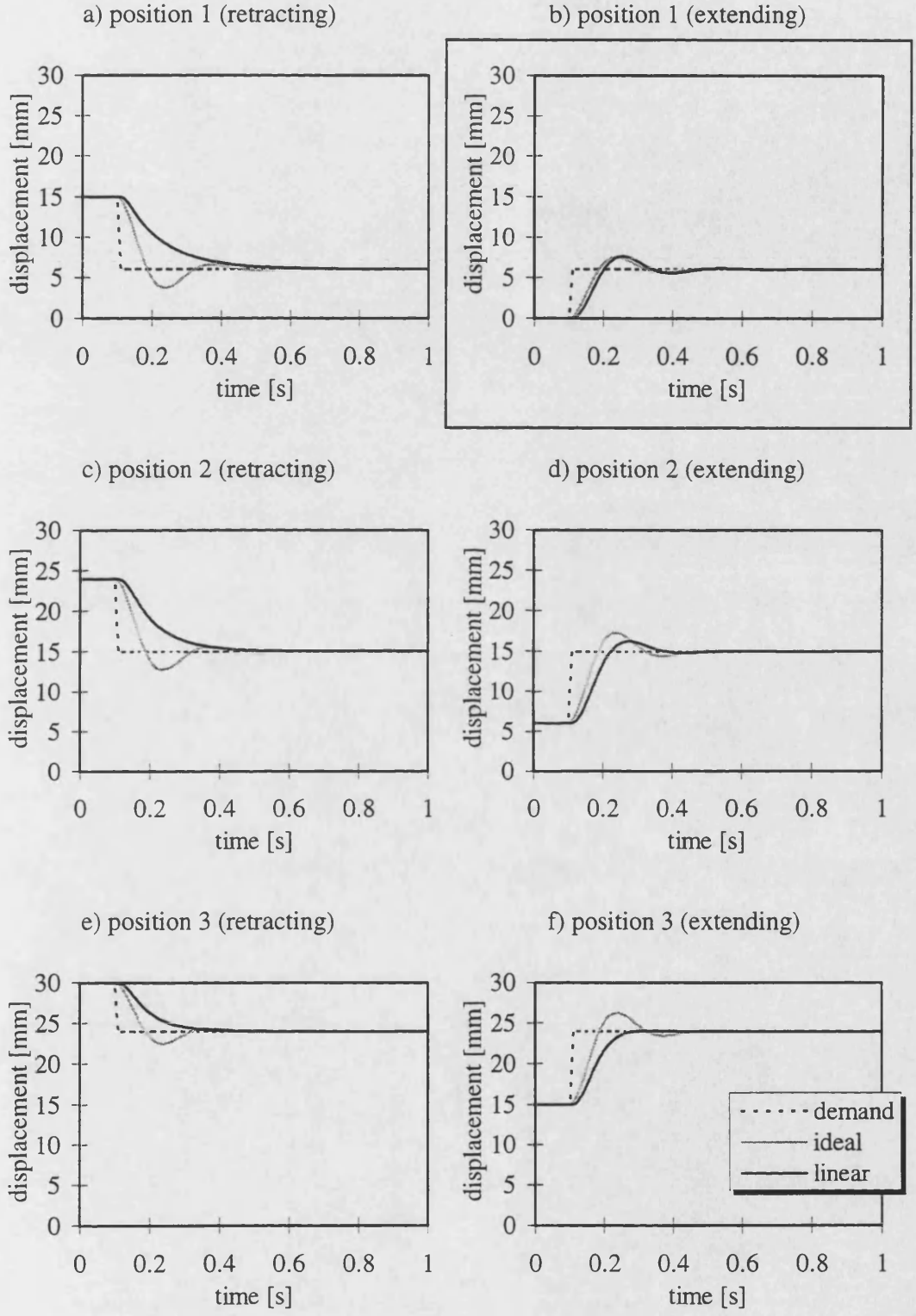

Figure 5.18 - Step response of linear model of pneumatic servo with unequal area actuator and gravity load (controller tuned for position 1 (6 mm), extension)

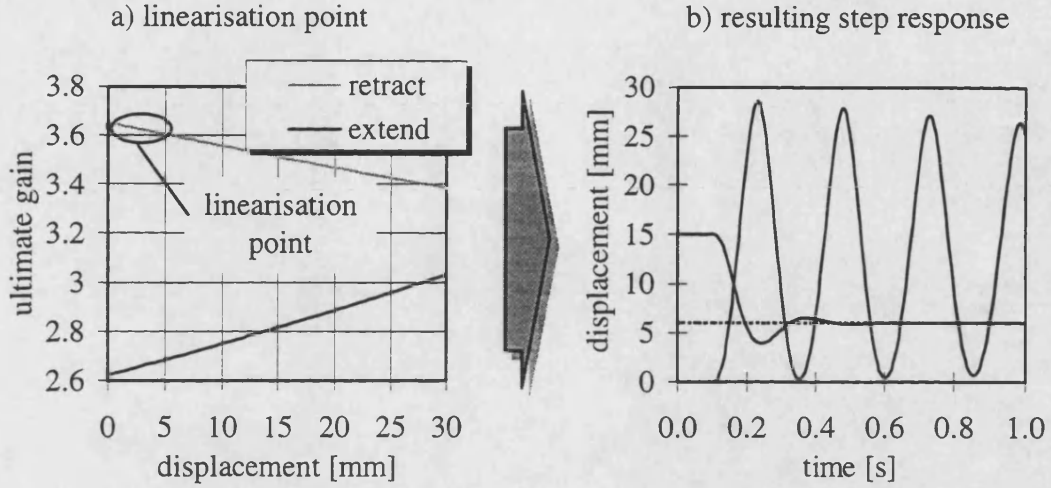

Figure 5.19 - Step response of linear model with controller tuned for position 1 (6 mm), retraction

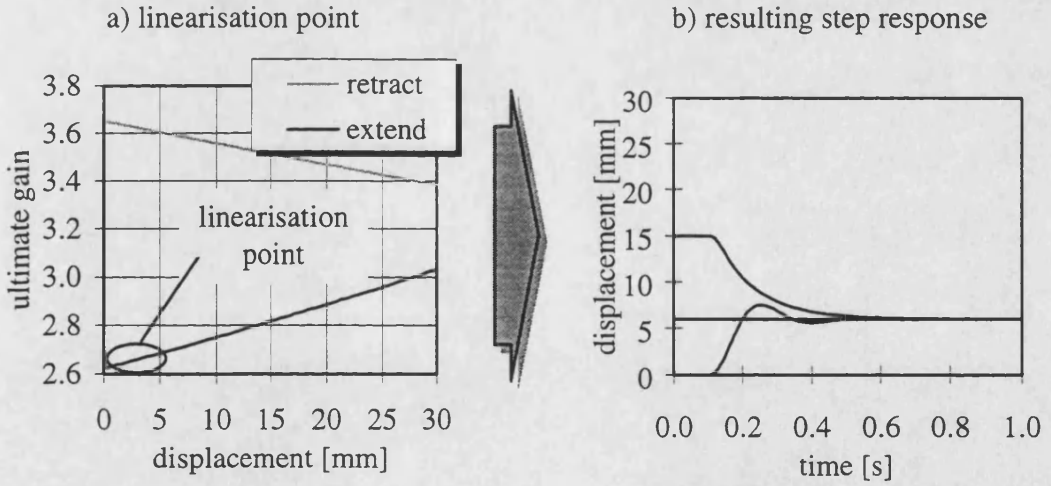

Figure 5.20 - Step response of linear model with controller tuned for position 1 (6 mm), extension

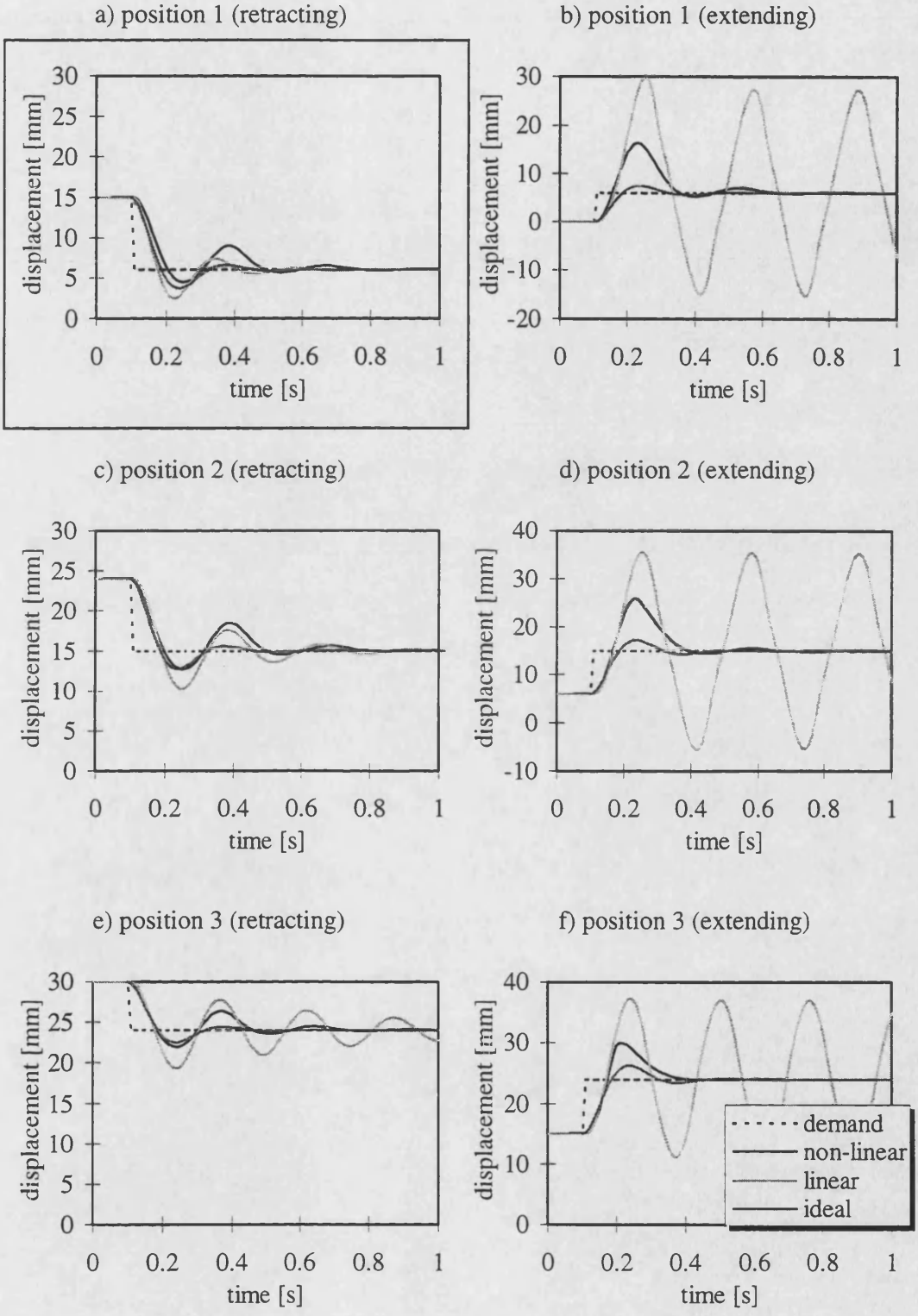

Figure 5.21 - Step response of linear and non-linear model of pneumatic servo with unequal area actuator and gravity load (controller tuned for position 1 (6 mm), retraction)

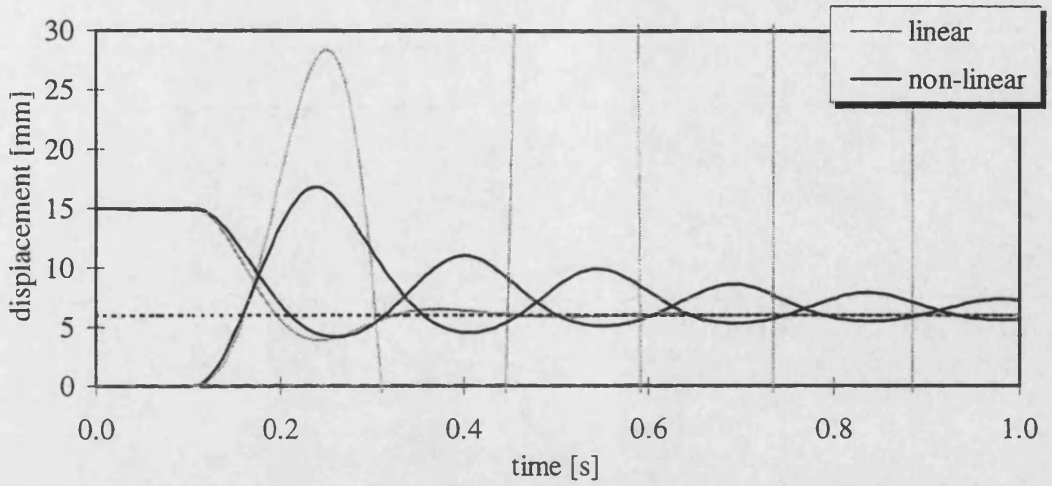

Figure 5.22 - Comparison of step response of linear and non-linear model

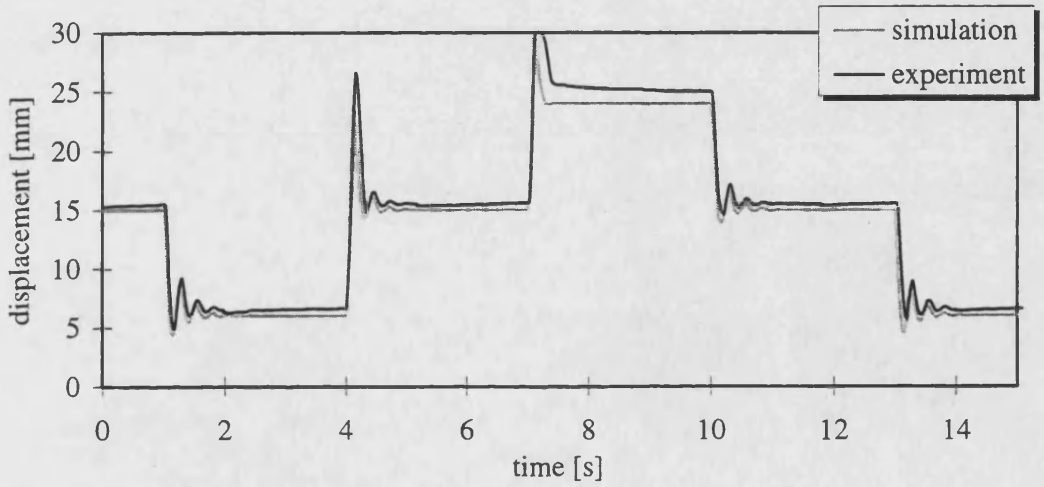

Figure 5.23 - Comparison of simulation and experimental results

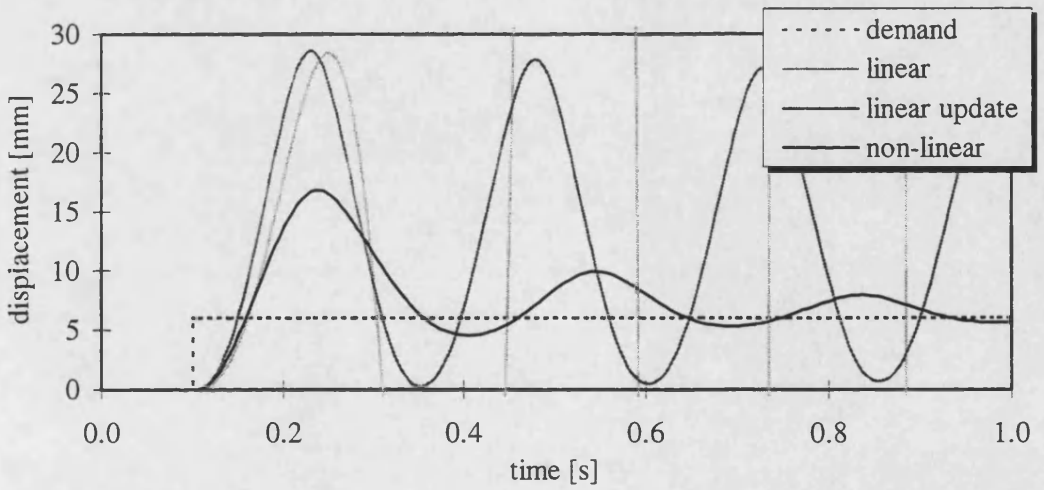

Figure 5.24 - Comparison of step response of linear, linear update and non-linear model

6 SLIDING MODE CONTROL

Sliding Mode control is a specific type of Variable Structure control which has, historically speaking, received most attention of the almost unlimited supply of Variable Structure control laws. The reason for the particular interest in sliding mode control lies in its many advantages like the insensitivity to plant parameter variations, the excellent disturbance rejection capabilities and the simplicity of the control algorithms. Nevertheless, serious difficulties can be encountered when applying Sliding Mode control to real physical systems.

The following chapter will introduce the basic concepts of Sliding Mode control (SLMC) in detail. Furthermore, a comprehensive overview of various aspects of sliding mode control, its advantages and disadvantages and also its discrete realisation will be given. Moreover, this chapter reviews and discusses most relevant references which deal with SLMC. The application of SLMC to a pneumatic positioning servo mechanism will be investigated then in Chapters 7 to 9.

6.1 CONTROL OF UNCERTAIN SYSTEMS

When modelling a physical plant for controller design purposes the degree of accuracy of this model is in general limited by the fact that either the dynamic behaviour of the plant is not fully known or that certain dynamics have to be neglected in order to reduce the complexity of the model. Furthermore, the dynamic characteristics of the plant might change during operation. When using a dynamic model of the plant now as a basis for controller design the resulting modelling inaccuracies (in form of parametric uncertainties or unmodelled dynamics) can have a significant influence on the dynamic behaviour of a closed-loop control system. Consequently, the need arises to take account of these uncertainties which are not part of the nominal system model and hence are considered as being external disturbances by a controller based on the nominal model. The two major and complementary approaches to dealing with these uncertainties are:

- *adaptive control* and
- *robust control.*

6.1.1 ADAPTIVE CONTROL

One way an adaptive controller deals with model uncertainties is by updating the system model during operation based on measured performance using for instance an on-line parameter estimation technique. Another possibility is to update the closed-loop feedback gains based on the difference in response between the nominal or reference model and the plant response. The former approach is called *self-tuning control* the latter is referred to as *model reference adaptive control* (MRAC).

Self-tuning controllers use input and output signals to and from the plant to estimate the plant dynamics and update the parameters of a chosen dynamic plant model. A controller based on this dynamic plant model is then designed on-line which in general explicitly places the poles of the closed-loop system to give the desired dynamic characteristics. In most cases, the only use for the estimated plant model is to determine the controller gains. In some cases, the system model can also be used for condition monitoring purposes (Pollmeier (1997)). A comprehensive review of self-tuning controllers based on model parameter identification and consecutive controller gain computation by means of pole-placement or eigenstructure assignment methods can be found in Åström and Wittenmark (1980), some examples for the application of these controllers to pneumatic systems can be found in Bobrow and Jabbari (1991), Shih and Huang (1992), McDonell and Bobrow (1993) and Shih and Tseng (1994).

In model reference adaptive control (MRAC) a reference model describing the desired dynamic behaviour of the plant to be controlled is excited by the same external inputs as the adjustable closed-loop system including plant and adjustable controller. The difference between the dynamic state of the reference model and that of the adjustable system is then used by an adaptation algorithm to modify the control parameters or to generate an auxiliary control signal in order to minimise this difference. An excellent introduction into MRAC has been given by Landau (1979) and Slotine and Li (1991). The application of MRAC to pneumatic systems is for instance described by Tse and Leung (1990), Araki and Yamamoto (1990) and Fok *et al* (1995).

It has been shown by Landau (1981) that both approaches are in some cases equivalent and both control methods have resulted in excellent closed-loop performance in numerous applications as reported in a vast and rapidly growing number of publications (for instance Walters and Byoumi (1982), Edge and Figueredo (1987), Vaughan and Plummer (1990) and Anand *et al* (1993)).

Nevertheless, both methods entail certain drawbacks. Self-tuning control methods are often based on a recursive least-square identification algorithm which requires an input signal sufficiently rich in information to obtain accurate predictions of the system parameters. Moreover, in general a large number of samples have to be evaluated by the identification algorithm which often restricts the application of self-tuning controllers to plants which only change slowly over time.

In comparison to self-tuning control, one of the main advantages of model reference adaptive controllers is their high speed of adaptation. One of the main problems though is to choose an appropriate reference model whose dynamics can be followed by the plant to be controlled. Also, when synthesising the control algorithm the common inclusion of an integrator in the control law often requires persistent excitation or other measures in order to avoid integrator wind-up.

6.1.2 Robust Control

The concept of robust control was first introduced by Bode (1945). It was then basically neglected though until Horowitz introduced the theory of quantitative feedback theory in 1963. Unlike adaptive control, in robust control the system model is neither identified on-line nor used to update the controller gains. A typical robust controller consists of a nominal part based on a nominal plant model and an additional term dealing with model uncertainties. One approach to robust control is the so-called *Variable Structure Control* (VSC) in particular when it operates in *sliding mode*. Although by definition, sliding mode control (SLMC) belongs to the group of robust controllers, it significantly differs from other robust control methods. It not only guarantees stability and robustness to parameter variations, non-linearities and external disturbances but also precisely defines the dynamic properties of the closed-loop system by means of a so-called *sliding surface*. In VSC dynamic

uncertainties in the system model are dealt with by forcing the system state onto this sliding surface invariable of unmodelled dynamics or external disturbances. Against the background of MRAC, the sliding surface can also be interpreted as a reference model describing the desired dynamic system response. (In this context, de Almeida (1993) showed that using hyperstability theory (Landau (1979)) and choosing an integrator-free control law results in a similar control algorithm to the one obtained by using VSC theory.)

The dynamic phenomenon of a sliding mode was first envisaged in control systems using relay elements. It was initially regarded as being highly undesirable because the high speed switching action tended to wear out the relay element contacts. Only when the theory of Variable Structure systems was developed in the 1950's the advantages of sliding mode control were better understood. In this context sliding mode control can be classified as a specific mode of operation of VSC systems. However, practical application of the theory was and still is today limited by the lack of suitable high speed switching devices. Tsypkin (1984) presented a very thorough investigation into the occurrence of sliding modes in relay control systems and showed that *perfect* dynamic performance of the control system can in principle be achieved even in the presence of arbitrary parameter inaccuracies assuming full state switching. This perfect performance, however, is obtained at the price of extremely high control activity.

The classical VSC methodology was mainly developed in the literature from the Soviet Union by Emal'yanov (1959), Taran (1964) and Barbashin and Gerashchenko (1965). It was later described and extended by Itkis (1976) and Utkin (1978). The basic mathematical ideal was derived by Filippov (1960) constructing the equivalent dynamics while Drazenovic (1969) first established early results on the invariance of Variable Structure systems to a class of disturbances and parameter variations. An early survey paper by Utkin (1977) gives reference to many of these first Russian contributions available in English translation. More recent comprehensive survey papers and books have been written by Utkin (1983, 1987), Bühler (1986), de Carlo *et al* (1988), Zinober (1990) and Hung *et al* (1993).

As mentioned above, SLMC forces the system state onto a sliding surface. Once the system state has reached this sliding surface and the so-called *sliding mode*

has been established the system dynamics are then only determined by the dynamics of the sliding surface which in general are of a lower order than the plant dynamics. A sliding mode can be reached by switching between different controller structures depending on the position of the dynamic state of the system relative to the sliding surface or switching manifold in the state space. The individual controller structures may be unsatisfactory when used as fixed controllers over the whole operating space and may even result in an unstable closed-loop system response when used as such. Nevertheless, in certain regions of the state space these controller structures might have desirable properties. For instance, dynamically unstable systems often exhibit a very fast response which might be desirable in certain subspaces of the state space but not over the whole working space. The switching function $\sigma(x)$ determining the change of controller structure is a function of the dynamic states of the plant to be controlled (Itkis (1976)). Usually, there are two different types of controller structures used to achieve sliding mode. In one control algorithms the gains of a state feedback controller are switched according to the switching function. These algorithms are called switched gains algorithms. Alternatively, the controller output can be switched according to the sign of the switching function. These relay-like algorithms are called on/off or relay switching algorithms.

Assuming an ideal control plant the existence of a sliding mode requires a switching of the controller structures at an infinite frequency. Obviously, this infinite switching frequency cannot be obtained in real applications especially not with digital control systems. As a result, a high-frequency oscillation of the system state around the sliding surface can be observed. This in practice undesirable *chattering* not only leads to excessive wear in the control elements but might further excite high-frequency dynamics (e.g. structural modes of vibration, neglected time delays, etc.). These serious problems with sliding mode control have resulted in the fact that most recent research has been concentrating on the application of sliding mode control to non-ideal systems and especially on the development of sliding mode control algorithms avoiding the undesirable chattering and achieving an optimal compromise between control bandwidth and tracking precision. See in this context for example Sabanovic *et al* (1983), Slotine and Sastry (1983), Borojevic *et al* (1984), Walcott and Zak (1987), Min-Ho *et al* (1989), Xu *et al* (1989) and Zinober (1990).

In terms of application, the recent introduction of reasonably priced high bandwidth hydraulic and pneumatic control valves have made sliding mode control an interesting and important control alternative to conventional control methods for fluid power systems. Gamble (1992) applied sliding mode control to a proportional solenoid valve. De Almeida (1993) used a model reference adaptive controller with a Variable Structure switching logic to successfully control a 2DOF hydraulically actuated manipulator. Surgenor *et al* (1995) for the first time successfully applied sliding mode control to a pneumatic positioning servo-mechanisms. Lantto (1994) gives a detailed insight in various aspects of the application of sliding mode control to fluid power systems such as reduction of feedback transducers, low- and high-frequency disturbances, reduction of chattering and the effects of sampling.

6.2 SLIDING MODE CONTROL OF A SECOND-ORDER SYSTEM

The probably easiest way of getting familiar with sliding mode control is to consider a second-order plant as it was originally done by Emal'yanov (1967). This simple example allows for the dynamic behaviour of the system to be shown graphically on a phase plane plot.

Assume that the dynamics of the second-order system to be controlled can be described by the following differential equation:

$$\ddot{x}(t)+a\dot{x}(t)=bu(t) \tag{6.1}$$

where $x(t)$ represents the system state and $u(t)$ the controller output. A relay-like switching control strategy results in the following two distinct dynamic structures depicted in Figure 6.1:

$$\ddot{x}(t)+a\dot{x}(t)=bU_{\max} \tag{6.2}$$

$$\ddot{x}(t)+a\dot{x}(t)=bU_{\min} \tag{6.3}$$

As can be seen both of these structures are unstable yet velocity limited. The following switching function $\sigma(x)$ can now be chosen:

$$\sigma(x)=-c_1x-\dot{x} \tag{6.4}$$

whose null space $\sigma(x)=0$ describes a straight line in the phase plane and interestingly is of one order less than the dynamics of the second-order system to be

controlled (Equation (6.1)). This switching line $\sigma(x)=0$ divides the phase plane into two separate regions: $\sigma(x)>0$ and $\sigma(x)<0$. Assuming now that the initial system state lies in the phase plane region where $\sigma(x)<0$ the controller output will be $u = U_{max}$. The system state will therefore follow the structure depicted in Figure 6.2 until it reaches the switching line that is $\sigma(x)=0$. The motion of the system is determined by its own open-loop dynamic structure described by Equation (6.1). This is called the *reaching phase.* When the state trajectory crosses the switching line, that is $\sigma(x)>0$, the system switches to the second structure with $u = U_{min}$ until the switching line is reached again. It can be seen in Figure 6.2 that once the state point reaches the switching line defined by Equation (6.4) the controller switches between its two structures (Equations (6.2) and (6.3)) in order to keep the system state on this line. The motion of the system now does not follow its own dynamic structure anymore but the system dynamics are rather determined by the dynamics of the switching line. The system is said to be in *sliding mode.* It can be seen from Equation (6.4) that the closed-loop dynamics of the system are therefore now of one order less than the dynamics of the open-loop system to be controlled.

Ideally, the controller in sliding mode will switch with an infinite switching frequency and hence the system state will oscillate around the switching line with an infinite frequency and zero amplitude. In practice however, the controller structure switching is necessarily imperfect due to the fact that, for instance, the switching is not instantaneous. Furthermore, neglected higher-order system dynamics, time delays, the effects of digital implementation, non-linearities like hysteresis and the fact that the switching function $\sigma(x)$ is only known with finite precision will reduce the switching frequency and therefore increase the amplitude of the state point oscillation around the sliding line. This phenomenon is called *chattering* and is generally undesirable. Therefore, in practice perfect sliding mode is unachievable and only a so-called *quasi-sliding* or *pseudo-sliding* mode can be achieved. Although this distinction is made in many references, it is also common to refer to this mode as sliding mode, since in practice ideal sliding mode cannot be achieved. This convention will therefore be used in this thesis unless a distinction between both phenomena adds clarity to the explanations.

As shown above, in sliding mode the transient response of the closed-loop system is equivalent to that of a first-order system with a time constant given by the slope of the switching line $-c_1$. It can be seen in Figure 6.3 that sliding mode may not occur, if the slope of the switching line is steeper than the slope of the open-loop plant response. In this case the state point may be driven away from the switching surface and might reach the surface again in another quadrant of the phase plane. The slope of the open-loop plant response can be expressed as:

$$\frac{\partial \dot{x}}{\partial x} = \frac{bU_{max}}{\dot{x}} + a \quad \text{for } \dot{x} \neq 0 \tag{6.5}$$

Sliding mode now can be guaranteed if

$$c_1 < a \tag{6.6}$$

over the whole range space. If $c_1 > a$ the state point might not be forced onto the sliding surface if it is far away from the origin (that is if $\dot{x}$ is large), but by increasing the maximum control signal the region in which the state point is forced onto the surface can be increased. Nevertheless, it cannot be guaranteed that sliding mode can be established over the whole range space.

As can be seen in Figure 6.4 even if sliding mode cannot be established the resulting system response can change from an unstable response of the two individual structures to a damped though oscillatory response of the switched system. In the worst case, a limit cycle may be reached resulting in a sustained oscillation of the control system.

6.3 DESIGN OF SLIDING SURFACE

To describe the motion of the system in sliding mode mathematically the rigorous mathematical definition given by Filippov (1960) can be used. Following his definition, the motion of the system in sliding mode can be given an interesting geometric interpretation as an average of the system dynamics on both sides of the surface. A summary of this intuitive construction can be found in Itkis (1976) and Slotine and Li (1991). Although Filippov's method is mathematically rigorous it is rather inconvenient. Wonham (1963) proposed a much simpler method which can be

used instead. The formal procedure may be described as follows. In sliding mode the following equalities are required to hold:

$$\dot{\sigma} \equiv 0 \tag{6.7}$$

$$\sigma(x) = 0 \tag{6.8}$$

These two equalities imply that once sliding mode has been reached the state simply moves on the sliding surface without ever leaving it. In physical terms, the proposed procedure replaces the infinitely fast oscillation of the system state about the sliding surface by the slow average component of the motion on the sliding surface itself.

Since in sliding mode the dynamics of the sliding surface describe the dynamics of the closed-loop control system, it has to be made sure that the sliding surface itself describes a stable system response with the desired dynamic characteristics. When designing a linear surface, linear system theory can be used to determine the defining state gains (e.g. pole-placement and eigenstructure assignment techniques, frequency domain design methods (Konno and Hashimoto (1993)), solution of the Algebraic Riccati Equation (Diong and Medanic (1992))). Also, optimisation methods like the evolution strategy (Kim *et al* (1996a)) and genetic algorithms have been used to determine the surface parameters.

Using Slotine's (1991) formalism for defining a sliding surface:

$$\sigma(x) = \left(\frac{d}{dt} + \lambda\right)^{n-1} x \tag{6.9}$$

where λ is a strictly positive constant, a second-order surface can be expressed as:

$$\sigma(x) = \ddot{x} + 2\lambda\dot{x} + \lambda^2 x \tag{6.10}$$

The question is how to choose the sliding surface tuning parameter λ. In this case, λ can be interpreted as the natural frequency of the ideally damped control system in sliding mode. Therefore assuming reachability of the sliding surface (which will be discussed in Section 6.4), λ can be chosen to obtain the required system dynamics. Yet, there are other factors beside the closed-loop dynamics and reachability that may impose limits. For example in mechanical systems there are generally three factors limiting the tuning parameter λ and therefore the choice of the sliding surface:

- Unmodelled structural resonant modes:

$$\lambda \leq \lambda_{struc} \approx \frac{2\pi}{3} f_{struc} \tag{6.11}$$

- Neglected time delays:

$$\lambda \leq \lambda_{del} \approx \frac{1}{3T_{del}} \tag{6.12}$$

- Sampling rate of digital control circuit elements:

$$\lambda \leq \lambda_{samp} \approx \frac{1}{5T_{samp}} \tag{6.13}$$

6.4 REACHABILITY OF SLIDING SURFACE

As could be seen in the simple example given in the Section 6.2, it is very important that the system state is forced onto the sliding surface to establish sliding mode. Therefore, in order to guarantee stability of the closed-loop system it has to be ensured that:

- firstly, the sliding surface results in a stable response of the control system in sliding mode as discussed in the previous section
- secondly, the sliding surface is reachable by the system state from any initial condition over the whole range space.

The condition for having the state trajectory directed towards the switching line can be formulated by looking at the following candidate of a Lyapunov function describing the square of the distance of the state point from the sliding surface:

$$L = \frac{1}{2}\sigma^2(x) \tag{6.14}$$

The above function is positive semidefinite. It is in fact positive everywhere in the state space except on the switching surface $\sigma(x) = 0$ itself. To ensure reachability of the sliding surface and hence stability of closed-loop control system (if the dynamics described by the sliding surface are stable) the first derivative of L has to be less than zero for all $x \neq 0$ that is:

$$\lim_{\sigma \to 0} \dot{L} = \lim_{\sigma \to 0} \sigma(x)\dot{\sigma}(x) < 0, \quad \forall x \neq 0 \tag{6.15}$$

This inequality represents a necessary condition for the reachability of the sliding surface and is commonly used in the design and stability proof of sliding mode

control systems. If condition (6.15) is satisfied, the function L is by definition a conditional Lyapunov function for the system to be controlled relative to the subspace $\sigma(x)=0$ and the system is therefore conditionally stable relative to this manifold (Itkis (1976)). If this condition is verified for the whole state space (with exception of the origin) the system state will reach the sliding surface from any possible initial condition and hence, assuming a sliding surface defining a stable dynamic response of the closed-loop control system, is stable. The range of the state space the system exists in is called *range space*. If any state vector in this range space will be driven towards a stable sliding surface, the control system is said to be globally stable.

Considering again the second-order plant presented in Section 6.2, the reachability condition (Equation (6.15)) yields the same condition for the existence of sliding mode as the one obtained by comparing the slope of the open-loop plant response with the slope of the switching line (Equation (6.6)).

Another way of looking at the problem of reachability of a given sliding surface is to use relay theory (Tsypkin (1984)). Re-writing for example the equation defining a linear second-order sliding surface:

$$\sigma = -c_1 x - c_2 \dot{x} - c_3 \ddot{x} \tag{6.16}$$

yields:

$$\begin{aligned} \sigma_1 &= -c_1 x - c_2 \dot{x} \\ \sigma &= \sigma_1 - c_3 \ddot{x} \end{aligned} \tag{6.17}$$

As can been seen from Figure 6.5, σ_1 is the demand input to the innermost feedback loop spanning the relay element depicted in Figure 6.6. Differentiating Equation (6.17) yields:

$$\dot{\sigma} = \dot{\sigma}_1 - c_3 \dddot{x} \tag{6.18}$$

Substituting Equation (6.18) into Equation (6.15) gives:

$$\lim_{\sigma \to 0} \sigma \left(\dot{\sigma}_1 - c_3 \dddot{x} \right) < 0 \tag{6.19}$$

According to Tsypkin (1984) reachability of the chosen sliding surface can hence be guaranteed, if at any moment the external (relative to the part of the system

containing the relay and being spanned by the inner feedback loop) action σ_1 varies more slowly than the inner feedback action $c_3\ddot{x}$. That is, if at any moment:

$$|\dot{\sigma}_1| < |c_3\ddot{x}| \tag{6.20}$$

Having now designed the sliding surface and assured its reachability it can be also of interest to determine the duration of the reaching phase before sliding mode is established since in general it is desirable to drive the system state as rapidly as possible towards the sliding surface. It is easy to determine the time taken by the system to reach the sliding surface from any initial condition even when the system is excited by a step input. However, this can only be done assuming that the plant is well known and linear. In this context it might be interesting that Eydinov (1965) proposed an approximate method for predicting this reaching time which can be used to minimise the reaching phase.

6.5 EQUIVALENT CONTROL

Solving the equations describing a control system in sliding mode formally for the control signal yields the so-called *equivalent control* signal u_{eq}, which can be seen as the continuous control action that would maintain the system state on the sliding surface. The equivalent control signal can also be seen as an average value of the switched control signal in ideal sliding mode. To obtain this equivalent control signal though the system dynamics have to be known precisely:

$$\dot{x} = Ax + Bu_{eq} \tag{6.21}$$

As shown in Section 6.3 in sliding mode the following equalities are required to hold:

$$\sigma(x) = s^T x = 0 \tag{6.22}$$

$$\dot{\sigma}(x) = s^T \dot{x} = 0 \tag{6.23}$$

The continuous equivalent control action replacing the control signal switching at an infinite frequency is hence:

$$u_{eq} = -\left(s^T B\right)^{-1} s^T Ax \tag{6.24}$$

Assuming now that the equivalent control action is synthesised by means of the following relay-like control signal:

$$u = -U_{\max} \operatorname{sgn}(\sigma) \tag{6.25}$$

where $U_{\max}$ represents the switching gain, the equivalent gain factor of the relay element (see Figure 6.6) can be determined as the ratio of the output to the input signal (Tsypkin (1955)):

$$K_{eq} = \frac{U_{\max} \operatorname{sgn}(\sigma)}{\sigma} = \frac{V}{|\sigma|} \tag{6.26}$$

The smaller the input signal, the larger is the equivalent gain K_{eq} In the limit of $\sigma \to 0$:

$$\lim_{\sigma \to 0} K_{eq} = \infty \tag{6.27}$$

Therefore, when the system is operating in sliding mode, it contains an element equivalent to an amplifier with infinite gain and therefore of infinite power overcoming all parametric and external disturbances acting on the system. Considering the second-order example used by Tsypkin (1984) shows that in sliding mode the innermost feedback loop spanning the relay and the system parameter dependent part of the system dynamics can be replaced by the reciprocal of the feedback element. Since this feedback element contains no plant dependent terms, the closed-loop response of the system in sliding mode is invariant to changes of system parameters.

It is now possible to construct a control law consisting of an equivalent term and a switching term (Yallapragada *et al* (1996)) such as:

$$u = u_{eq} + u_{switch} = -K_{eq} x - U_{\max} \operatorname{sgn}(\sigma) \tag{6.28}$$

In this case, the switching part u_{switch} of the control law forces the system state onto the sliding surface while the equivalent part u_{eq} operates like a state-feedback controller and keeps the state on this surface. Like this, no switching is required once the sliding surface has been reached. As mentioned above, in order to compute the equivalent gain, the dynamics of the system have to be known precisely. Therefore applying the above control law to a real system, the equivalent control signal only keeps a nominal system on the sliding surface while the switching control has to compensate for discrepancies between the physical plant and the nominal model used

as a basis for control design. Furthermore, the relay-like switching part of the control law provides robustness to plant parameter changes and the action of external disturbances.

6.6 SWITCHED GAINS CONTROL LAWS

Other control laws than the relay-like algorithm presented in Equation (6.25) can be used to establish sliding mode. In particular for higher-order systems the following *linear feedback with switched gains* algorithm has been considered (Utkin (1977), Utkin (1978), Zinober (1990), Chern and Wu (1991), Hung *et al* (1993)):

$$u = -\sum_{i=1}^{k} \psi_i x_i \qquad (1 \le k \le n) \tag{6.29}$$

where

$$\psi_i = \begin{cases} \alpha_i & x_i \sigma > 0 \\ \beta_i & x_i \sigma < 0 \end{cases} \tag{6.30}$$

For sliding motion, the required inequality conditions for the values of the individual state-dependent switching gains α_i and β_i can be obtained using the standard sliding condition (see Equation (6.15)) provided that the range of the expected plant parameter variations are known (Itkis (1976)).

One reason for using switched gains control laws like the one presented in Equation (6.29) is the fact that the relay-like control term $U_{max}\,\mathrm{sgn}(\sigma)$ which is normally used in relay-type sliding mode control is not present in the control algorithm. This term is usually the reason for excessive switching activity (chattering).

Further switching laws commonly used in VSC systems can be found in Hung *et al* (1993).

6.7 SLIDING DOMAINS

As shown by Bühler (1990), due to the fact that only a limited control action U_{max} is available to the control system (because of power limitation in the actuators)

sliding will not be possible over the whole sliding surface but rather will be restricted to an area around the origin called the *sliding domain*. The boundary of the sliding domain for a given sliding surface can easily be found by setting the equivalent control signal u_{eq} equal to the maximum available control signal $U_{\max}$:

$$u_{eq} = U_{\max} \tag{6.31}$$

This yields:

$$0 = s^T \left(Ax \pm BU_{\max} \right) \tag{6.32}$$

According to Equation (6.32) the dynamics of the sliding surface given by s^T and the maximum values of the components of the system state x determine the limits of the sliding domain for a given maximum control action $U_{\max}$. As demonstrated by Bühler (1990), for a second-order system and a linear first-order sliding surface the sliding domain is limited by two points on the straight sliding line. In general now, for a second-order system:

$$\ddot{x} + 2\zeta\omega_n \dot{x} + \omega_n^2 x = \pm bU_{\max} \tag{6.33}$$

with a damping ratio $\zeta < 1$ the sliding domain increases with a decrease in the slope c_1 of the sliding surface. Therefore, a slower system response in sliding mode can be achieved over a larger state-space region as shown in Figure 6.6. (Hence by definition, the sliding domain is bounded by the *time optimal phase trajectory*). The size of the sliding domain can further be increased by increasing the maximum control signal as depicted in Figure 6.8. According to Bühler (1986) similar relations exist for higher-order systems.

Although the closed-loop response of the control system in sliding mode is invariant to changes in the system parameters it can be deducted from Equation (6.32) that the size of the sliding domain is not. Increasing for instance the damping ratio ζ of the second-order dynamics increases the sliding domain until it reaches infinity for $\zeta = 1$ and $c_1 = \omega_n$ as can be seen in Figure 6.9. Increasing the natural frequency ω_n of the second-order dynamics on the other hand decreases the sliding domain as shown in Figure 6.10.

Concluding the above discussion, the existence of the sliding domain mainly results in two guidelines for the design of sliding mode control systems:

- When choosing the parameters of the sliding surface it should be ensured that the sliding domain exists over the whole state space the system operates in. In the case of changing system parameters the *worst case* system matrices $\boldsymbol{A}$ and $\boldsymbol{B}$ resulting in the smallest possible sliding domain should be chosen when determining its size
- The maximum control signal U_{max} should be chosen large enough to obtain a sufficient size of the sliding domain

6.8 NON-LINEAR AND OTHER SLIDING SURFACES

In order to extend the sliding domain, to improve reachability of the sliding surface or to obtain a faster transient response of the control system in sliding mode, non-linear sliding surfaces can be designed. In general, a non-linear sliding surface matches more closely the so-called time optimal system trajectory limiting the sliding domain as demonstrated in Section 6.7. Therefore, it can be made sure that the dynamics of the sliding surface do not exceed the dynamic limits of the controlled plant. Various approaches have been mentioned in literature, for instance:

- piecewise linear surfaces (Makarov and Rakhmankulov (1969))
- non-linear surfaces (Matthews *et al* (1987), Sira-Ramiréz (1987), Dwyer and Sira-Ramiréz (1988), Lee and Youn (1989), Zhu and Chen (1990), Kwatny and Kim (1990), Lee *et al* (1991), Qi and Hoft (1994))
- velocity limited surfaces (Bose (1985))
- constant deceleration surfaces (Harashima *et al* (1985), Feller and Benz (1987), Workman *et al* (1987), Gilbert (1989))
- constant jerk surfaces (Gamble (1992))
- adaptive surfaces (Zinober (1975), (1977), Nouri *et al* (1994), ParraVega and Arimoto (1995), Lee and Kwok (1995a), (1995b), Bekiroglu *et al* (1995))
- fuzzy surfaces (Kung and Liao (1994), Xu and Smith (1994), Ashrafzadeh *et al* (1996), Kim *et al* (1996b))
- time-varying surfaces (Fossas and Martinez (1993), Park and Lee (1993), Kim *et al* (1993), Choi and Park (1994), Bartoszewicz (1995))
- *Lagrangian* surfaces (Jumarie (1996))
- moving surfaces (Choi *et al* (1994), Gayed *et al* (1995), Lee *et al* (1995))

As reported, all these methods have been developed and implemented successfully. A comparison of the above mentioned approaches can be found in Harashima *et al* (1985) and Hashimoto and Harashima (1987).

In general, the realisation of complex non-linear sliding surfaces requires a digital or hybrid implementation of the VSC controller.

6.9 INVARIANCE OF CONTROL SYSTEMS IN SLIDING MODE

As first shown by Drazenovic (1969), sliding regimes have an important property: the motion of the system in sliding mode is independent of changes in the plant parameters and of external disturbances. In the second-order control system considered as an example in the Section 6.2 the performance of the closed-loop system is independent of the plant time constant a as long as it remains in sliding mode. As shown above, in sliding mode the closed-loop system dynamics are only governed by the sliding surface time constant c_1.

In general, the dynamics of a linear plant acted upon by an arbitrary disturbance vector $F(t)$ can be described by the state-space equation:

$$\dot{x}(t) = Ax(t) + Bu(t) + EF(t) \tag{6.33}$$

The dynamics of a system with changing system parameters can be expressed as:

$$\dot{x}(t) = (A + \Delta A)x(t) + Bu(t) \tag{6.34}$$

where ΔA is a matrix representing the parameters variations. The system now is invariant to disturbances or parameter changes, if there are matrices $\Lambda_D(t)$ and $\Lambda_A(t)$ such that the following relations:

$$E(t) = B\Lambda_D(t) \tag{6.35}$$

$$\Delta A(t) = B\Lambda_A(t) \tag{6.36}$$

are true (Utkin (1978), Gao and Hung (1993)). One important conclusion from Equations (6.35) and (6.36) is that the invariance of a VSC system in sliding mode to external disturbances and parameter changes only depends on the magnitude of these disturbances and not on their frequency content or their rate of change. In this respect

sliding mode control is far superior to self-tuning or adaptive control (Guzzella and Geering (1990)).

Yet, it has to be mentioned again that disturbance rejection and robustness to parameter changes can only be guaranteed if the system is in sliding mode with an infinite switching frequency. If the switching frequency is not infinite which is the case for all real physical applications, it can be easily shown that the system state will deviate from the sliding surface in-between two control structure switching instants due to external disturbances acting on the system. Also, changes in plant parameters will result in similar deviations of the system state from the sliding surface. Therefore, robustness to parameter changes and the disturbance rejection capability of a real (as opposed to an ideal) control system in sliding mode (or better quasi-sliding mode) have to be investigated carefully.

Furthermore, if the power limits of the control system are exceeded by external disturbances or parameter changes sliding mode may break down. One way of exceeding the power limits of the control system is for example to exert an external force to the system which is larger than the force available from the plant's actuators to compensate for this disturbance. The system state might be forced away from the sliding surface by the external disturbance force and therefore, the reachability conditions might not be fulfilled anymore.

When reachability of the sliding surface is guaranteed for the nominal plant model and a given minimum switching gain, an increase in this switching gain which will result in an increase in the magnitude of the available control action will improve the system's robustness and disturbance rejection capabilities. In case of fluid power positioning systems for instance, the switching gain can be increased by increasing the control valve size or the supply pressure.

Finally, external disturbances and system parameter changes will distort the phase trajectories in the reaching phase which occurs prior to the establishment of sliding mode. However, if the reachability conditions (see Equation (6.15)) are not violated by these disturbances the system will proceed to reach sliding mode (Itkis (1976)).

6.10 CHOICE OF SYSTEM STATES

According to Drazenovic (1969), the invariance conditions of a control system in sliding mode can only be fulfilled, if the system model used as a basis for controller design is in its *controllable canonical* form. In this case, the system state to be controlled and its derivatives are chosen as state variables. The canonical model of the system dynamics in state-space representation is:

$$\dot{x} = Ax + Bu + d \tag{6.37}$$

with:

$$x = \left(x_1\ \dot{x}\ \ddot{x} \cdots x^{(n-1)}\right)^T \tag{6.38}$$

$$A = \begin{pmatrix} 0 & 1 & 0 & \cdots & 0 & 0 \\ \vdots & \vdots & \vdots & \ddots & \vdots & \vdots \\ 0 & 0 & 0 & \cdots & 0 & 1 \\ -a_1 & -a_2 & -a_3 & \cdots & -a_{n-1} & -a_n \end{pmatrix}, \quad B = \begin{pmatrix} 0 \\ \vdots \\ 0 \\ b_0 \end{pmatrix} \tag{6.39}$$

The system order and the number of states is n while the excess of poles over zeros (the relative degree) is r. Here, x is the system state, u the control signal, y the system output and d a vector describing external disturbances. The switching function now can have the form:

$$\sigma(x) = s^T x = -c_1 x - c_2 \dot{x} - \ldots - c_n x^{(n-1)} \tag{6.40}$$

This equation defines a linear switching plane of order n-1 in the n^{th}-order state space.

In general, when obtaining the required derivatives of the plant state to be controlled severe problems might be encountered (for instance, additional noise and phase lags due to differentiation, high costs for additional transducers, etc.). These problems increase with the order of the plant. Hence, in many applications more accessible internal states are used or a *reduced-order* switching law is employed ignoring higher-order derivatives completely (White (1983), (1986)).

If other states than the canonical ones are chosen to synthesis the switching function sliding mode might still exist. The resulting motion though contains plant dependent terms. Therefore, the response of the closed-loop system will not be robust to changes in these terms.

6.10.1 REDUCED-ORDER VARIABLE STRUCTURE CONTROL (VSC) SYSTEMS

Omitting the highest system states when synthesising the switching function results in the so-called *reduced-order switching*. Although in many cases acceptable dynamic performance of the control system can be obtained when ignoring the highest system states (White (1983, 1986)) it can be shown that reducing the order of the sliding surface always results in a finite switching frequency. Therefore, a stable limit cycle might be established resulting in the fact that the system can ideally only reach quasi-sliding mode. Thus, the transient response of the closed-loop system is not invariant to changes in the plant parameters or to the action of external disturbances.

Considering again the second-order system presented in Section 6.2 as an example and omitting the velocity signal in the switching function results in the closed-loop response shown already in Figure 6.4.

For switched gains VSC systems an approximation to sliding mode can be produced by means of compensation techniques. This is not possible though for VSC systems with relay-type control algorithms. Consequently, only quasi-sliding motion can be achieved with these control systems.

In terms of relay control theory, the requirement for full state switching in order to achieve sliding mode is equivalent to the statement that the index (excess of poles over zeros) of the forward and feedback path of the innermost loop spanning the relay element must be one (Tsypkin (1984)).

6.10.2 OBTAINING THE SYSTEM STATE

In VSC, as in other state-feedback strategies, the dynamic state of the plant has to be either measured directly or derived in some way from measurements of other plant variables. From the standpoint of a control engineer, it is always the better alternative to measure the system state directly. Nevertheless, in most cases it is not possible to do so because suitable transducers are not available, too expensive or cannot be incorporated into the system. Hence, the need arises to obtain the missing information by other means. The possible techniques available are:

- State observation
- Differentiation or integration of measured system states
- Measuring of non-canonical system states

6.10.2.1 The Use of State Observers for Obtaining the System State

One way of determining the dynamic state of a system is to use a state observer. State observers are in general based on a linear model of the plant dynamics and use measured data to predict the system states which cannot be measured. Obviously, the accuracy of the obtained information on the unmeasureable system states depends on the accuracy of the system model being the basis of the observer.

In case of a linear Luenberger observer unmodelled dynamics and changes in system parameters can result in large errors between the real system state and the one predicted by the observer. Hence, when using this observer in combination with a sliding mode controller these measurement errors result in the system response being highly sensitive to changes in the plant parameters even in sliding mode (Nadam and Sen (1987, 1988, 1990). Therefore, the use of Luenberger observers degrades one of the most interesting features of sliding mode control, the robustness to plant parameter changes.

One way of accounting for changing system parameters is to use an adaptive observer which not only predicts the system state but also updates its plant model based on the measured data. Nevertheless, the introduction of an adaptive observer increases the complexity of the control system significantly and hence might reduce the available sampling rate especially when using the digital processor of a personal computer. Furthermore, the introduction of an adaptive observer might introduce some or all of the problems with adaptive systems like the need for sufficient excitation of the system, integrator wind-up etc.

6.10.2.2 Differentiation of Measured System States

When directly differentiating measured system states, the applied differentiation methods usually amplify the high-frequency content of the measured

signal which means they amplify the high-frequency noise. Furthermore, the application of numerical differentiation routines introduces an additional phase lag into the differentiated signal because past system state information is required in order to use backwards differencing schemes. This phase lag can be decreased by increasing the sampling frequency but at the same time an increase in sampling frequency also increases the sensitivity to noise of the differencing scheme.

In order to attenuate the high-frequency content of the differentiated signal and therefore noise, low-pass filters are generally used. These filters introduce additional phase lags into the system. Therefore, using a direct differentiation method always results in a trade-off between noise attenuation and an additional phase lag.

6.10.2.3 Measuring Non-Canonical System States

As mentioned at the beginning of this chapter Drazenovic (1969) showed that when using a non-canonical system representation for controller synthesis robustness to system parameter changes and maximum disturbance rejection cannot be guaranteed.

One way of looking at this fact is to consider the desired dynamic behaviour of the plant. This desired dynamic behaviour directly translates to a desired behaviour of the canonical system states, e.g. position error (for example), velocity and acceleration, no matter whether the system parameters change or external disturbances act upon the system. It is not possible to say the same about for instance the differential pressure of a pneumatic or hydraulic positioning system because it must change with changes in the system parameters and in the presence of external disturbances in order to make the system behave as desired.

Nevertheless, Pandian *et al* (1997) successfully applied sliding mode control to a pneumatic servo using position, velocity and differential pressure feedback and therefore avoiding acceleration feedback. The experimental results presented show that under nominal conditions the system is behaving well while changes in pay load resulting in changes in the differential pressure lead to an oscillatory response about the reference trajectory.

6.11 Switching Frequency of Control Systems in Quasi-Sliding Mode

Theoretically, a VSC system requires an infinite switching frequency in order to operate in sliding mode. As mentioned already, an infinite switching frequency cannot be achieved with a real physical system. Therefore, only a so-called quasi-sliding mode can be realised. The motion of the control system in quasi-sliding mode can be interpreted as the existence of a sustained oscillation due to a limit cycle. The frequency and amplitude of this limit cycle determines frequency and amplitude of the chattering in the control system. When determining the switching frequency of the control system in quasi-sliding mode the following effects have to be taken into account for an analogue control system:

- unmodelled plant dynamics, not considered when designing the sliding surface (i.e. neglected higher order dynamics, structural modes)
- neglected time delays
- signal filters (i.e. noise filters, non-ideal differentiators)

For a digital system, additionally the effects arising from the discretisation and numerical differentiation have to be considered. These are:

- latency introduced by sampling process
- computing delay
- phase lag due to numerical differentiation (due to backwards differencing scheme)

It is worth mentioning that these effects are a function of the sampling frequency of the digital system. Therefore, an increase in the frequency will decrease the adverse influence of the above factors on the system dynamics.

Due to the fact that the limit cycle is caused by the switching of a non-linear relay element its existence cannot be predicted by means of linear control theory. There are a number of methods though which can be used in order to predict the existence of a limit cycle in VSC systems and determine its frequency and amplitude. On possibility is to use the Tsypkin method (Tsypkin (1984), Atherton (1981)). This method results in an exact prediction of limit cycles based on an assumed relay output waveform rather than its input. Assuming a relay without deadzone, the output of this non-linearity will be a square wave with known amplitude. Because

this square wave is transmitted to the relay element input through the linear components of the closed-loop system, the relay input can be expanded to a Fourier series. The relay input now must be determined so that it generates the assumed square wave at the correct time. The resulting non-linear algebraic equation can then be solved for the limit cycle frequency. When the relay element has a dead zone the similar method yields two algebraic equations which give the limit cycle frequency and pulse width.

Another simpler way of determining the existence and dynamic characteristics of a limit cycle in a non-linear control system is to use describing functions. These describing functions can be conveniently used regardless whether the non-linearity is continuous (*soft*) or discontinuous (*hard*), as it is the case for a relay (see Nagarth and Gopal (1982), D'Azzo and Houpis (1986)). The advantage of using describing functions is that by substituting the non-linear element (relay) by its linear describing function, linear control theory can be applied to analyse the control system.

Although the more complex Tsypkin method produces an exact solution to the problem unlike the approximate describing function method it is also based on a linear plant model which is only an approximation of the real plant's dynamics. Therefore, the results are not necessarily more accurate when applying this method to non-linear systems. Additional validation of the results using computer simulations of the system dynamics are in both cases advisable.

Furthermore, Atherton (1981) showed that the difference in the results between the Tsypkin method and the describing function method is small if the linear elements in the control system are good low-pass filters. Hence, in the following the describing function method will be explained in more detail and used for the analysis of the limit cycles occurring in the control system under investigation.

6.11.1 Describing Function of a Relay Element

The application of describing functions to limit cycle analysis is based on the fact that the form of the signals in a limit-cycling system is usually approximately sinusoidal. If there is a limit cycle in the system, then the system signals must all be

periodic. Since, as a periodic signal, the input to the linear elements of the system can be expanded as the infinite sum of harmonics, and since the linear element, because of its low-pass filter properties, filters out higher frequency signals, the output of the linear element must be composed mostly of the lowest harmonics.

The describing function for a relay-type non-linearity without dead zone (see Figure 6.6) is:

$$N(\hat{\sigma}) = \frac{4U_{max}}{\pi \hat{\sigma}} \tag{6.41}$$

U_{max} represents the switching step height while $\hat{\sigma}$ is the amplitude of the input signal (switching function) into the relay element. One can observe three features of this describing function:

- When the input is infinitely small, the describing function is infinitely large.
- When the input is infinitely large, the describing function converges towards zero.
- The describing function has no imaginary part. Hence, the relay element does not produce a phase shift.

Ideally, the input signal into the switching or relay element of the SLMC system is equal to zero hence the gain of the non-linear element increases to infinity which corresponds to the equivalent gain results of Tsypkin (1984).

6.11.2 THE EXTENDED NYQUIST CRITERION

Having substituted the non-linear relay element by its linear describing function the slightly extended Nyquist criterion can be used to check for the existence of limit cycle oscillations in the system depicted in Figure 6.11. Assuming that a self-sustained oscillation of amplitude $\hat{\sigma}$ and frequency ω exists, the following equality must have a solution (Slotine and Li (1991)):

$$G(i\omega) = -\frac{1}{N(\hat{\sigma})} \tag{6.42}$$

In other words, the amplitude $\hat{\sigma}$ and frequency ω of the limit cycle in the system must satisfy Equation (6.42).

Particularly for higher-order systems, it is generally not easy to solve this equation using analytical methods. Therefore, a graphical approach is often used. The idea is to plot both sides of the complex Equation (6.42) in the complex plane and find the points where the two curves intersect. Limit cycles now exist, if the two curves intersect, and the values of $\hat{\sigma}$ and ω corresponding to the intersection point are the solutions of Equation (6.42). If points near the intersection and along the increasing amplitude $\hat{\sigma}$ side of the curve $-1/N(\hat{\sigma})$ are not encircled by the curve of the linear part $G(i\omega)$, the predicted limit cycle is stable. Otherwise, the limit cycle is unstable (Slotine and Li (1991)).

As mentioned already, for a relay element without hysteresis and backlash the describing function $N(\hat{\sigma})$ is real and therefore the plot of $-1/N(\hat{\sigma})$ always lies on the real axis of the complex plane. Resulting from this observation, it is also possible to examine the Bode plot of the frequency response of the linear part of the system $G(i\omega)$. The points where the phase of $G(i\omega)$ reaches -180° indicate the existence of stable limit cycles. Using the Bode plot method, it is easier to obtain frequency ω and amplitude $\hat{\sigma}$ of the limit cycles since frequency and oscillation amplitude are both plot parameters.

It seems to be important, to point out again that the above procedure only gives an approximate prediction of the existence of limit cycles. The validity and accuracy of this prediction should be confirmed by computer simulation as in Chapter 9 of this thesis where the limit cycles of the control system under investigation are analysed.

6.12 Boundary Layer

Since chattering is an inherent dynamic characteristic of quasi-sliding mode and is generally undesirable it has to be reduced if not eliminated in order to enable the controller to perform satisfactorily. As mentioned earlier, for switched gains VSC systems sliding mode can be approximated by means of compensation techniques. For relay VSC systems chattering reduction is usually achieved by means of a thin boundary layer neighbouring the switching surface (Slotine and Li (1991)). This

boundary layer smoothes out the control switching discontinuity by altering the control algorithm within this layer. Using a relay-like switching algorithm a boundary layer can be incorporated as shown in Figure 6.12 (Surgenor *et al* (1995)):

$$u = \begin{cases} U_{\max}\,\mathrm{sgn}(\sigma) & \text{when} \quad |\sigma| > \sigma_{BL} \\ U_{\max}\dfrac{\sigma}{\sigma_{BL}} & \text{when} \quad |\sigma| < \sigma_{BL} \end{cases} \tag{6.43}$$

or:

$$u = \frac{\sigma}{|\sigma| + \delta} \quad \text{with} \quad \delta > 0 \tag{6.44}$$

The boundary layer basically acts as a low-pass filter attenuating chattering by filtering the switching function σ. The cut-off frequency ω_{BL} of this low-pass filter can be determined as:

$$\omega_{BL} = \frac{b_0 c_n}{\sigma_{BL}} \max\{|u|\} = \frac{b_0 c_n}{\sigma_{BL}} U_{\max} \tag{6.45}$$

Recognising the filter-like structure allows for the tuning of the control law in order to achieve a trade-off between tracking precision and chattering reduction. The introduction of a boundary layer leads to tracking within a guaranteed precision rather than perfect tracking. As explained by Slotine and Li (1991), the thickness of the boundary layer can also be monitored and made time-varying in order to fully exploit the control bandwidth available (see also Dwyer *et al* (1989)).

Due to the fact that chattering is caused by unmodelled system dynamics (reduced-order switching) the cut-off frequency should by smaller than the lowest frequency of the unmodelled dynamics limiting the switching frequency:

$$\omega_{BL} \leq \omega_{unmodelled} \tag{6.46}$$

It can be shown that the closed-loop system dynamics of a control system with boundary layer can be similar to those of a system without boundary layer. In order to achieve this, the boundary layer has to be chosen sufficiently small (Lantto (1994)):

$$\omega_{BL} = \frac{b_0 c_n}{\sigma_{BL}} \min\left\{\frac{u_{\max} - u_{\min}}{2}\right\} >> \frac{|a_i| c_n}{c_i} \quad ; i = 1,2,\ldots,n \tag{6.47}$$

6.13 DIGITAL IMPLEMENTATION OF SLIDING MODE CONTROL

The dynamic characteristics of discrete-time VSC systems significantly differ from those of continuous-time VSC systems. The main difference is that in discrete-time systems the control action can only be activated at discrete sampling instants. The controller output is then held constant by the D/A-converter over each sampling period. As a result, the switching frequency of the discrete-time VSC system cannot exceed half of the sampling frequency of its digital elements (microprocessor, D/A- and A/D-converter). Therefore, discrete-time VSC systems (as all VSC systems with finite switching frequency) can only undergo quasi-sliding modes (Verghese *et al* (1988)) with the switching frequency limited by the sampling frequency. Often these dynamic modes are also called *pseudo*-sliding modes (Er and Wang (1993)) to emphasise the fact that the similarity between discrete-time sliding modes and continuous-time sliding modes disappears as the sampling frequency decreases.

In pseudo-sliding mode the state of the system approaches the switching surface but in general cannot stay on it. Hence, the switching surface is bounded by a sector repelling the system state trajectory as shown in Figure 6.13. Outside this sector the trajectory is still directed towards the switching surface. It was shown by Lim *et al* (1991) that, even if the switching frequency is equal to its maximum of half the sampling frequency, the system state does not necessarily stay within this repulsion sector surrounding the sliding surface for two consecutive sampling periods. Lim *et al* (1991) also used an application to demonstrate that the trajectory in the phase plane of a discrete-time VSC system is not necessarily symmetrical about $\sigma = 0$ in particular, if the controller gains vary for e.g. positive and negative input signals. It was shown that this unsymmetrical switching about the sliding surface can lead to steady-state control errors. Baida (1993) showed, using a simple example, that the implementation of a discrete-time VSC controller may also lead to both high- and low-frequency chattering. This result was confirmed by Lantto (1994) in a simulation study. Unlike the high-frequency chattering though, the low-frequency chattering cannot be filtered out by the system.

As a result of the limited switching frequency, discrete-time VSC systems (as all VSC systems only reaching quasi-sliding mode) do not possess the invariance properties found in ideal continuous-time VSC systems with an infinite switching

frequency. Therefore, the robustness issues of discrete-time VSC systems have to be investigated carefully (Hung *et al* (1993)). In this context, Milosaviljevic (1985) showed for example that disturbances acting on the system at intersample instants prohibit exact tracking of the sliding surface $\sigma = 0$. Research in this area is still ongoing.

To determine now the switching frequency of a discrete-time VSC systems one has to consider the influence of the sampling process on the system dynamics and also additional time lags being inherent to the discrete-time dynamics. Since each sampled controller output value $u(kt)$ is held constant by the D/A-converter until the next value has been made available by the control computer, the continuous value of $u(t)$ consists of steps that lag behind the sampled values $u(kt)$ by $T_{samp}/2$ on average as can be seen in Figure 6.14. A further time lag might be introduced by the time required by the control computer to do the necessary computation steps. Finally, numerical differentiation routines add a further lag into the system since they require past information of the signal to be differentiated in order to calculate an approximation of the derivative.

In general, there are two possible ways of analysing time delays in discrete-time control systems: One can either incorporate the time delays resulting from the discrete character of the control system into the continuous analysis of the digital system or alternatively look at a discrete model of the system under consideration. When analysing a continuous equivalent of the discrete control system the characteristics of the D/A-converter can be modelled by including the Laplace-domain transfer function of a zero-order-hold (ZOH) into the continuous model of the system. The Laplace-domain transfer function of a ZOH with sampling time of T_{samp} is:

$$G_0(s) = \frac{1 - e^{-sT_{samp}}}{s} \tag{6.48}$$

As can be seen from Equation (6.48) the time delay model does not result in a polynomial. Therefore, to investigate the effects of time delay on the dynamics of the system the transcendental function has to be either approximated or the phase conditions have to be applied directly to the system. The most common means of finding such an approximation is to use the so-called Padé approximation (Houpis

and Lamont (1985)). This approximation consists of matching the series expansion of the transcendental function describing the time delay with the series expansion of a rational function whose numerator is polynomial of degree p and whose denominator is a polynomial of degree q. The result is commonly referred to as the (p,q)-Padé approximation. To give an example, the (1,1)- and (0,1)-Padé approximations of a time delay T_d are:

$$\begin{aligned} &(1,1): \quad e^{-T_d s} \cong \frac{1-(T_d s/2)}{1+(T_d s/2)} \\ &(0,1): \quad e^{-T_d s} \cong \frac{1}{1+T_d s} \end{aligned} \tag{6.49}$$

The additional phase lag introduced to the system by a time delay T_d can also be directly calculated as follows (see Figure 6.15) and added to the system's phase:

$$\varphi_d = -\frac{\omega}{\omega_d} \times 360^\circ = -\frac{\omega T_d}{\pi} \times 180^\circ \tag{6.50}$$

It can generally be said that, if an average delay of half the sampling time is incorporated into the continuous analysis of a digital system without any further computing time delays, excellent agreement results for many reasonable sampling frequencies (Franklin *et al* (1994)).

Rather than using the above approximations for the delays in discrete-time systems in combination with a continuous-time analysis method, an often better approach is to analyse the entire discrete-time system using an exact discrete-time analysis technique. To do this the z-transform (Dorf and Bishop (1995)) is usually employed. For discrete-time systems the z-transform plays the same role as the Laplace-transform does for continuous-time systems.

When performing a discrete analysis of a control system containing some discrete elements, the first step is to determine the discrete transfer functions of the continuous elements. The discrete transfer function $G(z)$ of continuous plant described by $G(s)$ and preceded by a ZOH element as depicted in Figure 6.16 is:

$$G(z) = (1-z^{-1}) Z\left\{\frac{G(s)}{s}\right\} \tag{6.51}$$

The discrete transfer function $G(z)$ is an exact discrete equivalent of the continuous system under consideration because the ZOH element models the dynamic behaviour of the system in-between sampling instants exactly. It is also possible to use approximation methods which make different assumptions about what happens in-between sampling instants. One method is called Tustin's method or bilinear approximation (Phillips and Nagle (1990)). The method is based on the trapezoidal integration formula substituting:

$$s = \frac{2}{T_{samp}}\left(\frac{1-z^{-1}}{1+z^{-1}}\right) \tag{6.52}$$

Other methods are the matched pole-zero (MPZ) method and the modified matched pole-zero (MMPZ) method. There description can be found in Franklin *et al* (1990). A very helpful tool for converting the continuous-time transfer function $G(s)$ into its discrete-time equivalent $G(z)$ is the *c2dm* routine in MATLAB (MathWorks (1992)). This routine allows for the use of either the exact ZOH method or the above approximation techniques.

In the case that velocity and acceleration cannot be measured directly, these signals can be obtained from the measured displacement signal $x(k)$ using the following backwards differencing:

$$v(k) = \frac{1}{T_{samp}}(x(k) - x(k-1)) \tag{6.53}$$

$$a(k) = \frac{1}{T_{samp}^2}(x(k) - 2x(k-1) + x(k-2)) \tag{6.54}$$

It is also possible to use the bilinear transformation to compute velocity and acceleration. This transformation results in zero phase shift for frequencies below the Nyquist frequency and maximum phase shift for frequencies above the Nyquist frequency. Nevertheless, using the bilinear transformation does not give an exact system representation in the sampling points resulting in distorted amplitude and phase in the high-frequency range. Velocity and acceleration obtained by the bilinear transformation are:

$$v(k) = \frac{2}{T_{samp}}(x(k) - x(k-1)) - v(k-1) \tag{6.55}$$

$$a(k) = \frac{4}{T_{samp}^2}(x(k) - 2x(k-1) + x(k-2)) - 2a(k-1) - a(k-2) \qquad (6.56)$$

The additional phase lags introduced to the system dynamics by the above mentioned factors at a sampling rate of T_{samp} = 1 ms can be seen in Figures 6.17 to 6.18. Obviously, these phase lags depend on the sampling time. It can be seen that at the sampling frequency of f_{samp} = 1 kHz the numerically differentiated velocity signal lags 180° and the numerically differentiated acceleration signal lags 360° behind the ideal response. In order to keep these significant phase lags small, the sampling time has to be as short as possible.

6.13.1 SAMPLING FREQUENCY

The previous analysis indicates that (for the same plant to be controlled), a much higher sampling frequency is required for digital VSC systems than for conventional digital control systems due to the adverse effects of a low sampling frequency on the switching frequency in sliding mode. This result is further confirmed by Dote *et al* (1982), Hashimoto and Harashima (1987), Hashimoto *et al* (1988), MacCarley and Meyer (1991) and Surgenor *et al* (1995).

In order to successfully implement a continuous-time VSC algorithm digitally much higher sampling frequencies than the bandwidth of the plant are mentioned in literature, for example:

- Åström and Wittenmark (1990) — 20 times the system bandwidth
- Gamble (1993) — 75 times the system bandwidth
- Hwang *et al* (1993) — 100 times the system bandwidth
- Lin and Chen (1994) — more than 100 times the system bandwidth

As a comparison, Franklin *et al* (1994) mention a sampling frequency of 20 times the system bandwidth to be used for the digital implementation of conventional control methods.

According to the above authors, the listed sampling frequencies are sufficient to enable the digital sliding mode controller to emulate the action of an analogue controller. If the system is further subject to disturbances with a frequency content above the bandwidth of the system, an even faster sampling time has to be used in

order to fulfil the invariance conditions reasonably. Hence, the highest disturbance frequency can also determine the required sampling frequency (Lantto (1994)).

One way of determining the minimum sampling rate required in order to obtain a satisfactory system response is to use the Lyapunov exponent method. This method can be used to estimate the rate of change of distance between neighbouring trajectories of non-linear chaotic dynamic systems. Using the Gramm-Schmidt algorithm allows for the calculation of the Lyapunov exponent as a function of the sampling rate (Grantham and Athalye (1990)). Depending on whether the exponent is negative, zero or positive the distance between trajectories decreases, remains constant or increases. Furthermore, Yu and Potts (1992) proposed a relationship for determining the upper bound for the sampling rate which should not be exceeded when implementing a continuous-time VSC controller digitally. The proposed relationship is based on the *best* discretisation scheme.

Another way of obtaining a lower bound for the sampling frequency is to require the system state to stay within a certain region around the switching surface once the surface has been reached. MacCarley and Meyer (1991) derived the following equation relating the maximum sampling time to the maximum deviation of the system state from the switching surface:

$$T_{samp} \leq \frac{\delta \|s\|}{2\left|s^T \mathbf{B} U_{\max}\right|} \tag{6.56}$$

where δ is a Euclidean norm bound on state deviations from the switching surface during a single sampling period T_{samp}. In practice, δ may be selected based upon some maximum acceptable deviation of each system state $|\Delta x_i| \leq \alpha_i$:

$$\delta = \min\left|s^T \alpha\right| \quad \text{with} \quad \alpha = \begin{pmatrix} \alpha_1 \\ \vdots \\ \alpha_n \end{pmatrix} \tag{6.57}$$

Equation (6.57) requires very little knowledge about the plant dynamics and therefore represents a simple criterion for choosing the sampling time for uncertain systems.

A comparable method is presented by Zhao and Utkin (1996) to determine the effect of the sampling frequency on the tracking error for a path tracking VSC controller.

6.13.2 Discrete Sliding Mode Control (DSLMC)

If the sampling rate cannot be made high enough one way of dealing with the problem of limited switching frequency in discrete-time VSC systems due to low sampling rates is to use discrete sliding mode (DSLM) theory when designing the controller. The aim of DSLM theory is to ensure the existence of pseudo-sliding mode in discrete-time VSC systems. When designing DSLMC systems, the control law is usually derived on the basis of a discrete-time Lyapunov function (Furuta (1990)) or contraction mapping (Utkin and Yang (1978), Utkin and Drakunov (1989)) and hence takes into account the effect of sampling on the control system dynamics.

The reachability condition for the sliding surface can be derived from a difference equation instead of a derivative equation (Milosaveljevic (1985)):

$$\lim_{\sigma(k)\to 0^+}[\sigma(k+1)-\sigma(k)]\le 0 \quad ; \quad \lim_{\sigma(k)\to 0^-}[\sigma(k+1)-\sigma(k)]\ge 0 \tag{6.58}$$

In practice though, it is in general impossible for the system state to approach the sliding surface close enough. Therefore, the conditions $\sigma(k)\to 0^+$ and $\sigma(k)\to 0^-$ are rarely fulfilled. Hence, the following condition can be used to determine whether a discrete-time sliding mode (pseudo-sliding mode) exists or not:

$$[\sigma(k+1)-\sigma(k)]\sigma(k)\le 0 \tag{6.59}$$

A further condition for the existence of pseudo-sliding mode often quoted is:

$$|\sigma(k+1)|<|\sigma(k)| \quad \text{(Sarpturk } et\ al \text{ (1987))} \tag{6.60}$$

or equivalently:

$$\sigma^2(k+1)<\sigma^2(k) \quad \text{(Furuta (1990))} \tag{6.61}$$

$$|\sigma(k)\sigma(k+1)|<\sigma^2(k) \quad \text{(Sira-Ramiréz (1987))} \tag{6.62}$$

As shown by Spurgeon (1992) though, Condition (6.60) and its equivalents are sufficient but do not have to be satisfied necessarily, if Condition (6.59) is satisfied.

In general, a switched gains type control law similar to the one described in Section 6.6 is used for discrete-time VSC systems. Using Condition (6.59) lower bounds for the state gains α_i and β_i can easily be found. Yet, the existence of asymptote hyperplanes, on which the system trajectory diverges from the switching surface imposes another restriction on the choice of the state gains. An algorithm which determines the upper bounds for the state gains by ensuring that the system trajectory stays within the state space region bounded by these asymptote hyperplanes can be found in Yu (1994).

A comprehensive overview over various approaches to sliding surface design for DSLMC systems and a comparison between those methods and the ones used for CSLMC systems can be found in Iordanou and Surgenor (1997).

Although it was found that for low sampling rates DSLMC could improve the system response significantly in comparison to CSLMC, DSLMC is not as robust to parameter changes as CSLMC (Iordanou and Surgenor (1997)). This is due to the fact, that DSLMC is taking the model of the system dynamics into account on a more basic design level than CSLMC in order to compensate for chattering introduced by the reduction of the switching frequency caused by discretisation. Hence, changes in the plant parameters have a more dramatic effect on DSLMC systems than on CSLMC.

A detailed analysis of DSLMC can be found in the recently published thesis of Iordanou (1998).

6.14 Implementation of Sliding Mode Control - Analogue Versus Digital

In general, there are three different approaches to the implementation of sliding mode control. These are:

- Analogue implementation using analogue switching circuit cards, amplifiers and filters (e.g. Dote *et al* (1982), Bengiamin and Kauffmann (1984), Feller and Benz (1987), Mestha and Yeung (1991)).

- Digital implementation using fast microprocessors, dedicated processors or Digital Signal Processors (DSP) to realise the control algorithm (e.g. Hashimoto *et al* (1988), Min-Ho *et al* (1989), Leung *et al* (1992), Surgenor *et al* (1995), Chern *et al* (1997)).
- Hybrid implementation using digital and analogue elements to realise specific control tasks best suited for these elements (Bellini *et al* (1989), Gamble (1992)).

Each of these approaches has its advantages and disadvantages:

- Digital control offers an increased flexibility of the system. The implementation of non-linear switching surfaces and additional functions can be done easily. Nevertheless, when using a digital sliding mode controller the switching frequency achieved by the control system depends on the sampling frequency of the processor and often the switching frequencies of control systems using conventional processors are not sufficient to guarantee sliding motion.
- Analogue controllers, on the other hand, are cheaper and offer higher speeds of operation at the cost of a reduced flexibility and user-friendliness.
- One way of combining the advantages of digital and analogue controllers is to use a hybrid approach to implementation. Gamble (1992) described a hybrid controller using an analogue filter to obtain the acceleration feedback signal from the measured velocity signal. The control algorithm was realised using a DSP with a maximum sampling frequency of 4 kHz. By using the analogue differentiation filter to obtain the acceleration signal the switching frequency could be increased greatly without the need of increasing the processor speed used to compute the switching surface.

6.15 CLOSURE

The above review on sliding mode control confirms the conclusion already drawn from the results of the preliminary study presented in Appendix A1: for the control of the *n*DOF pneumatically actuated figure sliding mode control seems to be the most appropriate control approach.

Moreover, due to its greater invariance to changes in the system parameters and its better disturbance rejection capabilities the continuous version (CSLMC) seems to be of more interest than the discrete version (DSLMC).

In the remainder of this thesis the development and implementation of a CSLM controller for the animated figure will therefore be described.

FIGURES

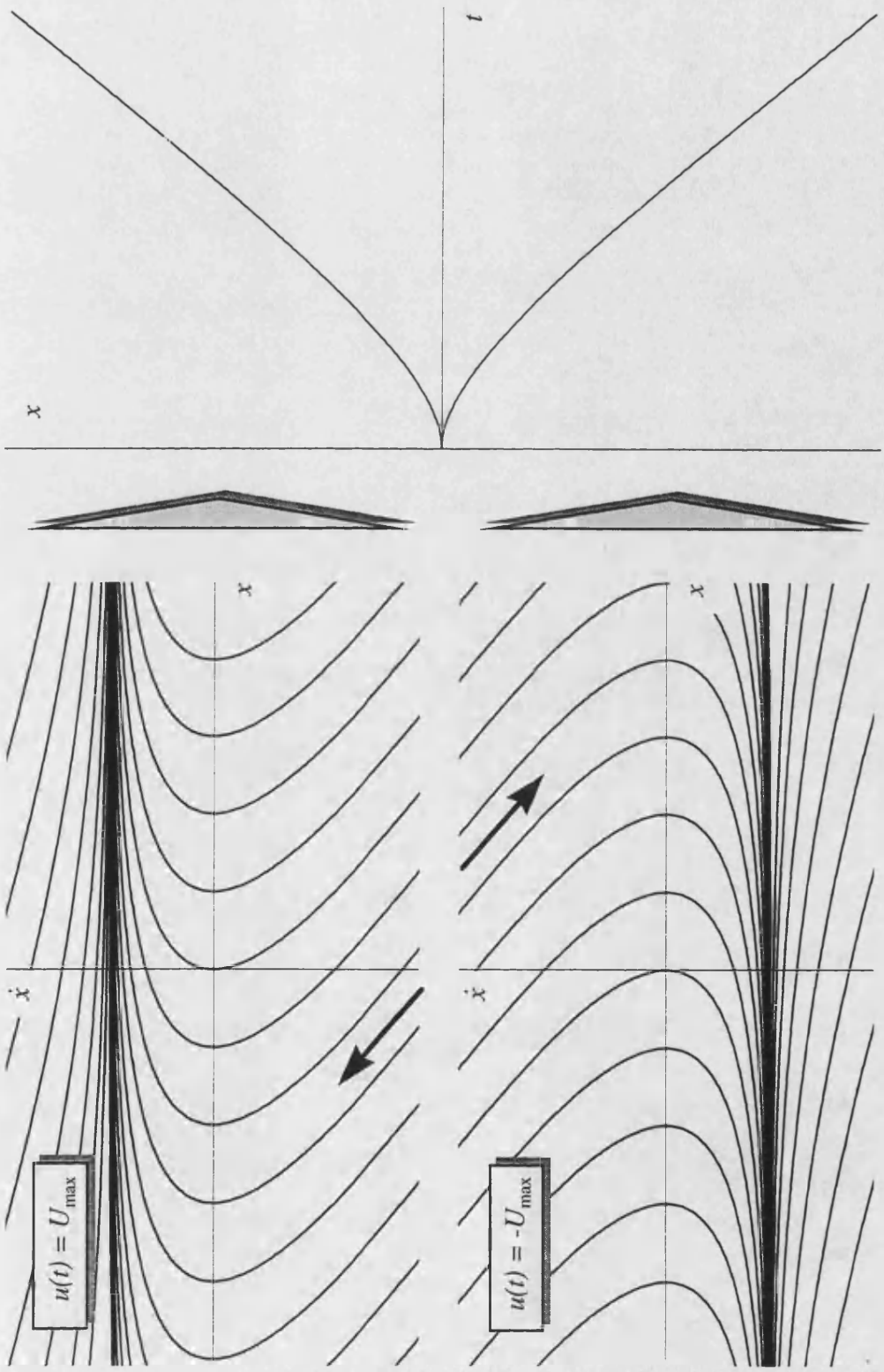

Figure 6.1 - Open-loop dynamics of second-order system

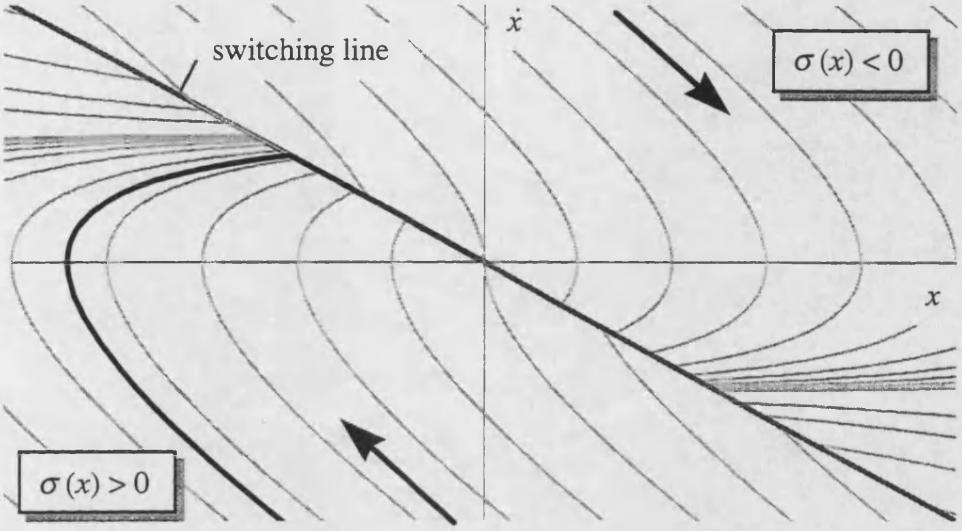

Figure 6.2a - Phase plane plot of the dynamics of a second-order system ($c_1 < a$)

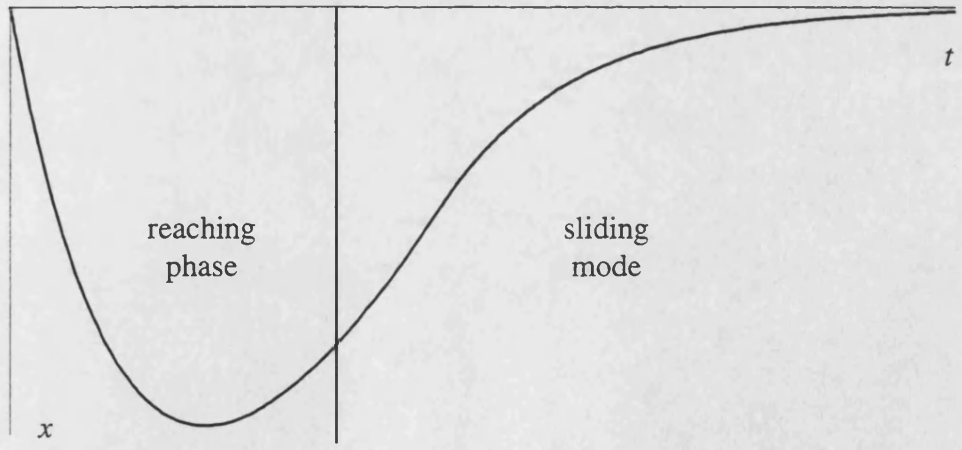

Figure 6.2b - Dynamic response of a second-order system ($c_1 < a$)

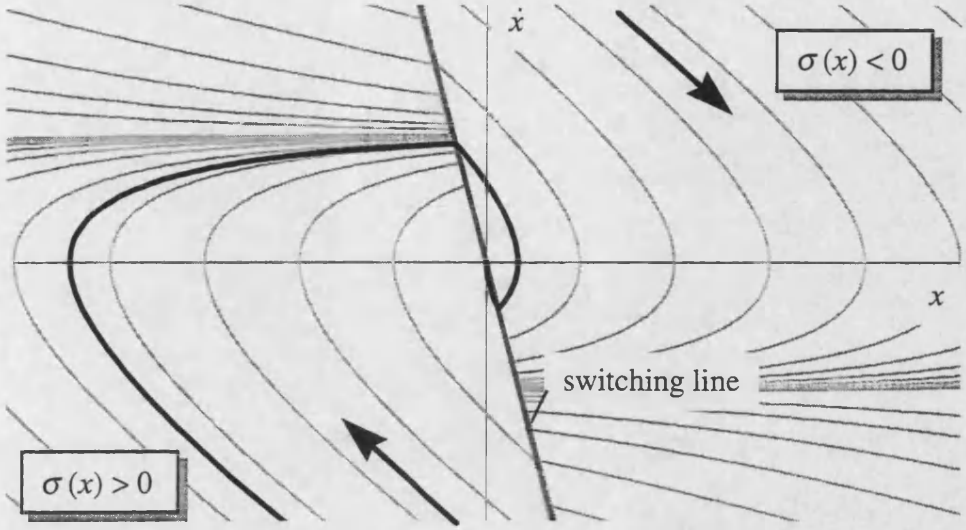

Figure 6.3a - Phase plane plot of the dynamics of a second-order system ($c_1 > a$)

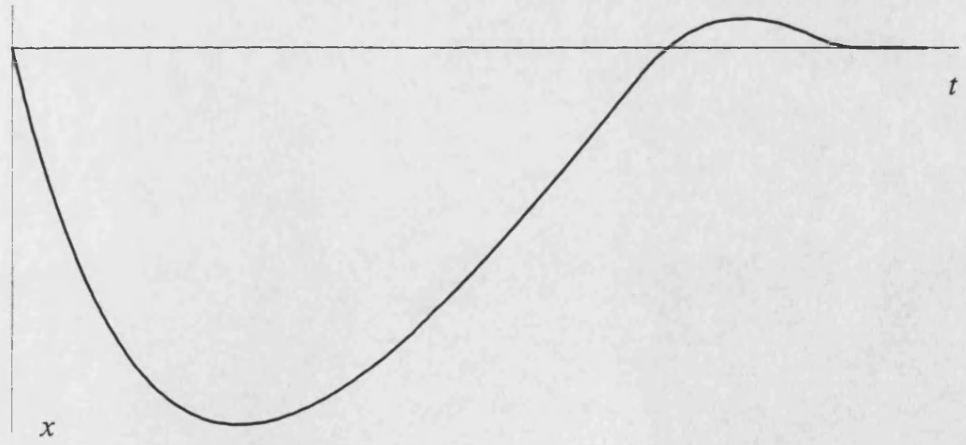

Figure 6.3b - Dynamic response of a second-order system ($c_1 > a$)

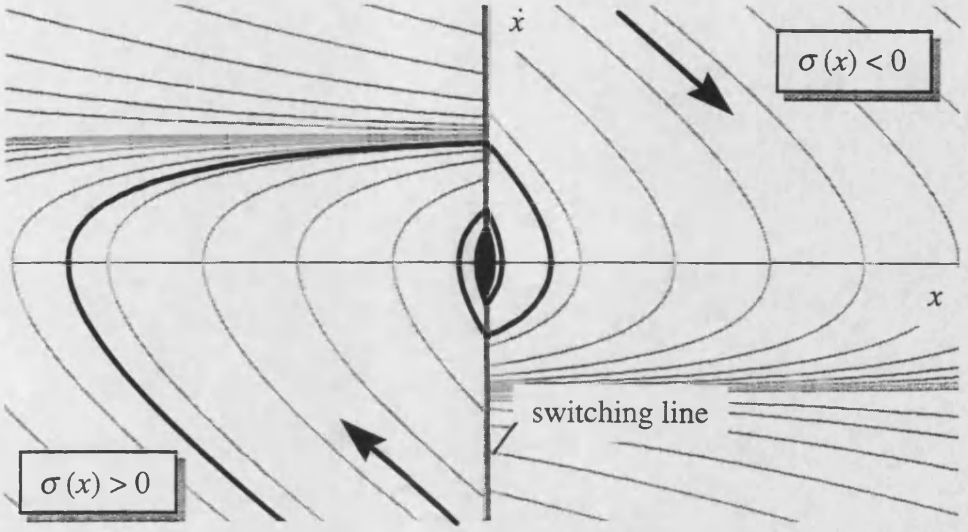

Figure 6.4a - Phase plane plot of the dynamics of a second-order system ($c_1 > a$)

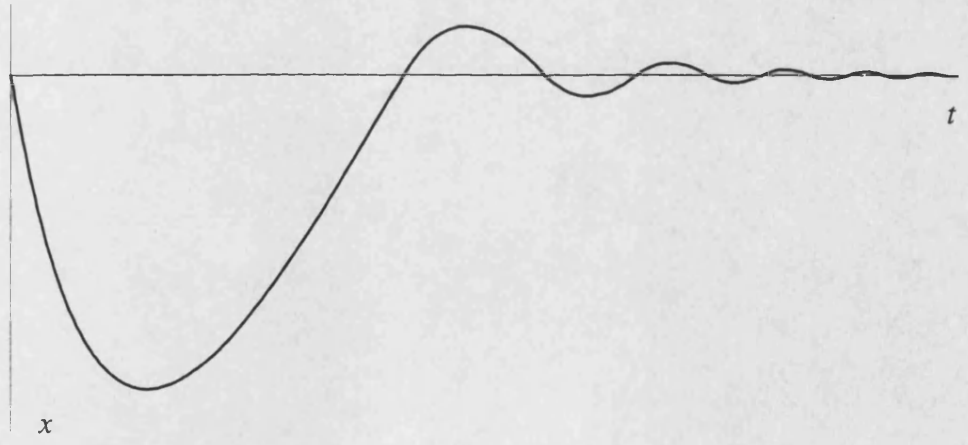

Figure 6.4b - Dynamic response of a second-order system ($c_1 > a$)

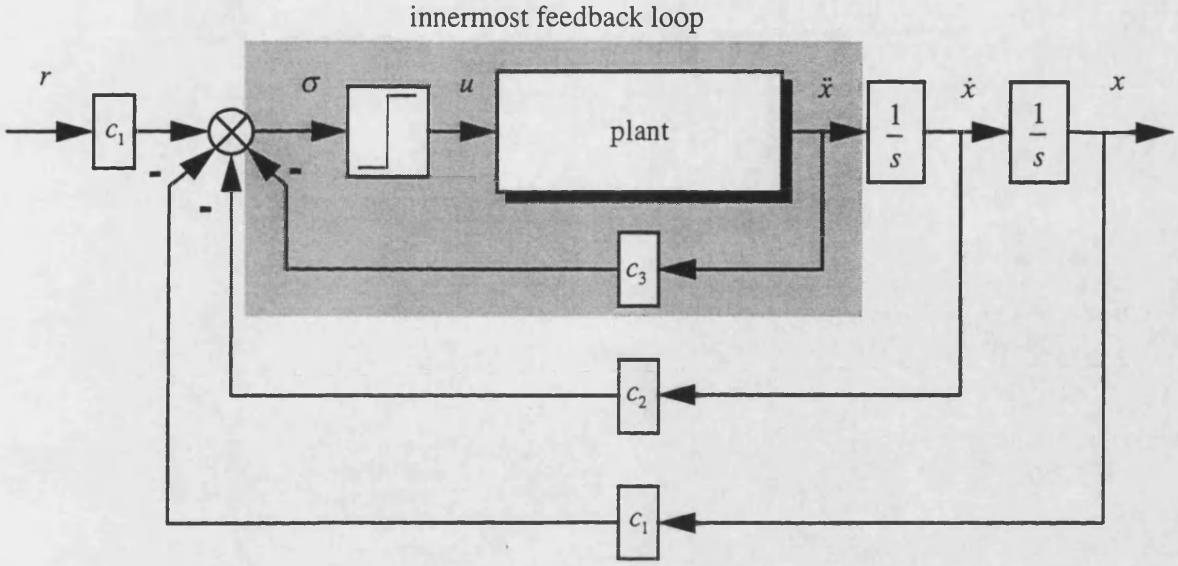

Figure 6.5 - System under relay control

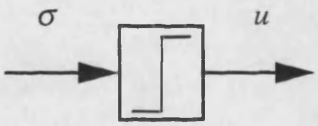

Figure 6.6 - Relay-like switching element

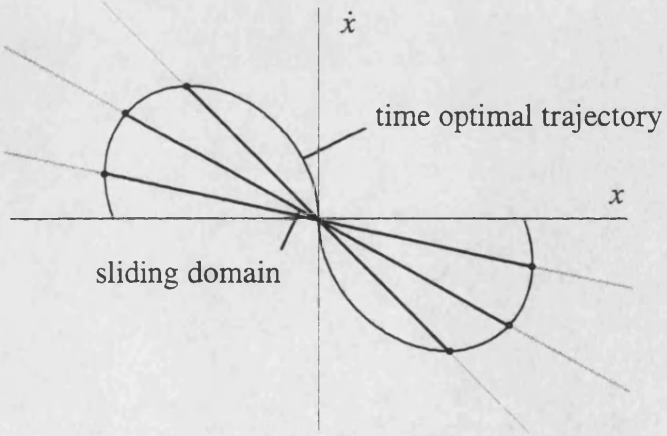

Figure 6.7 - Sliding domain of second-order system with a damping ratio of $\zeta < 1$

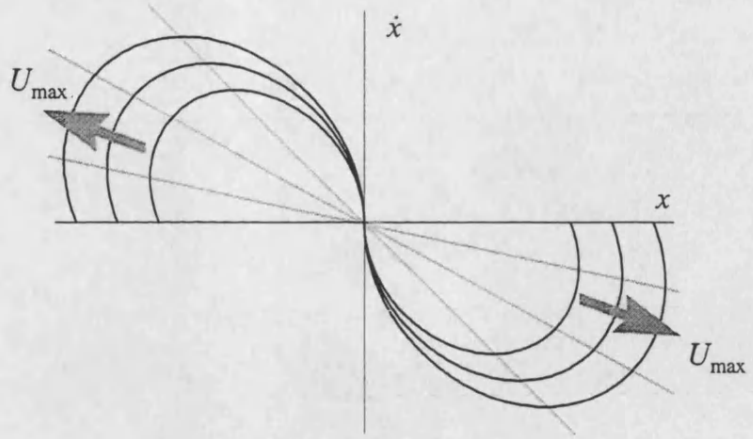

Figure 6.8 - Sliding domain for increasing control signal U_{max}

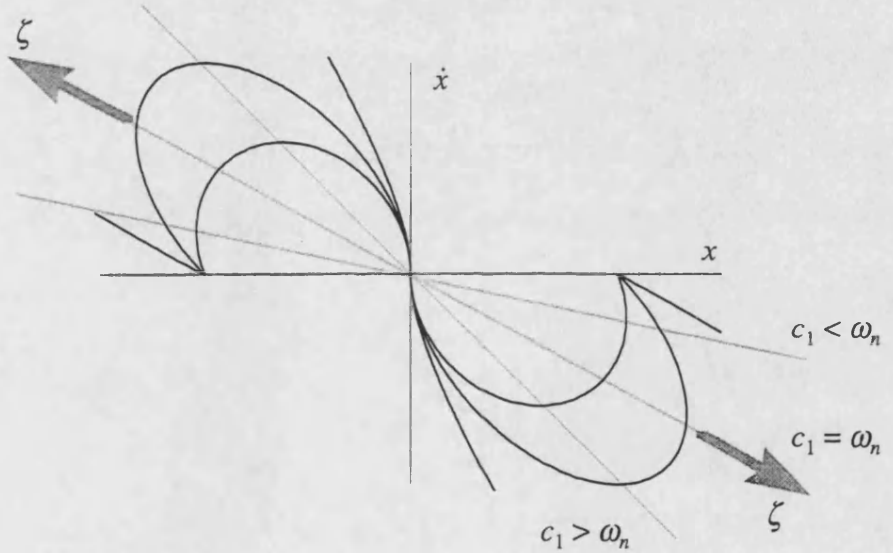

Figure 6.9 - Sliding domain for increasing damping ratio ζ

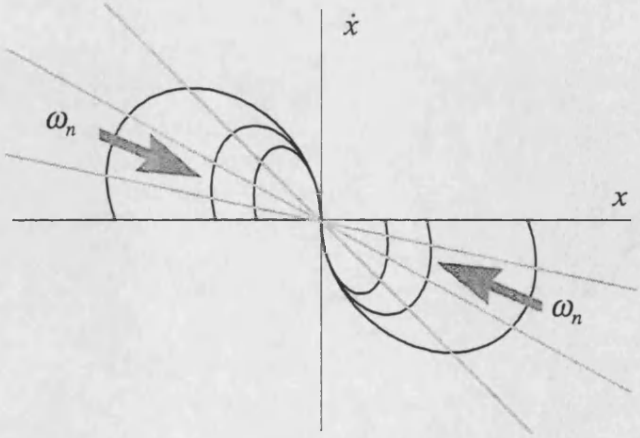

Figure 6.10 - Sliding domain for increasing natural frequency ω_n

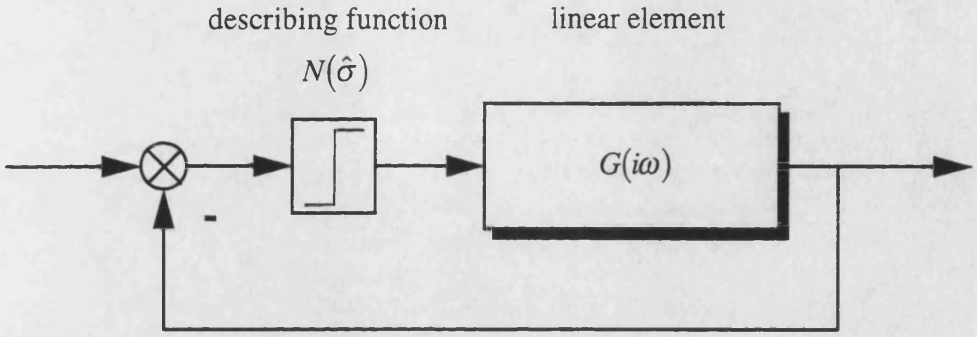

Figure 6.11 - Describing function analysis

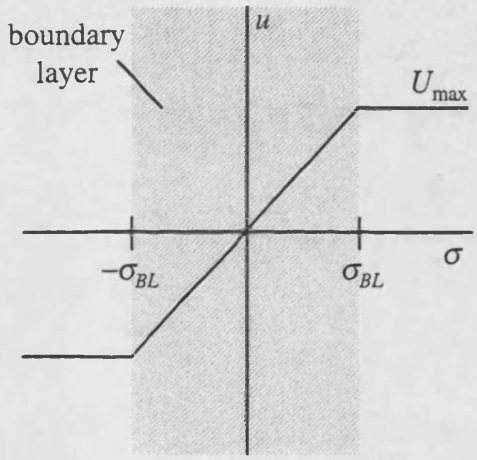

Figure 6.12 - Boundary layer neighbouring the switching surface $\sigma = 0$

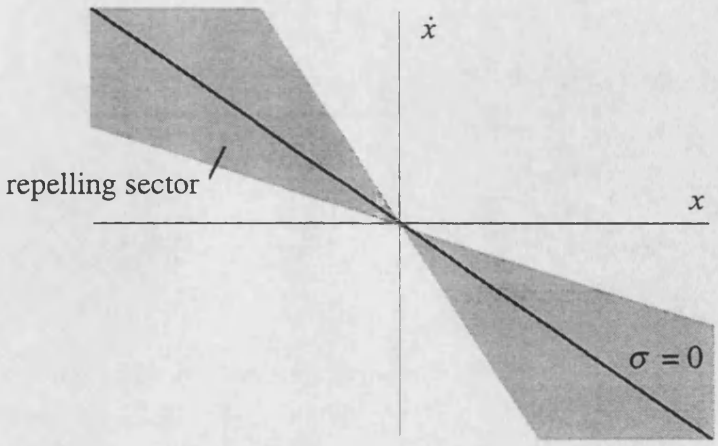

Figure 6.13 - Repelling sector around the switching surface $\sigma = 0$

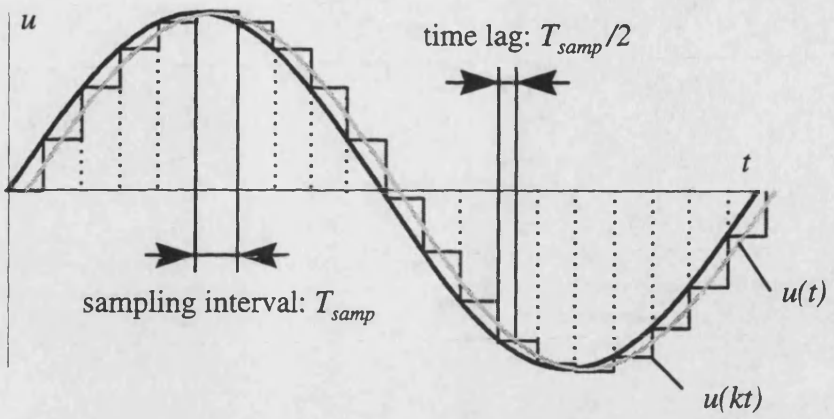

Figure 6.14 - Time lag due to sampling

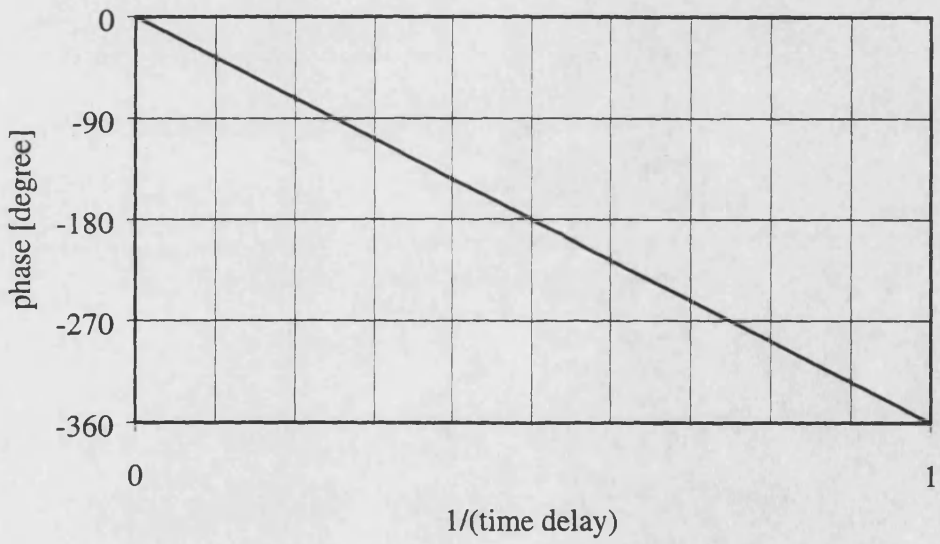

Figure 6.15 - Additional phase lag due to time delay

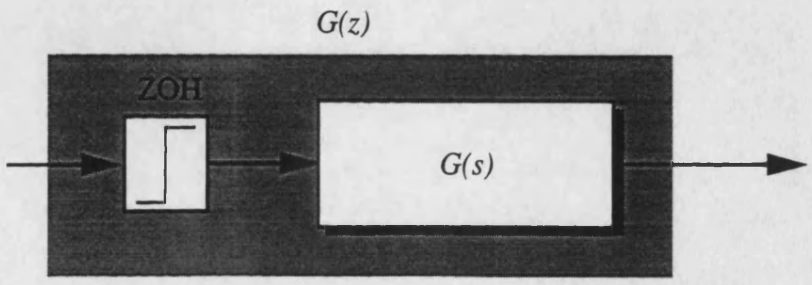

Figure 6.16 - Discrete transfer function *G(z)*

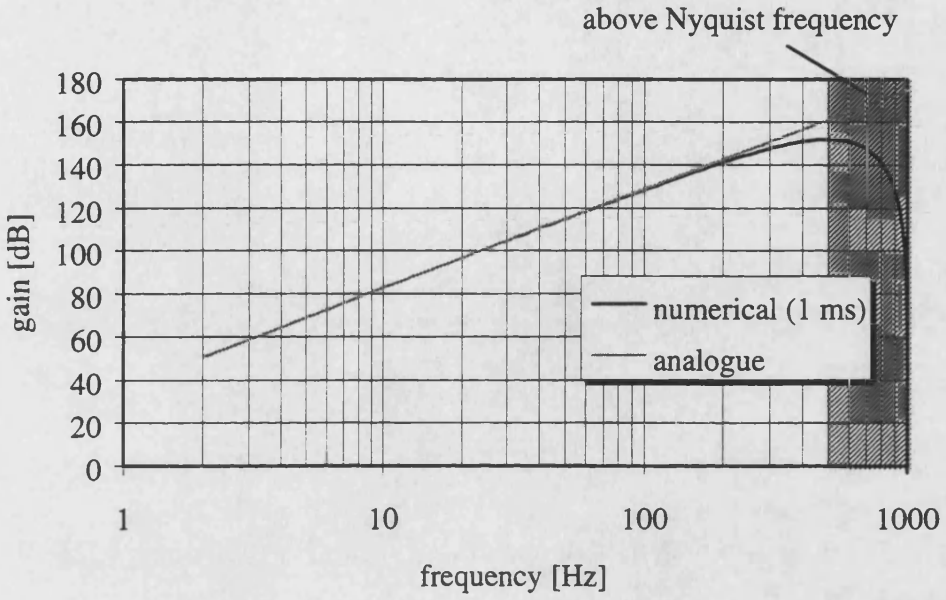

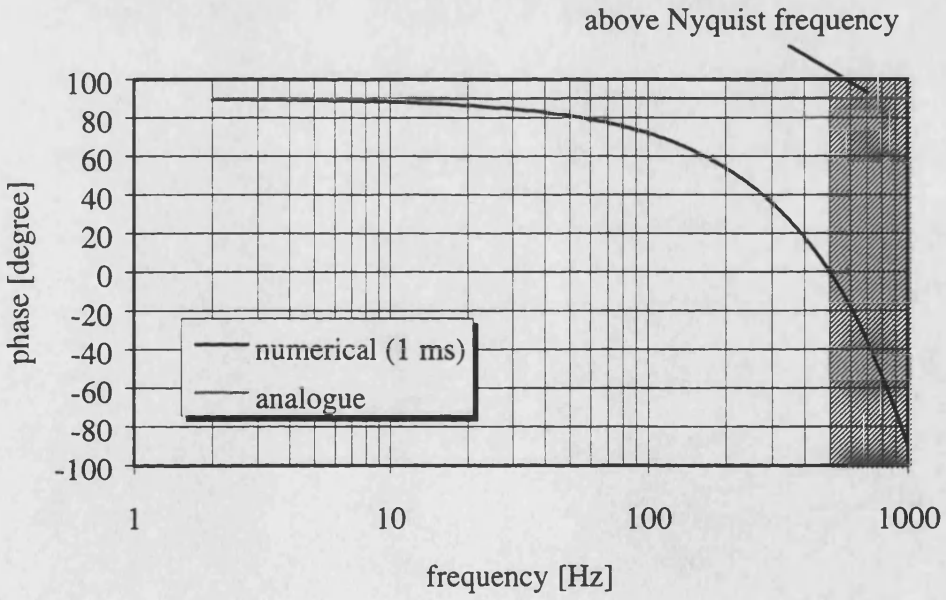

Figure 6.17 - Bode plot of discrete differentation routine (T_{samp} = 1 ms)

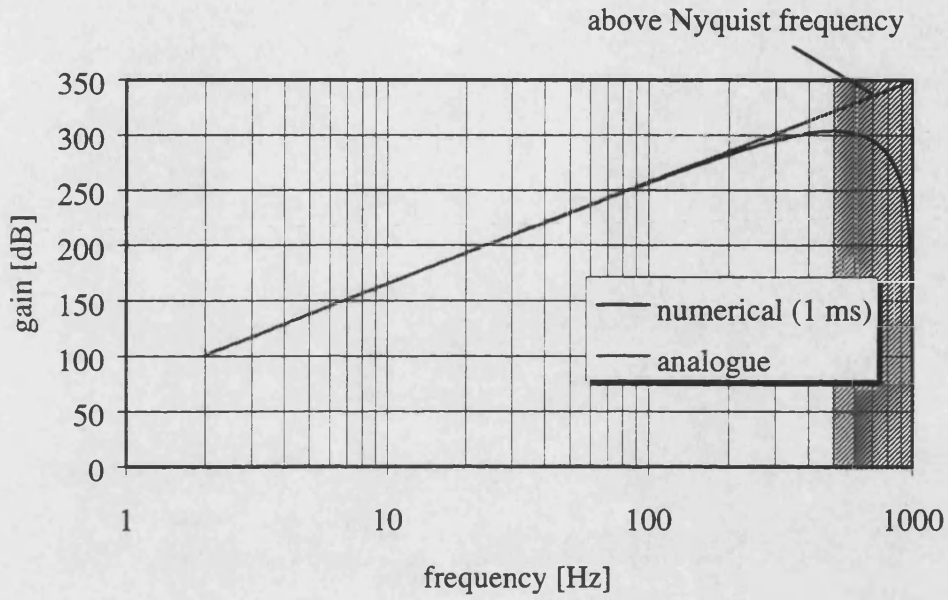

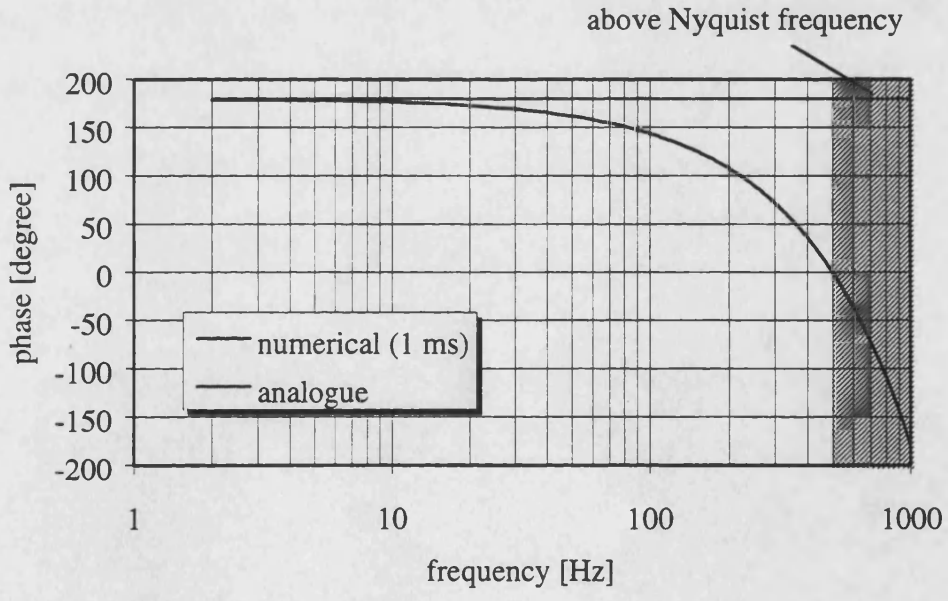

Figure 6.18 - Bode plot of discrete double-differentation routine (T_{samp} = 1 ms)

7 BASIC DESIGN OF A SLIDING MODE CONTROLLER FOR A PNEUMATIC SERVO

As mentioned already, it was decided to develop a CSLMC algorithm instead of a DSLMC one because CSLMC generally offers greater robustness to parameter changes and the action of external disturbances provided that, when implementing it digitally, the sampling frequency is sufficiently high (Iordanou and Surgenor (1997)). A CSLM controller therefore seems to be better suited for the animated figure (and other *n*DOF applications like industrial manipulators) where parameter changes and external disturbances are of major concern.

In this chapter therefore, a continuous-time sliding mode controller (CSLMC) for the pneumatic actuation system of the animated figure described in Chapter 3 will be designed. The design will be based on the advanced linear model of the pneumatic servo system introduced in Section 5.2. Critical design questions in the context of the reachability condition will be discussed and its limitations as a design tool for CSLM controllers will be analysed. The CSLMC design procedure will be completed in Chapter 8 by means of a limit cycle analysis using the extended Nyquist criterion. In Chapter 9 the CSLM control algorithm is then validated by means of computer simulations using the non-linear simulation model presented in Chapter 4 and experimental results.

7.1 DESIGN PROCEDURE

The first step when designing a sliding mode controller is to decide on a nominal system model and to choose a sliding surface accordingly. The sliding surface has to fulfil the following requirements:

- It has to be of sufficient order.
- Since it defines the system's closed-loop dynamics it has to be stable.
- It has to be reachable by the system state over the whole range space.

The CSLMC design aspects presented in this chapter will in particular concentrate on these requirements by analysing the reachability condition for a given

sliding surface, a realistic system range space and the nominal model of the servo dynamics. At this stage the influence of parameter changes are included in the analysis by using the parameter update model introduced in Section 5.3.3. The results of this procedure are the state gains of the chosen sliding surface which guarantee that the sliding surface is reachable by the nominal system model.

7.2 SURFACE ORDER

As demonstrated in Section 6.2, the order of a continuous-time switching surface along which the system state is driven towards its origin is generally n-1 for an n^{th}-order plant to be controlled. Although all physical systems have an infinite order, the dominant dynamics of a pneumatic servo mechanism including the valve spool dynamics as described in Chapter 5 can be expressed as a fifth-order linear transfer function resulting in the need for a fourth-order sliding surface. In order to synthesise this surface based on the canonical representation of the system dynamics, the system displacement (or displacement error) and the first four of its derivatives have to be available. From the implementation standpoint this can be very difficult if not impossible. Even in the ideal case of displacement, velocity and acceleration being measurable the output of the accelerometer still has to be differentiated twice introducing significant noise into the system and also an additional phase lag if this is done numerically or a noise filter is used.

Since the animated figure is only fitted with a potentiometer-type displacement transducer it was decided to neglect the fast dynamics of the servo valve and only to use a third-order servo model. A linear second-order sliding surface can now be constructed by means of the system displacement (or displacement error) and only the first two of its derivatives (velocity and acceleration or for path tracking velocity error and acceleration error):

$$\sigma(x) = -c_1(x - x_d) - c_2\dot{x} - c_3\ddot{x} \quad \text{(positioning)} \tag{7.1}$$

$$\sigma(x) = -c_1(x - x_d) - c_2(\dot{x} - \dot{x}_d) - c_3(\ddot{x} - \ddot{x}_d) \quad \text{(path tracking)} \tag{7.2}$$

Obviously, neglecting the valve dynamics will only yield reduced-order switching with the neglected valve dynamics being treated as external disturbances by the reduced-order CSLMC system. As will be demonstrated and discussed in Chapter 8,

the reduction of the order of the plant model and hence of the switching surface results in the fact that the bandwidth of the neglected valve dynamics limits the switching frequency of the control system.

7.3 SURFACE DYNAMICS

The sliding surface can be interpreted as a description of the desired response of the closed-loop control system. It can therefore be seen as comparable to the reference model in model reference adaptive control (MRAC) (de Almeida (1993)). Hence, when tuning the chosen second-order sliding surface the following relations can be used relating natural frequency ω_n and damping ratio ζ of the desired system response to the state gains of the sliding surface (Surgenor *et al* (1995)):

$$c_1 = \omega_n^2 ; \quad c_2 = 2\zeta\,\omega_n ; \quad c_3 = 1 \tag{7.3}$$

These again can be related to the following performance specifications in the time-domain:

$$T_{sett} = \frac{4}{\zeta\,\omega_n} \quad \text{and} \quad M_p = 100e^{\frac{-\pi\zeta}{\sqrt{1-\zeta^2}}} \tag{7.4}$$

where T_{sett} is the $\pm$ 2% settling time and M_p the precentage overshoot. The sliding surface will be designed to achieve a critically damped system response with the damping ratio ζ set to unity. The settling time T_{sett} of the closed-loop system in the sliding mode has to be chosen under the requirement of guaranteed reachability within the system range space as will be shown in the following.

7.4 REACHABILITY OF SLIDING SURFACE AND SLIDING DOMAIN

To determine whether a chosen switching surface is reachable by the system, state Condition (6.15) derived in Section 6.4 has to be verified. For a dynamic system with changing system parameters (like a pneumatic servo mechanism) described by:

$$\dot{x} = (\boldsymbol{A}_0 + \Delta\boldsymbol{A})x + (\boldsymbol{B}_0 + \Delta\boldsymbol{B})u + d \tag{7.5}$$

the reachability condition can be written as:

$$\lim_{\sigma\to 0} \sigma\dot{\sigma} = \sigma\, s^T(\boldsymbol{A}_0 x + \boldsymbol{B}_0 u + \Delta\boldsymbol{A}x + \Delta\boldsymbol{B}u + d) < 0 \tag{7.6}$$

where ΔA and ΔB are matrices containing the maximum parameter variations from their nominal values A_0 and B_0. The vector d here represents external disturbances.

The following equivalent control signal is required to keep the system state of the nominal model of the pneumatic servo on the sliding surface defined by s^T once it has been reached:

$$u_{eq} = -K_{eq}x = -\left(s^T B_0\right)^{-1} s^T A_0 x = -\begin{pmatrix} 0 \\ \dfrac{c_1 - c_3 a_1}{c_3 b_0} \\ \dfrac{c_2 - c_3 a_2}{c_3 b_0} \end{pmatrix} \begin{pmatrix} x \\ \dot{x} \\ \ddot{x} \end{pmatrix} \tag{7.7}$$

Here the parameters a_1, a_2 and b_0 describe the system's open-loop dynamics as shown in Section 5.2. Using now the on/off-relay control law:

$$u = u_{switch} = -U_{\max} \operatorname{sgn}(\sigma) \tag{7.8}$$

the sliding domain on the sliding surface can be determined by requiring that the absolute value of the switching control signal u_{switch} has to be greater or equal to the absolute value of the equivalent control signal u_{eq}. Therefore, just considering the nominal system model the following inequality has to hold true:

$$|u| = |u_{switch}| = U_{\max} \geq |u_{eq}| = |u_{nom}| = |\mathbf{K}_{eq} x| = \left| \frac{c_1 - c_3 a_1}{c_3 b_0} \dot{x} + \frac{c_2 - c_3 a_2}{c_3 b_0} \ddot{x} \right| \tag{7.9}$$

Including the effects of parameter changes due to actuator piston position and direction of motion results in an additional control signal u_{par} necessary to assure that the pneumatic servo system remains in sliding mode once the sliding surface has been reached:

$$\begin{aligned} u_{par} &= -\left(s^T (B_0 + \Delta B)\right)^{-1} \left(s^T \Delta A - s^T \Delta B \left(s^T B_0\right)^{-1} s^T A_0\right) x \\ &= -\frac{1}{b_0 + \Delta b_0} \begin{pmatrix} 0 \\ -\Delta a_1 - \dfrac{\Delta b_0}{c_3 b_0}(c_1 - a_1 c_3) \\ -\Delta a_2 - \dfrac{\Delta b_0}{c_3 b_0}(c_2 - a_2 c_3) \end{pmatrix} \begin{pmatrix} x \\ \dot{x} \\ \ddot{x} \end{pmatrix} \end{aligned} \tag{7.10}$$

Therefore, the sliding domain is limited by the following condition:

$$|u| = |u_{switch}| = |U_{\max}| \geq |u_{nom} + u_{par}| = |u_{eq}^*| \tag{7.11}$$

7.5 SYSTEM RANGE SPACE

As mentioned before, the reachability of the sliding surface (and the existence of the sliding domain) has in general to be guaranteed over the whole system's range space. It is therefore important to determine the range space boundaries that is, considering the positioning switching function (Equation (7.1)), maximum and minimum displacement error, velocity and acceleration achievable by the pneumatic servo. When implementing the path tracking switching function (Equation (7.2)) limits also have to be determined on the demand velocity and acceleration.

The dynamic limits of the linear model can easily be obtained by evaluating the frequency response of the system's open-loop linear transfer function $G(s)$ (Equation (4.26)) and its derivatives $sG(s)$ and $s^2G(s)$. These are shown Figure 7.1. The following velocity and acceleration limits were obtained using the linear pneumatic servo model and the dynamic parameters listed in Table 5.2. It was further assumed that the displacement is limited by the actuator stroke:

$$|x| \le 0.03\text{m}; \quad |\dot{x}| \le 0.75\,\text{m/s} \quad \text{and} \quad |\ddot{x}| \le 95\,\text{m/s}^2 \tag{7.12}$$

Please note, that the system jerk is also limited. The amplitude of the frequency response of the system jerk $s^3G(s)$ is 12696 m/s^3. With increasing frequency the system jerk then converges towards 5225 m/s^3 for a fully open control valve.

The above velocity and acceleration limits are only relevant for the linear model. The non-linear system is further limited by the maximum mass flow rate through the control valve (due to choked flow) and a maximum available pressure force acting on the actuator piston. The maximum mass flow rate limits the piston velocity while the maximum pressure force limits the piston acceleration. Using Newton's law and the choked flow condition for exhausting the actuator chambers results in the following boundary values for the non-linear model:

$$\begin{aligned} |x| \le 0.03\text{m}; \quad & -0.25\,\text{m/s} \le \dot{x} \le 0.356\,\text{m/s} \quad \text{and} \\ & -67\,\text{m/s}^2 \le \ddot{x} \le 82\,\text{m/s}^2 \end{aligned} \tag{7.13}$$

From experimental data it was found that the smaller extreme velocity and acceleration values in Equation (7.13) fairly accurately represent the limits of the physical system.

7.5.1 System Range Space Based on Physical Limits of Servo

It can be deduced from the reachability condition (Equation (7.9)) that in order to freely control the sign of $\dot{\sigma}$ by switching between U_{max} and -U_{max} the following inequality has to hold true:

$$-c_3 b_0 U_{max} \leq (c_1 - c_3 a_1)\dot{x} + (c_2 - c_3 a_2)\ddot{x} \leq c_3 b_0 U_{max} \tag{7.14}$$

This inequality defines a space within which reachability is guaranteed by the fact that the sign of $\dot{\sigma}$ can be freely controlled by means of the switching control action. This space will therefore be called *controllability space* in the following. The area of the sliding surface contained within this controllability space represents the sliding domain. In general, it can be shown that even if the controllability space is smaller than the range space the reachability condition will still be satisfied if the sliding domain boundaries are outside the range space. This fact is illustrated in Figure 7.2 for a sliding surface with a settling time of T_{sett} = 0.25 s. It shows the rectangular box which defines the range space for the non-linear limits given in Equation (7.13). The grey regions signify regions which are within the range space but outside the controllability space. The light grey regions in the corners of the range space are the regions in which the system state is still forced towards the sliding surface. Only in the dark grey region is the system state repelled by the sliding surface. On the right hand side of Figure 7.2 it can be seen that the sliding domain boundary lies within the range space. Therefore, the reachability condition is not satisfied since the system state is not forced towards the sliding surface from above and below. On the left hand side though, the reachability condition is satisfied from both sides despite the limited controllability region due to the fact that the sliding domain boundary lies outside the range space. Hence, in order to guarantee reachability over the whole system range space, it has to be proved that the boundaries of the sliding domain on the sliding surface are outside the range space limits. Alternatively, it should be made sure that no regions where the system state is repelled from sliding surface (dark grey regions) exist within the range space .

Figure 7.3 emphasises the importance of choosing the appropriate range space boundaries. As can be seen, choosing the boundaries based on the linear system model result in large areas where the reachability condition is not satisfied (dark grey areas) while choosing the smaller range space boundaries based on the

physical limitations of the servo as depicted in Figure 7.2 results in a significant reduction of these areas. Yet it has to be mentioned that in the case of the chosen range space being smaller than the physical system's range space the reachability condition might be violated by the real physical system.

Similar to the case of a second-order plant and a first-order surface as demonstrated in Section 6.7 the sliding domain decreases with a decrease in sliding surface settling time assuming a fixed maximum control signal U_{max} as can be seen in Figures 7.4 to 7.6.

Figure 7.7 shows the settling time of a linear second-order sliding surface as a function of the maximum fractional valve opening under the condition that the surface is globally reachable by the nominal linear servo model. It can be seen that with a supply pressure of P_s = 6.5 bar the fractional valve opening has to be at least 1.2 in order to guarantee reachability of the sliding surface over the whole system range space. In particular for a fractional valve opening of 1 (representing valve dimensions of the 1DOF pneumatic servo test-rig) the sliding surface is not globally reachable by the nominal model even for long settling times. In this case there are two ways of assuring global reachability:

- Increasing the valve size (fractional valve opening)
- Increasing the supply pressure P_s

Doubling the valve flow rate (fractional valve opening = 2) results in a sliding surface with a settling time of T_{sett} = 0.05 s being globally reachable. Increasing the supply pressure to P_s = 10 bar yields that a sliding surface with a settling time of T_{sett} = 0.143 s is globally reachable even for a fractional valve opening of 1 and less.

Considering the effects of system parameter changes (due to actuator piston position and direction of valve opening) by using the parameter update model introduced in Section 4.3.3 results in an increase of the achievable settling times of T_{sett} = 0.02 s as can be also seen in Figure 7.7. Therefore, parametric uncertainties have an adverse influence on the reachability of a sliding surface and obviously require a larger control action for compensation.

The above results have been obtained by verifying the reachability condition over the whole specified range space for a linear second-order sliding surface. As a result, the fastest globally reachable sliding surfaces are determined representing the fastest achievable closed-loop system response in sliding mode.

It should be noted, that the above results are only valid assuming that the control action is solely used to force the system state onto the sliding surface and keep it there. In this case no control action is available to compensate for further parameter changes or the influence of external disturbances.

7.5.2 Range Space Based on Representative State Trajectories

The fact that no linear second-order sliding surface is globally reachable by the dynamic state of the pneumatic servo mechanism with a given supply pressure of $P_s = 6.5$ bar and a fractional valve opening of 1 (nominal valve flow rate of 2 SCFM at 100 psi) would usually require the introduction of non-linear switching strategies or the alteration of the physical plant (larger valve size, larger supply pressure). An increase in supply pressure or the use of a larger valve size were outside the scope of this project though and non-linear switching strategies result in rather complex controllers which are more difficult to tune and rule out the possibility of an easy analogue implementation.

Nevertheless, although ideally reachability should be guaranteed over the whole range space, in general a real physical dynamic system operates in a fairly limited region of its theoretical space of existence based on the physical limitations as defined in this case by Equation (7.13). This limited space of existence depends on possible initial conditions, demand signals and also on external disturbances. It can for instance be assumed that for positioning control, initial velocity and acceleration of the actuator piston are zero or close to zero. Therefore, it is an appropriate assumption to define only these initial conditions and the open-loop state trajectories starting from these initial conditions as the system range space. It was found that based on the above initial conditions and the requirement that the reachability condition is not violated at any time along the state trajectory very fast sliding

surfaces with a settling time of $T_{sett} = 0.1$ s are now reachable by the system state for a fractional valve opening of 1 as shown Figure 7.7.

Another factor that should be considered when designing the sliding surface is its orientation relative to the range space. The orientation of the sliding surface might result in the fact that although a decrease in sliding surface settling time reduces the closed-loop system response time *in sliding mode* significantly, the reaching phase before the establishment of sliding mode might increase leaving the system response sensitive to parameter changes and external disturbances for an extensive period of time. It can be seen in Figures 7.4 and 7.6 that a faster sliding surface ($T_{sett} = 0.05$ s) despite offering a smaller sliding domain also only covers a smaller displacement error region than a slower surface ($T_{sett} = 0.09$ s). Therefore, when choosing a slower surface for a positioning VSC controller the reaching phase will be shortened and the surface will be reached faster even though the displacement error is still significant. When choosing a faster surface on the other hand, most of the set point approach will be performed during the reaching phase and not in sliding mode. Therefore, it might not always be advisable to choose a fast sliding surface although reachability might be guaranteed. In this case sliding mode might only be established shortly before the set point has been reached.

In some cases a fast surface can be reachable all along a given state trajectory while a slower surface results in the reachability condition being violated. This is again due to the fact that changing the settling time of the sliding surface not only alters the sliding domain but also changes its orientation (compare Figures 7.6 and 7.9). Since the open-loop response is fixed for a given initial condition and a given maximum valve opening, the open-loop trajectory might enter the region outside the controllability space where it is repelled by the sliding surface in case of a slow surface and not in case of a faster one. An example demonstrating this phenomenon is given in Figure 7.10 and 7.11 for the settling time of $T_{sett} = 0.05$ s and $T_{sett} = 0.02$ s, respectively.

It can be concluded from the above analysis that for the system under consideration a linear second-order sliding surface with a settling time of $T_{sett} = 0.07$ s (as shown in Figure 7.5) would represent a satisfactory compromise between fast closed-loop dynamics of the VSC system in sliding mode and the region

within the range space in which it is reachable. The resulting state weights are the following:

$$c_1 = 3265.3\frac{1}{s^2}; \quad c_2 = 114.3\frac{1}{s} \quad \text{and} \quad c_3 = 1 \tag{7.15}$$

Computer simulations showed that the time of the reaching phase is T_{reach} = 0.065 s assuming an initial velocity and acceleration of zero and an initial displacement of x_i = 30 mm (stroke of the actuator). A representative CSLMC response with the chosen surface is depicted in Figure 7.12. It should be noted that for the chosen initial conditions the reachability condition is violated once. Yet, the system response seems satisfactory.

It seems interesting and important to mention that the reachability method described above can generally be used to size physical system components or parameters like valve size or supply pressure in order to enable the control system to meet certain dynamic criteria. All that has to be done is to determine the equivalent control action for a given dynamic response and to confirm that this control action can be achieved by the system.

7.5.3 Sustained Oscillations as a Violation of Reachability Condition

Temporary violations of the reachability condition prior to sliding mode can deteriorate the CSLMC system response noticeably. However, the dynamically worst response occurs when the system falls into a mode of sustained oscillation. As mentioned already in Section 6.2 although this mode of oscillation can occur in the case of non-ideal switching (due to a limited switching frequency because of reduced-order switching, discretisation, time delays etc.) it can also occur if the sliding surface settling time is chosen too fast. Therefore, another way of determining the fastest *reachable* sliding surface is to use the extended Nyquist criterion as explained in Section 6.11.2 and determine if limit cycles exist. Reachable in this context means that the system does not fall into a mode of sustained oscillation. As will be demonstrated in Section 8.1.1 the extended Nyquist criterion reveals that no limit cycles occur when choosing a settling time of T_{sett} = 0.07 s. This confirms the results of the above analysis. Therefore, sliding mode can be established and the system is not falling into a mode of sustained oscillation although the reachability

condition might be violated temporarily. According to the Nyquist criterion, the minimum settling time of a sliding surface not causing a limit cycle is $T_{sett} = 0.018$ s.

It has to be stressed again, that in the above analysis the valve spool dynamics were neglected. Therefore, what can be said at this point of the investigation is that limit cycles that might exist in the control system are not due to the choice of the dynamic parameters of the sliding surface but result from its order or other factors reducing the switching frequency.

7.6 EXTERNAL DISTURBANCES

Having chosen the sliding surface state weights the definition of the equivalent control action (Equation (7.7)) and the sliding domain (Equation (7.9)) can now be used to determine the systems robustness to additional parameter changes and the action of external disturbances. This can be done by estimating the difference between the maximum control action $U_{\max}$ and the equivalent control action u_{eq}^{*} (including parameter changes due to piston position and direction of valve opening) required to establish sliding mode.

The difference in control signal voltage between $u_{eq}^{*} = u_{nom} + u_{par}$ (black solid line in Figure 7.13) and the maximum voltage of $U_{\max} = 5$ V (fully open control valve) can be used to compensate for additional parameter changes or external disturbances. It can be seen in Figure 7.13 that this voltage decreases with a decrease in sliding surface settling time. It should be noted that the sliding surface settling times presented in Figure 7.13 are based on the requirement that the sliding surface does not yield a limit cycle and not on global reachability of the chosen sliding surface.

Assuming that all the remaining voltage can be used to reject external disturbances yields the maximum external disturbance vector $d_{\max}$ allowed to act on the system without changing the reachability properties of the sliding surface defined by s^{T}:

$$\left|s^T d_{\max}\right| = \left|s^T \begin{pmatrix} \dot{d}_{\max} \\ \ddot{d}_{\max} \\ \dddot{d}_{\max} \end{pmatrix}\right| \leq \left|s^T \left[(A_0 + \Delta A)x + (B_0 + \Delta B)u_{\max}\right]\right| \tag{7.16}$$

Figure 7.14 shows as an example the maximum allowable disturbance acceleration as a function of the sliding surface settling time, assuming that no disturbance velocity and jerk are acting on the system.

7.7 CLOSURE

In this chapter the requirements on the closed-loop CSLMC dynamics and the reachability condition were used to choose an appropriate second-order sliding surface.

Although this approach gives a good insight into the functioning of sliding mode control it is rather limited. The result presented above can be seen as a first CSLMC design step. They show that global reachability cannot be assured with the chosen control valve and supply pressure.

Despite violations of the reachability condition no limit cycles (sustained oscillations) are induced by the choice of the dynamic parameters of the sliding surface, only its order as will be demonstrated in the next chapter.

Since the CSLMC system under investigation is of reduced-order, limit cycles are an inherent part of the closed-loop dynamics. Amplitude and frequency of these limit cycles will be analysed in the next chapter to conclude the CSLMC design.

FIGURES

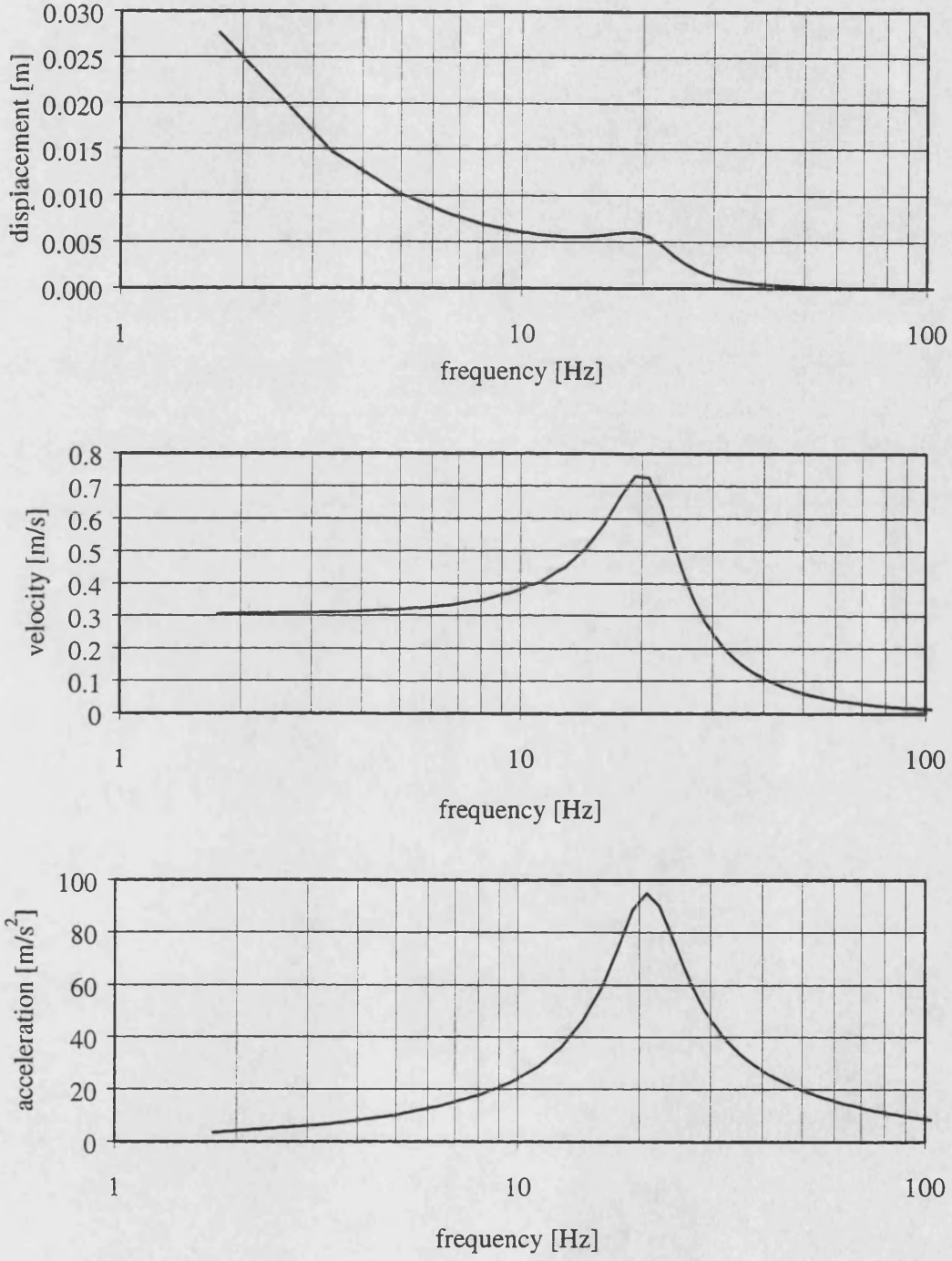

Figure 7.1 - State limits of linear model of pneumatic servo

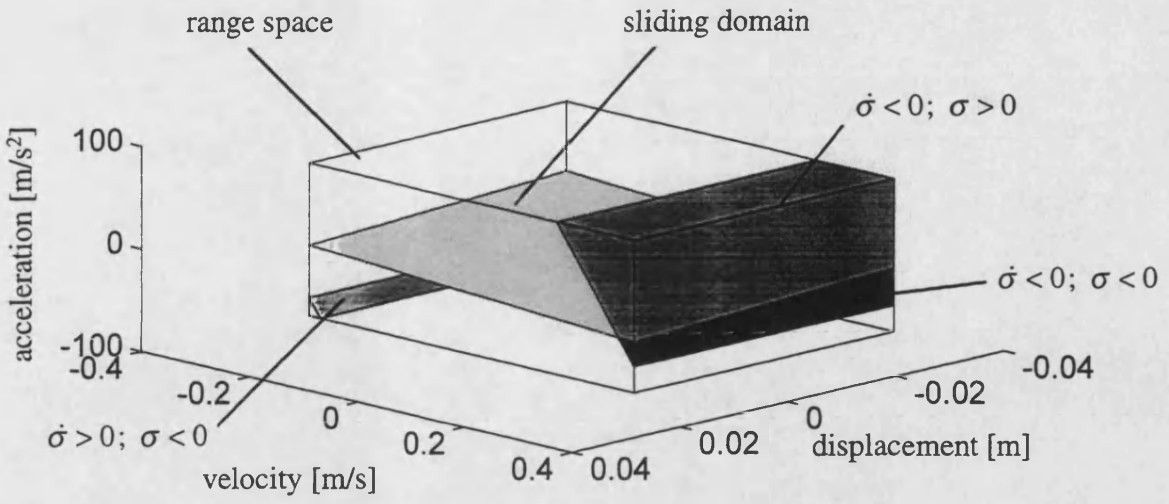

Figure 7.2 - Range space and sliding domain (T_{sett} = 0.25 s)

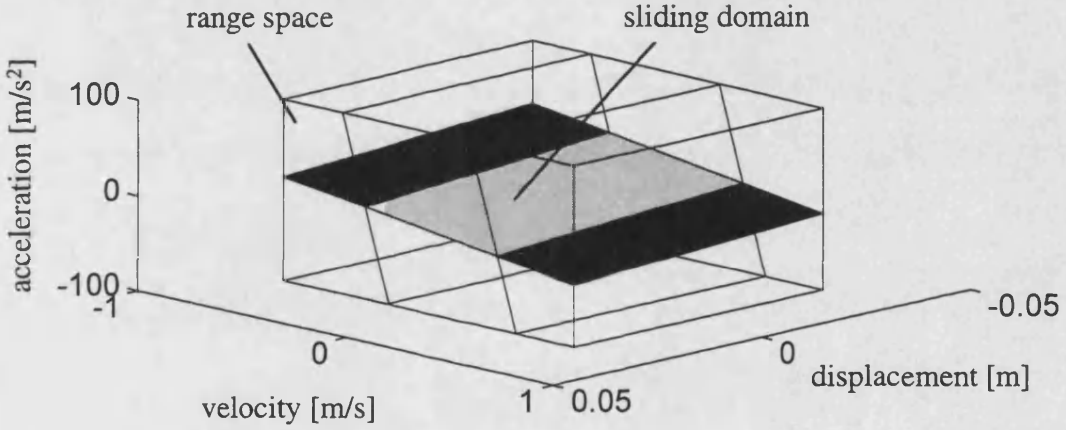

Figure 7.3 - Choice of range space boundaries (limits of linear model)

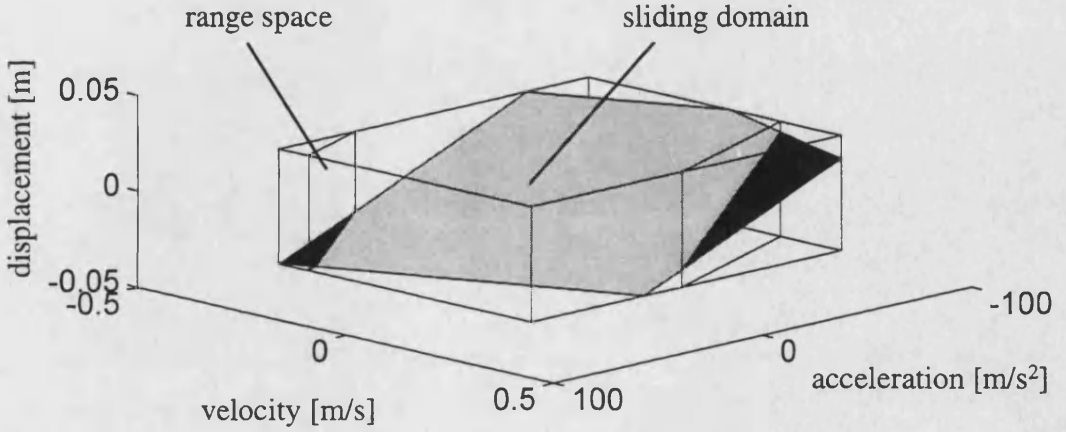

Figure 7.4 - Range space and sliding domain (T_{sett} = 0.09 s)

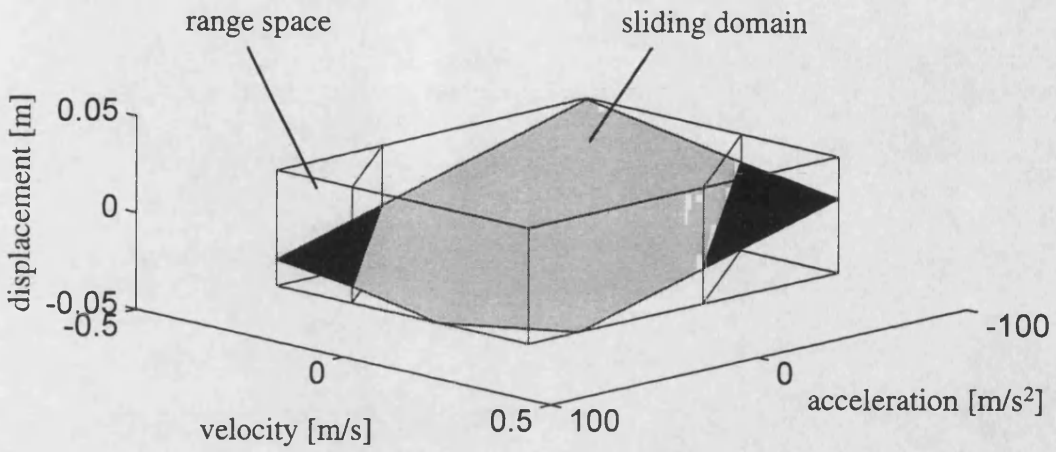

Figure 7.5 - Range space and sliding domain (T_{sett} = 0.07 s)

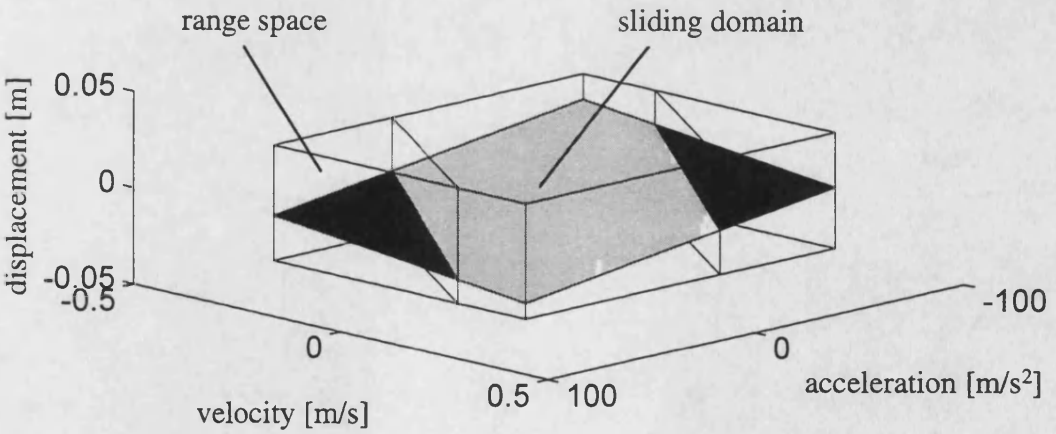

Figure 7.6 - Range space and sliding domain (T_{sett} = 0.05 s)

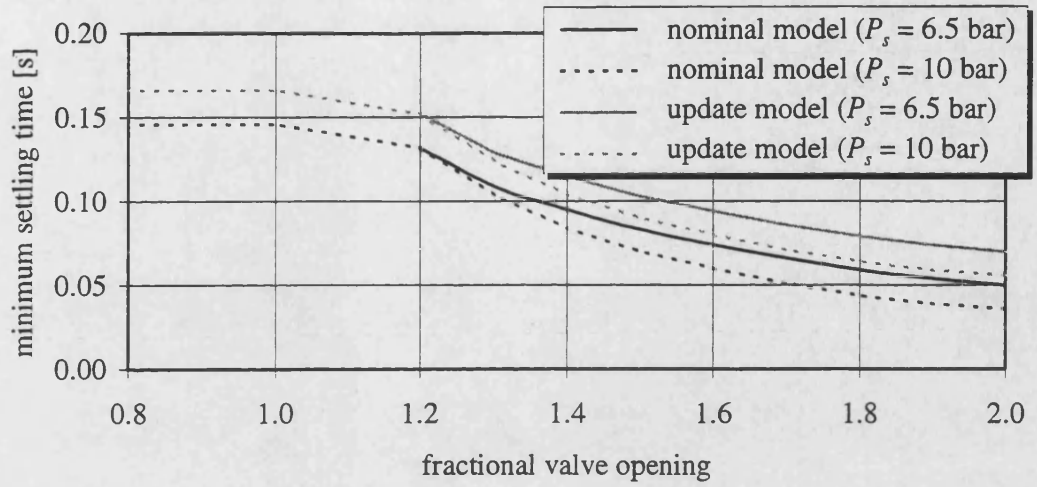

Figure 7.7 - Settling time of reachable sliding surface

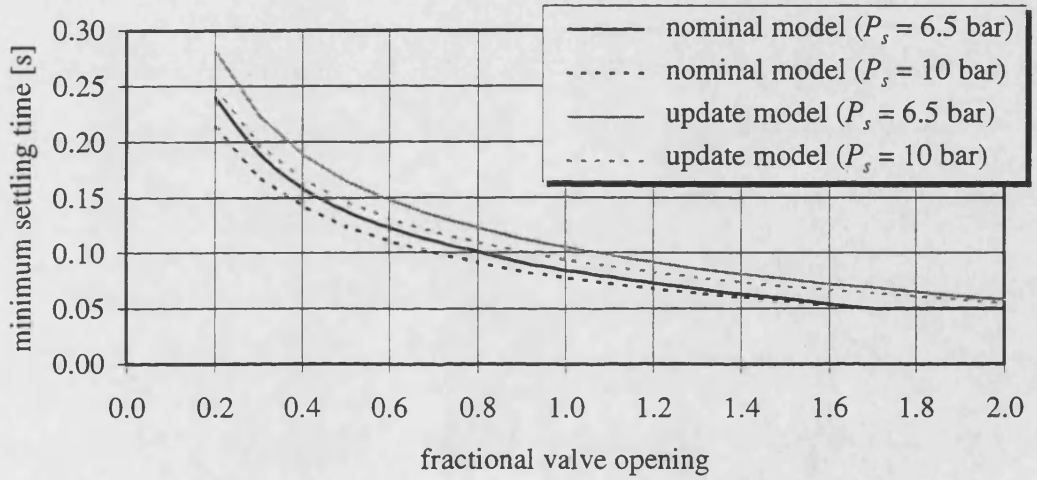

Figure 7.8 - Settling time based on representative system trajectories

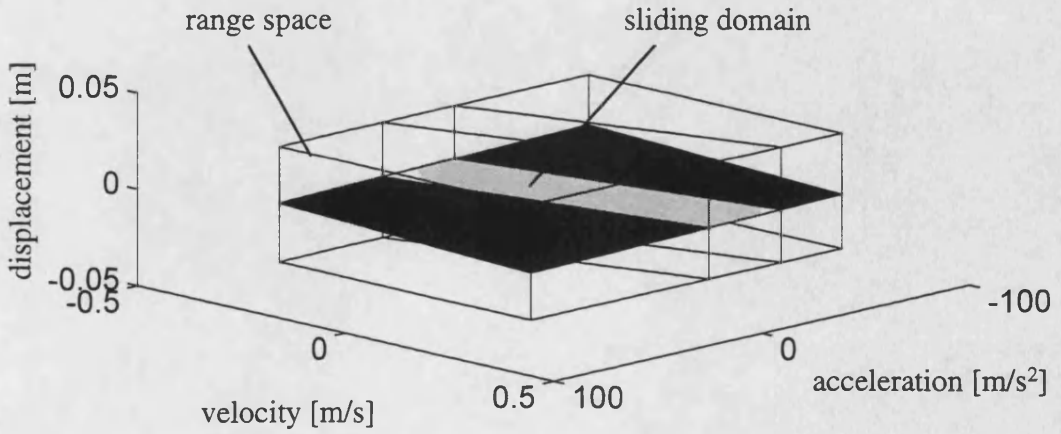

Figure 7.9 - Range space and sliding domain (T_{sett} = 0.02 s)

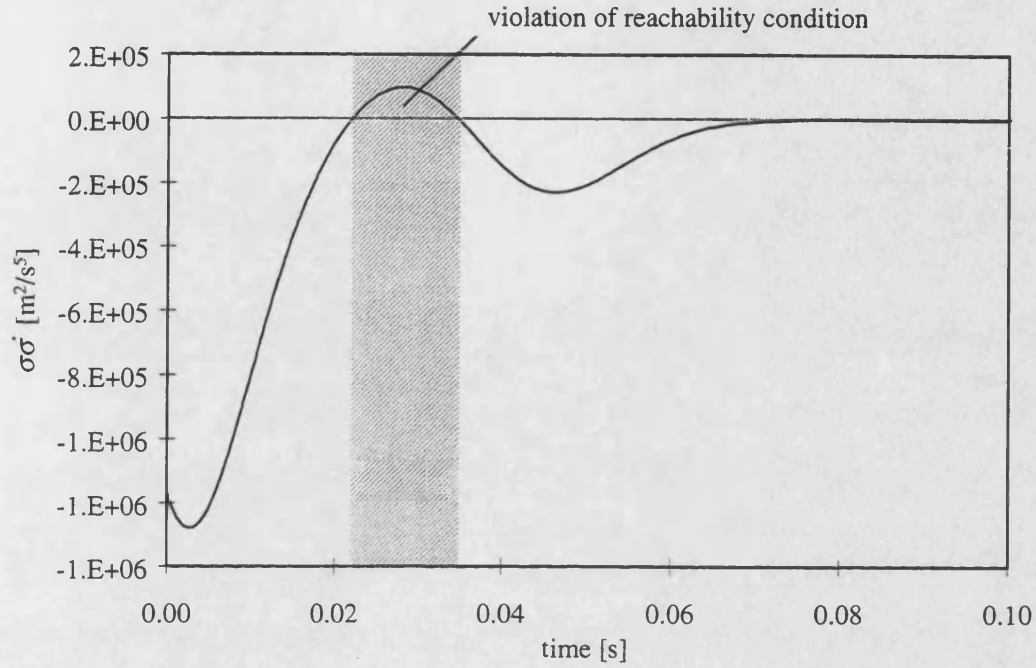

Figure 7.10 - Reachability of sliding surface with $T_{sett} = 0.05$ s

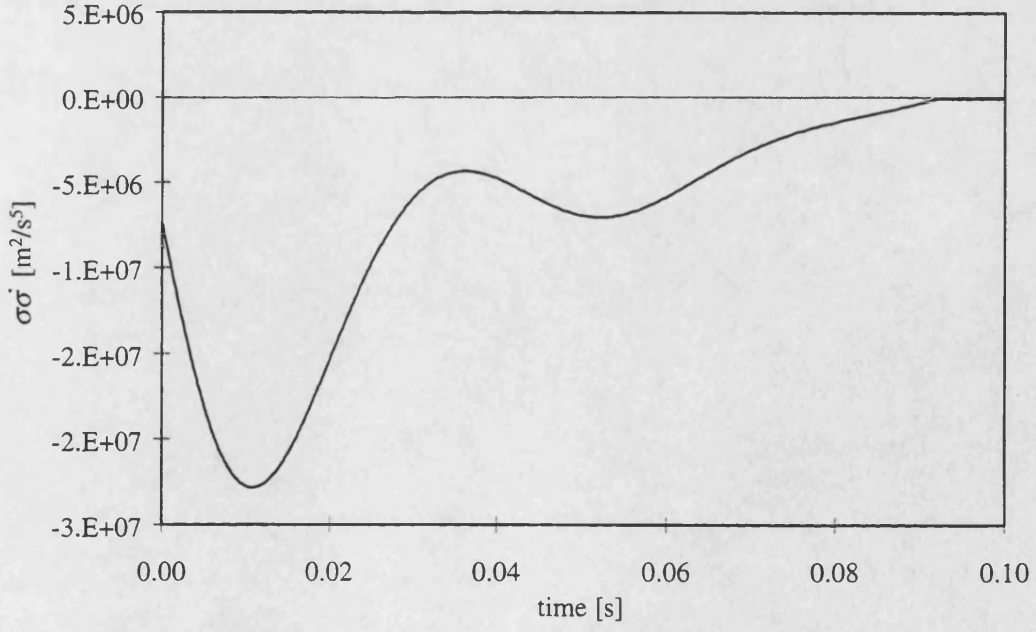

Figure 7.11 - Reachability of sliding surface with $T_{sett} = 0.02$ s

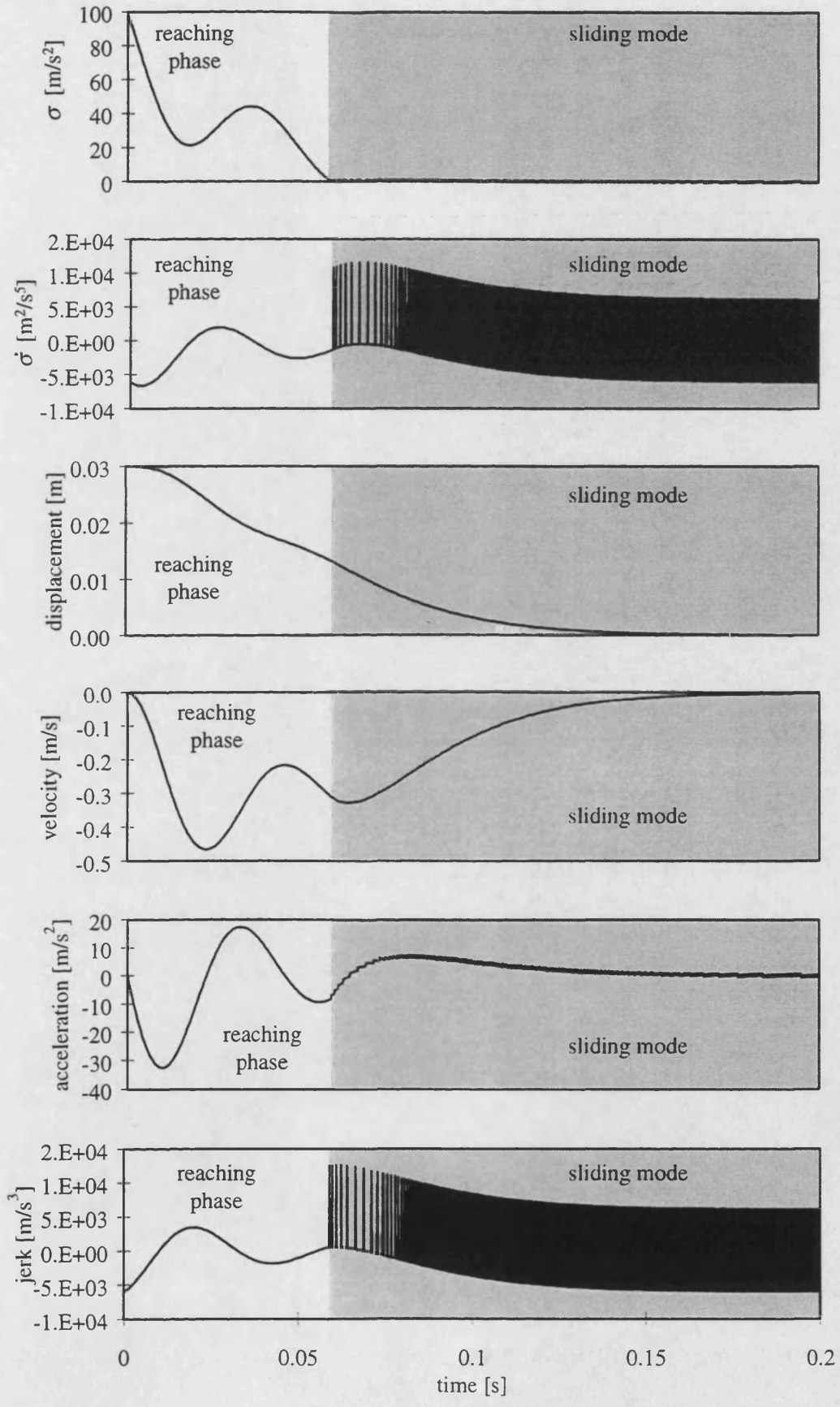

Figure 7.12 - CSLMC response of linear model (T_{sett} = 0.07 s)

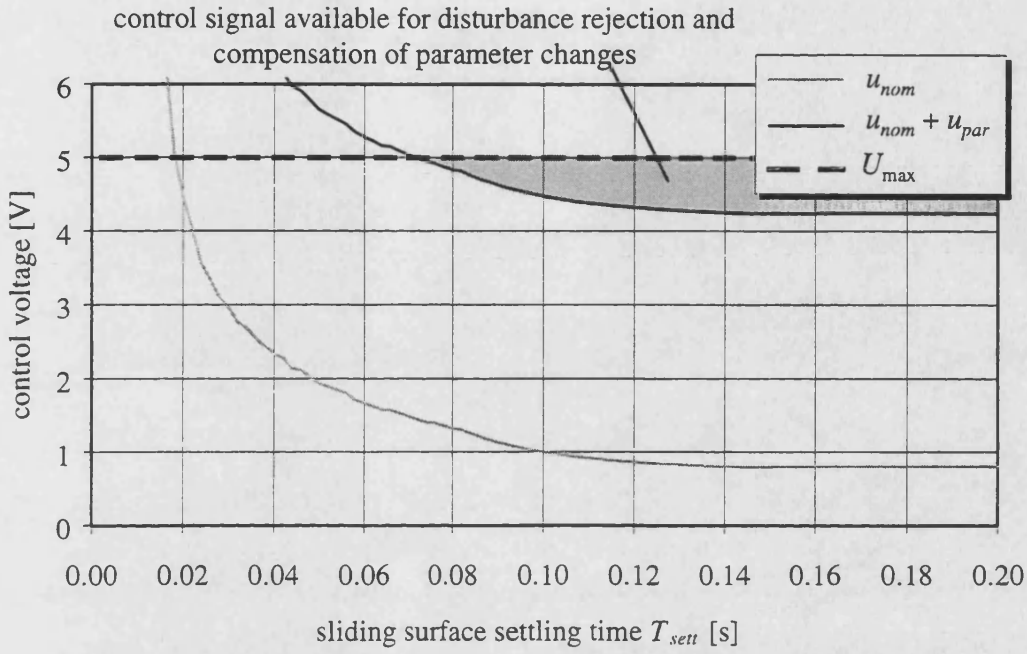

Figure 7.13 - Disturbance rejection capability and robustness to parameter changes

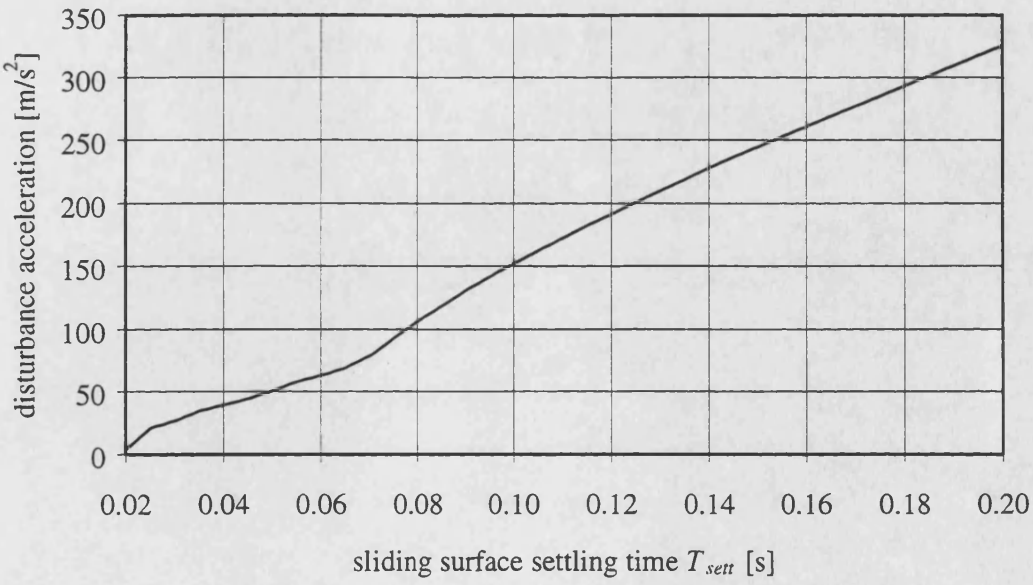

Figure 7.14 - Maximum rejectable disturbance acceleration

8 LIMIT CYCLE ANALYSIS OF THE CSLMC SYSTEM

In this chapter a limit cycle analysis of the CSLM control system for the pneumatic servo will be performed. This is of major importance for two reasons:

- Firstly, as shown in Chapter 7 global reachability cannot be achieved with the control system due to its physical limitations. However, it has to be ensured that for the ideal CSLMC system (full-order switching and no additional time delays) no limit cycles exist due to the choice of the dynamic parameters of the switching surface.
- Secondly, amplitude and frequency of the limit cycles resulting from the reduced-order of the CSLMC system and also from additional time lags have to be determined. By means of this analysis it can be decided how to synthesis the velocity and acceleration signals which cannot be measured. Furthermore, the question of whether an analogue, hybrid or digital implementation of the CSLM controller should be chosen can be answered.

In the following the influence of the following factors on the switching frequency will be investigated:

- sliding surface settling time
- neglected valve dynamics (reduced-order switching)
- second-order Butterworth filter of position feedback (e.g. LVDT)
- sampling of the system state (digital implementation)
- numerical differentiation of the displacement signal in order to synthesise velocity and acceleration

The limit cycle analysis is based on the extended Nyquist criterion as described in Section 6.11.2. To verify the results obtained by this method linear and non-linear simulation results of the closed-loop CSLMC system will be presented.

8.1 ANALOGUE CSLMC SYSTEM

8.1.1 PNEUMATIC SERVO SYSTEM WITHOUT VALVE DYNAMICS

To determine whether limit cycles due to the choice of the dynamic parameters of the sliding surface are induced into the CSLMC system, a closed-loop system consisting only of the linear model of a pneumatic servo mechanism and a relay element as depicted in Figure 8.1 is considered. The transfer function $G_1(s)$ of the linear part of this closed-loop system can be written as:

$$G_1(s) = \frac{\sigma(s)}{u(s)} = \left(c_3 s^2 + c_2 s + c_1\right) \cdot \frac{b_0}{s\left(s^2 + a_2 s + a_1\right)} \tag{8.1}$$

The Bode plot of this transfer function with a chosen surface settling time of $T_{sett} = 0.07$ s shown in Figure 8.2 reveals that the phase angle does not reach -180 degree. Therefore the system exhibits no limit cycles. Hence, the switching frequency of the control system in sliding mode is infinite.

These results can be verified by using the linear and non-linear simulation model in Bath*fp* described in Chapters 4 and 5. In simulation the switching time interval in sliding mode reduces to the minimum integration time interval of the simulation programme. Comparing the response of the linear and the non-linear simulation model in Figure 8.3 shows that both responses are equal. Therefore as predicted by theory, CSLMC in sliding mode compensates for the system's non-linearities (Tsypkin (1984)). Furthermore it should be appreciated that both responses are similar to the ideal response the control system is tuned for.

Reducing the sliding surface settling time and performing the same analysis described above it was found that a limit cycle occurs only when reducing the sliding surface settling down to $T_{sett} = 0.013$ s and less. Therefore, the ideal system will only fall into a mode of sustained oscillation if the sliding surface settling time is less or equal to $T_{sett} = 0.013$ s.

Interestingly, the good agreement between Nyquist and simulation results confirms the suitability of the use of the describing function approximation to represent the dynamics of the relay element as presented in Section 6.11.1.

8.1.2 PNEUMATIC SERVO SYSTEM WITH VALVE DYNAMICS

To determine the influence of the neglected valve dynamics on the closed-loop response of the CSLMC system a second-order model representing the valve spool dynamics is included in the plant model as shown in Figure 8.4. The resulting transfer function of the linear part of the control system is:

$$G_2(s) = \left(c_3 s^2 + c_2 s + c_1\right) \cdot \frac{\omega_v^2}{\left(s^2 + 2\zeta_v \omega_v s + \omega_v^2\right)} \cdot \frac{b_0}{s\left(s^2 + a_2 s + a_1\right)} \tag{8.2}$$

with ω_v being the natural frequency of the valve spool and ζ_v being its damping ratio. The Bode plot of the above transfer function is depicted in Figure 8.5. The results indicate the existence of a limit cycle with a frequency of f_{limit} = 203.4 Hz and an amplitude of A_{limit} = 3.84 m/s^2 as listed in Table 8.1. As expected, the bandwidth of the servo valve of 200 Hz limits the switching frequency of the CSLMC system.

Including the valve dynamics into the Bath*fp* simulation circuit yields the simulated step response results presented in Figure 8.6. The responses of the linear and the non-linear model now lag behind the ideal response while the non-linear response also exhibits a steady-state error of e_{sim} = 0.46 mm.

As can be seen in Figure 8.7 the limit cycle predicted by simulation of the response of the linear model has a frequency of f_{limit} = 204.1 Hz and an amplitude of A_{limit} = 3.73 m/s^2 which compares well with the theoretical results. Using the full non-linear model in simulation results in a limit cycle with a frequency of f_{limit} = 204.9 Hz and an asymmetric amplitude of A_{limit} = +3.43 m/s^2 and -2.80 m/s^2. The reason for this asymmetry is the difference in switching gain for different switching directions as is the case for the non-linear model where the transfer function numerator b_0 is dependent on the direction of valve opening (see Section 5.2). According to Lantto (1994) this asymmetry in the switching results in the observed steady-state errors. The maximum possible steady-state error e can be approximated to be:

$$\max(e) = \frac{\max(\sigma) - \min(\sigma)}{\omega_{switch}} \tag{8.3}$$

Using Equation (8.3) a theoretical maximum steady-state error due to asymmetric switching of e_{theo} = 0.47 mm can occur which compares well with the observed error of e_{sim} = 0.46 mm.

One interesting conclusion from Equation (8.3) is that the steady-state error due to asymmetric switching can be reduced by increasing the switching frequency in sliding mode.

8.1.3 Pneumatic Servo System with Valve Dynamics and Second-Order Butterworth Filter

8.1.3.1 Butterworth filter acting on the full system state

One possibility of measuring the system displacement is to use a LVDT position sensor. In this device a second-order Butterworth filter in the demodulation stage with a bandwidth of 500 Hz is used to filter out noise partly due to the exciting carrier frequency of the LVDT. Assuming that the position is measured using the LVDT and velocity and acceleration signals are derived from this LVDT signal without introducing any further time delays, the second-order Butterworth filter influences the whole system state. The resulting control system is depicted in Figure 8.8. The transfer function of the linear part of the closed-loop control system is:

$$G_3(s) = \frac{\left(c_3 s^2 + c_2 s + c_1\right)\omega_v^2}{\left(s^2 + 2\zeta_v \omega_v s + \omega_v^2\right)} \cdot \frac{b_0}{s\left(s^2 + a_2 s + a_1\right)} \cdot \frac{\omega_f^2}{\left(s^2 + 2\zeta_f \omega_f s + \omega_f^2\right)} \tag{8.4}$$

Using the Nyquist criterion (see Figure 8.9), the system exhibits a limit cycle with a frequency of f_{limit} = 148.6 Hz with an amplitude of A_{limit} = 6.55 m/s^2 listed Table 8.2. Hence, the Butterworth filter in the demodulation stage of the LVDT reduces the CSLMC switching frequency significantly due to the fact that it introduces an additional phase shift into the system state used to synthesis the switching function.

Figure 8.10 shows the simulated step response of the linear and the non-linear model. As in the previous case the responses of the linear and the non-linear model lag behind the ideal response and the non-linear model exhibits an additional steady-state error. As can be seen in Figure 8.11 the limit cycle predicted by simulation of the response of the linear model has a frequency of f_{limit} = 143.7 Hz and an amplitude

of A_{limit} = 6.57 m/s^2. This compares well again with the theoretical results listed in Table 8.2. Using the full non-linear model in simulation results in a limit cycle with a frequency of f_{limit} = 142.5 Hz and an asymmetric amplitude of A_{limit} = +6.37 m/s^2 and -4.57 m/s^2. The steady-state error in this case is e_{sim} = 1.3 mm which agrees with a maximum steady-state error of e_{theo} = 2.01 mm predicted by Equation (8.3).

Therefore, the additional Butterworth filter reduces the switching frequency and increases the steady-state error considerably.

8.1.3.2 Butterworth filter acting only on position and velocity

Assuming now that the Butterworth filter only acts on the position and velocity signal and not on the acceleration as shown in Figure 8.12 results in the following closed-loop transfer function:

$$G_4(s) = \left(c_3 s^2 + \frac{(c_2 s + c_1)\omega_v^2}{\left(s^2 + 2\zeta_v \omega_v s + \omega_v^2\right)} \right) \cdot \frac{b_0}{s\left(s^2 + a_2 s + a_1\right)} \cdot \frac{\omega_f^2}{\left(s^2 + 2\zeta_f \omega_f s + \omega_f^2\right)} \tag{8.5}$$

This transfer function corresponds to the case where position is measured by means of a LVDT and differentiated to obtain the velocity. Acceleration is measured using a separate accelerometer.

From the Bode plot depicted in Figure 8.13 it can be seen that the switching frequency now is 202.7 Hz and the amplitude is 3.73 m/s^2. These results are similar to ones obtained without the Butterworth filter which is confirmed by simulation as shown in Figures 8.14 and 8.15. All results can be found in Table 8.3.

8.1.4 Conclusions from the Limit Cycle Analysis of the Analogue CSLMC System

The conclusions that can be drawn from the results listed in Tables 8.1 to 8.3 is that only a phase shift in the highest system state (here acceleration) reduces the switching frequency of the CSLMC system in sliding mode. In other words, the bandwidth of the innermost (acceleration) feedback loop spanning the relay element limits the bandwidth of the CSLMC system and hence the switching frequency of the

system in sliding mode. This corresponds to the results found by Tsypkin (1984) using relay theory.

As a result, for an analogue implementation of a sliding mode controller for the pneumatic servo system under investigation the following two system set-ups are advisable:

- Displacement is measured using a potentiometer, velocity and acceleration are obtained by differentiating the displacement signal without introducing an additional phase lag. This can for instance be done by means of an analogue differentiation filter.
- Displacement is measured using a LVDT. Velocity is obtained by differentiating the displacement signal. Acceleration is measured separately.

If the above guidelines are adhered to only the bandwidth of the servo valve limits the switching frequency of the analogue CSLMC system.

Another interesting finding is that the bandwidth of the innermost feedback loop (acceleration) limits the switching frequency. Therefore, applying the extended Nyquist criterion just to the innermost feedback loop results in the same limit cycle prediction as applying it to the whole system. This fact can be utilised when looking at discrete or hybrid implementations of sliding mode controllers. Especially for hybrid systems it can be very difficult to synthesise a system model when part of the feedback loops are closed using analogue filters and others are closed numerically. Modelling just the inner feedback loop whether it is digital or analogue is comparably easy and will yield the same results.

8.2 Digital CSLMC System

8.2.1 Measuring and Sampling the System State

To obtain first of all a discrete system model of the pneumatic servo mechanism assuming that position, velocity and acceleration are measured the zero-order-hold (ZOH) approach can be used. The resulting discrete transfer function can be obtained by adding a ZOH element to its continuous counterpart. This can be

easily done using the MATLAB simulation software. The description of the *c2dm.m* routine in MathWorks, Inc. (1992) and Section 6.14 give further explanation. The circuit diagram of the discrete system without valve dynamics and Butterworth filter can be seen in Figure 8.16. The transfer functions of the systems with valve dynamics and the Butterworth filter can be obtained in a similar manner.

Figures 8.17 to 8.19 demonstrate the influence of the ZOH element with a sampling frequency of f_{samp} = 1 kHz on the switching frequency of the following three CSLMC systems:

- ideal system without valve dynamics
- system with valve dynamics and
- system with valve dynamics and Butterworth filter acting on all system states

As mentioned in Chapter 3 the sampling frequency of 1 kHz is the maximum achievable by the control PC and the software used. The resulting switching frequencies and amplitudes obtained using the extended Nyquist criterion are listed in Table 8.4. As can be seen from these results the ZOH element reduces the switching frequency significantly while the switching amplitude decreases only slightly at higher frequencies. In Figure 8.17 the maximum switching frequency achievable with the discrete CSLMC system without valve dynamics and Butterworth filter is half the sampling frequency. In this case the controller switches at every sampling instance.

Simulating the step responses of the discrete CSLMC systems using the linear and non-linear models with and without valve dynamics yields the limit cycles listed in Tables 8.5 and 8.6. Again Nyquist and simulation results are in good agreement. The step response results can be found in Figures 8.20 to 8.23. It can be observed that the response of the linear model now also exhibits a steady-state error while the response of the non-linear model shows an additional low-frequency oscillation. The results in Figures 8.21 and 8.23 show clearly an additional low-amplitude oscillation at the sampling frequency being superposed to the switching function due to the influence of the discrete-time sampling and updating of the control signal.

The steady-state error in the linear model is due to the fact that the state trajectories for discrete-time switching are asymmetrical around the switching surface even though the switching gain is independent of the switching direction (see Gamble (1992)). Interestingly, the introduction of the valve dynamics reduces the steady-state error as can be seen in Figure 8.22. These valve dynamics act like a low-pass filter and therefore reduce the high-frequency switching asymmetry as can be seen when comparing the switching amplitudes in Tables 8.5 and 8.6.

An explanation of the origin of the observed low-frequency oscillation in the non-linear model response can be found in Baida (1993). The reason for this oscillation is again the direction dependent denominator b_0 of the transfer function of the plant model in combination with the switching being only possible at discrete instants. Lantto (1994) reported similar results when simulating the dynamic response of a discrete second-order CSLMC system with direction dependent switching gains.

As expected, an increase in sampling frequency improves the dynamic response of both the linear and the non-linear model significantly as can be seen in Figures 8.24 and 8.25. The resulting limit cycle frequencies and amplitudes obtained using simulation of the linear and non-linear model response can be found in Tables 8.7 and 8.8, respectively. For very high sampling frequencies of for example 10 kHz the response of the discrete CSLMC system approaches the response of the continuous system as can seen by a comparison between Figure 8.24 and Figure 8.3 and between Figure 8.25 and Figure 8.6.

8.2.2 Sampling Displacement and Differentiating Numerically

As mentioned in Section 6.14 when differentiating the system output numerically using the backwards differencing scheme described by Equations (6.53) and (6.54) an additional phase lag is introduced into the system states and hence the closed-loop dynamics of the CSLMC system. In order to model this phase lag due to numerical differentiation the following discrete switching function has to be considered:

$$\sigma(k) = \left[\left(\frac{c_3}{T_{samp}^2} + \frac{c_2}{T_{samp}} + c_1\right)x(k) - \left(\frac{2c_3}{T_{samp}^2} + \frac{c_2}{T_{samp}}\right)x(k-1) + \frac{c_3}{T_{samp}^2}x(k-2)\right]$$
$$= \left[\left(\frac{c_3}{T_{samp}^2} + \frac{c_2}{T_{samp}} + c_1\right) - \left(\frac{2c_3}{T_{samp}^2} + \frac{c_2}{T_{samp}}\right)z^{-1} + \frac{c_3}{T_{samp}^2}z^{-2}\right]x(k) \qquad (8.6)$$
$$= D(z)x(k)$$

In order to obtain the closed-loop transfer function *G(z)* of the discrete CSLMC system as depicted in Figure 8.26, the open-loop transfer function *F(s)* of the plant has to be transformed from the continuous Laplace-domain into the discrete *z*-domain. The ZOH approach as explained in Section 6.14 is chosen. The discrete transfer function of the servo without valve dynamics is of the form:

$$F(z) = \frac{x(k)}{u(k)} = \frac{a_1 z^{-1} + a_2 z^{-2} + a_3 z^{-3}}{1 + b_1 z^{-1} + b_2 z^{-2} + b_3 z^{-3}} \qquad (8.7)$$

The parameters a_i and b_i are determined using the *c2dm* routine in MATLAB (MathWorks (1992)). Similarly, the discrete transfer function of the plant with valve dynamics can be obtained.

The Bode plot of the resulting closed-loop transfer function

$$G(z) = D(z)F(z) = \frac{\sigma(k)}{u(k)} \qquad (8.8)$$

for the system without and with valve dynamics and a sampling frequency of f_{samp} = 1 kHz can be seen in Figures 8.27 and 8.28. Clearly, the introduction of the numerical differentiation routines reduces the switching frequency more significantly than the sampling of the system state.

The limit cycles of the CSLMC system without and with valve dynamics are listed in Tables 8.9 and 8.10. As in the previous examples the results obtained with the extended Nyquist criterion agree well with the simulation results. Increasing the sampling frequency f_{samp} increases the switching frequency but even for a sampling frequency of f_{samp} = 10 kHz the switching frequency stays considerably below the Nyquist frequency of $f_{samp}/2$ for the system without valve dynamics and also below the valve's natural frequency f_v for the system with valve dynamics.

The simulation step response and switching function results for a sampling frequency of f_{samp} = 1 kHz can be found in Figures 8.29 to 8.32. It can be seen, that

the response of the linear model without valve dynamics exhibits a larger steady-state error than the comparable response of the system with measured system states depicted in Figure 8.20.

The additional valve dynamics result in a visible chattering in the displacement signal at a frequency of about 80 Hz. The response of non-linear model shows again the low-frequency oscillation which has already been observed in the discrete system with sampled system states. The oscillation frequency now is lower while the amplitude is higher than in the discrete case with measured system states.

8.2.3 Conclusions from the Limit Cycle Analysis of the Digital CSLMC System

From the above limit cycle analysis it can be concluded that a digital implementation of the CSLM controller with a sampling frequency of f_{samp} = 1 kHz results in a switching frequency below the bandwith of the control valve (chattering). In particular the low-frequency oscillation in the response of the non-linear model is highly undesirable.

Numerical differentiation has the strongest influence on the switching frequency of all the investigated factors. Differentiating the displacement signal to obtain velocity and acceleration reduces the frequency of this chattering further and increases its amplitude. The resulting system response is unacceptable. Numerical differentiation should therefore be avoided.

When increasing the sampling frequency to f_{samp} = 10 kHz the system response is satisfactory even when differentiating the displacement signal twice to obtain acceleration. Since this sampling frequency is not achievable though with the available hard- and software a digital implementation of the CSLM controller for the pneumatic servo under consideration cannot be recommended.

TABLES

Table 8.1 - Limit cycle of continuous CSLMC system with valve dynamics

	frequency [Hz]	**amplitude $\hat{\sigma}$ [m/s^2]**
Nyquist criterion	203.4	3.84
Simulation of linear model	204.1	3.73
Simulation of non-linear model	204.9	+3.43 / -2.80

Table 8.2 - Limit cycle of continuous CSLMC system with valve dynamics and Butterworth filter acting on displacement, velocity and acceleration

	frequency [Hz]	**amplitude $\hat{\sigma}$ [m/s^2]**
Nyquist criterion	148.6	6.55
Simulation of linear model	143.7	6.57
Simulation of non-linear model	142.5	+6.37 / -4.57

Table 8.3 - Limit cycle of continuous CSLMC system with valve dynamics and Butterworth filter acting on displacement and velocity

	frequency [Hz]	**amplitude $\hat{\sigma}$ [m/s^2]**
Nyquist criterion	202.7	3.73
Simulation of linear model	202.0	3.68
Simulation of non-linear model	200.5	+3.37 / -2.69

Table 8.4 - Limit cycle of discrete CSLMC system obtained using Nyquist criterion (f_{samp} = 1 kHz)

	frequency [Hz]	**amplitude $\hat{\sigma}$ [m/s^2]**
Servo	500.0	3.41
Servo+valve	145.1	6.35
Servo+valve+filter (all states)	115.2	8.22

Table 8.5 - Limit cycle of discrete CSLMC system without valve dynamics (f_{samp} = 1 kHz)

	frequency [Hz]	**amplitude $\hat{\sigma}$ [m/s^2]**
Simulation of linear model	500.0	+1.91 / -3.29
Simulation of non-linear model	492.6	not constant

Table 8.6 - Limit cycle of discrete CSLMC system with valve dynamics (f_{samp} = 1 kHz)

	frequency [Hz]	**amplitude $\hat{\sigma}$ [m/s^2]**
Simulation of linear model	148.3	+4.88 / -5.35
Simulation of non-linear model	140.9	not constant

Table 8.7 - Limit cycle of discrete CSLMC system obtained using simulation of linear model

	sampling frequency [kHz]	**frequency [Hz]**	**amplitude $\hat{\sigma}$ [m/s^2]**
Servo	1	500.0	+1.91 / -3.29
Servo+valve		148.3	+4.88 / -5.35
Servo	2	1000.0	+0.99 / -1.58
Servo+valve		168.2	+4.84 / -5.51
Servo	10	5000.0	+0.22 / -0.28
Servo+valve		194.2	+4.01 / -4.08

Table 8.8 - Limit cycle of discrete CSLMC system obtained using simulation of non-linear model

	sampling frequency [kHz]	**frequency [Hz]**	**amplitude $\hat{\sigma}$ [m/s^2]**
Servo	1	500.0	not constant
Servo+valve		140.9	not constant
Servo	2	1000.0	not constant
Servo+valve		178.2	not constant
Servo	10	5000.0	not constant
Servo+valve		194.5	not constant

Table 8.9 - Limit cycle of discrete CSLMC system with differentiated velocity and acceleration (valve dynamics not included)

	sampling frequency [kHz]	**frequency [Hz]**	**amplitude $\hat{\sigma}$ [m/s^2]**
Nyquist	1	167.0	5.7
linear model		164.8	+5.5 / -7.2
non-linear model		144.3	not constant
Nyquist	2	334.0	2.8
linear model		330.0	+2.7 / -3.4
non-linear model		330.3	not constant
Nyquist	10	1667.7	0.5
linear model		1664.7	+0.6 / -0.7
non-linear model		1408.5	not constant

Table 8.10 - Limit cycle of digital CSLMC system with valve dynamics and differentiated velocity and acceleration

	sampling frequency [kHz]	**frequency [Hz]**	**amplitude $\hat{\sigma}$ [m/s^2]**
Nyquist	1	93.3	11.7
linear model		86.2	+13.3 / -14.4
non-linear model		92.5	not constant
Nyquist	2	126.4	7.9
linear model		117.7	+7.6 / -8.7
non-linear model		128.0	not constant
Nyquist	10	177.8	4.7
linear model		175.4	+4.9 / -5.0
non-linear model		175.8	not constant

FIGURES

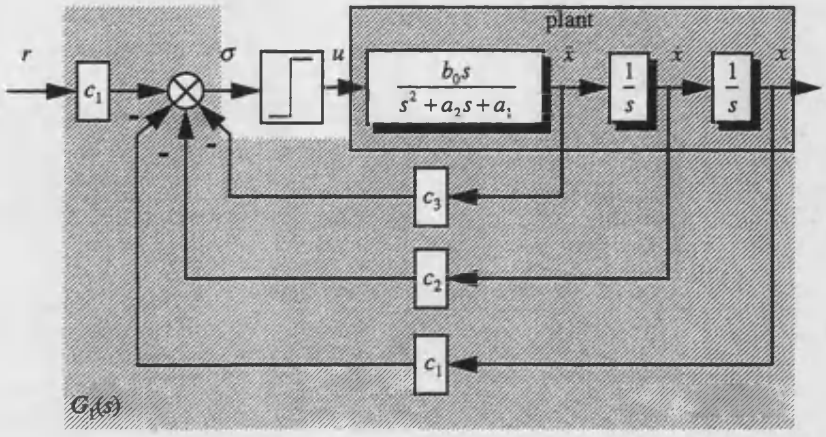

Figure 8.1 - Circuit diagram of closed-loop CSLMC system

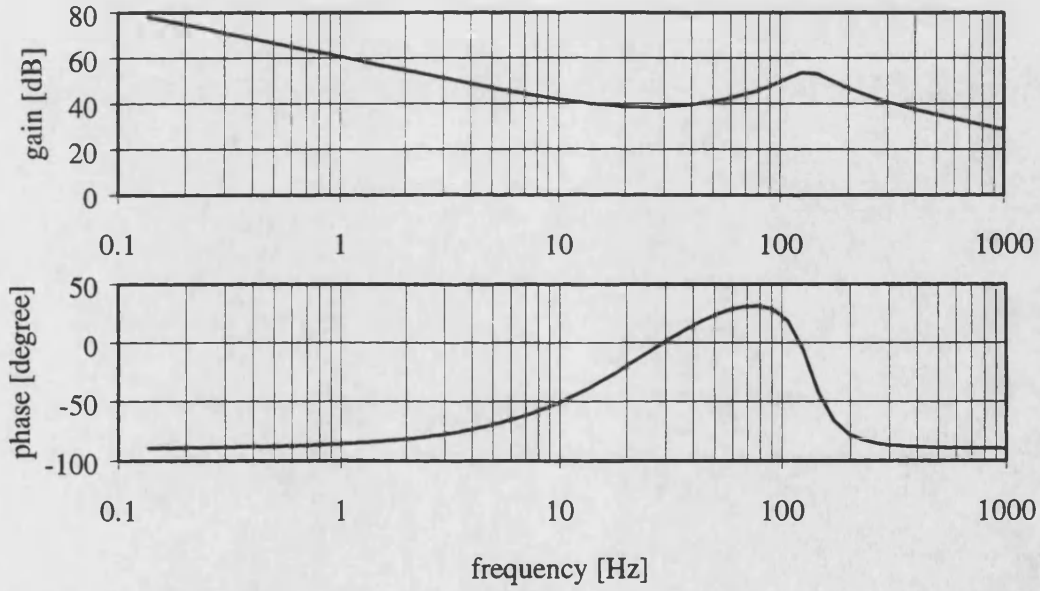

Figure 8.2 - Frequency response of CSLMC system

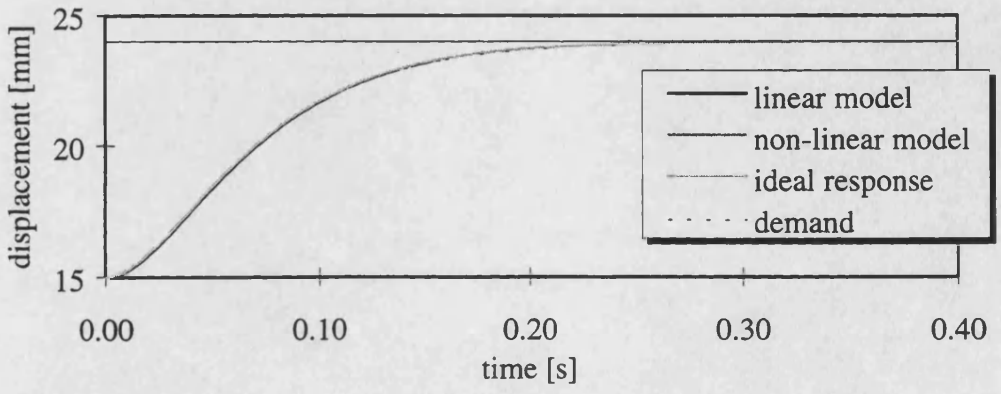

Figure 8.3 - Response of linear and non-linear model

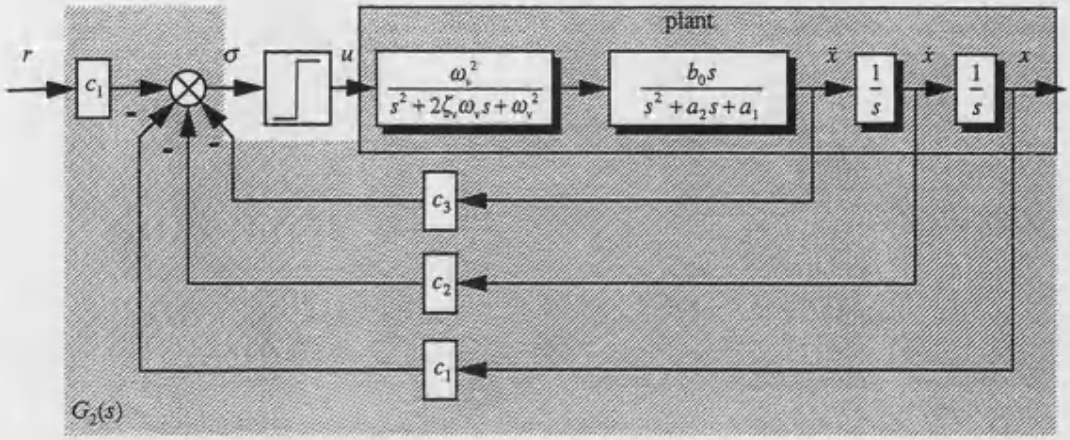

Figure 8.4 - Circuit diagram of closed-loop CSLMC system with valve dynamics

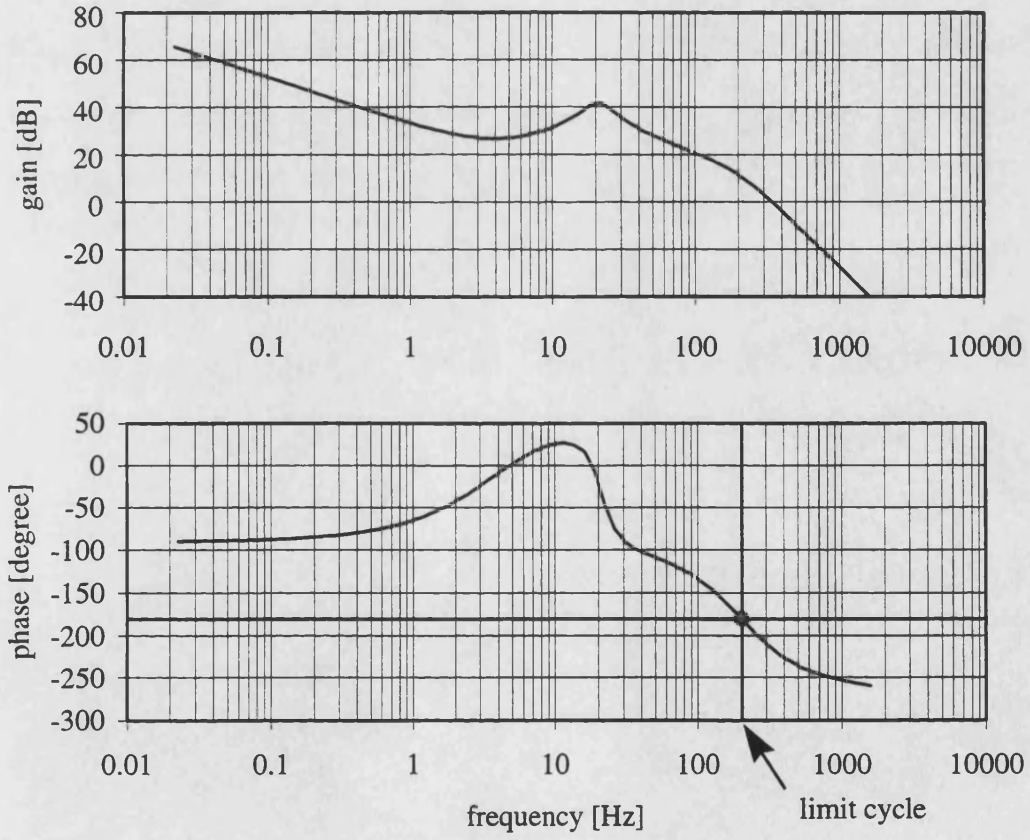

Figure 8.5 - Frequency response of transfer function G_2

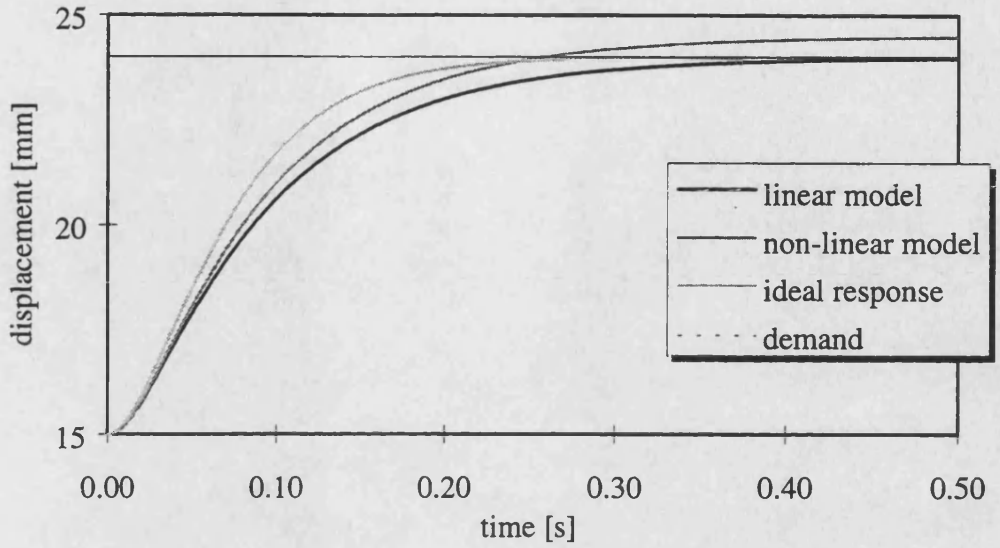

Figure 8.6 - Step response of linear and non-linear model including valve dynamics

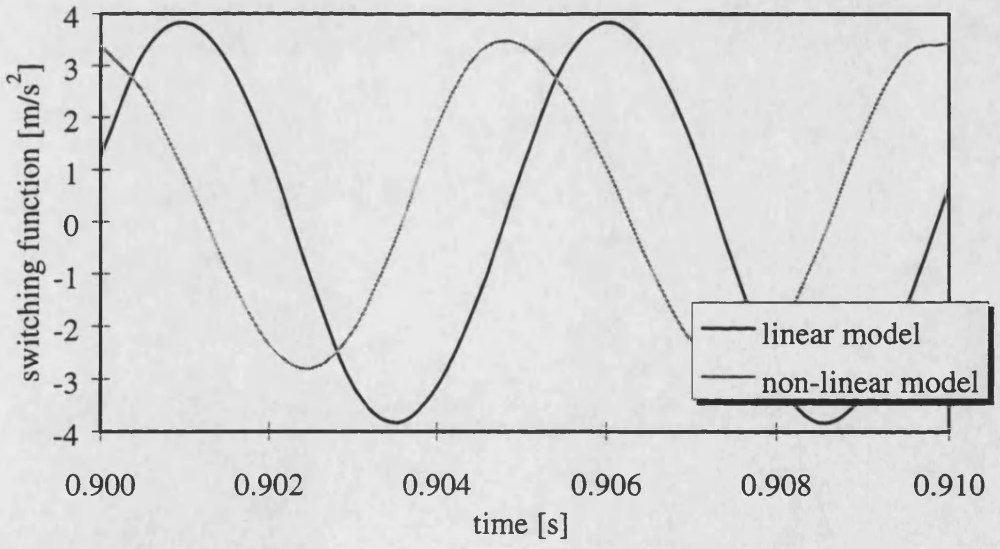

Figure 8.7 - Switching function of linear and non-linear model including valve dynamics

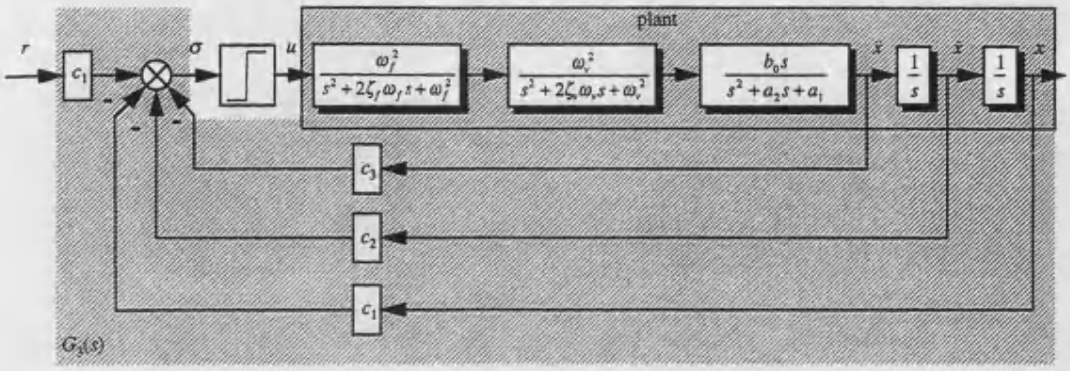

Figure 8.8 - Circuit diagram of closed-loop CSLMC system with valve dynamics and a second-order Butterworth filter

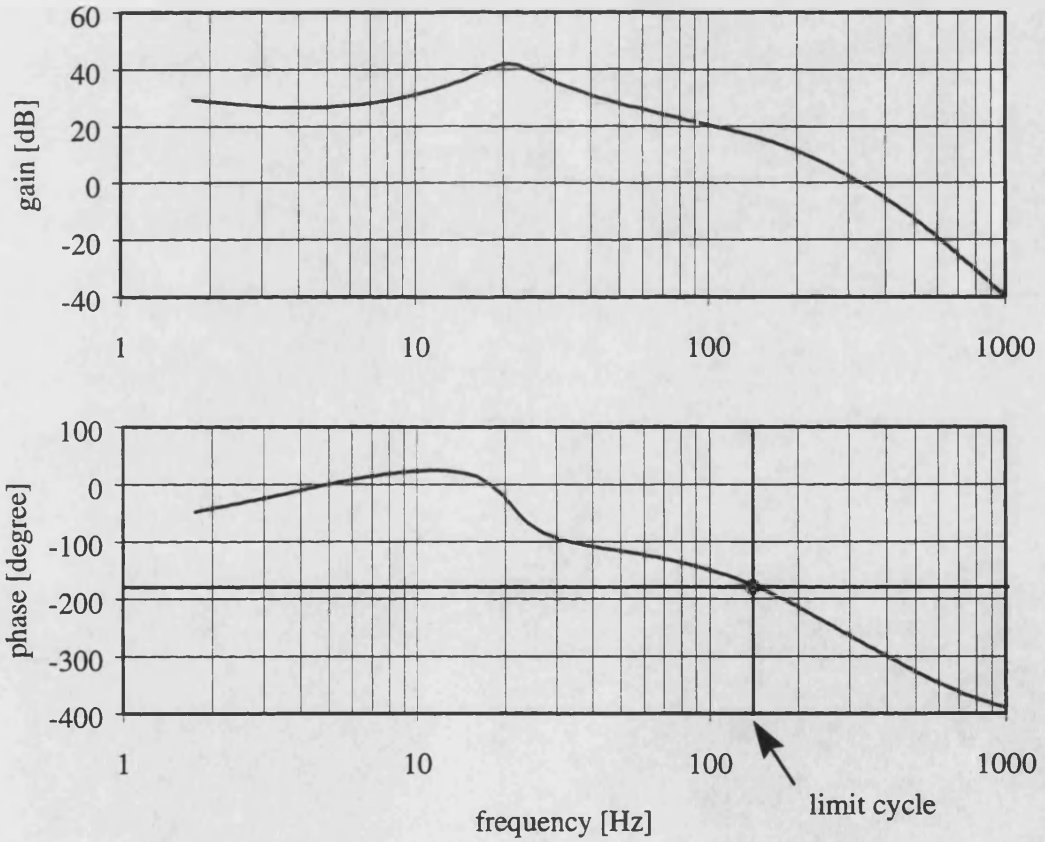

Figure 8.9 - Frequency response of transfer function G_3

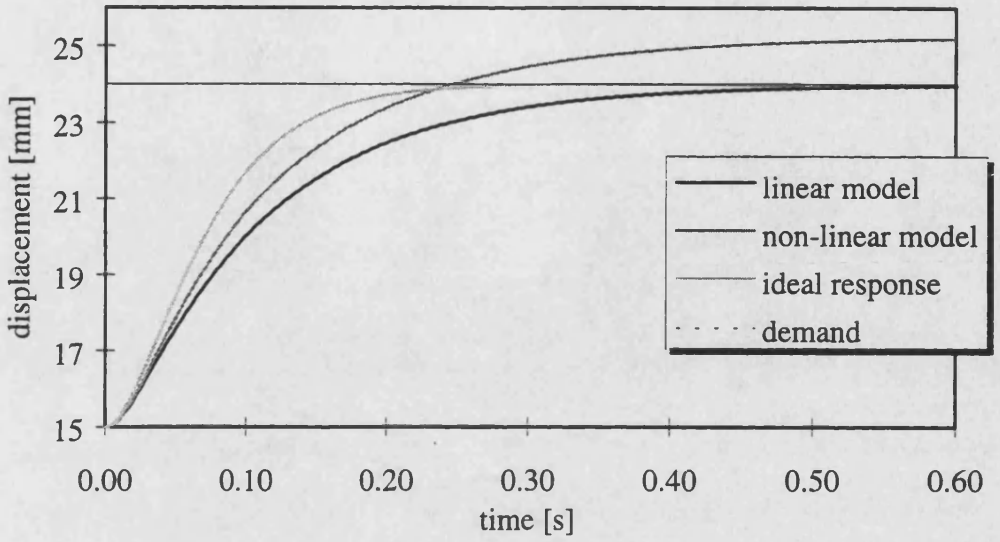

Figure 8.10 - Step response of linear and non-linear model including valve dynamics and a second-order Butterworth filter

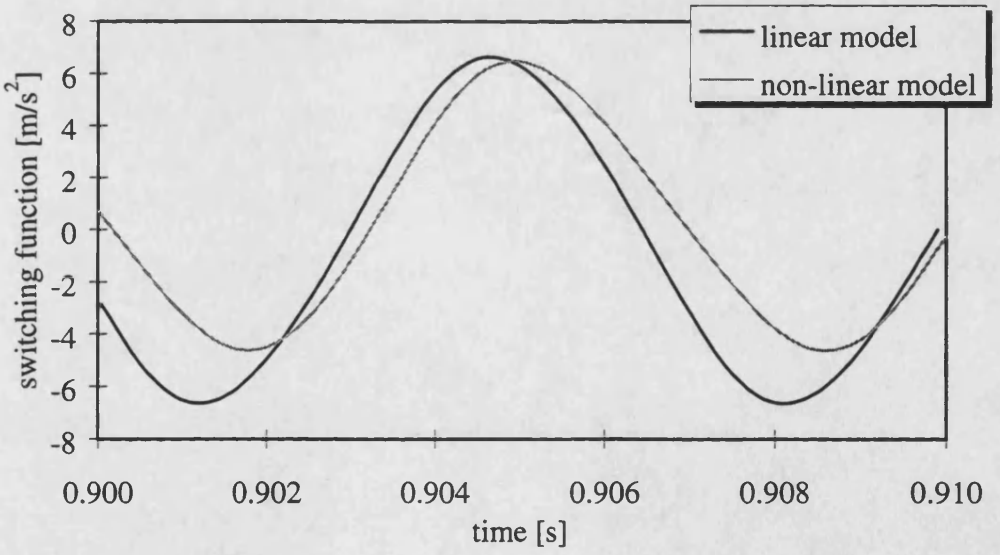

Figure 8.11 - Switching function of linear and non-linear model including valve dynamics and a second-order Butterworth filter

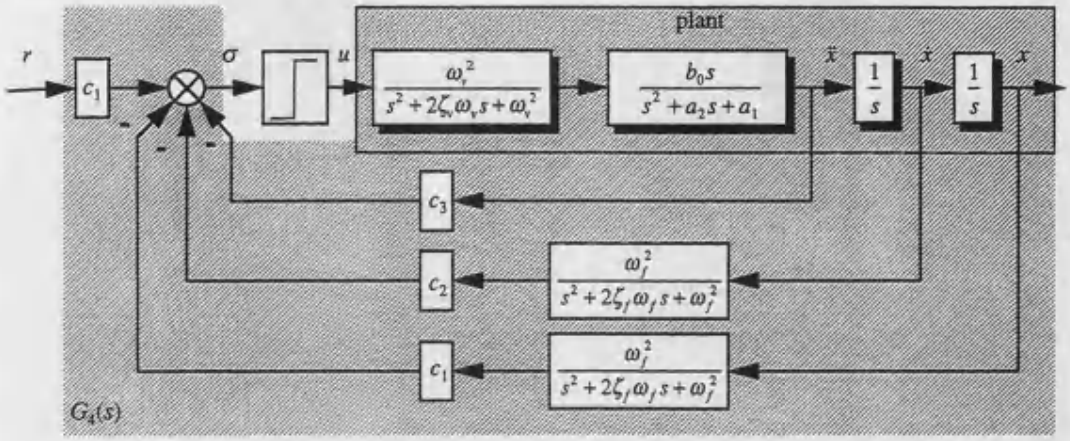

Figure 8.12 - Circuit diagram of closed-loop CSLMC system with valve dynamics and a second-order Butterworth filter acting on displacement and velocity

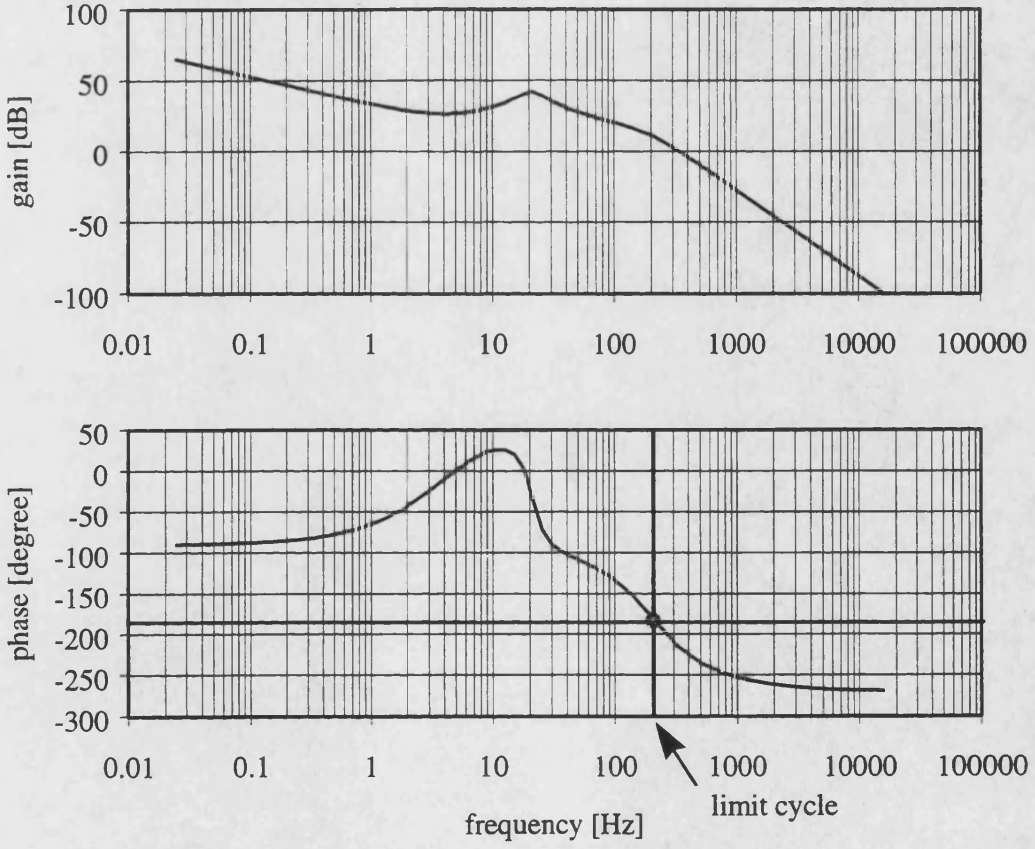

Figure 8.13 - Frequency response of transfer function G_4

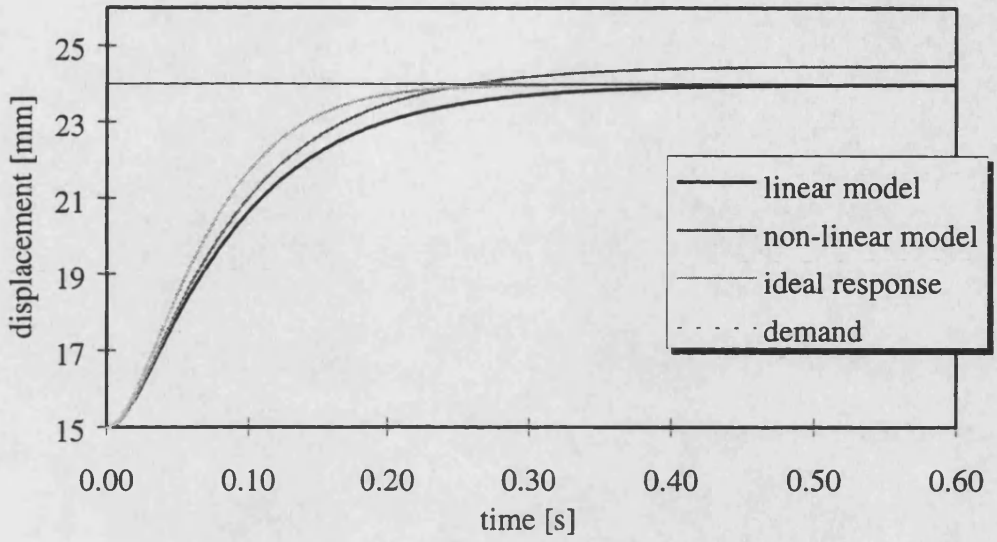

Figure 8.14 - Step response of linear and non-linear model including valve dynamics and a second-order Butterworth filter acting on displacement and velocity

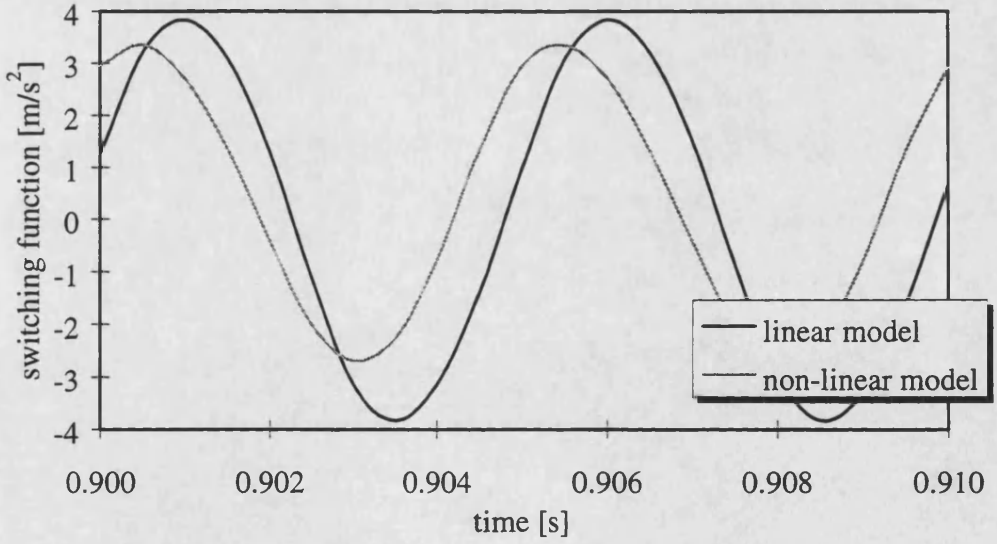

Figure 8.15 - Switching function of linear and non-linear model including valve dynamics and a second-order Butterworth filter acting on displacement and velocity

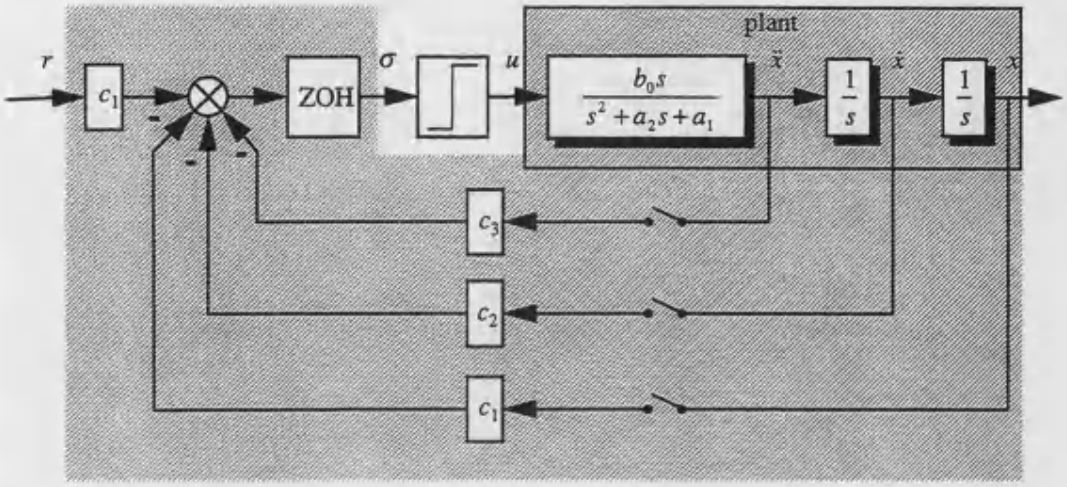

Figure 8.16 - Circuit diagram of discrete CSLMC system

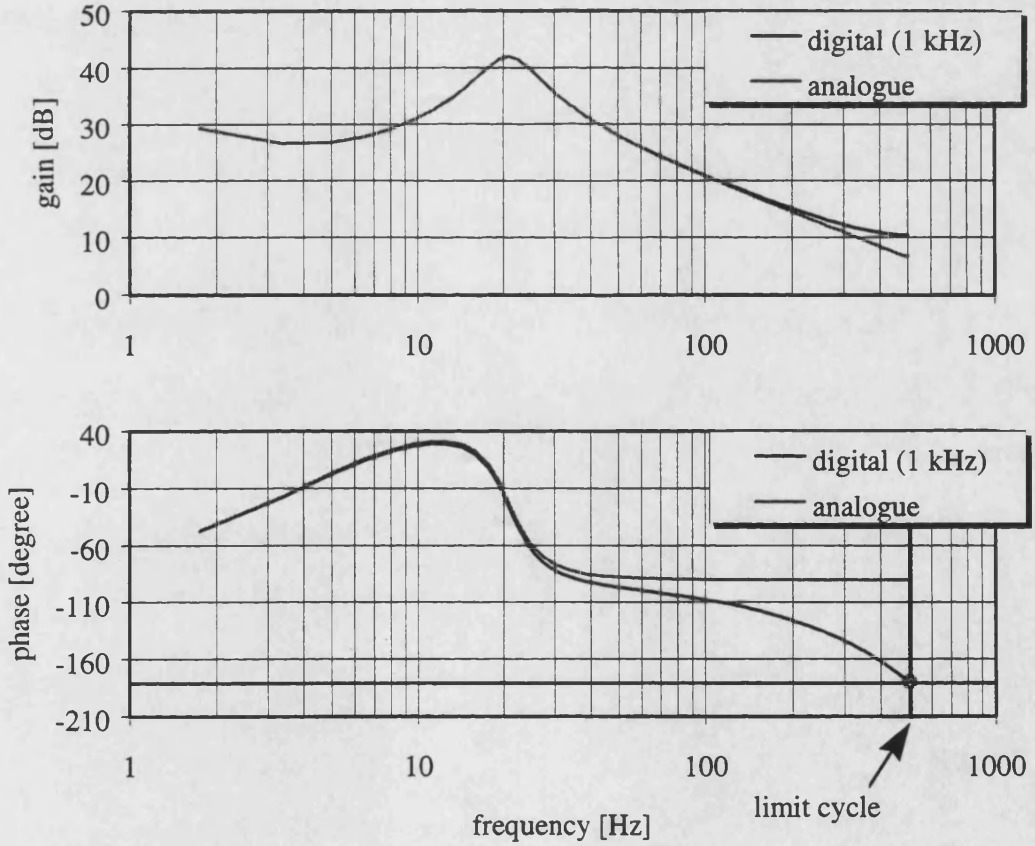

Figure 8.17 - Frequency response of discrete CSLMC system (f_{samp} = 1 kHz)

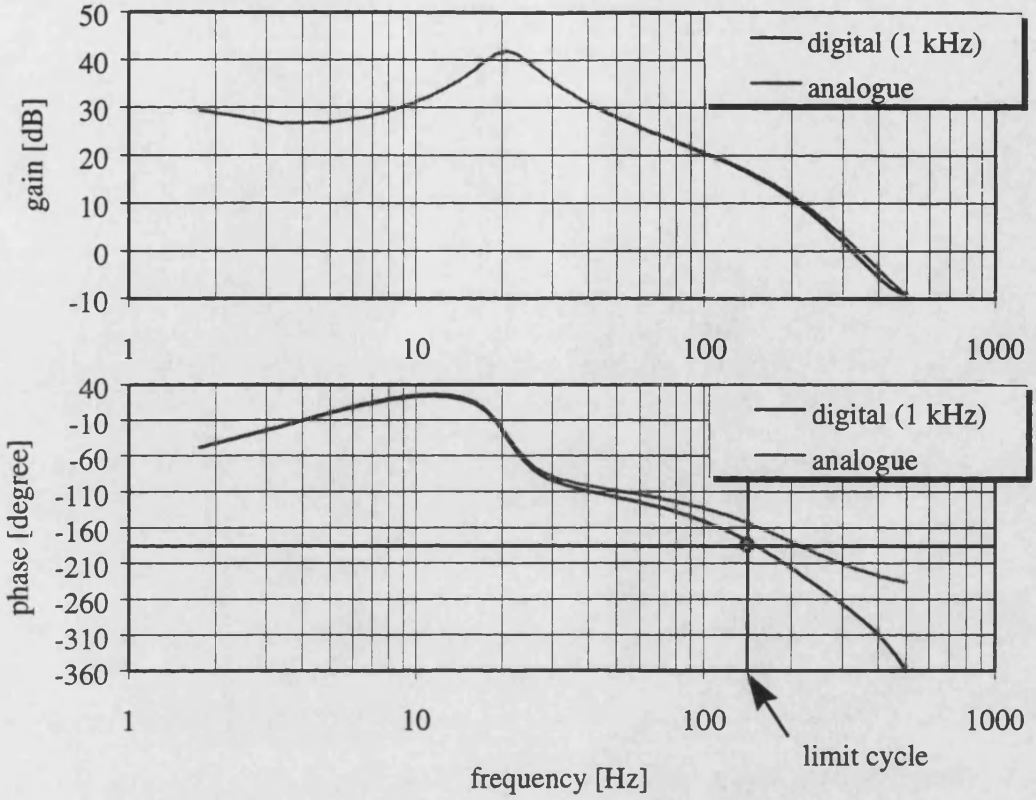

Figure 8.18 - Frequency response of discrete CSLMC system with valve dynamics (f_{samp} = 1 kHz)

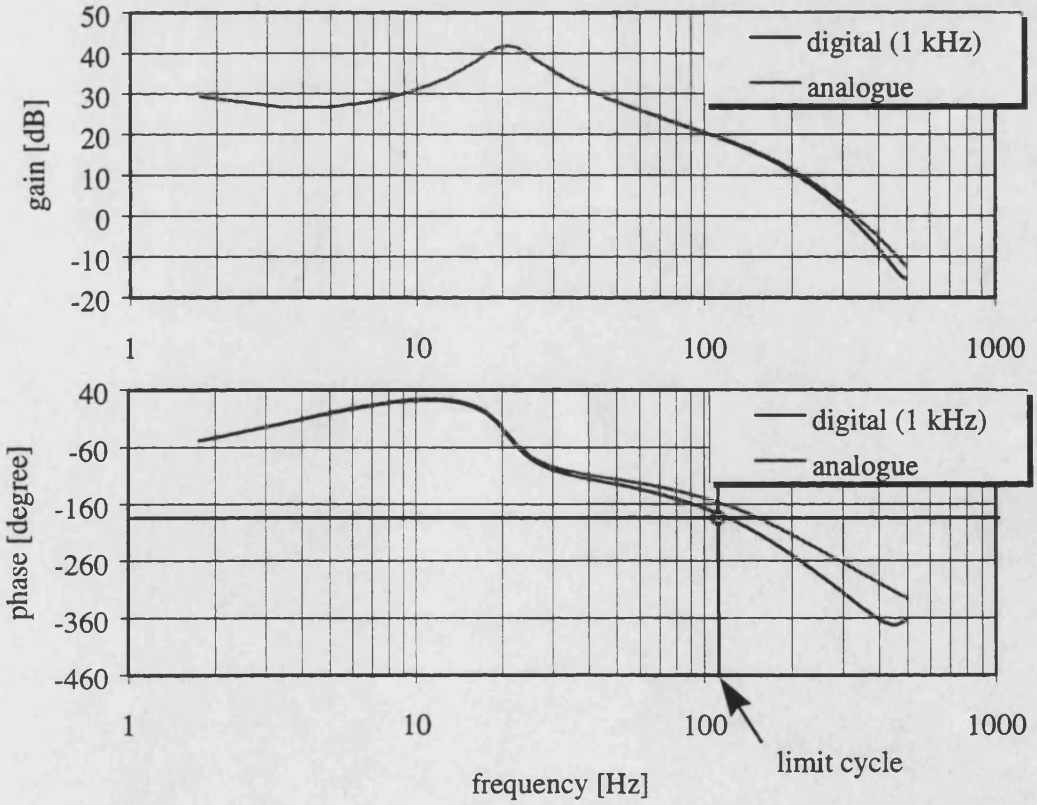

Figure 8.19 - Frequency response of discrete CSLMC system with valve dynamics and a Butterworth filter (f_{samp} = 1 kHz)

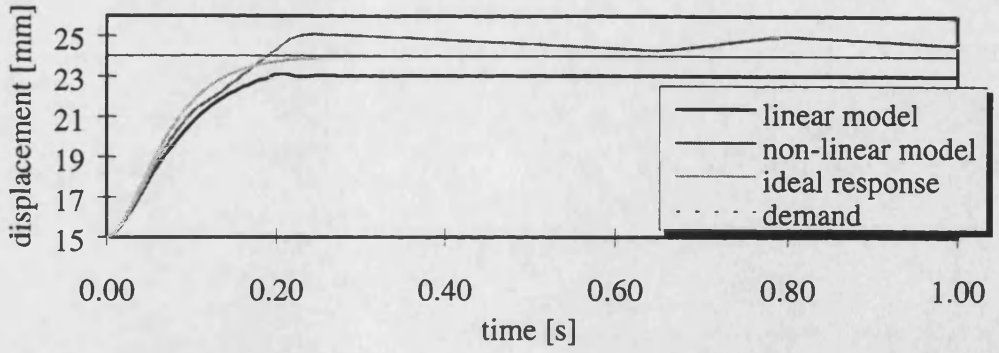

Figure 8.20 - Step response of discrete CSLMC system without valve dynamics

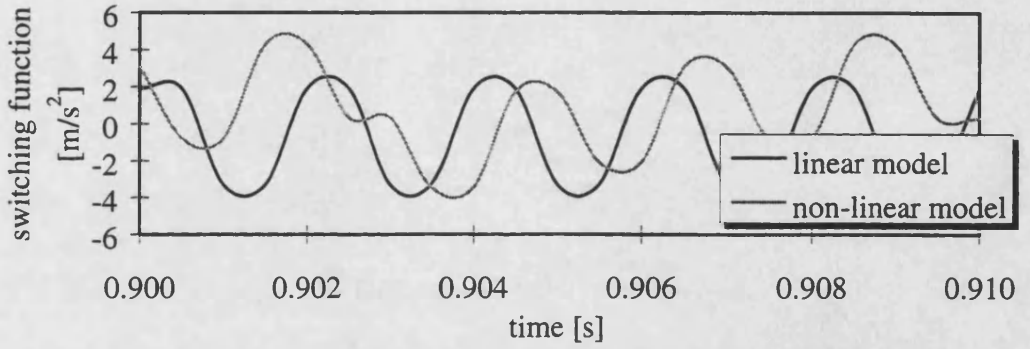

Figure 8.21 - Switching function of discrete CSLMC system without valve dynamics

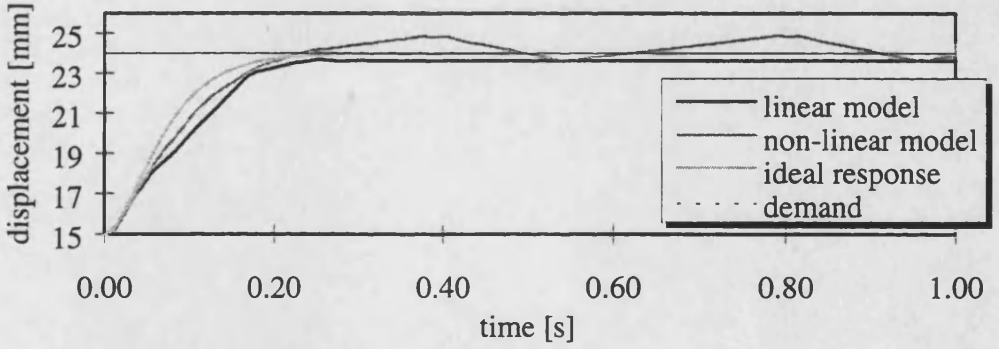

Figure 8.22 - Step response of discrete CSLMC system with valve dynamics

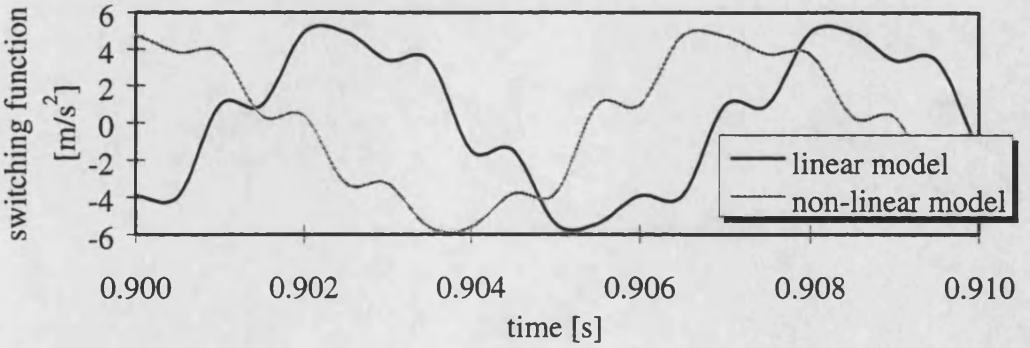

Figure 8.23 - Switching function of discrete CSLMC system with valve dynamics

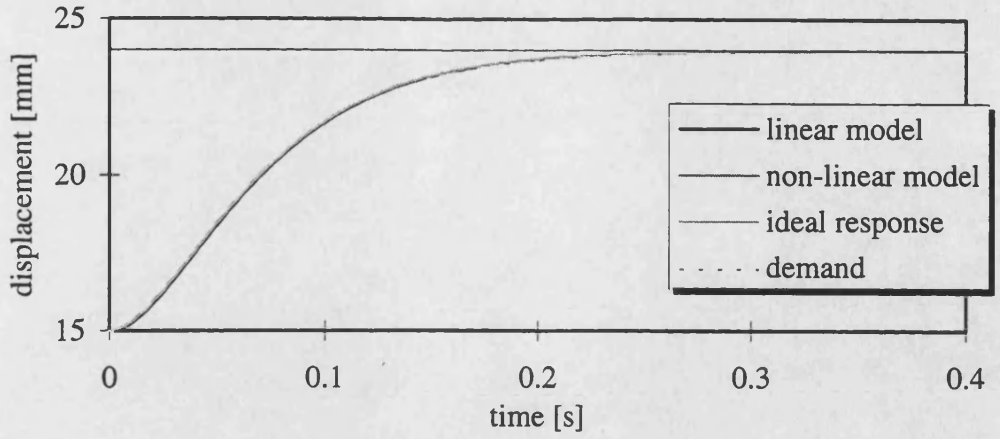

Figure 8.24 - Step response of discrete CSLMC system without valve dynamics and a sampling frequency of f_{samp} = 10 kHz

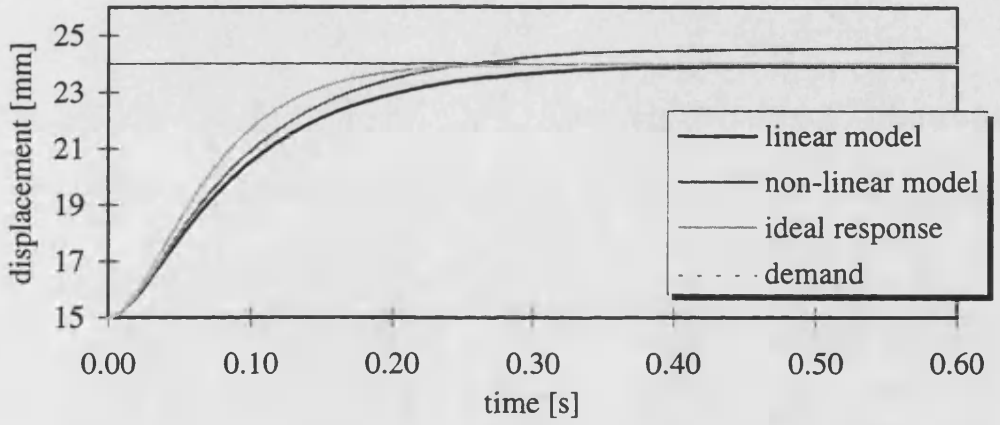

Figure 8.25 - Step response of discrete CSLMC system with valve dynamics and a sampling frequency of f_{samp} = 10 kHz

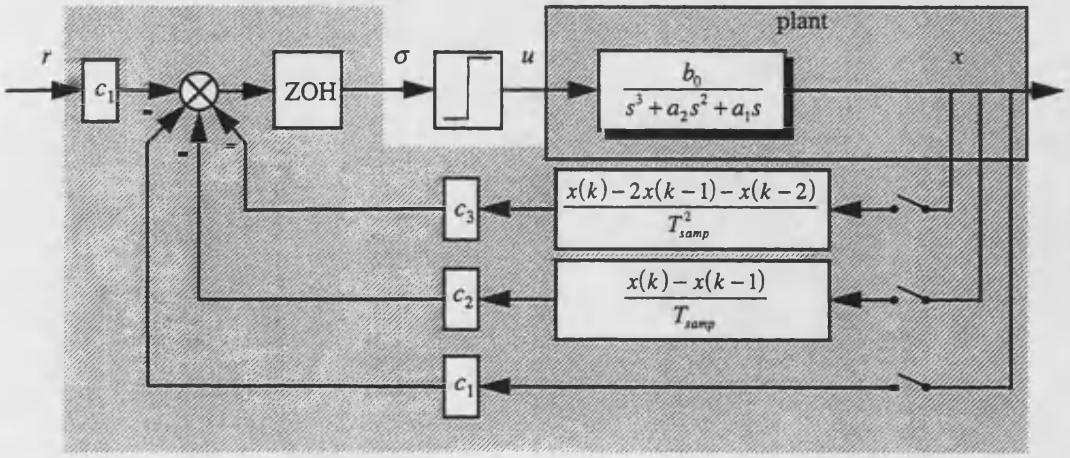

Figure 8.26 - Circuit diagram of discrete CSLMC system with numerical differentiation routines

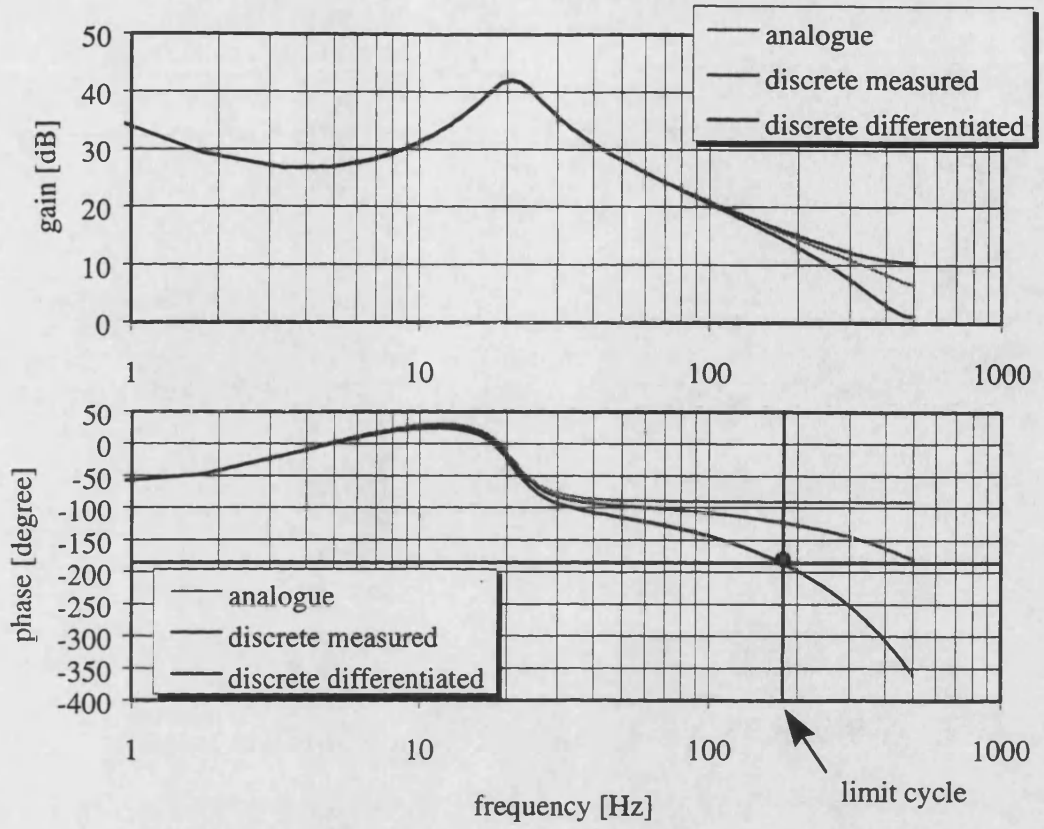

Figure 8.27 - Frequency response of transfer function *G(z)* (system without valve dynamics)

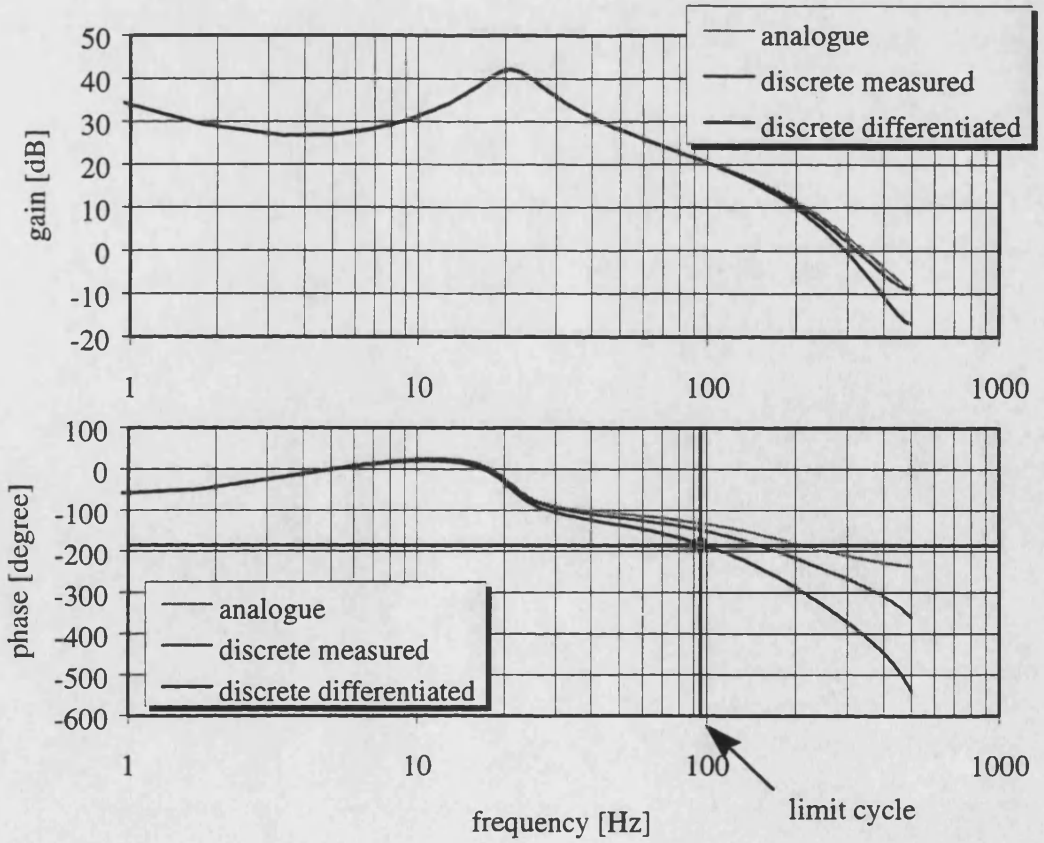

Figure 8.28 - Frequency response of transfer function *G(z)* (system with valve dynamics)

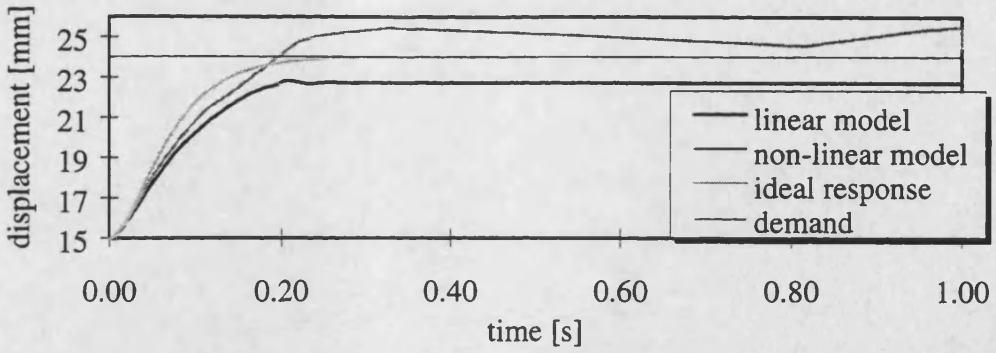

Figure 8.29 - Step response of discrete CSLMC system with differentiated velocity and acceleration (f_{samp} = 1 kHz)

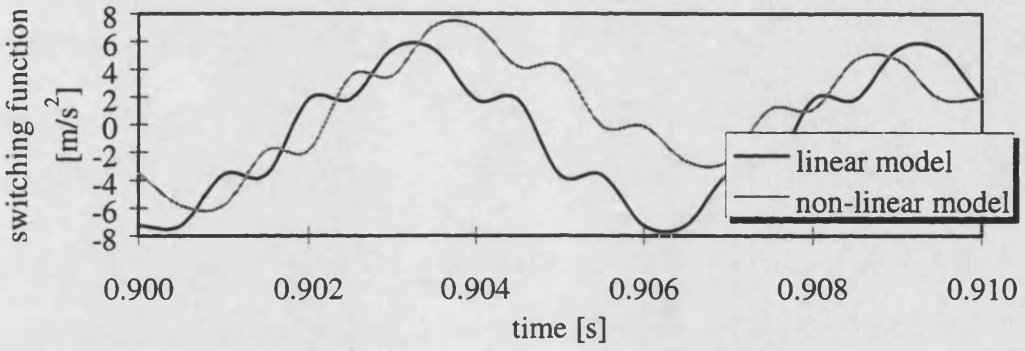

Figure 8.30 - Switching function of discrete CSLMC system with differentiated velocity and acceleration (f_{samp} = 1 kHz)

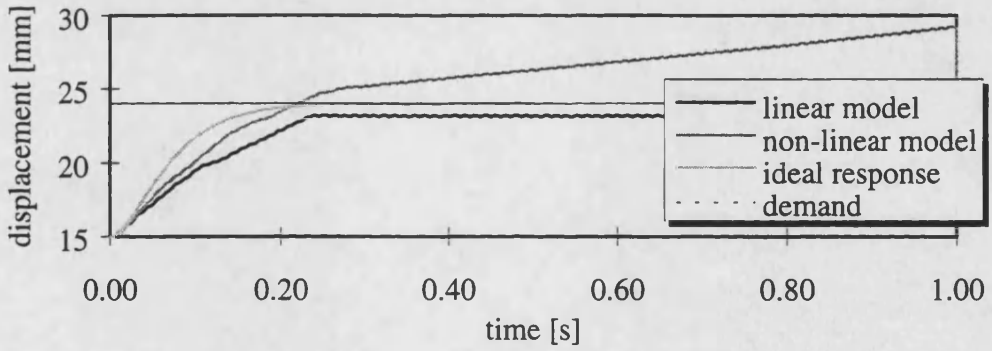

Figure 8.31 - Step response of discrete CSLMC system with valve dynamics and differentiated velocity and acceleration (f_{samp} = 1 kHz)

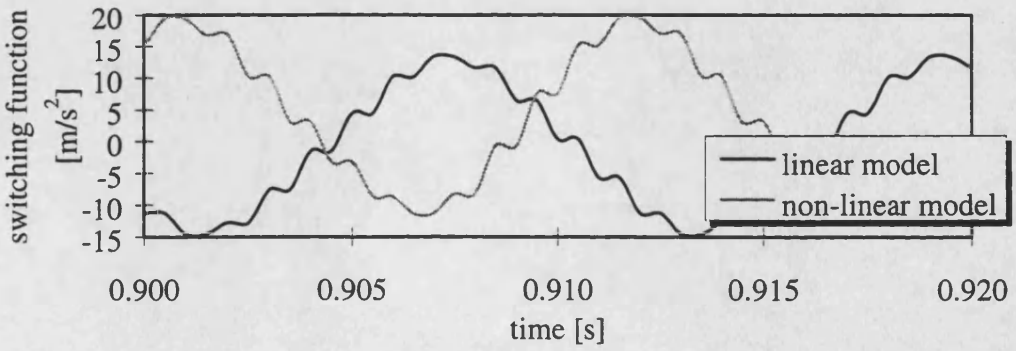

Figure 8.32 - Switching function of discrete CSLMC system with valve dynamics and differentiated velocity and acceleration (f_{samp} = 1 kHz)

9 IMPLEMENTATION OF THE CSLM CONTROLLER ON THE PNEUMATIC SERVO MECHANISM

In this chapter, the issues concerned with the implementation of the CSLM control algorithm designed in Chapters 7 and 8 will be discussed. For experimental testing the controller will be implemented on the single-axis test rig and on two axes of the pneumatically actuated figure.

Prior to the actual implementation of the CSLM controller though the effects of a limited sensitivity of the A/D-card will be investigated in this chapter. The results of this investigation are important in terms of further evaluating the feasibility of a digital CSLMC implementation. As the results of Chapters 7 and 8 indicate, a digital implementation of the control algorithm is not expected to yield a satisfactory dynamic behaviour of the control system. Nevertheless, it has been assumed in the theoretical analysis so far that chattering which occurs when implementing the CSLM controller digitally can be detected by the control system. Yet, when the CSLMC algorithm is implemented on the physical plant the sensitivity of the A/D-card determining the maximum switching frequency being detectable by the control system has to be considered. Therefore, at the beginning of this chapter the limit cycle results obtained in the previous chapters are reviewed taking into account the sensitivity of the A/D-card of the experimental rig.

Considering the problems with the digital implementation of CSLMC a novel analogue CSLM control card will then be presented which offers adjustable state gains, an adjustable boundary layer and the possibility to generate velocity and acceleration signals by means of analogue differentiation filters. This novel control card represents a new, effective, cheap and simple way of closed-loop control for systems of third-order being subject to significant external disturbances and system parameter changes.

To demonstrate the capabilities of the new control card its performance will be benchmarked against the performance of digital and hybrid CSLMC systems and also classical state-feedback control.

In order to test the robustness of the CSLMC system to parameter changes the mass to be moved is varied while the disturbance rejection capabilities are tested by means of the 2DOF implementation where the dynamic reaction torques and forces are treated as external disturbances by the single-axis controller and have to be compensated.

9.1 Maximum Detectable Switching Frequency

In Chapter 8 the maximum achievable switching frequencies of the digital and analogue implementation of the CSLM control system have been determined. The interesting question in this context is now how high the switching frequency has to be in order to avoid chattering. To determine this minimum switching frequency required the sensitivity of the A/D-card which is providing the information on which the calculation of the switching function is based must be examined. Theoretically, if the switching of the system cannot be detected by the microprocessor due to the limited sensitivity of the A/D-card no chattering will occur. A similar method has been used by Gamble (1992) and has also been successfully applied by Lantto (1994) to design a sliding mode control system.

For the chattering in the actuator piston displacement to remain undetected by the microprocessor, the amplitude of the oscillation being converted by the A/D-card must be less than half the value of the Least Significant Bit (LSB). The A/D-converter card used in this investigation is a DT2812A card by Data Translation® working on a 12-bit basis (see Section 3.3). For an actuator stroke of 30 mm this corresponds to a minimum piston displacement oscillation amplitude detectable by the microprocessor of:

$$x_{LSB} = \frac{1}{2} \times \frac{30\,\text{mm}}{2^{12}} = 3.662 \times 10^{-3}\,\text{mm} \tag{9.1}$$

Using the Bode plot of the frequency response of the servo system the maximum detectable switching frequency can now be obtained. It has to be mentioned though, that, as shown in Chapter 5, the servo dynamics change with actuator piston position and direction of motion. Hence, in order to guarantee

chatterfree operation of the system for all piston positions and directions of motion the *maximum* of this maximum detectable switching frequency has to be determined.

Figure 9.1 and Table 9.1 show the maximum detectable switching frequency at the piston mid position and two positions near the extreme ends of the piston stroke for both directions of motion. The servo valve dynamics are neglected in this case. Depending on the actuator piston position and its direction of motion the detectable switching frequency lies between f_{switch} = 163 Hz and f_{switch} = 233 Hz. The results imply that the system is most likely to exhibit chattering when the actuator piston is near the fully retracted position and moving outwards. This agrees with the results presented in Chapter 5, where it was shown that the above conditions exhibit the lowest system stability margin. It follows that in order to avoid chattering over the whole actuator stroke and for both directions of motion it should be insured that the switching frequency is higher than f_{switch} = 233 Hz.

As can be seen in Figure 9.2 and Table 9.2 including the dynamic response of the valve spool into the analysis reduces the maximum detectable switching frequency to between f_{switch} = 155 Hz and f_{switch} = 204 Hz.

So far it has been assumed that just displacement is measured and acquired by the A/D-card. If an additional accelerometer is used, the maximum resolution of the acceleration signal has to be checked as well. The minimum acceleration amplitude detectable by the A/D-converter is:

$$a_{LSB} = \frac{1}{2} \times \frac{322.57\,\mathrm{m/s^2}}{2^{12}} = 0.0394\,\mathrm{m/s^2} \tag{9.2}$$

Even for very high switching frequencies of up to f_{switch} = 950 Hz the acceleration amplitude exceeds A_{acc} = 0.04 m/s^2 as can be seen in Figure 9.3. As a result, switching in the acceleration signal is always detectable by the A/D-converter and hence will be affecting the switching function $\sigma(x)$.

The conclusion that can be drawn from comparing the maximum detectable switching frequency with the CSLMC limit cycle switching frequencies determined in Chapter 8 is that for a digital implementation with a sampling frequency of f_{samp} = 1 kHz chattering will always be detectable by the A/D-converter. Therefore,

only an analogue CSLMC card can achieve the required system performance. The design of this card will be described in the following section.

9.2 ANALOGUE CSLMC CARD

The analogue CSLMC card to be developed for the animated figure has to provide the following functions:

- Double differentiation of the measured displacement signal
- Synthesis of the switching function
- Provision of a boundary layer to reduce chattering
- Variable control voltage

9.2.1 DESIGN OF THE ANALOGUE DOUBLE DIFFERENTIATION FILTER

A circuit diagram of the analogue differentiation filter can be seen in Figure 9.4. The differentiator circuit is based on the operational amplifier CA3140 offering a very low bias current of 3.3 μV. A resistor R_p is also included to balance any offset due to the bias current flowing in R. In order to avoid differentiator instability which occurs when the differentiator frequency response reaches the open-loop response A_d of the operational amplifier as shown in Figure 9.5 the differentiator amplitude response is attenuated at high frequencies (Clayton (1979), Maddock and Calcutt (1994)). The amplitude attenuation also significantly reduces high-frequency noise contained in the differentiated signals. The resulting differentiator transfer function is as follows:

$$\frac{V_{out}}{V_{in}} = -\frac{i\omega CR}{(1+i\omega C_f R)(1+i\omega CR_s)} \tag{9.3}$$

In this case the two break frequencies are chosen equal. Hence:

$$f_0 = \frac{1}{2\pi CR_s} = \frac{1}{2\pi C_f R} \tag{9.4}$$

Derived from the transfer function the differentiator amplitude gain can be calculated to be:

$$-V_{out} = RC\frac{dV_{in}}{dt} \tag{9.5}$$

At frequencies below f_0 the basic differentiation function is still provided by the numerator. At high frequencies, the 20 dB roll-off indicates integration preventing excessive noise amplification.

Double differentiation of the measured displacement signal is realised by means of a series connection of two single differentiation circuits.

9.2.2 Design of the Analogue Control Card

The circuit diagram of the analogue CSLMC card can be found in Figure 9.6. Since only displacement can be measured on the animated figure two differentiation filters as described in Section 9.2.1 are connected in series in order to obtain velocity and acceleration signals. Both signals can also be picked up for display and measurement purposes and also to allow for a hybrid use of the control card. In this case for instance the filtering can be done by means of the analogue differentiation filters on the card while the generation of the sliding surface and the switching of the controller output can be realised by means of a control PC.

A second-order linear sliding surface is synthesised by means of state weights. These state weights can be adjusted by means of two potentiometers (P1 and P2). It should be noted that the additional gains introduced by the analogue differentiation filters (Equation (9.5)) have to be taken into account when setting the gains defining the switching surface.

A saturated operational amplifier realises the relay-like switching control action. An additional potentiometer (P4) allows for the adjustment of the switching voltage U_{max}.

The width of a boundary layer neighbouring the switching surface as described in Section 6.12 can be controlled by means of the potentiometer P3 in order to suppress chattering of the closed-loop system.

In order to test the disturbance rejection capabilities of the analogue CSLMC card two separate CSLM controllers as described above have been implemented on the card.

9.3 Experimental Testing of The CSLMC System

In order to validate the theoretical results derived in Chapters 7 and 8 and to proof that the new analogue CSLM controller is the best solution to the control problem under consideration experimental test have been performed. In the following the new control card will be benchmarked against the performance of the following control systems:

- Digital CSLMC system with measured position and numerically differentiated velocity and acceleration
- Digital CSLMC system with measured position and acceleration and numerically differentiated velocity
- Hybrid CSLMC system with digitally implemented control algorithm, measured position and velocity and acceleration being obtained by means of analogue differentiation filters
- Digital state-feedback system with measured position and numerically differentiated velocity and acceleration

9.3.1 Set up of Experimental Control Systems

The set up of the single-axis experimental control systems can be seen in Figures 9.7 to 9.9. The control computer used for the realisation of the digital controller, the numerical differentiation of the measured displacement signal and for data acquisition is a PC with a 166 MHz Pentium processor as described in Section 3.3.

In order to test the analogue controllers disturbance rejection capabilities both channels on the control card are set up as single-axis controllers for the 2 members of the arm of the animated figure depicted in Figure 3.1.

9.3.2 STEP RESPONSE OF DIGITAL CSLMC SYSTEM

The digital CSLMC system with numerically differentiated velocity and acceleration as depicted in Figure 9.7 is investigated first. Figure 9.11 shows the step response of this control system with the sampling times of T_{samp} = 1 ms and 2 ms and no boundary layer surrounding the switching surface. As suggested by the theoretical design the settling time of the ideally damped switching surface is chosen to be T_{sett} = 0.07 s. As already suspected from the simulation study in Chapter 8 the responses are far from being satisfactory. Both responses are extremely chattery. A steady-state condition is not being reached by either of the systems, rather a chattering around a position a significant distance away from the demanded set point. Decreasing the sampling time from T_{samp} = 2 ms to 1 ms reduces the distance but by no means improves the general result of the step response. Both sampling times yield an intolerable phase lag in the numerically differentiated acceleration signal.

Even introducing a fixed width boundary layer with φ = 5000 m/s^2 to reduce chattering as explained in Section 6.12 does not improve the system response as can be seen in Figure 9.12. The low-pass filter properties of the boundary layer do not reduce chattering but rather reduce the system response time in a similar manner as the low-pass valve dynamics. Varying the width φ of the boundary layer between 1000 m/s^2 and 20000 m/s^2 yields no improvement.

Introducing an additional accelerometer to the control system as shown in Figure 9.8 yields the step response depicted in Figure 9.13. Again no boundary layer is applied and the sampling times are chosen to be T_{samp} = 1 ms and T_{samp} = 2 ms. Still the system response is not satisfactory although it has improved significantly. Chattering is envisaged and expected since the switching frequency can be detected by the A/D-card as predicted by the limit cycle analysis. Furthermore, large steady-state errors occur.

It can be seen that with a sampling time of T_{samp} = 2 ms not only high-frequency chattering but also low-frequency oscillations occur, which have been predicted by simulation. As explained in Section 8.2 this phenomenon results from an unsymmetric switching around the switching surface due to direction dependent switching gains in combination with discrete time switching. A decrease in sampling

time to T_{samp} = 1 ms eliminates the low-frequency oscillation without affecting the high-frequency chattering or the steady-state error.

Introducing now a fixed width boundary layer of $\varphi = 5000$ m/s^2 results in an almost ideal step response of the digital CSLMC system as can be seen in Figure 9.14. The closed-loop response follows the dynamics of the sliding surface without overshoot or significant steady-state errors. The remaining slight chattering in the control signal in this case is partly due to noise in the measured displacement and the differentiated velocity signal. The influence of this noise disturbance can be reduced by introducing a digital (second-order) Butterworth filter. As shown in Section 9.1.3.2 filtering these signals does not result in a reduction in switching frequency and therefore does not increase the chattering amplitude.

As a conclusion from the above results it can be said that using an accelerometer to obtain the highest system state yields a satisfying system response even with a relatively low sampling frequency of 1 kHz if an appropriate boundary layer is chosen whereas numerical differentiation is not applicable.

Yet, as the use of an accelerometer is out of question for the control problem under consideration another means of obtaining the required acceleration signal is necessary.

9.3.3 Step Response of Hybrid CSLMC System

A schematic of the hybrid CSLMC system can be seen in Figure 9.9. Velocity and acceleration are obtained by means of analogue differentiation filters while the CSLMC algorithm is realised by means of the control PC.

The step response of the hybrid CSLMC system for sampling frequencies of T_{samp} = 1 ms and T_{samp} = 2 ms and no boundary layer is depicted in Figure 9.15. In both cases the response is very chattery. Increasing the sampling frequency does not yield visible improvements.

Introducing now a boundary layer of $\varphi = 5000$ m/s^2 improves the step response significantly as shown in Figure 9.16. A small steady-state error occurs at

the mid position set point while almost no steady-state error occurs at the near end position set point. Although the response has improved significantly it is still not ideal but rather jerky when compared to the response of the digital CSLMC system with an accelerometer depicted in Figure 9.14. The reason for the difference between both responses is mainly the noise of the measured displacement signal being amplified by the analogue differentiation filter. Using an additional low-pass noise filter on the differentiated acceleration filter would decrease the switching frequency though and is therefore not advisable.

9.3.4 Step Response of Analogue CSLMC System

In Figure 9.17 the step response results of the digital CSLMC system with accelerometer, the hybrid CSLMC system with the analogue differentiation filters and the analogue CSLMC system with the analogue CSLMC card are compared. It should be noted that with the digital and the hybrid CSLMC system a boundary layer of φ = 5000 m/s^2 is used. The exact width of the boundary layer used with the analogue card is difficult to determine since it depends on the setting of potentiometer P3 described in Section 9.2.2. In this case the ideal boundary layer can be identified by simply adjusting potentiometer P3 (described in Section 9.2.2) until a satisfactory step response is achieved.

The responses of the digital and the analogue system are virtually identical. Both responses exhibit precisely the closed-loop dynamics the system is designed for. The main difference between the two responses is a slight increase in the steady-state error from about 0.02 mm for the digital system to 0.3 mm for the analogue system.

Comparing the response of the analogue system to the response of the hybrid system reveals that omitting the control PC as the main switching frequency limiting factor yields excellent results. The jerky response of the hybrid system resulting from noise being amplified by the analogue differentiation filters is smoothed out by introducing the analogue CSLMC card and the resulting increase in switching frequency.

It can be concluded that the digital CSLMC system with the additional accelerometer and the analogue CSLMC system both yield the desired dynamic response of the single-axis pneumatic servo under nominal conditions.

Yet, in comparison to the digital CSLMC system the analogue CSLMC system offers the advantage of a significant reduction in hardware cost due to the fact that neither accelerometer nor a control PC are required. Furthermore, the digital CSLMC system does not lend itself to being applied to an *n*DOF application since the accelerometer measures the absolute acceleration. For control purposes only the acceleration of the actuator piston relative to the actuator is required though.

Therefore, for further testing in the following only the analogue CSLMC card will be used.

9.3.5 Sliding Surface Settling Time

By means of the extended Nyquist criterion is was predicted in Section 9.1.1 that the system would fall in a mode of sustained oscillation if a sliding surface settling time of less than $T_{sett} = 0.013$ s was chosen. To confirm this theoretical result and also to demonstrate the effect of the sliding surface settling time on the closed-loop system dynamics, step response tests with sliding surface settling times T_{sett} between 0.25 s and 0.01 s have been performed.

In order to tune the state gains of the analogue card (potentiometers P1 and P2) it proved to be advantageous to compare the resulting system response to the one obtained with the digital CSLMC system. In this system the state gains are precisely defined by the variables in the control programme on the PC. By matching the two responses the exact settings of the tuning potentiometers can be found easily.

It can be seen in Figure 9.18 that a settling time $T_{sett} = 0.07$ s results in a satisfactory system response. For a settling time of $T_{sett} = 0.02$ s the step response exhibits a slight undesired ripple near the set point. When reducing the settling time further to $T_{sett} = 0.01$ s the system falls into a mode of sustained oscillation as predicted by theory.

As a consequence the settling time of T_{sett} = 0.07 s determined in the theoretical analysis in Chapters 8 and 9 is confirmed by experiment.

9.3.6 Robustness to Changes in Mass and Disturbance Rejection Capabilities of The Analogue CSLMC System

So far the analogue CSLMC system has only been tested for nominal system conditions. Although the response of the highly non-linear pneumatic servo could be improved significantly when compared to the response of the system using classical state-feedback control as shown in Section 5.5.3 one of the most attractive features of CSLM control, robustness to changes in the dynamic system parameters and the capability to reject external disturbances, has not yet been tested.

Besides the servo's non-linearities the most important effects the CSLM control has to compensate for in the context of the pneumatically animated figure are changes in the effective mass to be moved and external disturbance torques and forces resulting from the kinematic and dynamic coupling of the individual members of the figure. Therefore, in the following two sections these influences will be analysed and experimentally investigated.

9.3.6.1 Robustness to Changes in Mass

In order to determine the robustness of the analogue CSLMC system to changes in the mass to be moved the mass was increased from m = 1.82 kg firstly to m = 6.82 kg and than to m = 11.82 kg. The chosen gravity loads approximately represent the range of change of mass for a single axis of the animated figure.

As can be seen from the results of the analogue CSLMC system depicted in Figure 9.19 increasing the mass only increases the steady-state error slightly. However, the dynamic characteristics of the response are not affected at all. The same results could be achieved with the digital CSLM controller including the accelerometer.

As a result the robustness of the CSLM controller to changes in the effective mass to be moved is as predicted by theory and sufficient for controlling the animated figure.

9.3.6.2 Disturbances Rejection Capabilities - 2DOF implementation

Since it is the aim of this research project to use the single-axis CSLM controller to control an animated figure with seven dynamically coupled axes of motion the disturbance rejection capabilities of the control system are of crucial importance. Therefore, in order to test the disturbance rejection capability of the system two analogue single-axes CSLM controllers were implemented on two axes of the animated figures. For this experiment the arm of the figure was chosen since it exhibits the most significant coupling disturbances. The two members of this arm can be interpreted as an inverted double pendulum as depicted in Figure 9.20.

The disturbance rejection capabilities of the analogue CSLMC card has been benchmarked against the classical state-feedback controller shown in Figure 5.12.

As can be seen from the results presented in Figures 9.21 and 9.22 when using the single-axis CSLM controllers instead of single-axis state-feedback controllers (which both treat coupling effects as external disturbances) coupling effects resulting from the reaction forces and torques are compensated for much more effectively. The displacement ripples being observed in the response of the state-feedback control system (Figure 9.22) are almost eliminated by the CSLM controller. Therefore, efficient decoupling of the dynamic responses of the individual members of the animated figure has been achieved by means of simple single-axis controllers without the need of an overall control algorithm.

Decoupling by means of single-axis controllers offers a major advantage since an overall control algorithm has to be based on the complete highly complex and non-linear *n*DOF system model taking account of all the main non-linear coupling effects. How involved this can be even in the case of a relatively simple inverted double pendulum is demonstrated in Appendix A1.

As a result of the individual single-axis control approach, individual members of the animated figure can be added or omitted without the need of changing an

overall control algorithm or even the individual single-axis controllers. As derived in Section 7.7 it only has to be made sure that the amplitude of the disturbance does not exceed a certain maximum level. The disturbance frequency content and its highly non-linear nature is of no consequence for the disturbance rejection capabilities of the *n*DOF control system.

It should be mentioned that the response of axis 1 of the animated figure shows the influence of high-frequency noise. This is due to the high noise level of the displacement transducer used on this member. As a result it has to be made sure that only high-quality low-noise transducers are used for CSLM control.

A further interesting result from applying CSLM control to the animated figure is the fact that the overall vibrations of the animated figure during operation are greatly reduced when comparing it to the state-feedback control results. Obviously, reducing the coupling between the individual members of the animated figure prevents these disturbances from travelling through the rigid structure of the figure. When accelerating one member of the figure the adjacent members will compensate for these disturbances and therefore the disturbance effects on the dynamic behaviour of the other members in the dynamic chain are greatly reduced.

9.3.7 EXPERIMENTAL FREQUENCY RESPONSE RESULTS

To investigate fully the performance of the analogue CSLM control card frequency response tests have been performed. Again the CSLM control card is benchmarked against the state-feedback controller depicted in Figure 5.12. The frequency response results of both control systems are shown in Figures 9.23 and 9.24.

Comparing both results one of the most interesting observations is the ability of the CSLM controller to compensate for the stick-slip effect which is a dominant feature of the dynamics of pneumatic servos in the case of small actuator velocities. This stick-slip effect can clearly be observed in the frequency response of the state-feedback control system with a demand frequency of $f = 1$ Hz as depicted in Figure 9.23. As described in Section 6.2.2 a vast number of publications deal with the stick-slip problem without given satisfying answers. Methods such as e.g.

additional dither signals (Surgenor and Wijesuriya (1992)) or stick-slip compensation components in the forward path of the control law (Abou-Fayssal and Surgenor (1997)) do not yield the required system response or entail drawbacks like complicated tuning procedures or the need for determining a detailed friction model.

As the results in Figure 9.24 clearly demonstrate the stick-slip motion problem is of no concern for the CSLMC system. The switching characteristic of CSLM control automatically prevents the actuator piston from exhibiting this highly undesirable behaviour. Since the system state in sliding mode oscillates around the sliding surface the actuator piston is constantly in motion and is therefore prevented from being subject to the adverse effects of stiction.

In Figure 9.25 the Bode plot of the frequency response of the CSLMC system and the state-feedback system is depicted. In order to allow a qualitative judgement both responses are benchmarked against the frequency response of the sliding surface dynamics (being the ideal system response) and the frequency response of the proportional-feedback system. It can be seen that the state-feedback amplitude response exhibits a peak at a frequency of about 12 Hz which can be observed in the response of the proportional-feedback system as well. This amplitude peak results from the third-order open-loop dynamics of the pneumatic servo depicted in Figure 9.26. The amplitude peak in the CSLMC system response is significantly smaller and its amplitude response follows more closely the response of the ideal second-order response of the sliding surface.

The phase shift of the CSLMC and the state-feedback system are larger than the phase shift of the sliding surface. For small frequencies of up to 8.5 Hz the phase shift of the CSLMC system is larger than the phase shift of the state-feedback system while it follows more closely the phase shift of the sliding surface for frequencies greater than 8.5 Hz.

It can be concluded that CSLM control is far superior to state-feedback control in providing second-order closed-loop dynamics for a predominantly third-order plant. Even the adverse effects of highly non-linear friction (stick slip) can be compensated effectively.

TABLES

Table 9.1 - Maxmimum detectable switching frequency for pneumatic servo system without valve dynamics

		actuator piston position		
		1.5 mm (near end)	15 mm (mid)	28.5 mm (near end)
direction of motion	extend	233 Hz	176 Hz	218 Hz
	retract	210 Hz	163 Hz	205 Hz

Table 9.2 - Maximum detectable switching frequency for pneumatic servo system with valve dynamics

		actuator piston position		
		1.5 mm (near end)	15 mm (mid)	28.5 mm (near end)
direction of motion	extend	204 Hz	165 Hz	196 Hz
	retract	190 Hz	155 Hz	187 Hz

FIGURES

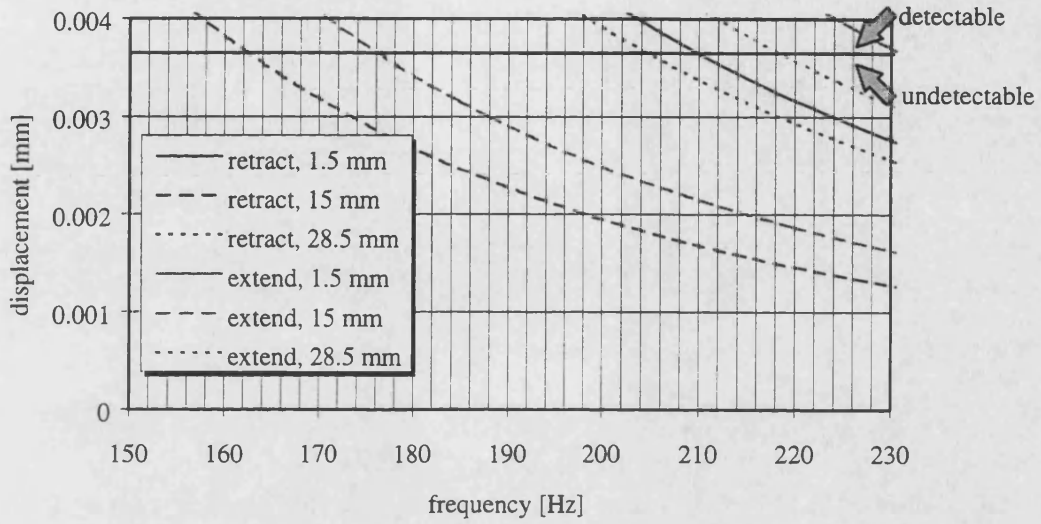

Figure 9.1 - Maximum detectable switching frequency (displacement signal) of digital CSLMC system without valve dynamics

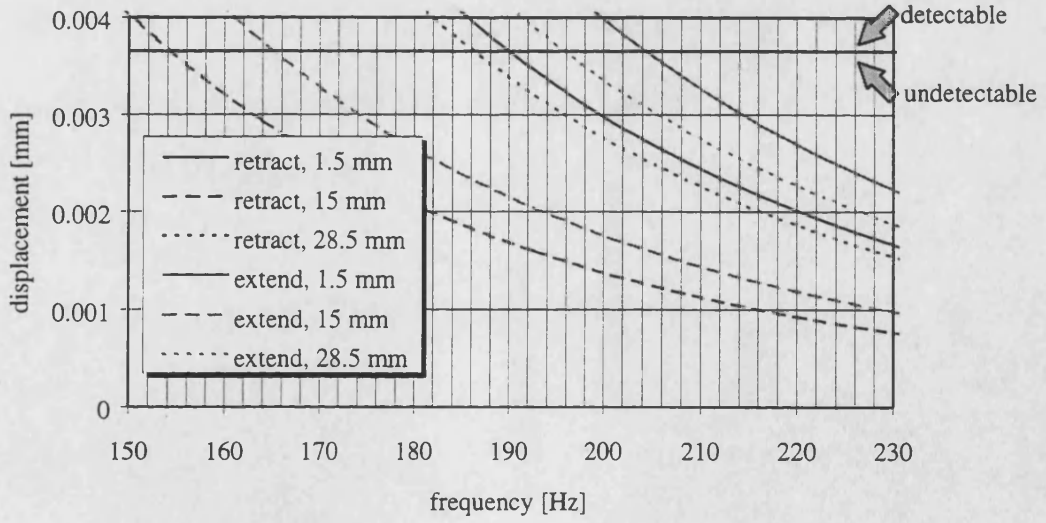

Figure 9.2 - Maximum detectable switching frequency (displacement signal) of digital CSLMC system with valve dynamics

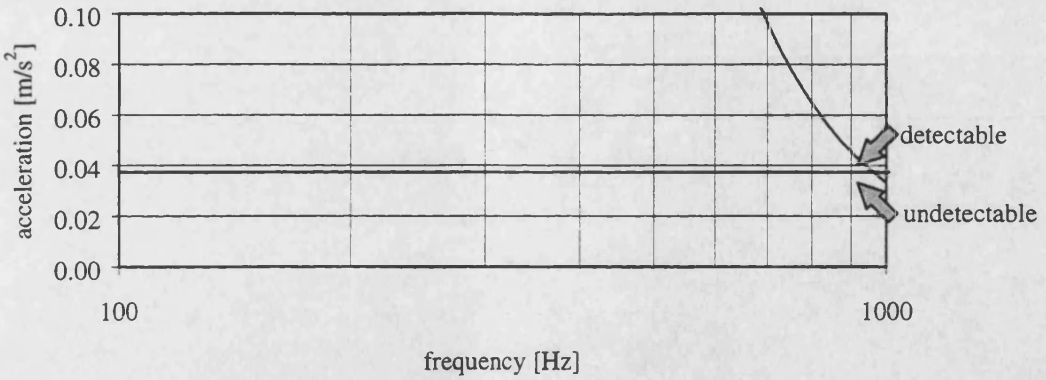

Figure 9.3 - Maximum detectable switching frequency (acceleration signal) of digital CSLMC system with valve dynamics

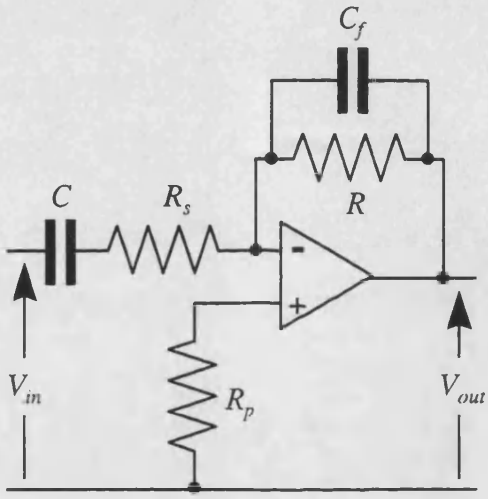

Figure 9.4 - Circuit diagram of the analogue differentiation filter

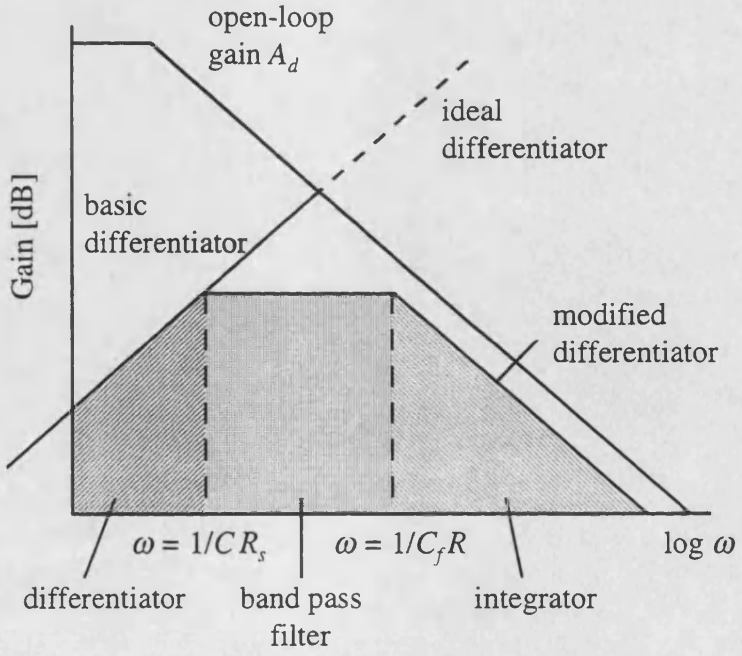

Figure 9.5 - Open-loop response of operational amplifier CA3140

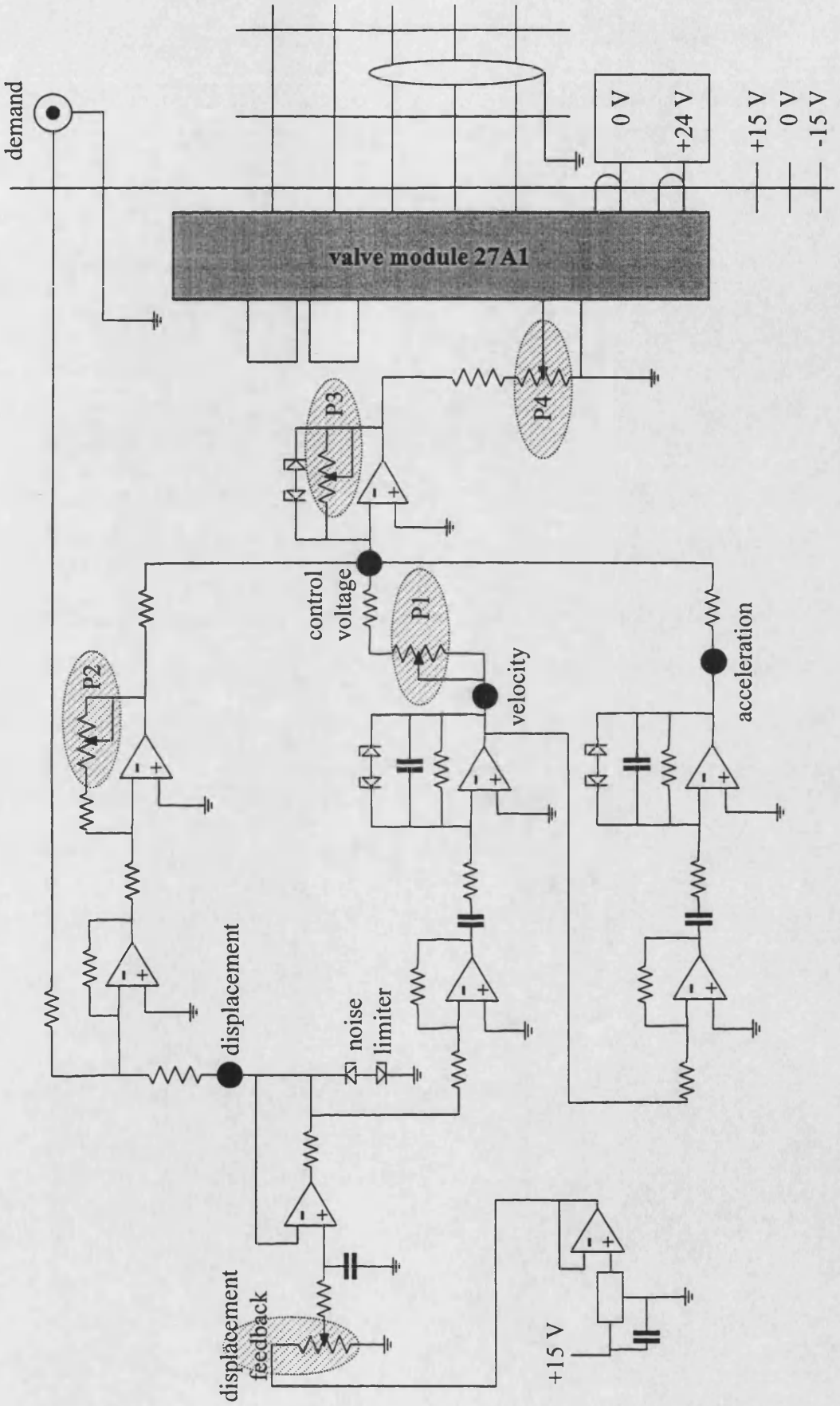

Figure 9.6 - Circuit diagram of novel analogue CSLM control card

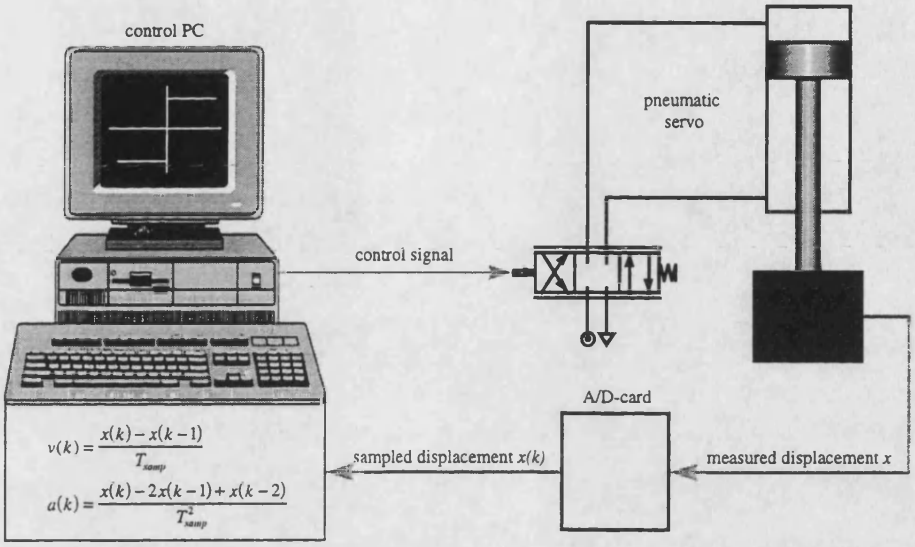

Figure 9.7 - Circuit diagram of digital CSLM control system

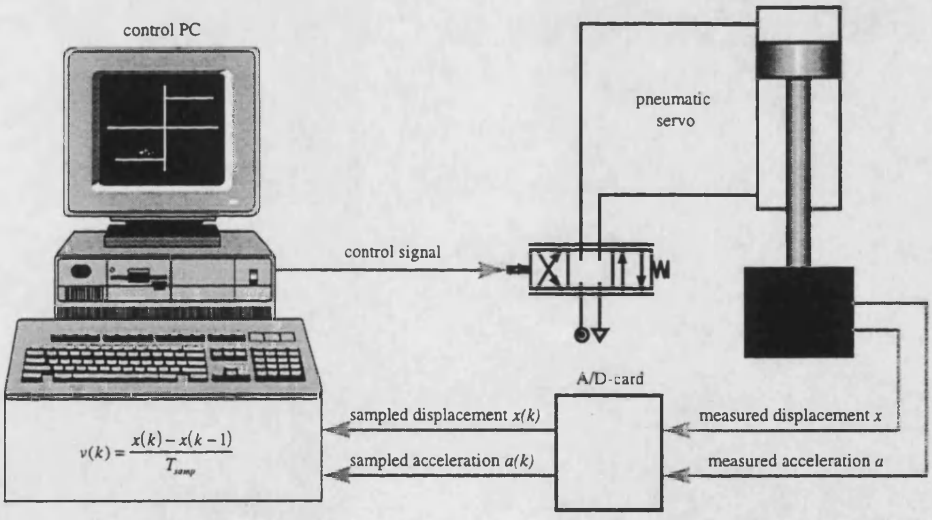

Figure 9.8 - Circuit diagram of digital CSLM control system with additional accelerometer

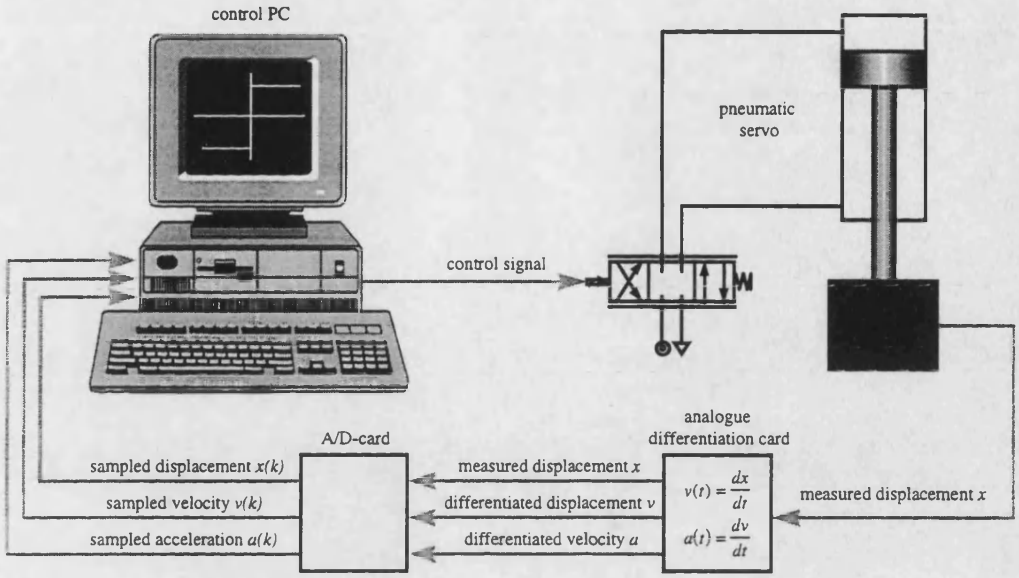

Figure 9.9 - Circuit diagram of hybrid CSLM control system

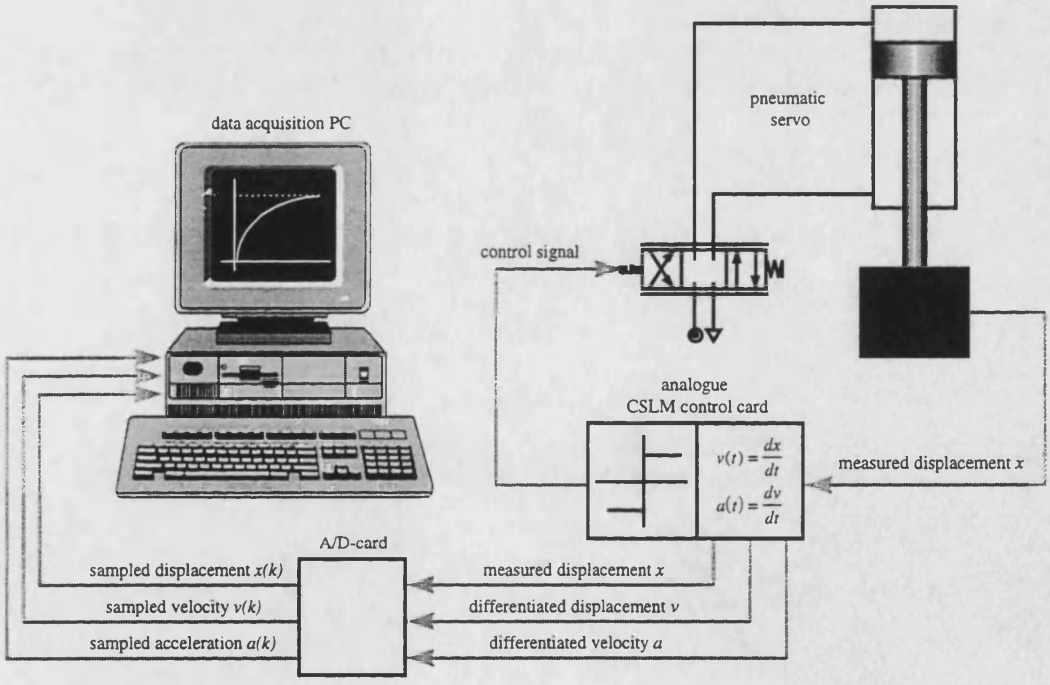

Figure 9.10 - Circuit diagram of analogue CSLM control system

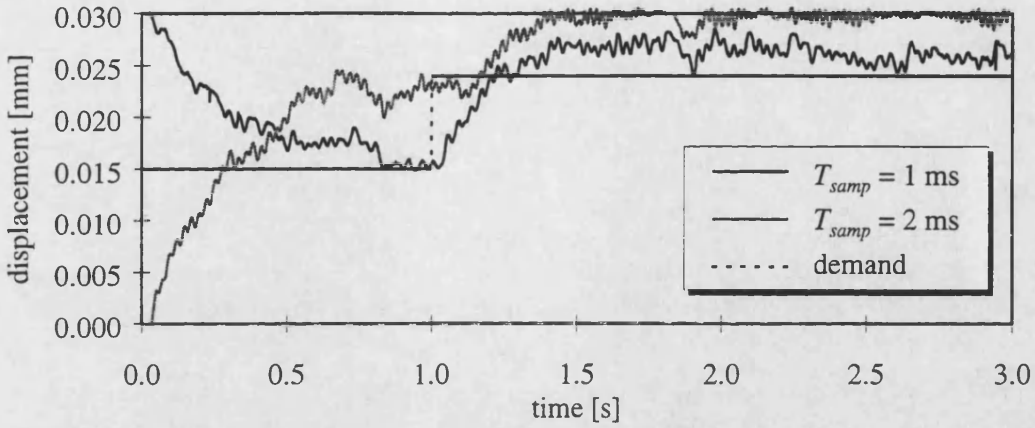

Figure 9.11 - Step response of digital CSLMC system with differentiated velocity and acceleration

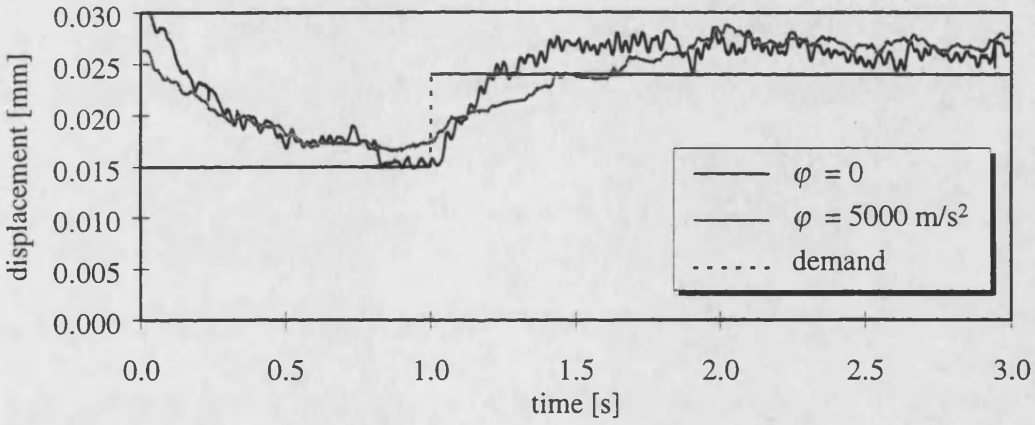

Figure 9.12 - Introduction of boundary layer (T_{samp} = 1 ms)

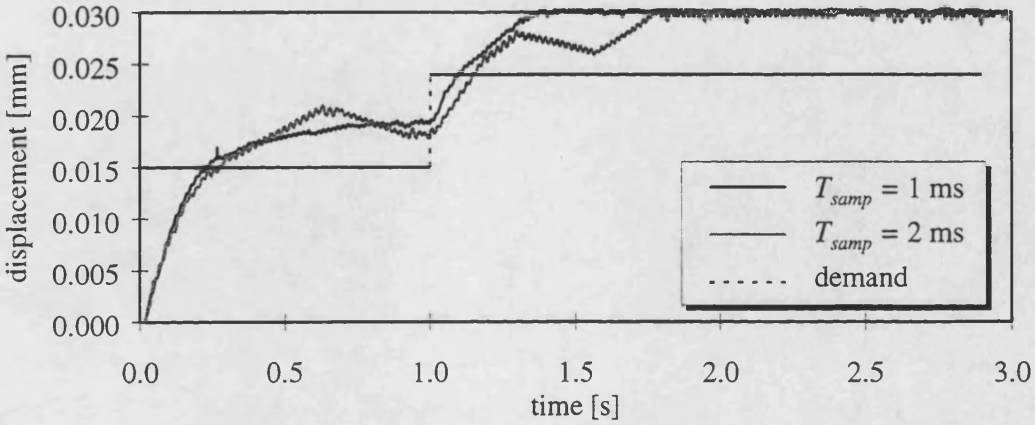

Figure 9.13 - Step response of digital CSLMC system with differentiated velocity and measured acceleration

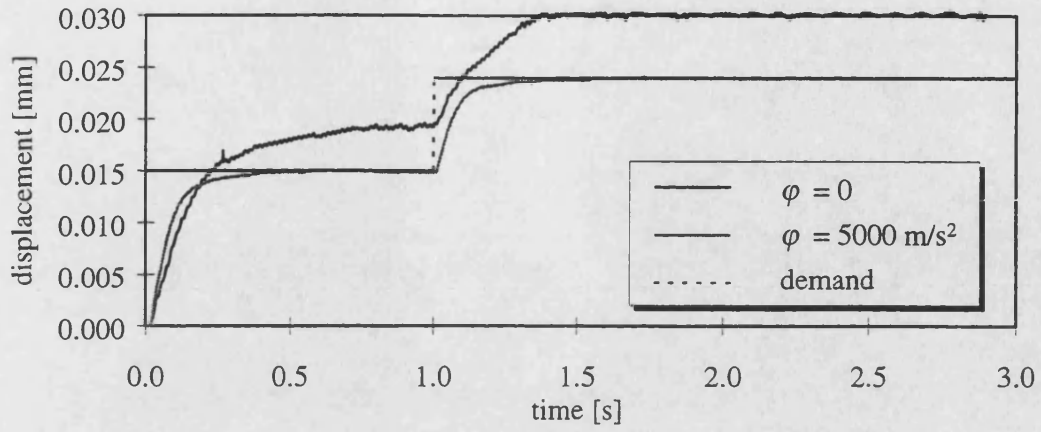

Figure 9.14 - Introduction of boundary layer (T_{samp} = 1 ms)

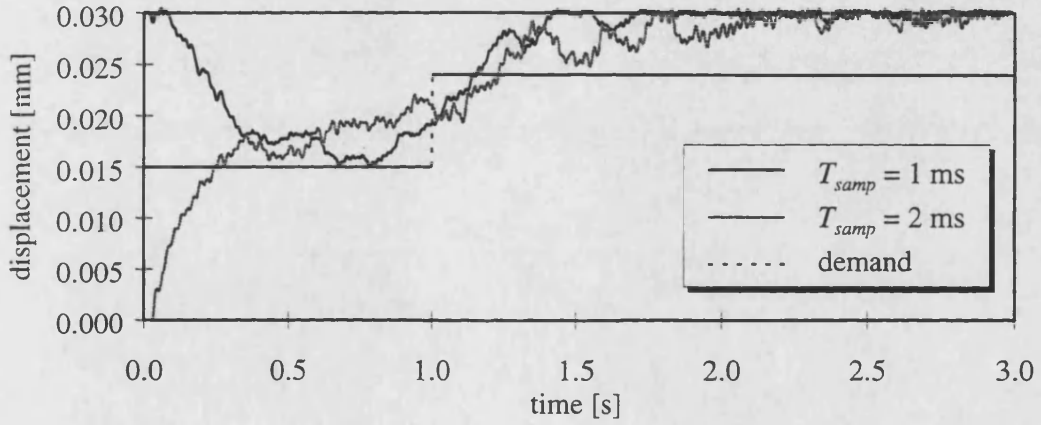

Figure 9.15 - Step response of hybrid CSLMC system with differentiated velocity and measured acceleration

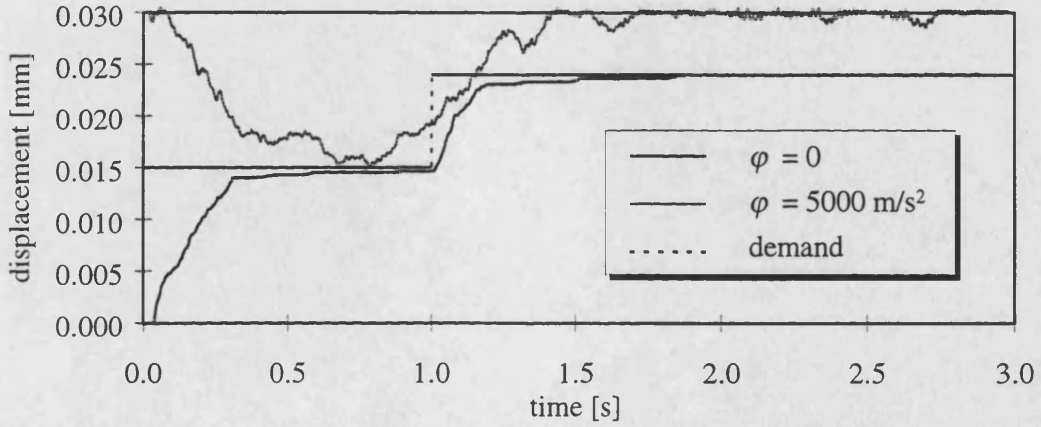

Figure 9.16 - Introduction of boundary layer (T_{samp} = 1 ms)

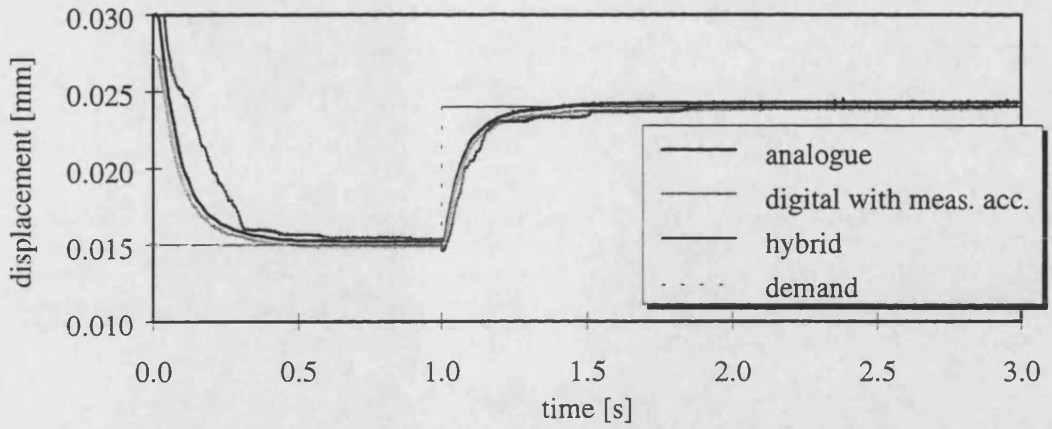

Figure 9.17 - Comparison between digital, hybrid and analogue CSLMC system

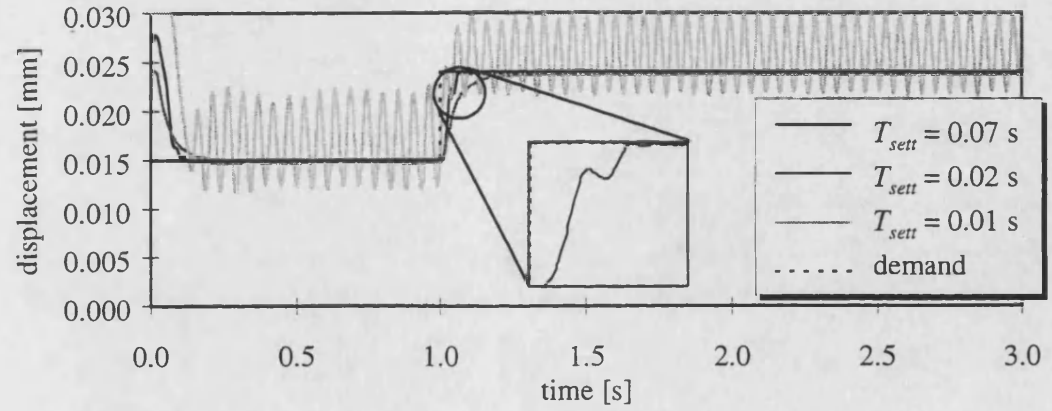

Figure 9.18 - Variation of sliding surface settling time T_{sett}

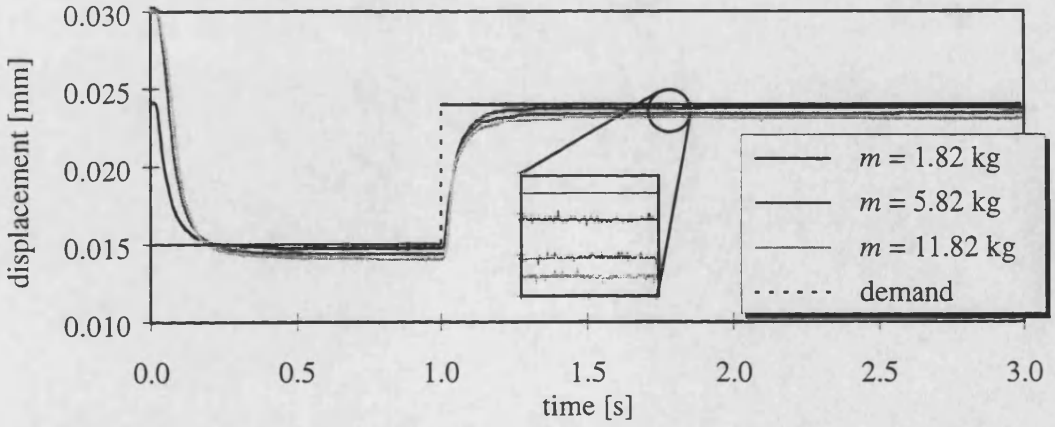

Figure 9.19 - Variation of effective mass to be moved

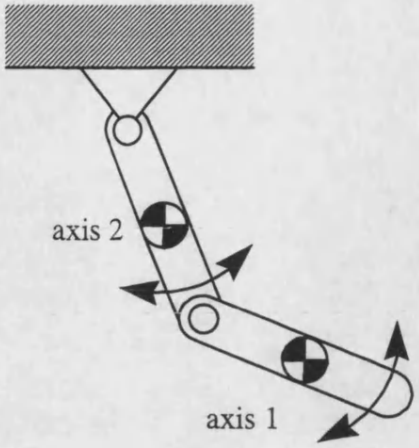

Figure 9.20 - Schematic diagram of inverted double pendulum

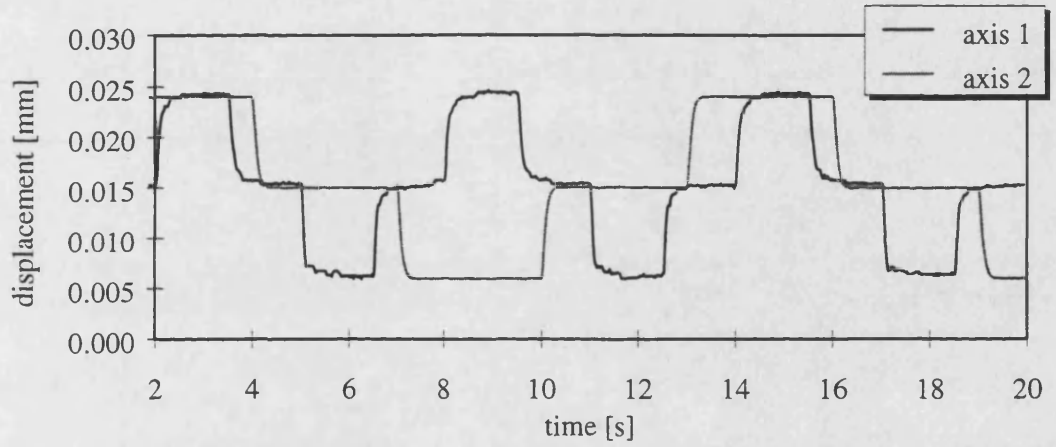

Figure 9.21 - Step response of arm under CSLM control

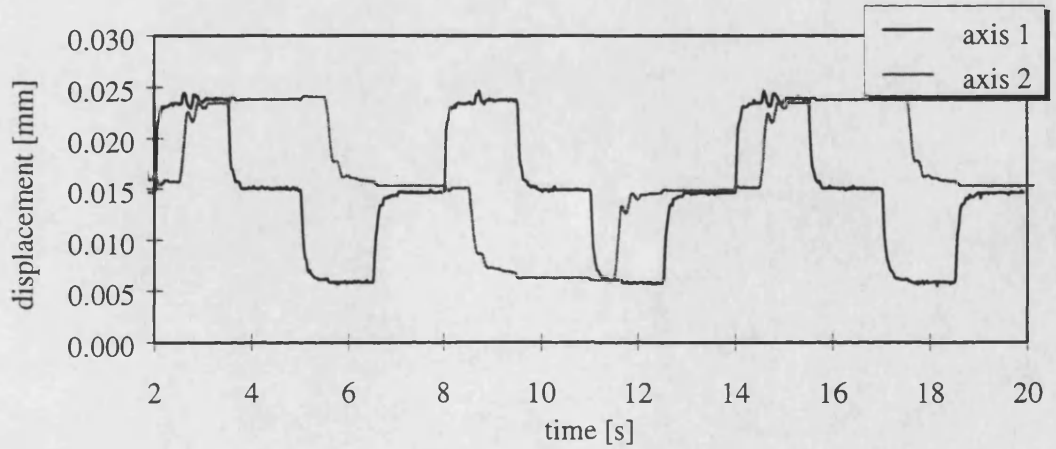

Figure 9.22 - Step response of arm under state-feedback control

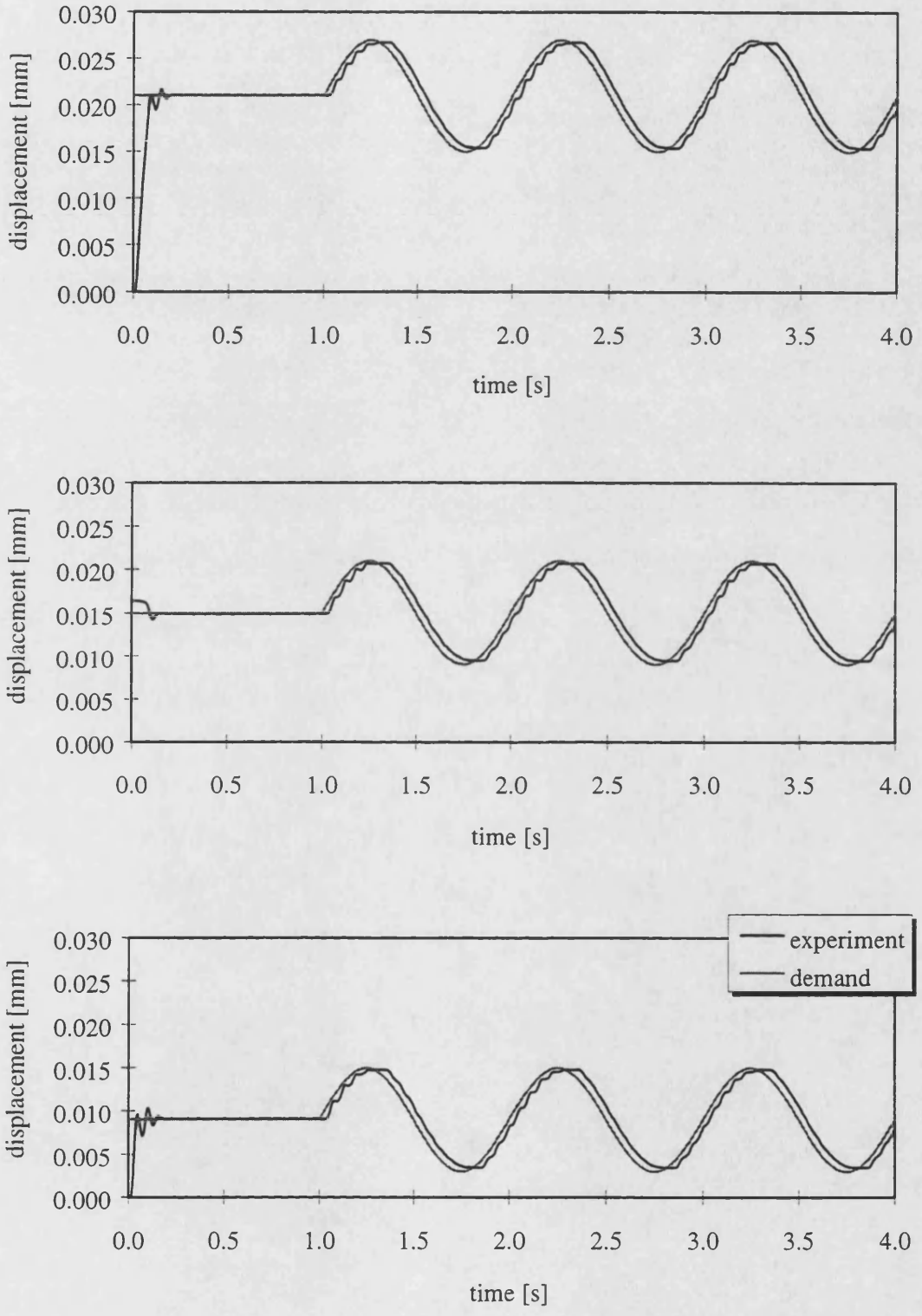

Figure 9.23 - Frequency response of state-feedback control system (f = 1 Hz)

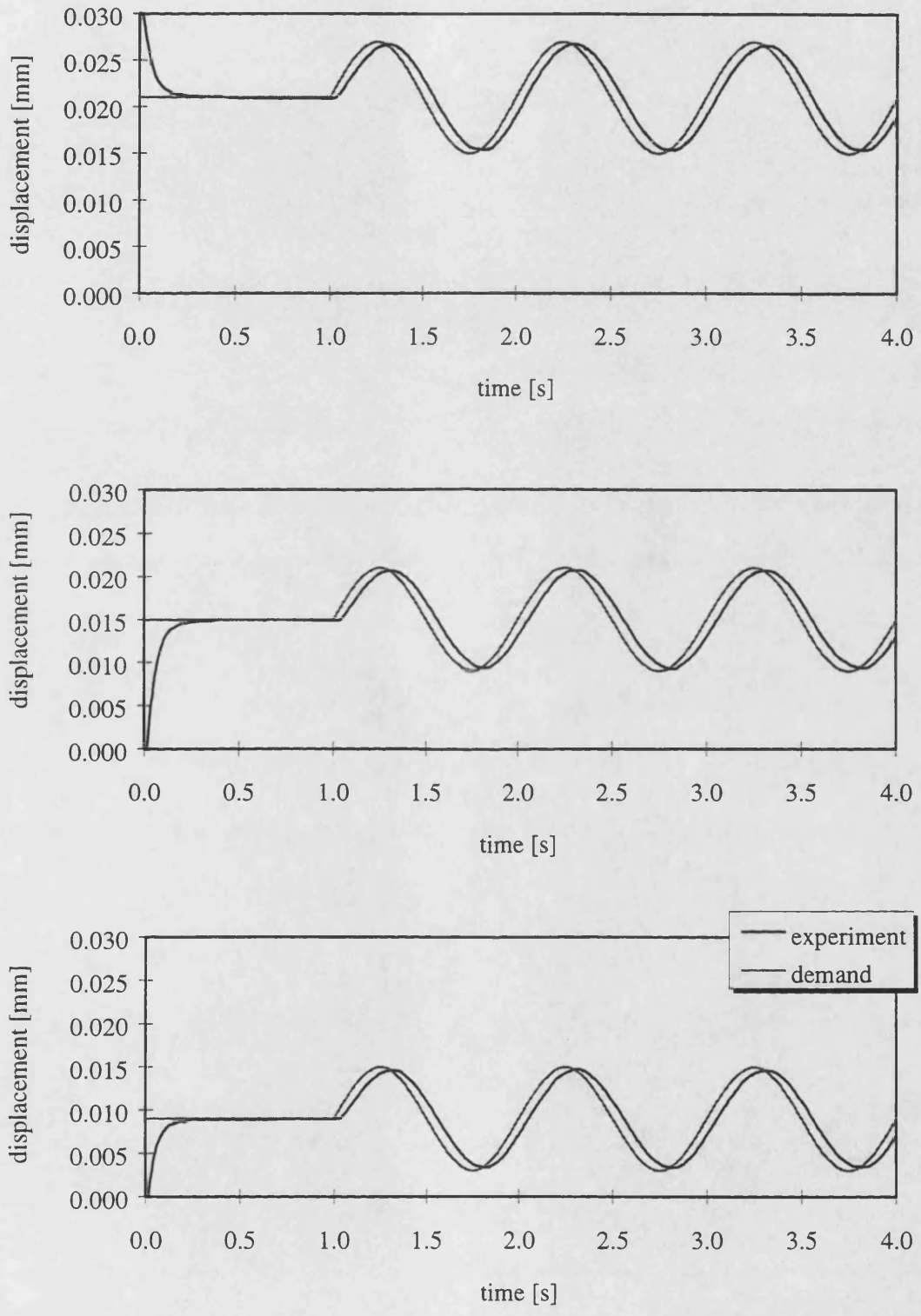

Figure 9.24 - Frequency response of CSLM control system (f = 1 Hz)

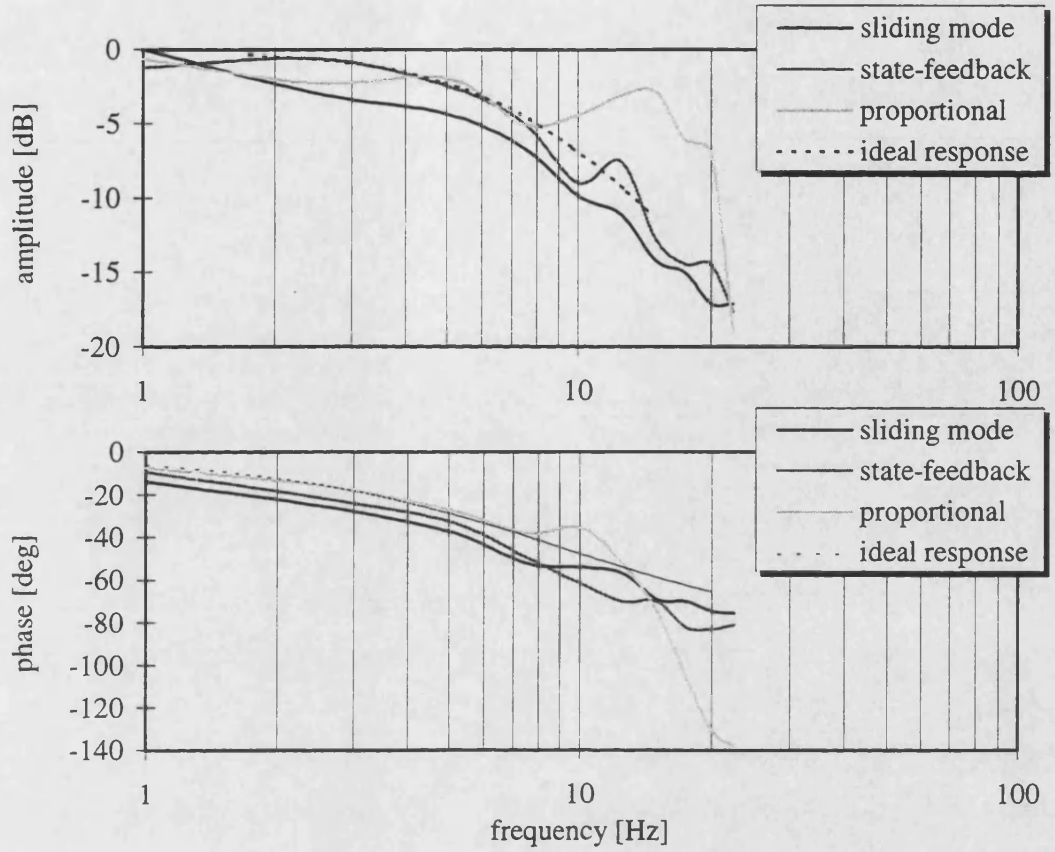

Figure 9.25 - Frequency response of CSLM control system

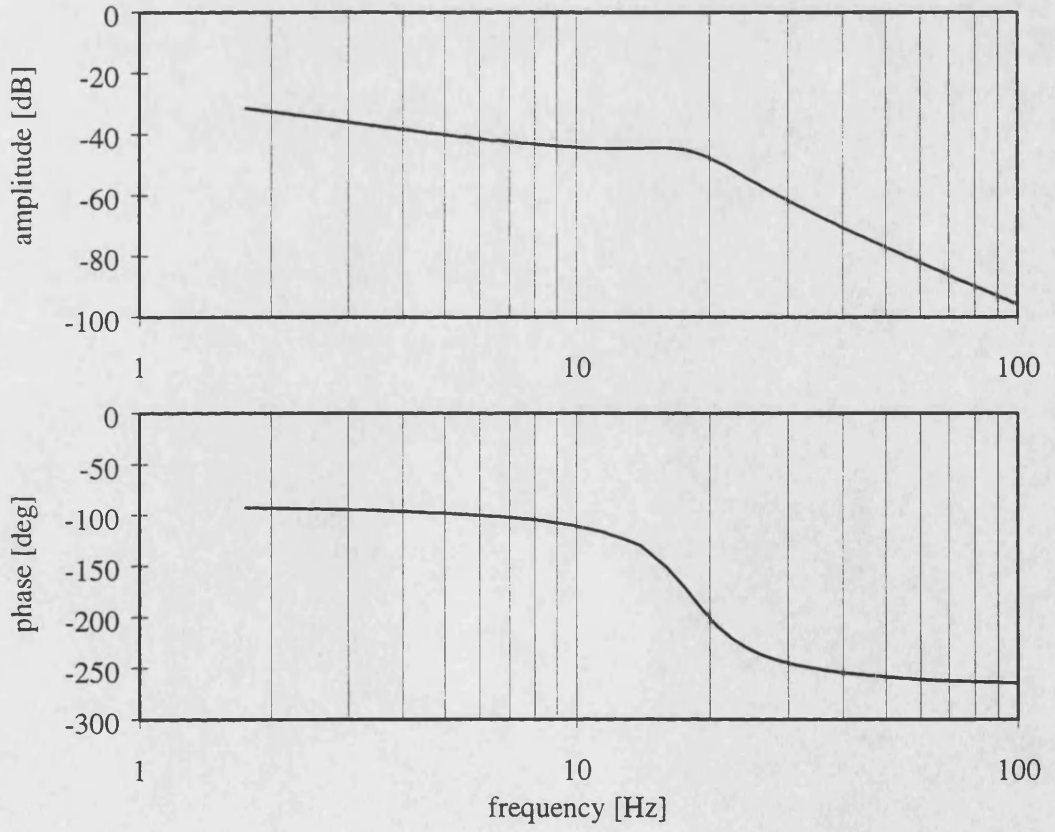

Figure 9.26 - Frequency response of open-loop pneumatic servo

10 CONCLUSIONS AND RECOMMENDATIONS FOR FUTURE WORK

The objective of the research project presented in this thesis was to develop a cheap, simple and robust controller for a multi-degree-of-freedom (*n*DOF) pneumatically actuated animated figure. In order to reduce the hardware costs to a minimum only an actuator displacement transducer was to be used.

The main achievements of the research work can be summarised under the following two headings:

- Derivation of an accurate linear and non-linear model for a pneumatic positioning servo system assisting with the analysis of these systems and enabling the development and design of suitable control methods.
- Proposal of a novel robust, low cost and easy to tune analogue CSLM control card which only requires system displacement as an input.

10.1 PNEUMATIC SERVO SYSTEM MODEL

The non-linear pneumatic component models developed within the Bath*fp* simulation environment provide a user-friendly tool to simulate and study the dynamic behaviour of highly non-linear pneumatic actuation systems. It was found during the investigation and the development of the pneumatic components for the Bath*fp* component library that an exact model of the pneumatic control valve is of crucial importance when simulating pneumatic systems. A detailed model of the direct drive servo valve HR 27A1 by HR Textron has been developed. It was found that the valve opening / flow area relationship was far from being linear. Also the discharge coefficient and the choking point proved to be valve opening and pressure ratio dependent. Therefore, as suggested by Andersen (1985) a large number of calibration tests had to be performed in order match the simulation results to the experimentally observed behaviour. In order to provide the experimental data necessary to perform the valve calibration a test routine was developed. This test routine was developed with the aim of enabling the provision of flow rate data without the need of using complicated or expensive flow measuring devices. It was

found that by charging and discharging constant dead volumes the flow rates for different valve openings and pressure ratios could be determined as a function of the polytropic index n. It was therefore decided to base the whole modelling methodology on the polytropic index n rather than on modelling heat exchange with the surrounding. Using this approach the agreement between simulation and experiment was excellent. Consequently, the developed simulation models provided an excellent tool to test the feasibility of various control methods for the pneumatic positioning servo.

The development of the linear model of a pneumatic positioning servo represents a significant extension to the basic models developed by Shearer (1956) and Burrows (1972) which are still widely used in literature. The new extended linear model takes into account the effects of unequal area actuator piston areas and constant gravity load resulting in unequal chamber pressures. These unequal chamber pressures result in a dependency on the direction of valve opening and consequent charging and discharging properties. Including these effects into the linear model results in the fact that even this relatively simple model describes position and direction of valve opening (and assuming zero initial velocity, direction of piston motion) dependent dynamic characteristics. In the context of linear controller design, the extended linear model eases the determination of the dynamically worst system state conditions to be used as a linearisation basis when synthesising a linear feedback controller. As a result the performance of pneumatic servo systems using conventional linear feedback controllers could be improved significantly.

10.2 CONTROLLER DESIGN

As a consequence of the decision to use a separate single-axis controller approach, the single-axis controller had not only to compensate for the non-linearities being an inherent characteristic of the pneumatic actuation system, but also had to be robust to severe system parameter changes due to the kinematic linking of the members of the manipulator. Furthermore, it had to provide excellent disturbance rejection capabilities in order to compensate for the coupling forces and torques resulting from the dynamic linking of the manipulator axes.

It was found that a continuous sliding mode control (CSLM) algorithm provided all the required features and hence would be best suited to the control problem. To achieve a sufficiently high switching frequency required by this controller in order to provide a satisfactory closed-loop system response it was found that working with a sampling rate of less than 10 kHz the innermost feedback loop (providing the feedback signal of the highest system state acceleration) could not be closed by means of a numerical differentiation routine. This sampling rate could not be achieved by the 166 MHz Pentium PC and the control software available for this project. An analogue double-differentiation filter was therefore designed providing the necessary information on the required system state (velocity and acceleration). Based on this double-differentiation filter a purely analogue CSLM control card was developed realising the relay-like switching action by means of a saturated operational amplifier. Experimentally testing the new analogue control card showed that it is far superior to linear state-feedback control in terms of robustness to system parameter changes (in particular the effective mass to be moved) and the action of external disturbances. Even the effects of non-linear stiction resulting in stick slip motion of the actuator piston in the case small velocities could be efficiently compensated for. Implementing the control card on two axes of a pneumatically actuated animated figure resulted in an excellent closed-loop system performance.

The new analogue control card therefore represents a simple and cheap device for a variety of third-order non-linear and linear control problems where disturbance rejection and robustness to system parameter changes are of major importance like for instance industrial manipulators. The tuning of the controller is simple and can be done by control engineers with only little prior knowledge of the system dynamics. The tuning parameters are closed-loop natural frequency or response settling time, damping ratio, maximum control action (controlling the disturbance rejection capabilities) and boundary layer width (smoothing the system response in the case of chattering). Additionally, the roll-off frequency of the differentiators can be tuned in order to minimise noise in the differentiated signals.

An interesting result that arose from the theoretical analysis of the control system in sliding mode and the reachability of the sliding surface was a way of determining important system design parameters like control valve bandwidth,

nominal valve flow rate and system supply pressure. By using equivalent control theory these parameters could be related to a desired system response and chosen accordingly. The same procedure can also be used for sizing of conventional control systems.

10.3 Recommendations for Future Work

An area into which the research presented in this thesis can be extended is the inclusion of direction dependent switching gains or integrator elements into the control algorithm. These elements would minimise the small steady-state errors which could be observed in experiment and simulation but did not prove to be of any consequence in the context of this research project. These steady-state errors result from unsymmetric switching around the sliding surface caused by direction of valve opening dependent changes in the charging and discharging conditions of the actuator chambers.

Furthermore, it would be interesting to increase the order of the sliding surface to take account of the valve spool dynamics which have been neglected here. Neglecting the valve spool dynamics resulted in a third-order dynamic model and hence a second-order sliding surface. The resulting closed-loop system can only achieve reduced-order switching. Including an additional accelerometer and differentiating the measured acceleration signal by means of analogue differentiation filters could yield a fourth-order sliding surface which would be of appropriate order for a dominantly fifth-order plant. In this case switching would not be limited by the bandwidth of the control valve but its dynamics would rather be an integral part of the sliding surface.

Implementing a non-linear switching surface could also improve the closed-loop dynamics and should therefore be investigated. By means of non-linear state gains the switching surface can approximate the so called time-optimal trajectory and therefore take fully account of the dynamics properties of the plant. A non-linear switching surface could be realised in the first instance by superposition of piecewise linear switching surfaces. These can for instance be implemented by means of a gain scheduling approach.

REFERENCES

Abou-Fayssal, H. and Surgenor, B. W., 1997
Experience with a pneumatic cartesian robot and the need for a practical friction compensator, *Proc. of the 10th Int. Fluid Power Workshop*, Bath, pp. 338-352

Anand, D. K., Anjanappa, M. and Sung, K. H., 1993
Adaptive control of a flexible manipulator with varying payload, *Proc. of the 12th World Congress IFAC*, Vol. 8, July, pp. 183-186

Anderson, B.W., 1985
The Analysis and Design of Pneumatic Systems, Robert E. Krieger Publishing Company, Florida, (corrected and revised edition)

Araki, K. and Yamamoto, A.., 1990
Model reference adaptive control of a pneumatic servo with a constant trace algorithm, *Journal of Fluid Control*, Vol. 20, No. 4, pp. 30-48

Ashrafzadeh, F., Nowicki, E. P., Boozarjomehry, R., Salmon, J. C., 1996
Optical synthesis of fuzzy sliding mode controllers, *Conference Record - IAS Annual Meeting (IEEE Industry Applications Society)*, Vol. 3, pp. 1741-1745

Åström, K. J. and Wittenmark, B., 1980
Self-Tuning Controllers based on pole-zero placement, *IEE Proceedings*, Vol. 127, Pt. D, No. 3, pp.120-120, May 1980

Åström, K. J. and Wittenmark, B., 1990
Computer controlled systems, 2nd ed., Prentice-Hall

Atherton, D. P., 1981
Oscillations in relay systems, *Trans. Inst. Measurement and Control*, Vol. 3(4), Oct.-Dec., pp. 171-184

Backé, W., 1986
Grundlagen der Pneumatik, Umdruck zur Vorlesung, IFAS, Aachen, 7. Auflage

Baida, S. V., 1993
Unit Sliding Mode Control in Continuous and Discrete Time Systems, *International Journal of Control*, 857, No. 5, pp. 1125-1132

Bailey, E. and Arapostathis, A., 1987
Simple sliding mode control scheme applied to robot manipulators, *Int. J. Cont.*, 45, pp. 1197-1209

Balestrino, A., DeMaria, G. and Sciavicco, L., 1983
An adaptive model following control for robot manipulators, *Trans. ASME, J. Dyn. Syst. Measmt. Control*, 105, pp. 143-151

Barbashin, E. A., and Gerashchenko, E. I., 1965
On Introduction to Sliding Modes in Control Systems, *Differential Equations*, 1, (1)

Bartoszewics, A., 1995
A time-varying sliding surface for fast and robust tracking control of 2nd-order uncertain systems, *Automatica*, Vol. 31, No. 12, pp. 1893-1895

Bekiroglu, N., IsilBozma, H. and Istefanopulos, Y., 1995
Model reference adaptive approach to sliding mode control, *Proc. of the American Control Conference*, Vol. 1, pp. 1028-1032

Bellini, A., Figalli, G., Pinello, P. And Ulivi, G., 1989
Realization of a control device for a robotic manipulator based on nonlinear decoupling and sliding mode control, *IEEE Trans. on Industry Applications*, Vol. 25, No. 5, pp. 790-799, Sept.-Oct.

Bengiamin, N. N. and Kauffmann, B., 1984
Variable structure position control, *IEEE Control System Magazine*, Vol. 4, No. 3, pp. 3-8, August

Bobrow, J. E. and Jabbari, F., 1989
Adaptive pneumatic force actuation and position control, *Proc. Am. Cont. Conf.*, pp. 1508-1513

Bobrow, J. E. and Jabbari, F., 1991
Adaptive pneumatic force actuation and position control, *Trans. of the ASME, Journal of Dynamic Systems, Measurement and Control*, Vol. 113, pp. 267-272, June

Bode, H. W., 1945
Network analysis and feedback amplifier design, Van Nostrad-Reinhold

Borojevic, D., Garces, L. and Lee, F. C., 1984
Soft variable structure control for DC motor position control, *Proc IEEE Industrial Applications Society Annual Meeting*, Vol. 1, pp. 283-288

Bose, H. W., 1985
Sliding mode control of an induction motor, *IEEE Trans. on Industrial Applications*, Vol. 21(2), pp. 479-486

Bouri, M., Richard, E., Thomasset, D. and Scavarda, S., 1994
Non-linear sliding mode control of an electropneumatic servodrive, *Proc. 7th Bath International Fluid Power Workshop*

Bouri, M., Thomasset, D. and Scavarda, S., 1996
Integral sliding mode controller of a rotational servo drive, *Proc. 3rd Intern. Symp. on Fluid Power*, Japan Hydraulics and Pneumatics Society, Tokyo

Bühler, H., 1986
Reglage par mode de glissement, Presses Polytechnique Romandes, Lausanne

Bühler, H., 1990
Sliding mode control with switching command devices, in Zinober, A. S. I., (ed) *Deterministic control of uncertain systems*, Peter Peregrinus, pp. 27-51

Burrows, C.R. and Webb, C.R., 1969
Further study of a low-pressure on-off pneumatic servomechanism, *Proc.Instn Mech Engrs*, 184, Pt 1, pp. 849

Burrows, C.R., 1972
Fluid Power Servomechanisms, Van Nostrand Reinhold Company

Chern, T. L. and Wu, Y. C., 1991
Design of integral variable structure controller and application to electrohydraulic velocity servosystems, *IEE Proc. Pt. D*, Vol. 138, No. 5

Chern, T. L., Chang, J. and Chang, G. K., 1997
DSP-based integral variable structure model following control for brushless DC motor drivers, *IEEE Transactions on Power Electronics*, Vol.12, No.1, January

Choi, S. B. and Park, D. W., 1994
Moving sliding surfaces for fast tracking control of second-order dynamical systems, *Trans. of the ASME: J. of Dynamic Systems, Measurement and Control*, March, Vol. 116, No. 1, pp. 154-158

Choi, S. B., Park, D. W. and Jayasuriya, S., 1994
Time-varying sliding surface for fast and robust tracking control of second-order uncertain systems, *Automatica*, May, Vol. 30, No. 5, pp. 899-904

Clayton, G. B., 1979
Operational amplifiers, 2nd edition, Butterworth & Co Ltd, London

Cotsaftis, M., Kobayashi, S. and Takamori, T., 1995
Dynamics and control of pneumatic actuators, *Proc. IEEE Int. Conf. Systems Man and Cybernetics*, pp. 159-154

Craig, J. J., 1986
Introduction to robotics: mechanics and control, Addison-Wesley Publishing Company

Craig, J. J., Hsu, P. and Sastry, S. S., 1987
Adaptive control of mechanical manipulators, *Int. J. Robotics Res.*, 6, pp. 18-28

D'Azzo, J. J. and Houpis, C. H., 1986
Feedback control system analysis and synthesis, 2nd edition, McGraw-Hill

de Almeida, F. G., 1993
Model Reference Adaptive Control of a Two Axes Hydraulic Manipulator, Ph.D. thesis, University of Bath

de Carlo, R. A., Zak, S. H. and Matthews, G. P., 1988
Variable strucutre control of non-linear multi-variable systems: a tutorial, *Proc. IEEE*, 76, pp. 212-232

Diong, B. M. and Medanic, J. V., 1992
State feedback simplex control design for systems with non-matching disturbances and uncertainties, *Proc. of the American Control Conference*, Vol. 4, pp. 3267-3271

Dorf, R. C. and Bishop, R. H., 1995
Modern control system, 7th edition, Addison-Wesley Publishing Company

Dote, Y., Takebe, M. and Ito, T., 1982
Variable structure control with sliding mode for DC drive speed regulation, *Proc. IEEE Pesc '82 Power Electronics Specialist Conference*, pp. 123-127

Drakunov, S. V., Hanchin, G. D., Su, W. C. and Ü. Özgüner, 1997
Nonlinear control of a rodless pneumatic servoactuator, or sliding mode versus Coulomb friction, *Automatica*, Vol. 33, No.7, pp. 1401-1408

Drazenovic, B., 1969
The invariance of conditions in variable structure systems, *Automatica*, 5, pp. 287-295

Dubowsky, S. and DesForges, D. T., 1979
The application of model reference adaptive control to robotic manipulators, *Trans. SME, J. Dyn. Syst. Measmt. Control*, 101, pp. 193-200

Dwyer, T. A. W. and Sira-Ramirez, H., 1988
Variable-structure control of spacecraft attitude maneuvers, *Journal of Guidance, Control, and Dynamics*, May-June, Vol. 11, No. 3, pp. 262-270

Dwyer, T. A. W., Karray, F. and Kim, J., 1989
Nonlinear robust variable structure control of pointing and tracking with operator spline estimation, *Proc.-IEEE Intern. Symp. on Circuits and Systems*, Vol. 3, p. 1606

Edge, K. A. and Figueredo, K. R. A., 1987
An adaptively controlled electrohydraulic servo-mechanism, Part 1and 2, *Proc. Instn. Mech. Engrs.*, Vol. 201, No. B3, pp. 181-189

Emal'Yanov, S. V., 1959
Use of non-linear correcting devices of switch type to inprove the quality of second order automatic control systems, *Avtomat. I Telemekh*, 20, (7), (in Russian)

Er, L. and Wang, Z., 1993
Discrete variable structure system with pseudo sliding mode, *Beijing Hangkong Hangtian Daxue Xuebao/Journal of Beijing University of Aeronautics and Astronautics*, April, No. 2, pp. 43-48, (in Chinese)

Eydinov, R. V., 1965
Evaluation of the transient process time in automatic control systems with variable structure, *Engineering Cybernetica*, No. 5, pp. 129-135

Feller, P. and Benz, U., 1987
Sliding mode position control of a DC motor, *Proc. 10th IFAC Triennial World Congress*, Munich, pp. 333-338

Filippov, A. F., 1960
Differential equations with discontinuous right-hand side, *Mat. Sb.*, 54, No. 1, (in Russian)

Filippov, A. F., 1960
Am. math. Soc. Trans., 62 199

Fok, S. C., Wang, Z. and Dransfield, P. D., 1995
Digital simulation study of an adaptive controller for a pneumatic cylinder system, *Intern. J. of Computer Applications in Technology*, Vol. 8, No. 3-4, pp. 163-171

Fossas, E. and Martinez, L., 1993
On the use of sliding mode control in bidirectional converters, *Proc.-IEEE International Symposium on Circuits and Systems*, Vol. 4, pp. 2355-2358

Franklin, G. F., Powell, J. D. and Workman, M. L., 1990
Digital control of dynamic systems, 2nd edition, Addison-Wesley Publishing Company

Franklin, G. F., Powell, J. D. and Emami-Naeini, A., 1994
Feedback control of dynamic system, 3rd edition, Addison-Wesley Publishing Company

Furuta, K., 1990
Sliding mode control of a discrete system, *Systems and Control Letters*, Vol. 14, pp. 145-152

Gamble, J. B., 1992
Sliding mode control of a proportional solenoid valve, Ph.D. thesis, School of Mechanical Engineering, University of Bath

Gamble, J., 1993
Proportional flow regulation from switching solenoids using sliding mode control, *Proc. of the Third Scandinavian International Conference on Fluid Power*, Linköping University, Linköping, pp. 255-270

Gao, W. and Hung, J. C., 1993
Variable structure control of nonlinear systems: a new approach, *IEEE Trans. on Industrial Electronics*, Vol. 40, No. 1, February, pp. 45-55

Gayed, A., Benkhoris, M. F., Siala, S., LeDoeuff, R., 1995
Time-domain simulation of discrete sliding control of permanent magnet synchronous motors, *IECON Proc. (Industrial Electronics Conference)*, Vol. 2, pp. 754-759

Gilbert, J. M., 1989
Sliding mode control of an industrial robot, Ph.D. thesis, University of Hull

Goodwin, G. C. and Sin, K. S., 1984
Adaptive filtering prediction and control, Prentice-Hall

Grace, H. P. and Lapple, C. E., 1951
Discharge coefficients for small-diameter orifices and flow nozzles, *Trans. ASME*, Vol. 73, pp. 639-647

Grantham W. J. and Athalye, A. M., 1990
Discretisation chaos: feedback control and transition to chaos, *Control and Dynamic Systems*, Vol. 34, pp. 205-277

Guihard, M., Fontaine, J. G. and M'Sirdi, N. K., 1994
Comparative study of adpative controllers for a pneumatic driven leg, *Proc. IEEE Conf. on Intelligent Robots and Systems*, pp. 1165-1171

Guihard, M., Gorce, P., Fontaine, J. G. and M'Sirdi, N. K., 1995
A solution to control the dynamic behaviour of a pneumatic quadruped robot, *Proc. IEEE Int. Conf. on Robotics and Automation*, pp. 1001-1005

Guzzella, L. and Geering, H. P., 1990
Cannonical formulation and general principles of variable structure controllers, *Deterministic control of uncertain systems*, Zinober (ed), Peter Peregrinus, pp. 115-127

Harashima, F., Hashimoto, H. and Kondo, S., 1985
MOSFET converter-fed position servo system with sliding mode control, *IEEE Trans. on Industrial Electronics*, Vol. 32(2), pp. 238-244

Harris, R. M., 1990
The modelling and simulation of temperature effects in hydraulic systems, Ph.D. thesis, School of Mechanical Engineering, University of Bath

Hashimoto, H. and Harashima, F., 1987
Variable structure strategy in motion control, *Proc. 10th IFAC Triennial World Congress*, Munich, pp. 57-62

Hashimoto, H., Yamamoto, H., Yanagisawa, S. and Harashima, F., 1988
Brushless servo motor control using variable structure approach, *IEEE Trans. On Industrial Applications*, Vol. 24(1), pp. 160-170

Horowitz, I. M., 1963
Synthesis of feedback systems, Academic Press

Houpis, C. H. and Lamont, G. B., 1985
Digital control system - theory, hardware, software, McGraw-Hill

Hung, J. Y., Goa, W. and Hung, J. C., 1993
Variable Structure Control: A Survey, *IEEE Trans. on Industrial Electronics*, Vol. 40, No. 1, February 1993, pp. 2-22

Hwang, C. L., Lan, C. H. and Jieng, W. J., 1993
The trajectory tracking of an electrohydraulic servo-mechanism via sliding mode controller, *Proc. of the IMechE*, Part I, Vol. 207, No. 13, pp. 135-142

Iordanou, H. N. and Surgenor, B. W., 1997
Sliding surface design for discrete sliding mode control and application to a pneumatic positioning system, *Proc. of the 10th International Fluid Power Workshop*, Bath

Iordanou, H. N., 1998
Continuous Versus Discrete Sliding Mode Control as Applied to a Pneumatic Positioning System, Ph.D. thesis, School of Mechanical Engineering, Queen's University, Kingston, Canada

Itkis, U., 1976
Control system of variable structure, Wiley

Jumarie, G., 1996
Tracking control of manipulators with active inertias by using sliding Lagrangian, *J. of Intelligent and Robotic Systems: Theory & Appl.*, July, Vol. 16, No. 3, pp. 245-267

Kautsky, J. and Nichols, N. K.,1983
Robust eigenstructure assignment in state feedback control, *Num. Anal. Rep.* Na/2/83, Flinders Univ., Australia

Kawamura, S., Miyata, K., Hanafusa, H. and Isida, K., 1989
PI-type hierarchical feedback control scheme for pneumatic robots, *IEEE Int. Conf. Rob. Autom.*, pp. 1853-1858

Kawashima, K., Fujita, T., Kagawa, T. and Jang, J., 1997
Characteristics measurement of pneumatic flow control valves using isothermal chamber, *Proc. of the 10th Int. Fluid Power Workshop*, Bath, pp. 324-337

Keller, H. and Isermann, R., 1993
Model-based non-linear adaptive control of a pneumatic actuator, *Control. Eng. Practice*, Vol. 1, No. 3, pp. 505-511

Kim, B. K. and Shin, K. G., 1983
An adaptive model following control of industrial manipulators, *IEEE Trans.*, AES-19, pp. 805-813

Kim, J. J., Lee, J. J., Park, K. B. and Youn, M. J., 1993
Design of new time-varying sliding surface for robot manipulator using variable structure controller, *Electronics Letters*, January 21, Vol. 29, No. 2, pp. 195-196

Kim, H. S., Park, J. H., Choi, Y. K., 1996a
Variable structure control of brushless DC motor using evolution strategy with varying search space, *Proc. of the IEEE Conf. on Evolutionary Comp.*, pp. 764-769

Kim, D. H., Kim, H. S., Kim, J. M., Won, C. Y.and Kim, S. C., 1996b
Induction motor servo system using variable structure control with fuzzy sliding surface, *IECON Proc. (Industrial Electronics Conference)*, Vol. 2, pp. 977-982

Kimura, T., Hara, S., Fujita, T. and Kagawa, T., 1995
Control for pneumatic actuator systems using feedback linearisation with disturbance rejection, *Proc. of the American Cont. Conf.*, Seattle, June, pp. 825-829

Konno, Y. and Hashimoto, H., 1993
Design of sliding mode dynamics in the frequency domain, *Advanced Robotics*, Vol. 7, No. 6, pp. 587-598

Kung, C. C. and Liao, C. C., 1994
Fuzzy-sliding mode controller design for tracking control of non-linear system, *Proc. of the American Control Conference*, Vol. 1, pp. 180-184

Kwatny, H. G. and Kim, H., 1990
Variable structure regulation of partially linearizable dynamics, *Systems & Control Letters*, July, Vol. 15, No. 1, pp. 67-80

Lai, J.Y., Menq, C.H. and Singh, R., 1990
Accurate Position Control of a Pneumatic Actuator, *ASME J. of Dynamic Systems Measurement and Control*, Vol. 112, pp. 734-739

Landau, Y. D., 1979
Adaptive Control - The Model Reference Approach, Marcel Dekker, New York

Landau, Y. D., 1981
Model Reference Adaptive Control and Stochastic Self-Tuning Regulators - A Unified Approach, *Trans. ASME, Journal of Dyn. Sys. Meas. and Control*, Vol. 103, December, pp. 404-416

Lantto, B., 1994
On fluid power control with special reference to load-sensing systems and sliding mode control, Ph.D. thesis, Department of Mechanical Engineering, Linköping University

Lee, D. S. and Youn, M. J., 1989
Controller design of variable structure systems with nonlinear sliding surface, *Electronics Letters*, December 7, Vol. 25, No. 25, pp. 1715-1717

Lee, D. S., Kim, M. G., Kim, H. K. and Youn, M. J., 1991
Controller design of multivariable variable structure systems with nonlinear switching surfaces, *IEE Proc., Part D: Control Theory and Applications*, September, Vol. 138, No. 5, pp. 493-499

Lee, C. K. and Kwok, N. M., 1995a
BLDCM servo system using a variable structure controller with an adaptive switching slope, *PESC Record - IEEE Annual Power Electronics Specialists Conference*, Vol. 2, pp. 1352-1357

Lee, C. K. and Kwok, N. M., 1995b
Variable structure controller with adaptive switching surfaces, *Proc. of the American Control Conference*, Vol. 1, pp. 1033-1034

Lee, C. K., Kwok, N. M. and Leung, T. P., 1995
Brushless dc motor velocity regulator using a variable structure controller with varying switching surfaces, *Proc. of the International Conference on Power Electronics and Drive Systems*, Vol. 1, pp. 297-302

Leung, N. C. M., Li, C. K. and Kung, P. K., 1992
Design of a DSP-based discrete variable structure controller with improved robustness, *Microprocessing and Microprogramming*, Vol. 35, No.1-5, September, pp. 713-718

Li, W. and Cheng, X., 1994
Adaptive high-precision control of positioning tables - theory and experiments, *IEEE Trans. on Control Systems Technology*, Vol. 2, No. 3, September, pp. 265-270

Lim, K. W., Low, T. S, Rahman, M. F. and Wee, L. B., 1991
A Discrete Time Variable Structure Controller for a Brushless dc Motor Drive, *IEEE Trans. on Industrial Electronics*, Vol. 38, No. 2, April, pp. 102-107

Lin, S. C. and Chen, C. H., 1994
A microprocessor-based electrohydraulic servo system, *Journal of the Chinese Institute of Engineers*, Vol. 7, No. 1, pp. 55-60

Lin, X. F., Thomasset, D., Richard, E. and Scavarda, S., 1993
Non-linear position control for a long pneumatic actuator, *Proc. 3rd Scandinavian Int. Conf. on Fluid Power*, Linköping, Sweden

Lin, Y. and Kortüm, W., 1992
Identification of System Physical Parameters for Vehicle Systems with Nonlinear Components, *Vehicle System Dynamics*, Vol. 20, University of California, Institute of Transportation Studies, Berkley

Liu, S. and Bobrow, J. E., 1988
An Analysis of a Pneumatic Servo System and its Application to a Computer-Controlled Robot, *Trans. ASME*, Vol. 110, September, pp. 228-235

Lo, J.K.W. and Tilley, D.G., 1993
Simulation of Pneumatic Systems using BATHfp Fluid Power Simulation Package, Internal report, Fluid Power Centre, University of Bath

Lo, J. K. W., 1995
Mathematical modelling of mixed gas breathing equipement and associated systems, Ph.D. thesis, School of Mechanical Engineering, University of Bath

MacCarley, C. A. and Meyer, D. G., 1991
Sample rate selection for discrete time switching controls, *IFAC Symposia Series - Proc. of a Triennial World Congress*, Vol. 3., pp. 305-309

Maddock, R. J. and Calcutt, D. M., 1994
Electronics for engineers, 2nd edition, Longman Scientific & Technical

Makarov, I. M. and Rakhmankulov, V. Z., 1969
Improvement of variable structure system time response by the combination of slipping hyperplanes, *Automation and Remote Control*, No. 6, pp. 72-81

Mannetje, J. J., 1981
Pneumatic servo design method improves system bandwidth twenty-fold, *Control Eng.*, June, pp. 79-83

MathWorks, Inc., 1992
MATLAB Reference Guide: High Performance Numeric Computation and Visualization Software, The MathsWorks Inc., Natick, Massachusetts

Matthews, G. P., DeMarco, C. and DeCarlo, R. A., 1987
Decentralised variable structure control design for two interconnected synchronous machines, *Proc. of the American Control Conference*, pp. 96-101

McCloy, D. and Martin, H. R., 1980
Control of Fluid Power: Analysis and Design, John Wiley, New York

McDonell, B. W. and Bobrow, J. E., 1993
Adaptive tracking control of an air powered robot actuator, *Trans. of the ASME, Journal of Dynamic Systems, Measurement and Control*, Vol. 115, pp. 427-433

Mestha, L. K. and Yeung, K. S., 1991
Sliding mode controller for RF cavity tuning loop, *Conf. Rec. 19 IEEE Part. Accel. Conf.*, No. 1991, pp. 783-785

Middleton, R. H. and Goodwin, G. C., 1988
Adaptive computed torque control for rigid link manipulators, *Syst. Control Lett.*, 10, pp. 9-16

Milosaviljevic, C., 1985
General conditions for the existence of a quasisliding mode on the switching hyperplane in discrete variable structure systems, *Automation and Remote Control*, pp. 307-314

Min-Ho, P., Young-Real, K. and Kyung-Seo, K., 1989
Chattering reduction in the position control of induction motors using the sliding mode, *Proc. IEEE PESC '89 Power Electronics Specialist Conf.*, Vol. 1, pp. 438-445

Miyasato, Y. and Oshima, Y., 1989
Non-linear adaptive control for robotic manipulators with continuous control inputs, *Int. J. Control*, 49, pp. 545-599

Moler, M. W., Little, J., Bangert, S. and Kleiman, S., 1987
PC-MATLAB, The MathWorks Inc., MA

Moore, P. R., Weston, R. H. and Thatcher, T. W., 1985
Compensation in pneumatically actuated servomechanisms, *Trans. Inst. M.C.*, Vol. 7, No. 5, Oct.-Dec.

Nagarth, I. J. and Gopal, M., 1982
Control systems engineering, 2nd edition, Wiley

Nadam, C. and Sen, P. C., 1987
Observer-based sliding mode control for variable speed drives, *Proc. IEEE Industrial Applications Soc. Annual Meeting*, Vol. 1, pp. 209-214

Nadam, C. and Sen, P. C., 1988
Sliding mode speed control of a SCSM using an adaptive state observer, *Proc. 3rd Conference on Power Electronics and Variable Speed Drives*, pp. 315-318

Nadam, C. and Sen, P. C., 1990
A comparative study of a Luenberger observer and adaptive observer-based VS speed control system using a SCSM, *IEEE Trans. on Industrial Electronics*, Vol. 37(2), pp. 127-132

Noritsugu, T. and Takaiwa, M., 1995
Robust positioning control of pneumatic servo system with pressure control loop, *Proc. IEEE Int. Conf. on Rob. and Autom.*, pp. 2613-2618

Nouri, A. S., Gauvert, C., Tondu, B. and Lopez, P., 1994
Generalized variable structure model reference adaptive control of one-link artificial muscle manipulator in two operating modes, *Proceedings of the IEEE International Conference on Systems, Man and Cybernetics*, Vol. 2, pp. 1944-1950

Pandian, S. R., Hayakawa, Y., Kanazawa, Y., Kamoyama, Y. and Kawamura, S., 1997, Practical design of a sliding mode controller for pneumatic actuators, *Proc. IEEE Conf. Decision and Control*, San Antonio, pp. 2155-2156

Park, K. B. and Lee, J. J., 1993
Variable structure controller for robot manipulators using time-varying sliding surface, *Proc.-IEEE Intern. Conf. on Robotics and Automation*, Vol. 1, pp. 89-92

ParraVega, V. and Arimoto, S., 1995
Exponentially convergent adaptive sliding mode control of robot manipulators, *International Journal of Systems Science*, December, Vol. 26, No. 12, pp. 2263-2276

Perry, J. A., 1949
Critical flow through sharp edged orifices, *Trans. ASME*, October

Phillips, C. L. and Nagle, H. T., 1990
Digital control system analysis and design, Prentice-Hall, Englewood Cliffs, New Jersey

Pollmeier, K., 1997
Parallel computing for real-time simulation and condition monitoring of fluid power systems, Ph.D. thesis, University of Bath

Pu, J. and Weston, R. H., 1990
Steady-state analysis of pneumatic servo drives, *Proc. of IMechE Part C, Journal of Mech. Eng. Science*, Vol. 204, No. 6, pp. 377-387

Pu, J., Weston, R. H., Harrison, R., Carrot, A. and Moore, P. R., 1991
Programmable machine control and software transmission elements for material handling systems, *Advances in Computer Science Applications to Machinery, CAD of Machinery*, Beijing, China, pp. 527-533

Pu, J., Weston, R. H. and Moore, P. R., 1992
Digital motion control and profile planning for pneumatic servos, *Trans. of the ASME*, Vol. 114, December, pp. 634-640

Qi, W. and Hoft, R. G., 1994
Induction motor sliding mode control performance results, *Conf. Proc.-IEEE Applied Power Electronics Conf. and Exposition-APEC*, Vol. 1, pp. 507-513

Richard, E. and Scavarda, S., 1989
Nonlinear control of pneumatic servodrives, *Proc. 2nd Bath Fluid Power Workshop*, September, pp. 59-75

Richards, R. J. and Reay, D. S., 1992
The real-time application of VSS controllers: implementation on elements of a 'direct-drive' arm, a Syke robot and PUMA robot, *Trans. Inst. Measmt. Control*, 14, pp. 139-152

Rogers, G. F. C and Mayhew, Y. R., 1973
Engineering Thermodynamics Work and Heat Transfer, Longman

Sabanovic, A., Izosimov, D. B., Bilalovic, F. and Music, O., 1983
Sliding mode in controlled motor drives, *Proc IFAC Symposium Lausanne, Control in power electronics and electrical drives*, Pergamon Press, Oxford, pp. 325-330

Sarpturk, S. Z., Istefanopulos, Y. and Kaynak, O., 1987
The stability of discrete-time sliding mode control systems, *IEEE Trans. on Automatic control*, Vol. 32, pp. 930-932

Scholz, D., 1990
Auslegung servopneumatischer Antriebssysteme, Dissertation, RWTH Aachen, Germany

Seraji, H., 1989
Decentralised adaptive control of manipulators: theory, simulation and experimentation, *IEEE Trans. on Robotics and Automation*, Vol. 5, No. 2, April

Shearer, J. L., and Lee, S. Y., 1956
Selecting power control valves. II - their design and performance, *Control Engng.*, 3, No. 4, 73

Shearer, J. L., 1956
Study of pneumatic processes in the continuous control of motion with compressed air, Parts I and II, *Trans.ASME*, 78, pp. 233

Shearer, J. L., 1957
Non-linear analogue study of a high pressure servo mechanism, *Trans. ASME*, 79, 1957, pp. 465

Shih, M. C. and Huang, Y. F., 1992
Pneumatic servo-cylinder position control using a self-tuning controller, *JSME Intern. J., Series 2: Fluids Engineering, Heat Transfer, Power, Combustion, Thermophysical Properties*, Vol. 35, No. 2, May, pp. 247-254

Shih, M. C. and Tseng, S. I., 1994
Pneumatic servo-cylinder position control by PID-self-tuning controller, *JSME International Journal*, Series C, Vol. 37, No. 3, pp. 565-572

Shoureshi, R., Momot, M. E. and Roesler, M. D., 1990
Robust control for manipulators with uncertain dynamics, *Automatica*, 26, pp. 353-359

Sira-Ramiréz, H., 1987
Spacecraft reorientation maneuvers via linearizing variable structure control, *Conf. Record - Asilomar Conference on Circuits, Systems & Computers*, pp. 477-480

Slotine J.-J. E., 1985
The robust control of robot manipulators, *Int. J. Robotics Research*, 4, pp. 49-64

Slotine J.-J. E. and Li, W., 1988
Adaptive manipulator control: a case study, *IEEE. Trans.*, AC-33, pp. 995-1003

Slotine J.-J. E. and Li, W., 1991
Applied Nonlinear Control, Prentice-Hall, Englewood Cliffs, New Jersey

Slotine, J.-J. E. and Sastry, S. S., 1983
Tracking control of non-linear systems using sliding surfaces, with application to robot manipulators, *Int. J. Control*, Vol. 38 (2), pp. 465-492

Spong, M. W. and Vidyasagar, 1989
Robot Dynamics and Control, John Wiley & Sons, Inc., Singapore

Spurgeon, S. K., 1992
Hyperplane design techniques for discrete-time variable structure control systems, *International Journal of Control*, Vol. 55, pp. 445-456

Stenning, A.H., 1955
An experimental study of two-dimensional gas flow through valve type orifices, *ASME*, paper No. 54-4-45

Stoten, D. P., 1990
Model Reference Adaptive Control of Manipulators, Research Studies Press Ltd., Taunton, England

Surgenor, B. W. and Wijesuriya, E. T., 1992
Experience with an intelligent optimal controller as applied to a high-friction pneumatic actuator, *ASME DSC Intelligent Control Systems*, Vol. 45, pp. 93-103

Surgenor, B. W., Uebing, M. and Vaughan, N. D., 1995
Continuous sliding mode control of a pneumatic positioning system, *Proc. of the 8th International Fluid Power Workshop*

Taha, Z. and Nor, K. M., 1989
Microcomputer control of a pneumatic robot, *Proc. 28th SICE Ann Conf.*, pp. 1057-1060

Tang, J. and Walker, G., 1995
Variable structure control of a pneumatic actuator, *Trans. of the ASME*, Vol. 117, March

Taran, V. A., 1964a
Improving the dynamic properties of automatic control system by means of non-linear corrections and variable structure, Translation from *Avtomatika I Telemkhanika*, Vol. 25, No. 1, pp. 140-149, (UDC 62-50.51)

Taran, V. A., 1964b
The control of linear systems by means of floating-control regulators with variable structure without using pure derivatives in the control law, Translation from *Avtomatika I Telekhanika*, Vol. 25, No. 11, pp. 1558-1565, (UDC 62-5051)

Thomasset, D., Richard, E., Scavarda, S., Lin, X. F., Sesmat, S. and Bouhal A., 1993
Control of an electropneumatic servodrive: a state affine or a sliding approach, *Proc. IFAC World Congress*, Sydney

Tse, P. and Leung, S. W., 1990
Simulation of model reference adaptive control used in high speed hydraulic and pneumatic driven system, *Proc. 29th SICE Annu. Conf.*, Vol. 2, pp. 805-808

Tso, S. K., Xu, Y. S. and Shum, H. Y., 1991
Variable structure model reference adaptive control for robotic manipulators, *Proc. Of IEEE International Conference on Robotics and Automation*, pp. 2148-2153

Tso, S. K., Xu, Y. S., Shum, H. Y. and Law, P. L., 1992
Model based variable structure adaptive control for robot manipulators: experimental study, *Proc. of 8th International Conference on CAD/CAM Robotics and Facturies of the Future*

Tso, S. K. and Law, P. L., 1992
Design and performance studies of model based variable structure adaptive controllers for industrial manipulators, *Proc. Instn. Mech. Engrs.* Vol. 206, No. 14

Tsypkin, Y. Z., 1984
Relay Control Systems, Cambridge

Uebing, M., Vaughan, N. D., and Surgenor B. W., 1997
On linear dynamic modelling of a pneumatic servo system, *Proc. 5th Scandinavian Int. Conf. on Fluid Power SICFP'97*, pp. 363-378

Utkin, V. I., 1977
Variable Structure systems with sliding modes, *IEEE Trans.*, AC-22, pp. 212-222

Utkin, V. I., 1978
Sliding Mode Control and its Application to Variable Structure Systems, Mir, : Moscow

Utkin, V. I. and Yang, K. D., 1978
Methods for constructing discontinuity planes in multidimensional variable structure systems, *Automat. Remote Control*, 10, pp. 72-77

Utkin, V. I., 1983
Variable structure systems present and future, *Automat. Remote Control*, 44, pp. 1105-1120

Utkin, V. I., 1987
Variable structure control state of the art, *Proc. IFAC Conf.*, München, Germany

Utkin, V. I. and Drakunov, S. V., 1989
On discrete-time sliding mode control, *Proc. of IFAC Symposium on Nonlinear Control Systems (NOLCOS)*, Italy, pp. 484-489

Vaughan, N. D. and Plummer, A. R., 1990
Robust Adaptive Control for Hydraulic Servosystems, *ASME Winter Annual Meeting*, Dallas, Texas

Verghese, G., Fernandez, R. B. and Hedrick, J. K., 1988
Stable, robust tracking by sliding mode control, *Syst. Contr. Lett.*, Vol. 10, pp. 27-34

Virvalo, T., 1995
Improving the use of the stroke of a pneumatic servo cylinder, *Proc. 4th SICFP'95*, Sept. 26.-29., Tampere, Finland, pp. 528-544

Walcott, B. L. and Zak, S. H., 1987
Laboratory Investigation in Microprocessor-Based Variable Structure Control, *IEEE Trans. on Education*, Vol. E-30, No. 4, pp. 227-243

Walters, R. G. and Byoumi, M. M., 1982
Application of self-tuning pole-placement regulator to an industrial manipulator, *IEEE Proc. on CDC*, pp. 323-329

White, B. A., 1983
Reduced order switching functions in variable structure control systems, *Proc. IEE Pt. D Control Theory*, Vol. 130(2), pp. 33-40

White, B. A., 1986
Range space dynamics of variable structure control systems, *Proc. IEE Pt. D Control Theory*, Vol. 133(1), pp. 35-41

Wonham, W., 1963
Optimal bang-bang control with quadratic performance index, *4th Joint Automatic Control Conference*, Minneapolis

Workman, M. L., Koust, R. L. and Franklin, G. F., 1987
Adaptive proximate time-optimal servomechanisms: continuous-time case, *Proc. IEEE American Control Conference*, pp. 589-594

Xu, J.-X., Hashimoto, H., Slotine, J.-J. E., Arai, Y. and Harashima, F., 1989
Implementation of VSS control to robotic manipulators - smoothing modification, IEEE Trans. on Industrial Electronics, Vol. 36 (3), pp. 321-329

Xu, M., Smith, S. M., 1994
Use of fuzzy logic in adaptive `morphological' controllers, *Proc. 1994 1st Int. Jt. Conf. NAFIPS IFIS NASA*, pp. 253-254

Yallapragada, S. V., Heck, B. S., Finney, J. D., 1996
Reaching conditions for variable structure control with output feedback, *J. of Guidance, Control, and Dynamics*, July-August, Vol. 19, No. 4, pp. 848-853

Ye, N., Scavarda, S., Betemps, M. and Jutard, A., 1992
Models of a Pneumatic PWM Solenoid Valve for Engineering Applications, *ASME Jrnl Dynamic Systems Measurement and Control*, Vol. 144, pp. 680-688

Yeung, K. S. and Chen, Y. P., 1988
A new controller design for manipulators using theory of variable structure systems, *IEEE Trans.*, AC-33, pp. 200-206

Young, K. K. D., 1978
Controller design for a manipulator using theory of variable structure systems, *IEEE Trans.*, SMC-8, pp. 101-109

Yu, X., 1994
Digital variable structure control with pseudo-sliding modes, *Lecture Notes in Control and Information Science 193*: *Variable Structure and Lyapunov Control*, Zinober (ed), Springer-Verlag, London

Yu, X. H. and Potts., R. B., 1992
Computer controlled variable structure systems, *Journal of the Autralian Mathematical Society, Series B - Applied Mathematics*, Vol. 34, No. Pt1, pp. 1-17

Zhao, F., Utkin, V. I., 1996
Adaptive simulation and control of variable-structure control systems in sliding regimes, *Automatica*, July, Vol. 32, No. 7, pp. 1037-1042

Zhu, W. and Chen, H., 1990
A global asymptotic stable variable structure algorithm using sliding mode observer, *Proc. of the 1990 IEEE International Conf. on Robotics and Automation.*, No. 1990, pp. 130-135

Zinober, A. S. I., 1975
Adaptive relay control of second-order system, *Int. Journal of Control*, Vol. 21(1), pp. 81-98

Zinober, A. S. I., 1977
Analysis of an adaptive 3rd-order relay control system using nonlinear switching surface theory, *Proc. of the Royal Soc. of Edinburgh*, Vol. 76A, pp. 239-254

Zinober, A. S. I., 1990
Deterministic Control of Uncertain Systems, Peter Peregrinus Ltd, London, ISBN 0863411703

A1 CONTROL OF MULTI-AXES MANIPULATORS WITH IDEAL ACTUATORS

This appendix presents the results of a preliminary study of the problems in connection with the control of *n*DOF manipulator systems. In this context the particular problems of coupling between the individual members of the manipulator and state dependent changes in the system parameters are addressed. In order to investigate these problems a 2 degree of freedom (2DOF) manipulator as shown in Figure A1.1 is examined and different well known and established control methods are compared.

The control of a 2DOF manipulator exhibits the same problems as the control of a higher degree of freedom system. Therefore and for convenience of presentation, only a 2DOF manipulator is considered here, although 3DOF and 4DOF manipulators have been investigated with similar results. In order to clarify the dynamic effects of the mechanical system and to compare the controllers' ability to overcome its undesired characteristics (dynamic coupling, unknown and state dependent changes of system parameters), the actuator dynamics have been neglected at this stage. They will be the subject of interest in the main part of the thesis.

The appendix is organised as follows: Section A1.1 describes the general problems in manipulator control. Section A1.2 then derives the mathematical model of the manipulator dynamics using Lagrange's method. A state-space representation of the manipulator dynamics is also obtained. Section A1.3 compares the suitability of three different conventional control strategies for manipulator tracking control. These are single axis proportional and differential (PD) feedback control, state-feedback control and computed torque control. Section A1.4 then introduces a model-based variable-structure adaptive control algorithm which is known to overcome problems of parameter uncertainties in the manipulator model used to synthesise the controller. All control strategies are compared in terms of step response simulation results and the robustness in case of system parameter variations.

The results of this preliminary study lead to the conclusion that due to the complexity and non-linearity of the mathematical models describing even relatively simple system like a double inverted pendulum depicted in Figure A1.1 individual single-axis controllers based on simple linear axis models are the preferable choice. However, these individual single-axis controllers have to provide superior disturbance rejection capabilities and robustness to system parameter changes.

A1.1 General Problems in Manipulator Control

In general, when designing a control system for a manipulator the following problems have to be considered (Stoten (1990)):

- **Non-linear dynamics:** Non-linear dynamics can be classified in terms of their mathematical properties as *continuous* or *discontinuous*. Because discontinuous non-linearities cannot be locally approximated by linear functions, they are also called *hard* non-linearities. Continuous non-linearities can be classified as steady-state non-linearities, such as gravity forces which are a function of position only, and transient non-linearities. The latter are due to centrifugal and Coriolis forces caused by the velocity of the manipulator links and actuator dynamics. Hard non-linearities are for example backlash, hysteresis, stiction and end stops.
- **Dynamic coupling between manipulator links:** These coupling effects are a natural consequence of Newton's Third Law. The acceleration of one link of the manipulator causes reaction torques at the other links which have to be controlled by an effective co-ordination of all control signals.
- **Internal parameter variations:** These parameter variations may be due to changes in hydraulic oil viscosity for hydraulically actuated manipulators, heat exchange with the environment for pneumatics, wear in joints, and changes in masses to be manipulated.
- **Unmodelled dynamics:** These dynamics are typically due to the flexibility of links, joints and mountings, which are otherwise considered to be rigid. If one of these high-frequency modes is excited, the system behaviour may change significantly. Furthermore, actuator dynamics are often neglected when the bandwidth of the actuators is higher than the bandwidth of the mechanical structure.

- **External disturbances:** External disturbances are e.g. noise, and forces due to interaction with a work piece or the environment.
- **High speeds of response:** In most applications high speeds of response are required to reduce cycle times to make processes more effective. This problem further exacerbates the non-linear dynamics and dynamic coupling problems.
- In general a controller for a manipulator has to enable the manipulator to fulfil one of the following two tasks: **reaching a desired position** along a path determined by the manipulator dynamics or **following a desired trajectory**. The latter task is the more demanding one because it requires the closed-loop error dynamics to converge towards zero which puts a higher burden on the controller and demands trajectory velocity and acceleration as an input. To obtain these velocities and accelerations generally a smooth path for the manipulator to track is required. This can for instance be realised in the trajectory programming stage or by means of a filter which smoothes out abrupt changes in the demand signals and hence enables their numerical differentiation.

Regarding the desired behaviour of the non-linear control system, a designer has to consider the following characteristics:

- **Stability** must be guaranteed for a nominal model (the model used for design), either in a local sense or in a global sense. The regions of stability and convergence are also of interest.
- **Robustness** is the sensitivity to effects which are not incorporated in the controller design such as external disturbances, measurement noise, unmodelled dynamics, etc. The system should be able to withstand these neglected effects within certain boundaries when performing the task of interest.
- **Accuracy and speed of response** may be considered for some 'typical' motion trajectories in the region of operation. For some classes of systems, appropriate controller design can actually guarantee consistent tracking accuracy independently of the desired trajectory.

Considering general non-linear systems, stability does not imply the ability to withstand persistent disturbances of even small magnitude, because the stability of a non-linear system is defined with respect to initial conditions, and only temporary disturbances may be translated as initial conditions. This situation is different from

that of linear system control, where stability always implies the ability to withstand bounded disturbances (assuming of course that the system does not leave its linear range). The effects of persistent disturbances on non-linear system behaviour are addressed by the concept of robustness. It should be noted, that the qualities of stability and robustness can conflict to some extent, and a good control system can often only be obtained via a compromise between stability and robustness.

A1.2 MANIPULATOR DYNAMIC EQUATION

In this section a dynamic model of the manipulator is generated using the *Lagrange equation*. This model is used for control system design and furthermore it provides the basis for the simulation work presented in Sections A1.3 and A1.4.

For the use of the Lagrange equation it is required to calculate the total kinetic energy T and the total potential energy U of the system. These energies together with the known externally applied forces and torques can then be used to generate the dynamic model of the manipulator in a fairly straightforward manner. Lagrange's equation is

$$\frac{d}{dt}\left(\frac{\partial(T-U)}{\partial \dot{q}_i}\right)-\frac{\partial(T-U)}{\partial q_i}=Q_i\,,\quad (i=1,\ldots,n) \tag{A1.1}$$

where the q_i are the generalised co-ordinates of each degree of freedom and Q_i are generalised forces applied externally at each co-ordinate q_i.

The manipulator is modelled as a set of 2 moving rigid bodies connected in a serial chain with one end fixed to the ground and the other end free as can be seen in Figure A1.1. The bodies are joined together with rigid revolute joints. A torque actuator and viscous friction are acting at each joint. Here q_i will be the transducer co-ordinate ϑ_i (relative angle of displacement) for each link, and Q_i will be the difference τ_i - k_i between actuator torque and the linear viscous friction torque applied to each link. The vector equation of motion of such a manipulator can be written in the form:

$$\tau = M(\Theta)\ddot{\Theta} + V\left(\Theta,\dot{\Theta}\right) + F\left(\dot{\Theta}\right) + G(\Theta) + \tau_d \tag{A1.2}$$

where $M(\Theta)$: position dependent inertia matrix

$V(\Theta,\dot{\Theta})$: vector representing torques caused by centrifugal and Coriolis effects

$F(\dot{\Theta})$: vector representing friction torques

$G(\Theta)$: vector representing gravity induced torques

τ_d: vector of unknown signals due to unmodelled dynamics and external disturbances

The parameters of the above matrices and vectors are detailed in Appendix A2.1.

Another way of formulating the dynamics of a non-linear system is by using a set of non-linear differential equations in the form:

$$\dot{x} = f(x,t) \tag{A1.3}$$

where f is a n x 1 non-linear vector function, and x is the n x 1 state vector. The number of states n is called *order* of the system. Equation (A1.3) does not explicitly contain the control input as a variable. Nevertheless, the equation is directly applicable to feedback control systems in the case where the control input is a function of system state x and time t.

Linear systems can be considered as a special class of non-linear systems. The equation of motion of a linear system can be written as the so called canonical state-space representation

$$\begin{aligned} \dot{x} &= \boldsymbol{A}x(t) + \boldsymbol{B}u(t) \\ y &= \boldsymbol{C}x(t) \end{aligned} \tag{A1.4}$$

where x represents the system's states, y the system's output and u an external input.

The system response has a number of interesting properties. First, it satisfies the *principle of superposition.* Second, the asymptotic stability of the system implies bounded-input bounded-output stability in the presence of u. Third, a sinusoidal input leads to a sinusoidal output of the same frequency.

The behaviour of non-linear systems is much more complex. Due to the non-linearities the superposition principle is not applicable and so non-linear systems respond to external inputs quite differently from linear systems. However, one will always be able to separate out the linear and non-linear terms in the equations of motion and obtain

$$\dot{x} = Ax(t) + Bu(t) + f(t) + g(t) \qquad \text{(A1.5)}$$

where the vector $f(t)$ contains all the transient non-linear components of the system dynamics and $g_g(t)$ all the steady-state non-linearities. The specific state matrices and vectors for a 2 DOF manipulator can be found in Appendix A2.2.

When designing a controller on the basis of the plant model presented in Equation (A1.5) the non-linear components are treated as external disturbances to be cancelled by the control action.

A1.3 CONVENTIONAL CONTROL STRATEGIES REVISITED

In this section several conventional control strategies are presented and compared. The control strategies use either a linear plant model for control design purposes (single axis proportional and differential control, state-feedback control) or a non-linear plant model (computed torque control).

To illustrate the system's behaviour with different controllers simulation results are shown which were produced using the simulation package Bath*fp* (Lo and Tilley (1993)). The results of Bath*fp* simulations provide both steady-state and transient performance data. This is achieved using the sophisticated numerical integration algorithm LSODA, which monitors the characteristics of the differential equations during the course of the simulation and selects the most appropriate integration method from a range of variable time step algorithms. These algorithms are able to deal with any system discontinuities.

As mentioned earlier, for convenience of presentation and discussion only a 2DOF manipulator (joint 1 shoulder, joint 2 elbow) is considered as shown in Figure A1.1, although an extensive study has been carried out using 3DOF and 4DOF manipulator models. The manipulator is modelled as described in Section A1.2. For simulation purposes the manipulator properties detailed in Table A1.1 are assumed. The numerical values are idealised to a certain extent, but nevertheless represent those of a realistic industrial robot. Although the masses and moments of inertia of the investigated animated figure are significantly smaller, the large values above have been chosen because they emphasise the dynamic non-

linearities and hence allow an easy comparison of the different control strategies and their ability to cope with these non-linearities. Furthermore as mentioned above, it is assumed that the bandwidth of the actuators is much higher than the bandwidth of the mechanical structure so that the actuator dynamics can be neglected.

As path tracking is more demanding than set-point positioning the following investigation concentrates on this problem when synthesising the controller. Generally to enable a manipulator to follow a prescribed path, not only the desired displacement of the actuators but also the desired actuator velocities and accelerations are required. One way of providing this information is a second-order reference signal filter, which not only smoothes the input demand signal but also computes the demanded velocities and accelerations. The filter is tuned to have a critically damped response.

Furthermore, in all control systems mentioned below position dependent parameter changes due to gravity which causes steady-state errors are dealt with by means of a gravity compensator which feeds-forward the necessary torques to counteract these gravity effects. To enable a compensator like this to work satisfactorily the gravity influence on the manipulator must be well known since modelling uncertainties in the compensator can make the system behaviour worse. Another possibility to overcome errors due to steady-state non-linearities is the use of integral action. An integrator may slow down the system response and tend to reduce transient robustness in face of modelling errors and this may lead to instability.

A1.3.1 Independent Joint Proportional and Differential Feedback Control With Steady-State Non-Linearity Compensation

Most present commercial industrial robots use simple PD (proportional and differential) or PID (proportional, integral and differential) feedback controllers where each joint is controlled as a separate control system. Since no decoupling is being done, the coupling reaction forces are treated as external disturbances and hence the motion of each joint affects the motion of the other joints. These interactions have to be minimised by the control law of each axis.

For controller design purposes the highly non-linear plant is assumed to be linear. The non-linear dynamic behaviour is hence treated as an additional external disturbance. Due to the position dependence of the plant parameters (e.g. the inertia coefficients) it is impossible to select fixed gains which will critically damp the response to a demanded input for all configurations of the manipulator. A local linearisation in the neighbourhood of an operating point has to be carried out and gains have to be chosen which approximate critical damping around this operating point of the manipulator's workspace. Generally, the further away from this linearisation point that the manipulator operates the worse the system behaviour becomes. In various extreme configurations of the arm, the system can become significantly under- or overdamped.

In the case of an indirectly driven manipulator, as commonly used in industry, the changes in the plant parameters and the coupling effects are reduced for high gear ratios so that the plant behaviour under simple PD or PID feedback control is generally sufficient. Nevertheless, it should be noted that even with gear reduction the inertia may vary over a large range, perhaps an order of magnitude (Spong and Vidyasagar (1989)).

In the following a PD controller with reference acceleration feedforward is synthesised where each link will be in a closed-loop system as shown in Figure A1.2. A PD controller is the better alternative when compared to a PID controller where a steady-state error is allowed in the system response as already mentioned above (Stoten (1990)). For the animated figure under consideration, a small steady-state error caused by parameter uncertainties in the gravity compensator is acceptable, since accurate positioning is normally not one of the requirements of this figure. Hence, an integrator is not an advantage.

The dynamics of link i (i = 1, 2) are taken as the linear terms $\boldsymbol{A}_i$ and $\boldsymbol{B}_i$ from the state Equation (A1.4) to give the transfer function:

$$G_{pi} = \boldsymbol{C}_i\left(s\boldsymbol{I} - \boldsymbol{A}_i\right)^{-1}\boldsymbol{B}_i = \frac{a_i}{s^2 + sb_i} \tag{A1.6}$$

Hence

$$G_{p1} = \frac{3.077}{s(s+5.769)}, \quad G_{p2} = \frac{8.205}{s(s+4.103)} \tag{A.1.7}$$

so that each link has its own integrator. Considering an ideal critically damped step response of each closed-loop link with a settling time of about 1 s, the desired closed-loop characteristic equation is:

$$s^2 + 2\xi\omega_n s + \omega_n^2 = 0, \quad \text{where } \omega_n = 4\,\text{rad}^{-1} \text{ and } \xi = 1 \tag{A1.8}$$

Comparing this with the actual PD control closed-loop characteristic equation

$$s^2 + (b_i + a_i k_{Di})s + a_i k_{pi} = 0 \tag{A1.9}$$

yields the controller gains listed in Table A1.2.

Figure A1.3 shows the Bath*fp* simulation circuit. The simulation results of the full non-linear closed-loop system, following the reference input r_1 = 1.0 rad and r_2 = 0.5 rad can be seen in Figure A1.4.

Obviously, the transient terms are far from being satisfactory, although the steady-state values are as required due to the gravity compensator. Overshoots and coupling effects are present because the non-linear dynamic behaviour of the manipulator (Coriolis and centrifugal effects) and reaction torques are treated as external disturbances.

Since a controller is synthesised using a set of estimated plant parameters, in general the system behaviour becomes worse, if these estimated parameters do not compare with the real plant parameters. In the following it is assumed that all plant parameters are only known within a band of +/- 30% of their nominal values. It is not realistic to assume that all parameters have the same uncertainties, because it is easier to measure lengths and masses than it is to measure friction coefficients or moments of inertia. Nevertheless, the blanket approach is useful when comparing different controllers and makes their problems with parameter uncertainties obvious. It must be noted that some parameter variations might counteract each other e.g. an increase of the mass or the length of a member has a similar effect on the system's behaviour as a decrease of the friction coefficient. In order to account for this counteracting effects of parameter changes, the system parameters listed in Table A1.1 are assumed to examine the worst case.

The system behaviour shown in Figure A1.5 is observed. Coupling effects and overshoots are amplified as expected but also a steady-state error occurs since the gravity compensator is unable to remove the steady-state non-linearities

completely. Yet it must be mentioned, that the system behaviour is still stable, even though the controller is significantly detuned.

A1.3.2 STATE-FEEDBACK CONTROL

A state-feedback controller is an attempt to take account of coupling effects, at least on the basis of the linearised dynamic model of the manipulator. It is assumed that all elements of the state vector are measurable, which implies that both position and velocity of each link are measured. To avoid the application of additional velocity transducers, the displacement signal is differentiated numerically in the simulated system. This does not cause problems in absence of transducer noise.

As shown in Section A1.2 the state equation of motion for the manipulator is

$$\dot{x} = \mathbf{A}x(t) + \mathbf{B}u(t) + f(t) + g_g(t) \qquad \text{(A1.10)}$$

This equation is used as a basis for synthesising the state-feedback controller depicted in Figure A1.6. $\boldsymbol{K}$ is the 2 x 4 state-feedback gain matrix . The closed-loop dynamics are

$$\dot{x} = (\boldsymbol{A} - \boldsymbol{BK})x(t) + \boldsymbol{BK}r(t) + f(t) \qquad \text{(A1.11)}$$

The steady-state non-linearities $g_g(t)$ are again removed by the gravity compensator described in the previous section. To maximise the robustness of the closed-loop system, the feedback gain matrix $\boldsymbol{K}$ is synthesised using the MATLAB *place* algorithm (Moler *et al* (1987)). This algorithm is based on eigenstructure assignment (Kautsky and Nichols (1983)), and calculates the $\boldsymbol{K}$ matrix coefficients for a chosen set of eigenvalues of the matrix ($\boldsymbol{A}$-$\boldsymbol{BK}$). Choosing all eigenvalues at s = -4 to obtain a natural frequency for each link of $\omega_n = 4$ rads^{-1}, the *place* algorithm yields:

$$\boldsymbol{K} = \begin{pmatrix} 6.4 & 1.3 & 1.2 & 0.6 \\ 2.4 & 1.2 & 2.4 & 0.7 \end{pmatrix} \qquad \text{(A1.12)}$$

The Bath*fp* simulation circuit is shown in Figure A1.7. Using the same input signal as for the PD controlled system results in the system response shown in Figure A1.8. For comparison the response of the PD controlled manipulator is plotted again.

Accounting for the linear coupling effects when synthesising the controller obviously improves the transient behaviour of the manipulator significantly, but still the non-linearities in the plant dynamics cause overshoots and coupling. The same can be said when comparing the plant behaviour under state-feedback control and under PD control in presence of parameter uncertainties. Again assuming the parameters of the manipulator are only known within a tolerance band of +/- 30% of their nominal values results in a closed-loop system response shown in Figure A1.9. Even with the existence of parameter uncertainties the state-feedback controller is able to reduce overshoots and coupling compared with the PD controller. Again, the system is still stable although detuned.

It can be concluded that multivariable controllers like the state-feedback controller result in better closed-loop response of the manipulator to be controlled because by using the whole plant state as an input they are synthesised with the linear open-loop coupling as a design feature. Still the non-linear coupling which occurs in plants like robot manipulators can cause unsatisfactory closed-loop behaviour.

Another shortcoming of a multivariable controller is the fact that the joints of a manipulator are not treated independently so that the controller structure in itself becomes more complex. Furthermore, a change in the manipulator structure leads to a change in the controller structure and cannot be accounted for by simply retuning the controller parameters.

A1.3.3 COMPUTED TORQUE CONTROL

In general, the knowledge of the system structure and its parameters can be used to feedforward the required control signals to cancel out non-linearities. Like this the order of the system is reduced and only the remaining uncertainties and disturbances have to be controlled by a feedback controller. The burden of this feedback controller is much lighter and it is easier to assure stability. In order to feedforward control signals, the plant has to be well known because the controller can generate signals which will cause additional disturbances on top of the external disturbances and those caused by modelling errors.

Assuming a dynamic manipulator equation as derived in Section A1.2

$$\tau = M(\Theta)\ddot{\Theta} + V(\Theta,\dot{\Theta}) + F(\dot{\Theta}) + G(\Theta) + \tau_d \qquad \text{(A1.13)}$$

a similarly structured control law, which is sometimes referred to as the computed torque method (Craig (1986)) of manipulator control is used

$$\tau = M(\Theta)\Theta^* + V(\Theta,\dot{\Theta}) + F(\dot{\Theta}) + G(\Theta) \qquad \text{(A1.14)}$$

where

$$\Theta^* = \ddot{\Theta}_d + K_v\dot{E} + K_pE \qquad \text{(A1.15)}$$

is the feedback servo part of the control law. The n x n constant, diagonal gain matrices K_v and K_p define the systems natural frequency and damping. The servo error E is defined as

$$E = \Theta_d - \Theta \qquad \text{(A1.16)}$$

The control law is chosen because in the favourable situation of perfect knowledge of parameter values and no disturbances, the closed-loop error dynamics are given by

$$\ddot{E} + K_v\dot{E} + K_pE = M^{-1}(\Theta)\tau_d \qquad \text{(A1.17)}$$

Hence in this ideal situation, the feedback gain coefficients may be chosen to place closed-loop poles of each joint separately, and disturbance rejection will be uniform over the entire workspace of the manipulator.

The Bath*fp* simulation circuit can be seen in Figure A1.10. The closed-loop system response to the step input signal r_1 = 1.0 rad and r_2 = 0.5 rad can be seen in Figure A1.11. The system response is perfect and this can be said for the whole workspace. No overshoot or coupling can be observed since the non-linear control algorithm exactly calculates the torques necessary to overcome coupling reactions and non-linearities in the system dynamics. The control algorithm reduces the system to a decoupled second-order system of n masses, compliances and dampers. By choosing the feedback gains for each member separately the natural frequencies and damping ratios can be set individually for each of the members. Yet, because the feedback part of the computed torque controller is only designed to control a simple second-order dynamic system the closed-loop system response can easily become unstable in the case of parameter uncertainties as can be seen in Figure A1.12. Considering a parameter uncertainty of +/- 30% of the nominal values of all parameters, the feedforward part of the controller produces torques which result in

the depicted unstable response. For parameter uncertainties of less than +/- 20% the system response is stable. Yet, even in this case the response of the computed torque control system is worse than the response of the state-feedback control system.

A1.4 Model-Based Variable-Structure Adaptive Control

As seen in Section A1.3.3, it is possible to design a non-linear control algorithm assuming the dynamics of the manipulator can be described mathematically. This control algorithm (computed torque control) can provide perfect model following properties in case of perfect plant parameter knowledge. With degrading parameter knowledge the controller can easily lead the system to instability as demonstrated in Figure A1.12.

Many adaptive control schemes have been described in literature that deal specifically with high-performance robot-tracking applications (e. g. Middleton and Goodwin (1988), Slotine and Li (1988), Craig (1986), Tso *et al* (1991)) in the case of poor parameter knowledge. In general, a convenient linear dynamic model is selected in the model-following approach (Stoten (1990), Dubowsky and DesForges (1979), Kim and Shin (1983), Balestrino *et al* (1983), Craig *et al* (1987)) and the difference in performance between the physical manipulator and the chosen model representing the desired system behaviour is used to adjust on-line the controller parameters or control signals in order to minimise this difference. This approach is called model-reference adaptive control (MRAC). The choice of the reference model is part of the adaptive control system design. It has to satisfy two requirements. On one hand, it should reflect the performance specifications in the control task, such as rise time, settling time, overshoot or frequency domain characteristics. On the other hand, this demanded behaviour should be achievable for the adaptive control system, i.e., there are some inherent constraints on the structure of the reference model (for example, its relative degree and order) given the assumed structure of the plant. The choice of a linear reference model causes the adaptation algorithm to counteract not only reaction torques but also non-linearities in the system dynamics by changing the controller parameters. Therefore the adaptation algorithm is responsible for the system's stability which in general is very difficult to prove (Craig *et al* (1987)).

As shown in Section A1.3.3, however, the non-linear, coupled and time-varying features of the actual manipulator are fully represented in the computed torque method, and this has prompted the application of more realistic models in model-reference adaptive control (MRAC) schemes in recent years (Tso *et al* (1991), Tso *et al* (1992)). The uncertain parameters in the full dynamic model of the manipulator are subject to a continuous adjustment according to a theoretically convergent adaptation process, so that the tracking errors are driven towards zero. The intention is that, by matching model and plant as far as possible, the compensation brought about by the computed torque techniques becomes more complete, and independent PD joint control can be applied more effectively for a wider range of operating conditions.

In general, a successful application of conventional model reference adaptive control schemes depends on persistent excitation (Tso *et al* (1991)) especially in the case of unmodelled dynamics, and the convergence rate cannot in practice be prescribed by design.

A method to overcome these shortcomings has been proposed by Utkin (1977) and experimentally studied by Young (1978) and others. It is based on the application of a variable-structure control (VSC) law for the parameter adaptation, rather than a continuous adaptation law, thereby providing a high degree of robustness irrespective of parameter variations and input disturbances. This technique avoids the on-line parameter identification and hence guarantees stability even in the case of insufficient excitation of the control system. VSC provides non-linear switching control, which ensures that the tracking errors and their derivatives will always be driven to the *sliding surface* (see also Continuous Sliding Mode Control in Chapter 6) and will slide along the surface towards the origin. The combination of VSC with MRAC, called model-based VSAC, results in greater control flexibility and enables the convergence properties to be more readily influenced by design. The application of VSC control to the problem of manipulator control has been intensively studied which is reflected by a large number of publications e. g. Slotine and Sastry (1983), Slotine (1985), Bailey and Arapostathis (1987), Yeung and Chen (1988), Miyasato and Oshima (1989), Shoureshi *et al* (1990), Richards and Reay (1992), Tso and Law (1992).

Following the derivation of Tso *et al* (1990, 1991) one possible MRAC scheme maintaining the structure of the computed torque control method introduced in Section A1.3.3 is based on the ability to represent the manipulator torque equation in a linearly parameterised form

$$\tau = M(\Theta)\ddot{\Theta} + N(\Theta,\dot{\Theta}) = W(\Theta,\dot{\Theta},\ddot{\Theta})F \tag{A1.18}$$

where τ is the n x 1 vector of generalised joint torques supplied by the n actuators, ϑ is the n x 1 vector of joint variables, M is the n x n inertia matrix, N is the combined n x 1 vector of the Coriolis, centrifugal, gravitational and frictional torque components, F is the r x 1 vector of unknown parameters and W is the coefficient matrix corresponding to the choice of F.

It is desired to drive the manipulator along the trajectory described by $\{\vartheta_d, \dot{\vartheta}_d, \ddot{\vartheta}_d\}$. By applying the control according to

$$\tau^* = W(\Theta,\dot{\Theta},\ddot{\Theta}^*)\hat{F} = \hat{M}(\Theta)\ddot{\Theta}^* + \hat{N}(\Theta,\dot{\Theta}) \tag{A1.19}$$

where

$$\ddot{\Theta}^* = \ddot{\Theta}_d + K_v\dot{E} + K_pE \tag{A1.20}$$

and

$$E = \Theta_d - \Theta \tag{A1.21}$$

it follows that the tracking error E is governed by the dynamic relationship

$$\ddot{E} + K_v\dot{E} + K_pE = \hat{M}^{-1}W(\Theta,\dot{\Theta},\ddot{\Theta})(F - \hat{F}) \tag{A1.22}$$

In the above, $\hat{F}$, $\hat{M}$ and $\hat{N}$ are the estimates of the respective vectors or matrices, and K_v and K_p are n x n diagonal gain matrices. With the introduction of a filtered error vector (*sliding surface*) E_1 according to

$$E_1 = \dot{E} + \Psi E \tag{A1.23}$$

where Ψ is a positive n x n diagonal matrix, it is possible to establish (Tso *et al* (1991), Tso *et al* (1992)) that the following switching adaptation algorithm

$$\begin{aligned} \hat{f}_i &= f_{i\max} \quad \text{when} \quad \left(W^T\hat{M}^{-1}E_1\right)_i > 0 \\ \hat{f}_i &= f_{i\min} \quad \text{when} \quad \left(W^T\hat{M}^{-1}E_1\right)_i < 0 \end{aligned} \tag{A1.24}$$

where $f_{i\min}$ and $f_{i\max}$ are the parameter bounds will lead tracking errors to zero and is acceptable from the stability point of view. Unlike conventional MRAC schemes

(Middleton and Goodwin (1988)), the adaptation does not require the estimated parameters to converge to their true model values. By using the proposed algorithm, exponential stability is achieved irrespective of the nature of the excitation (Tso *et al* (1991), Tso *et al* (1992)). E_1 goes to zero in a finite time and thereafter remains zero on the sliding surface $E_1 = 0$.

For practical realisation of the VSAC algorithm, it is necessary to introduce a boundary layer (Utkin (1977), Miyasato and Oshima (1989), Shoureshi *et al* (1990)) to minimise switching once the tracking error E, and E_1, becomes small. So whenever $e_{1j} < \varepsilon_j$ (j=1,..., n), the switching law is modified according to

$$\hat{f}_i = \frac{f_{i\max} + f_{i\min}}{2} + \frac{|e_{1i}|\,\mathrm{sgn}\left(W^T \hat{M}^{-1} E_1\right)_i \left(f_{i\max} - f_{i\min}\right)}{2\varepsilon_i} \qquad \text{(A1.25)}$$

Figure A1.13 shows the structure of the system circuit within Bath*fp* used to simulate the behaviour of a 2DOF manipulator with negligible actuator dynamics under variable-structure adaptive control. The system response to a step input can be seen in Figure A1.14. The controller has to overcome a parameter uncertainty of +/- 30% of the nominal plant parameter values on all parameters. To assure stability, it is essential that the plant parameters lie within the parameter bounds set in the controller. Hence parameter bounds listed in Table A1.3 are chosen.

Facing a similar parameter uncertainty that leads the computed torque control system to instability as discussed in Section A1.3.3 the VSAC controller provides perfect system control independent of the operation point of the manipulator as can be seen in Figure A1.14. No overshoot or coupling occurs. Figure A1.15 shows the switching of the control parameters which are on-line adapted by the VSAC algorithm. It should be noted that parameter drift after reaching a steady-state condition, which is likely to occur with continuously adapting algorithms (Tso *et al* (1991), Tso *et al* (1992)), is not experienced, because all control parameters are bounded within the algorithm.

A1.5 CONCLUSIONS

The above investigation leads to the following conclusions for the further investigation into the problem of controlling a *n*DOF pneumatically animated figure:

- Conventional PD-feedback and state-feedback control are not capable of dealing with coupling effects and the influence of dynamic parameter changes. Yet, despite a significant deterioration of the dynamic response of the closed-loop system in the case of system parameter changes both linear control algorithms provide stability.
- The non-linear computed torque control algorithm based on the full non-linear model of the plant provided an ideal response of the nominal model but resulted in instability unlike the linear control methods tested. It was found that this computed torque control algorithm is very sensitive to changes in the system parameters. Considering the application of a comparable non-linear algorithm on the complex animated figure would not only result in an excessive modeling and computation effort but would also not guarantee stability of the closed-loop system since system parameters like masses or moments of inertia are very likely to change due to varying system configurations.
- The VS control algorithm based on the non-linear structure of the computed torque controller provides excellent closed-loop performance as long as the system parameters stay within predefined bounds. The disturbance rejection capability and the robustness to parameter changes are far superior to the other control algorithms tested. Furthermore, the computational burden of the VS algorithm is extremely low when compared to other adaptation methods because no parameter estimation techniques are used. Yet, one main requirement on the computer is a high operating frequency to allow for a high control structure switching frequency.

As a result of the above study the investigation presented in the main part of the thesis will concentrate on variable-structure control as a means of compensating for coupling effects and dealing with unknown and changing system parameters. The aim will be to develop a single-axis VS controller based on a simple but sufficient linear model of the axis including the dynamics of the pneumatic actuation system which will

not only provide an excellent response of the highly non-linear coupled plant but will also minimise the controller hardware costs.

TABLES

Table A1.1 - Dynamic parameters used for manipulator model

system parameter	nominal value	30% variation
mass of member 1: m_1	10 kg	13 kg
mass of member 2: m^2	10 kg	13 kg
moment of inertia 1: J_1	0.5 kgm2	0.65 kgm2
moment of inertia 2: J_2	0.5 kgm2	0.65 kgm2
distance centre of gravity 1 - joint 1: l_{c1}	500 mm	650 mm
distance centre of gravity 2 - joint 2: l_{c2}	500 mm	650 mm
length of member 1: l_1	1000 mm	1300 mm
friction coefficient 1: k_1	75 Nms	52.5 Nms
friction coefficient 2: k_2	10 Nms	7 Nms
actuator gain 1: k_1	40 NmV-1	-
actuator gain 2: k_2	20 NmV-1	-

Table A1.2 - PD-feedback controller gains

	member 1	member 2
proportional gain k_{pi}	5.2	1.95
velocity gain k_{Di}	0.7228	0.4758

Table A1.3 - Upper and lower parameter bounds used in VSAC algorithm

lower bound	system parameter	upper bound
f_{1min} = 6 kg	< m_1 <	f_{1max} = 14 kg
f_{2min} = 6 kg	< m_2 <	f_{2max} = 14 kg
f_{3min} = 0.3 kgm^2	< J_1 <	f_{3max} = 0.7 kgm^2
f_{4min} = 0.3 kgm^2	< J_2 <	f_{4max} = 0.7 kgm^2
f_{5min} = 45 Nms	< f_{c1} <	f_{5max} = 105 Nms
f_{6min} = 6 Nms	< f_{c2} <	f_{6max} = 14 Nms

FIGURES

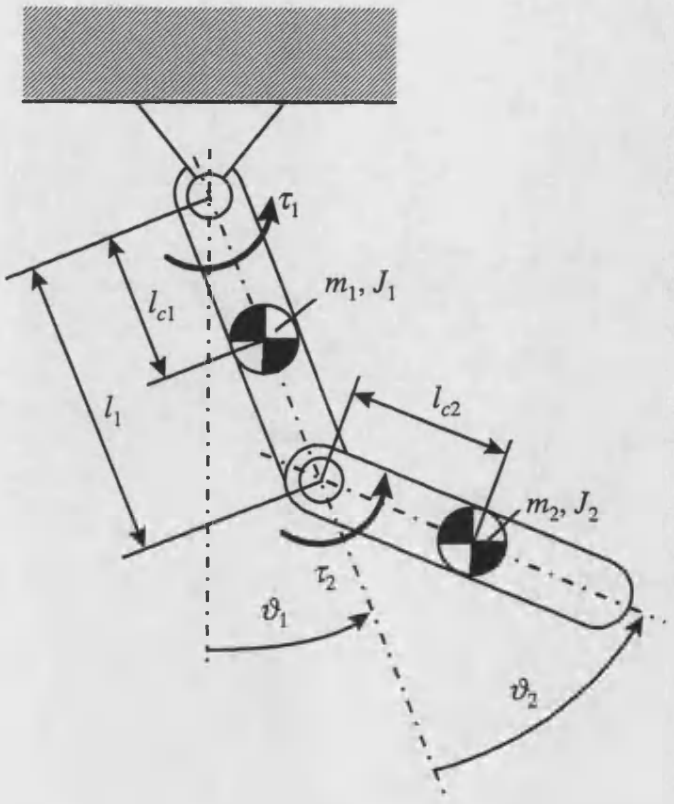

Figure A1.1 - Schematic of 2DOF manipulator

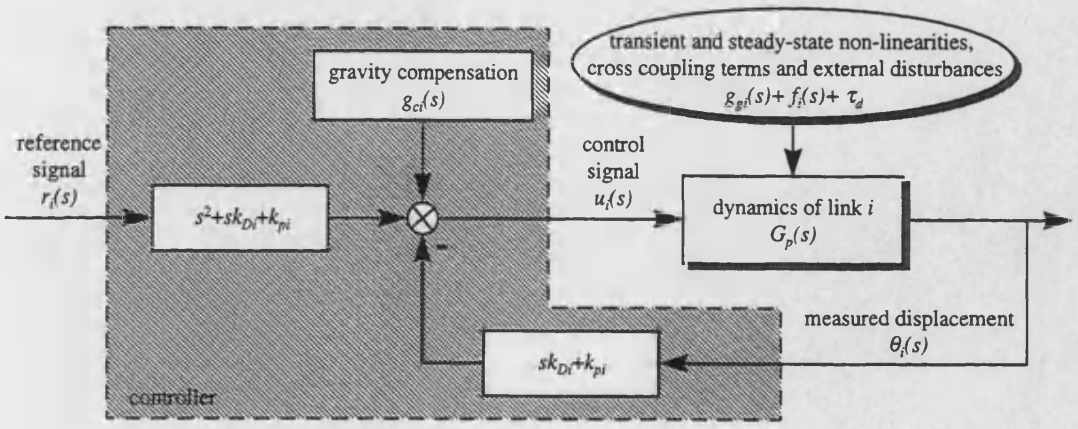

Figure A1.2 - Circuit diagram of individual link PD-feedback controller with reference velocity and acceleration feed-forward and gravity compensation

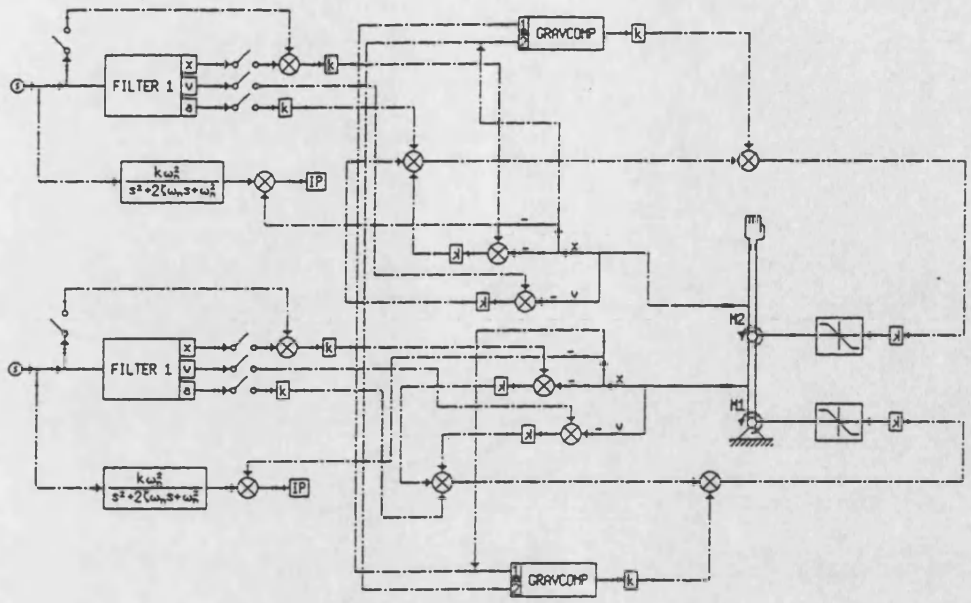

Figure A1.3 - Bath*fp* simulation circuit of 2DOF manipulator with PD control

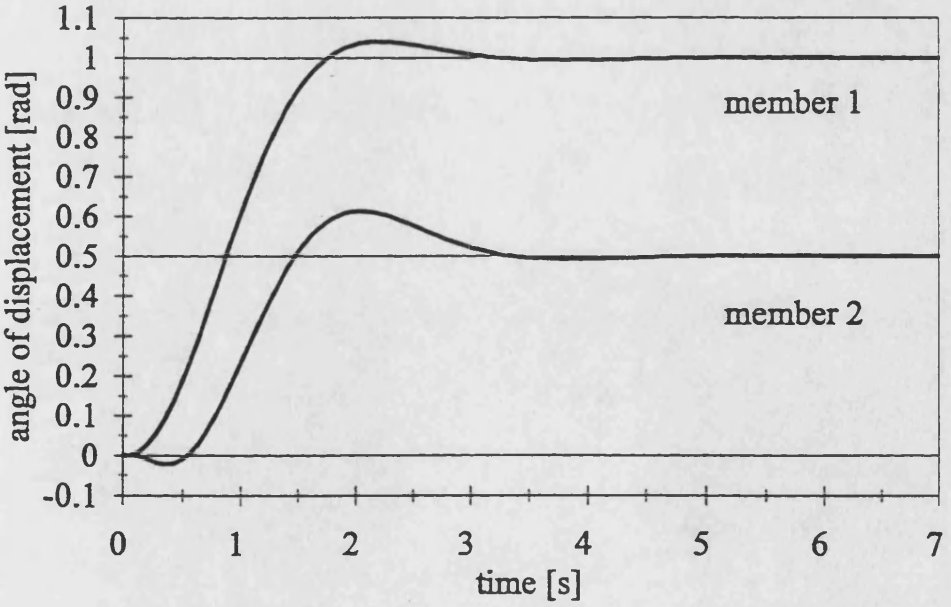

Figure A1.4 - Step response results of 2DOF manipulator with PD control

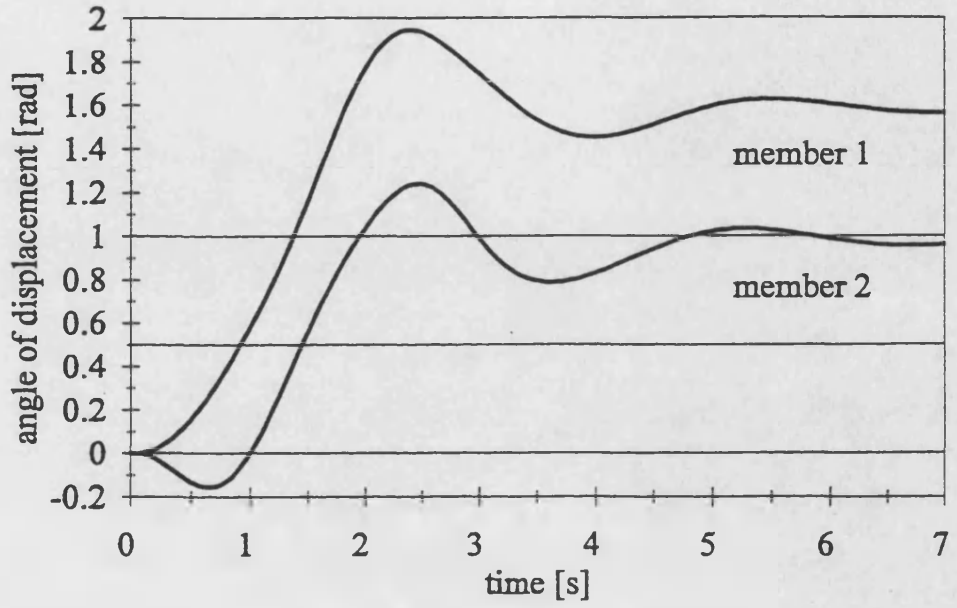

Figure A1.5 - Step response results of 2DOF manipulator with PD control and 30% parameter uncertainty

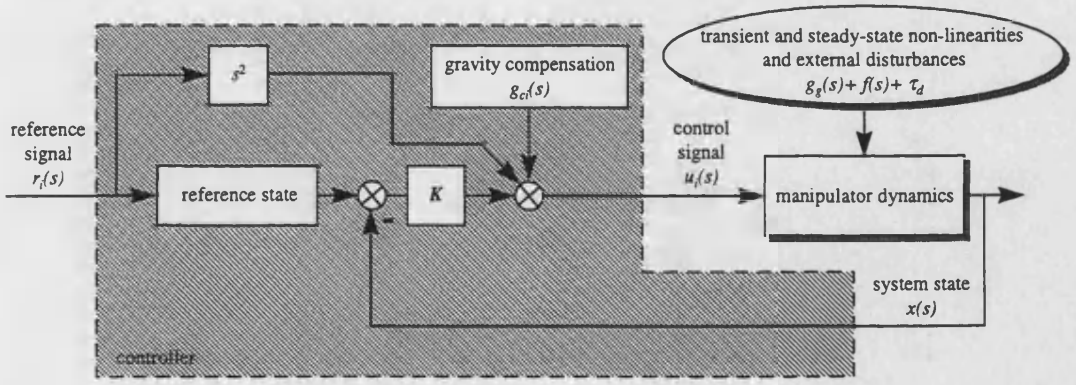

Figure A1.6 - Circuit diagram of state-feedback control system with reference acceleration feed-forward and gravity compensation

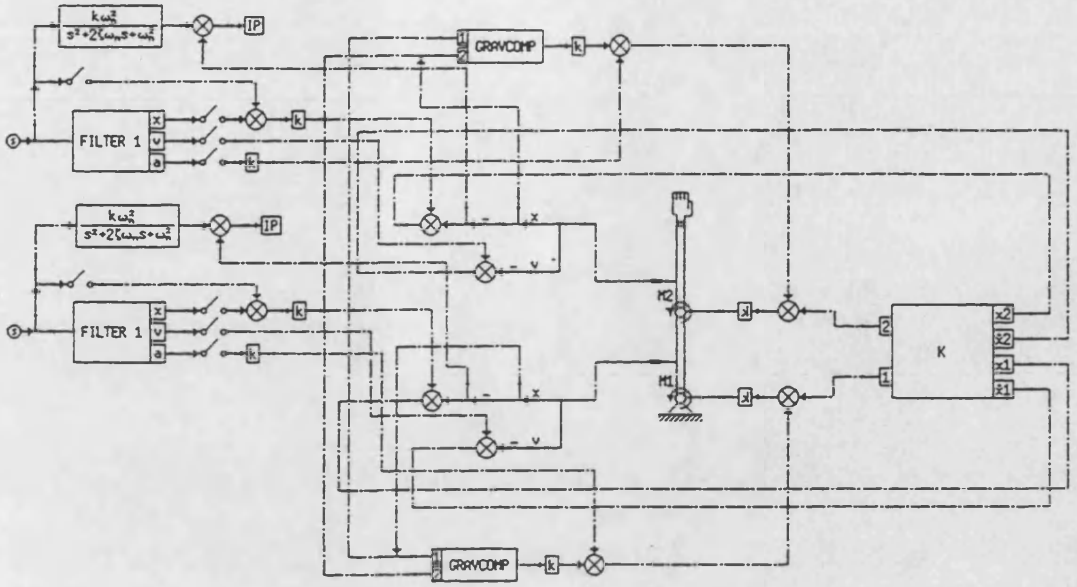

Figure A1.7 - Bath*fp* simulation circuit of 2DOF manipulator with state-feedback control

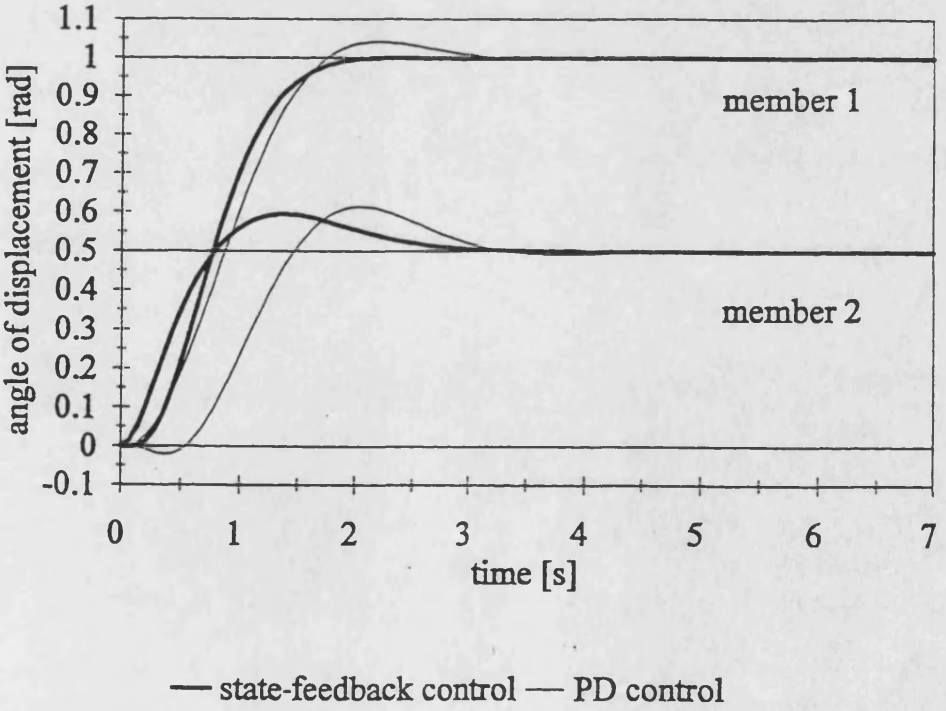

Figure A1.8 - Step response results of 2DOF manipulator with state-feedback control

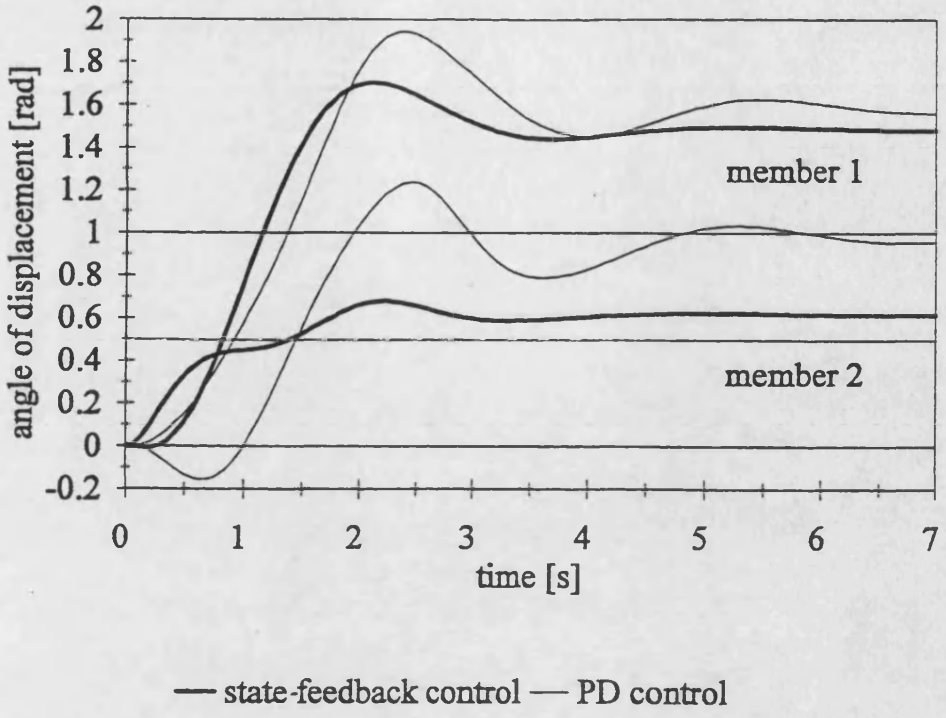

Figure A1.9 - Step response results of 2DOF manipulator with state-feedback control and 30% parameter uncertainty

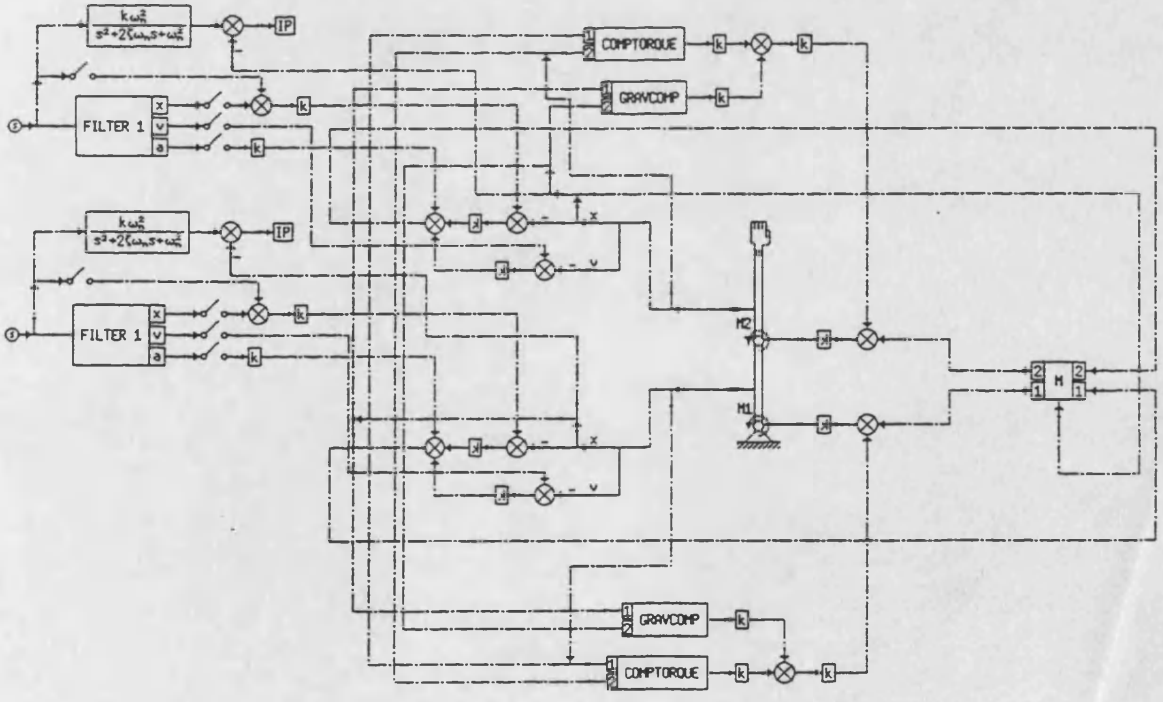

Figure A1.10 - Bath*fp* simulation circuit of 2DOF manipulator with computed torque control

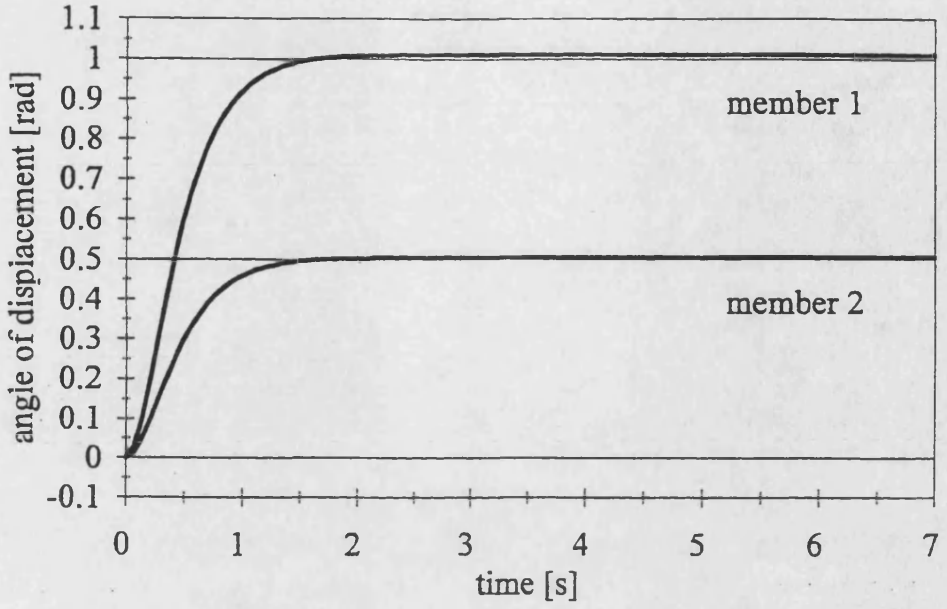

Figure A1.11 - Step response results of 2DOF manipulator with computed torque control

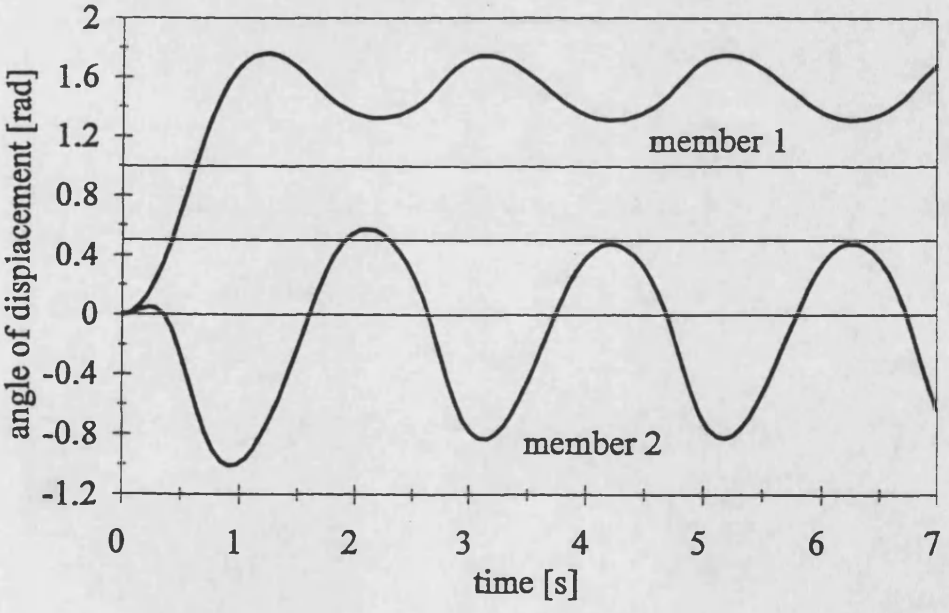

Figure A1.12 - Step response results of 2DOF manipulator with computed torque control and 30% parameter uncertainty

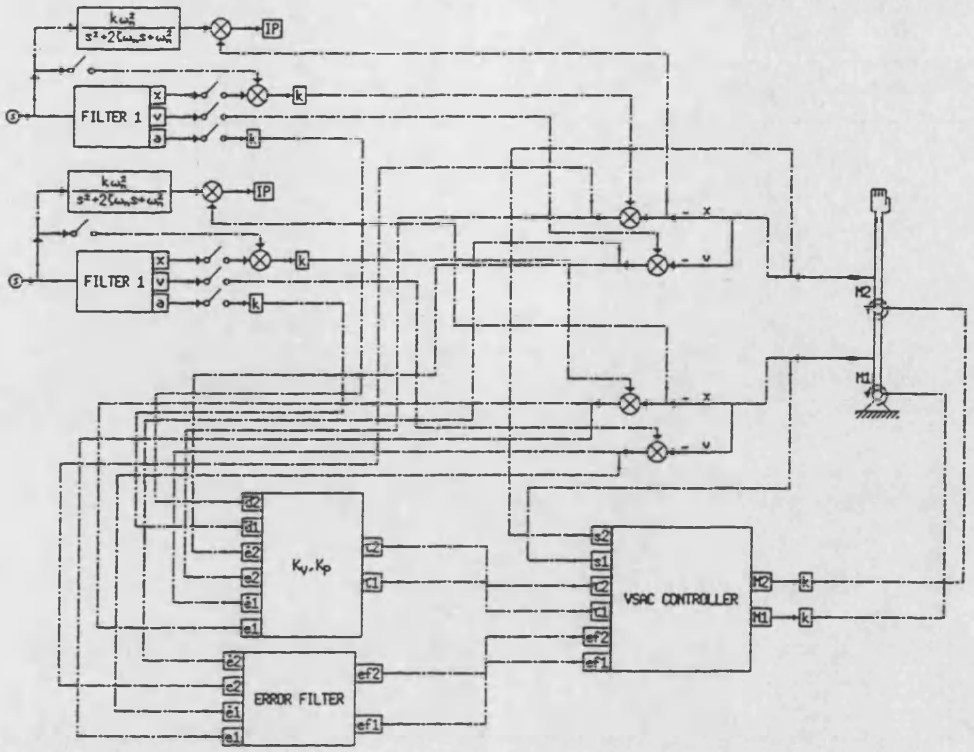

Figure A1.13 - Bath*fp* simulation circuit of 2DOF manipulator with VSAC control

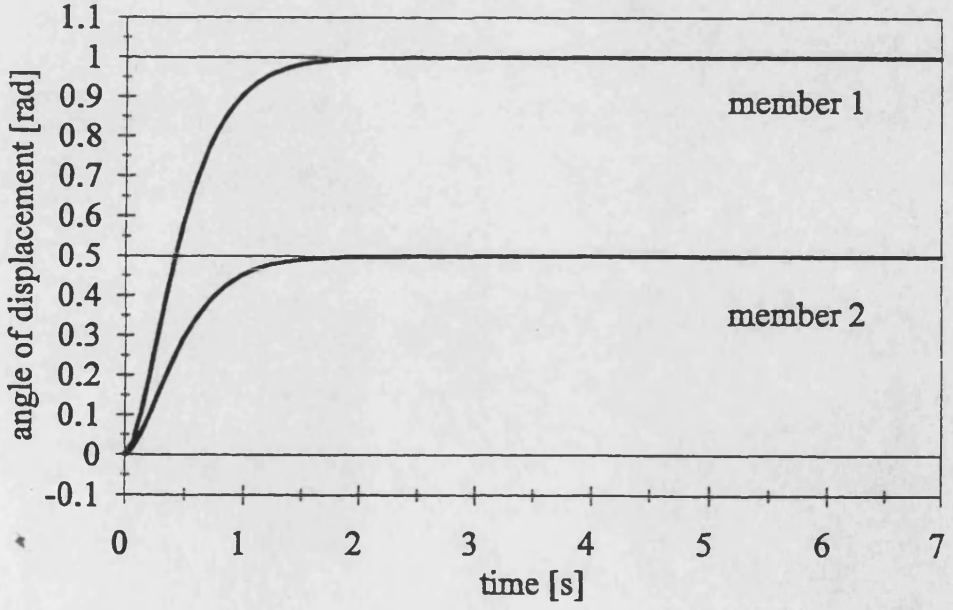

Figure A1.14 - Step response results of 2DOF manipulator with VSAC control and 30% parameter uncertainty

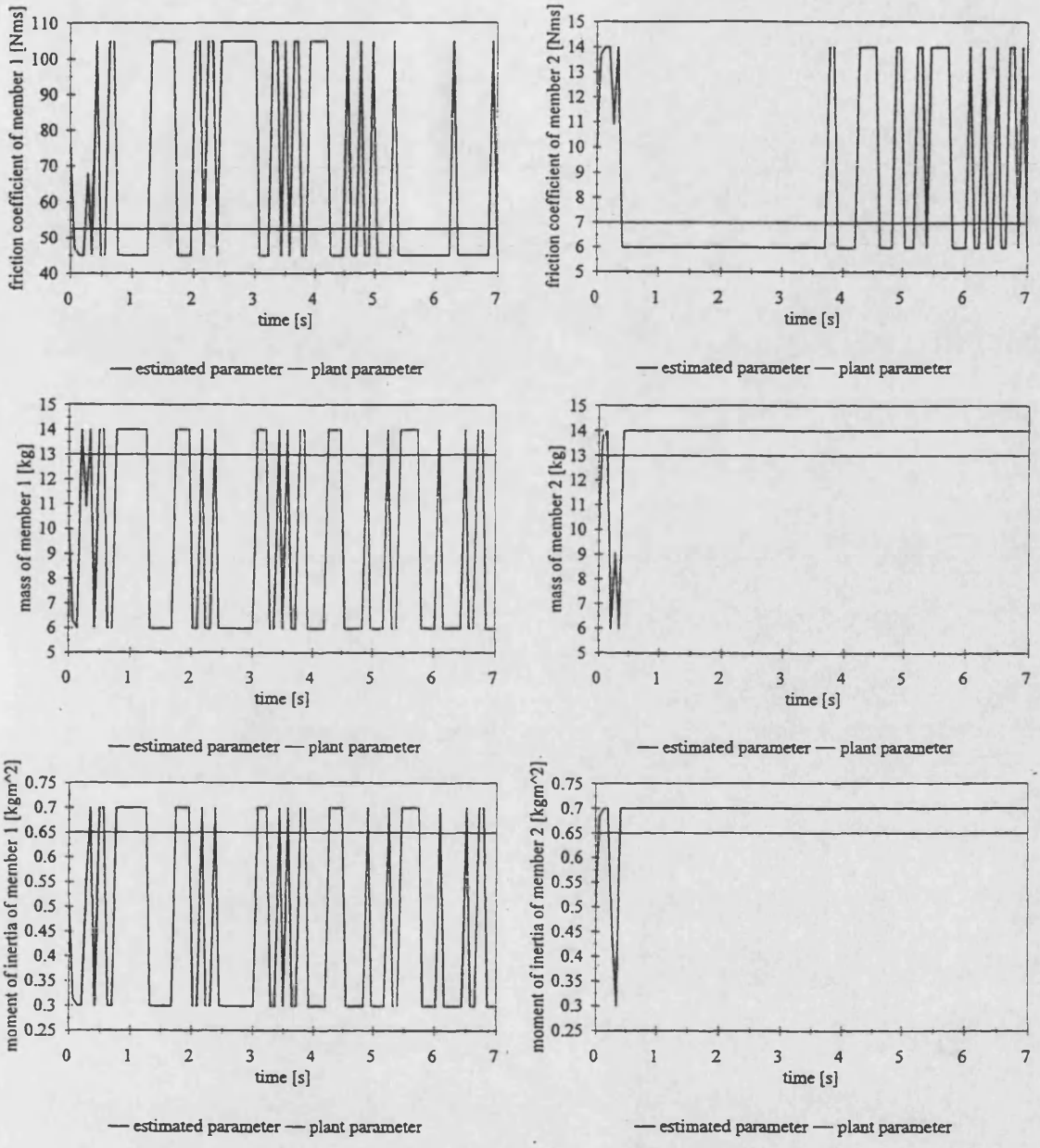

Figure A1.15a - Switching of plant parameters by VSAC algorithm to generate control signal for member 1 of the 2DOF manipulator

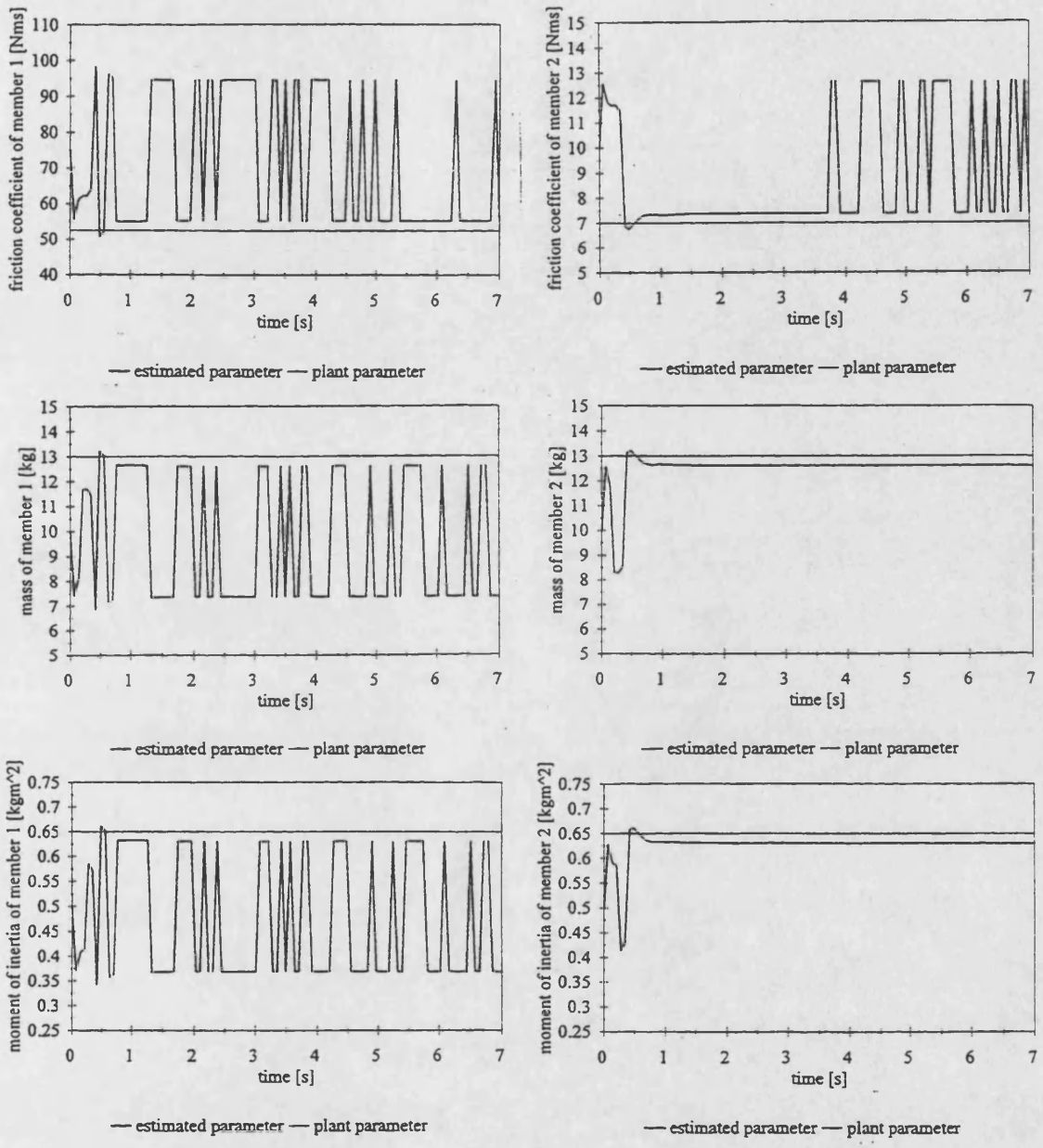

Figure A1.15b - Switching of plant parameters by VSAC algorithm to generate control signal for member 1 of the 2DOF manipulator

A2 DYNAMIC EQUATIONS OF A 2DOF MANIPULATOR

A2.1 DYNAMIC PARAMETERS OF LAGRANGE EQUATION

In the case of a 2DOF manipulator as depicted in Figure A1 the following dynamics system matrices and vectors for the Lagrange equation (A1.1) are obtained:

$$M(\Theta)=\begin{pmatrix} M_{11} & M_{12} \\ M_{21} & M_{22} \end{pmatrix} \tag{A2.1}$$

$$V(\Theta,\dot{\Theta})=\begin{pmatrix} -m_2 l_1 l_{c2}\dot{\vartheta}_2^2 \sin\vartheta_2 - 2m_2 l_1 l_{c2}\dot{\vartheta}_1\dot{\vartheta}_2 \sin\vartheta_2 \\ m_2 l_1 l_{c2}\dot{\vartheta}_1^2 \sin\vartheta_2 \end{pmatrix} \tag{A2.2}$$

$$F(\dot{\Theta})=\begin{pmatrix} k_1\dot{\vartheta}_1 \\ k_2\dot{\vartheta}_2 \end{pmatrix} \tag{A2.3}$$

$$G(\Theta)=g\begin{pmatrix} -m_1 l_{c1}\sin\vartheta_1 - m_2 l_1 \sin\vartheta_1 - m_2 l_{c2}\sin(\vartheta_1+\vartheta_2) \\ -m_2 l_{c2}\sin(\vartheta_1+\vartheta_2) \end{pmatrix} \tag{A2.4}$$

with

$$M_{12} = J_1 + m_1 l_{c1}^2 + J_2 + m_2 l_{c2}^2 + m_2 l_1^2 + 2m_2 l_1 l_{c2}\cos\vartheta_2 \tag{A2.5}$$

$$M_{12} = J_2 + m_2 l_{c2}^2 + m_2 l_1 l_{c2}\cos\vartheta_2 \tag{A2.6}$$

$$M_{21} = M_{12} \tag{A2.7}$$

$$M_{22} = J_2 + m_2 l_{c2}^2 \tag{A2.8}$$

A2.2 STATE-SPACE REPRESENTATION OF THE DYNAMIC EQUATIONS OF A 2DOF MANIPULATOR

Considering a 2DOF manipulator as depicted in Figure A1 the following vectors represent the system state, its derivative and the applied control signal:

$$x=\begin{pmatrix} \vartheta_1 \\ \dot{\vartheta}_1 \\ \vartheta_2 \\ \dot{\vartheta}_2 \end{pmatrix},\quad \dot{x}=\begin{pmatrix} \dot{\vartheta}_1 \\ \ddot{\vartheta}_1 \\ \dot{\vartheta}_2 \\ \ddot{\vartheta}_2 \end{pmatrix},\quad u=\begin{pmatrix} u_1 \\ u_2 \end{pmatrix} \tag{A2.9}$$

The matrices and vectors in the dynamic state-space equation (Equation (A1.5)) are:

$$\boldsymbol{A}=\begin{pmatrix} 0 & 1 & 0 & 0 \\ 0 & -\frac{c_1}{J_{t1}} & 0 & \frac{c_2}{J_{t1}} \\ 0 & 0 & 0 & 1 \\ 0 & \frac{c_1}{J_{t1}} & 0 & -c_1\left(\frac{1}{J_{t1}}+\frac{1}{J_{x2}}\right) \end{pmatrix} \tag{A2.10}$$

$$\boldsymbol{B}=\begin{pmatrix} 0 & 0 \\ \frac{k_1}{J_{t1}} & -\frac{k_2}{J_{t1}} \\ 0 & 0 \\ -\frac{k_1}{J_{t1}} & k_2\left(\frac{1}{J_{t1}}+\frac{1}{J_{x2}}\right) \end{pmatrix} \tag{A2.11}$$

$$f(t)=m_2 l_1 l_{c2}\begin{pmatrix} f_1 \\ f_2 \end{pmatrix} \tag{A2.12}$$

$$g_g(t)=g\begin{pmatrix} \frac{\sin\vartheta_1}{J_{t1}}\left(m_1 l_{c1}+m_2 l_1\right) \\ \frac{\sin\vartheta_1}{J_{t1}}\left(m_1 l_{c1}+m_2 l_1\right)-\frac{\sin\left(\vartheta_1+\vartheta_2\right)}{J_{x2}} m_2 l_{c2} \end{pmatrix} \tag{A2.13}$$

with

$$J_{xi}=J_i+m_i l_{ci}^2 \tag{A2.14}$$

$$J_{ti}=J_{xi}+m_i l_i^2 \tag{A2.15}$$

$$f_1=\frac{1}{J_{t1}}\left(-\left(\ddot{\vartheta}_1+\ddot{\vartheta}_2\right)\cos\vartheta_2+\left(\dot{\vartheta}_1^2+\dot{\vartheta}_2^2\right)\sin\vartheta_2+2\dot{\vartheta}_1\dot{\vartheta}_2\sin\vartheta_2\right) \tag{A2.16}$$

$$\begin{aligned} f_2=&\ddot{\vartheta}_1\left(\frac{1}{J_{t1}}+\frac{1}{J_{x2}}\right)\cos\vartheta_2+\ddot{\vartheta}_2\frac{1}{J_{t1}}\cos\vartheta_2-\dot{\vartheta}_1^2\left(\frac{1}{J_{t1}}+\frac{1}{J_{x2}}\right)\sin\vartheta_2 \\ &-\dot{\vartheta}_2^2\frac{1}{J_{t1}}\sin\vartheta_2-2\dot{\vartheta}_1\dot{\vartheta}_2\frac{1}{J_{t1}}\sin\vartheta_2 \end{aligned} \tag{A2.17}$$

In general the matrices $\boldsymbol{A}$ and $\boldsymbol{B}$ are of the form:

$$\boldsymbol{A}=\begin{pmatrix} \boldsymbol{A}_1 & \boldsymbol{A}_1^2 & 0 & 0 & \cdots & 0 \\ \boldsymbol{A}_2^1 & \boldsymbol{A}_1 & \boldsymbol{A}_2^3 & 0 & \cdots & 0 \\ 0 & \boldsymbol{A}_3^2 & \boldsymbol{A}_1 & \boldsymbol{A}_3^4 & \cdots & 0 \\ \vdots & \vdots & \vdots & \vdots & \ddots & \vdots \\ 0 & 0 & 0 & \cdots & \boldsymbol{A}_n^{n-1} & \boldsymbol{A}_1 \end{pmatrix} \tag{A2.18}$$

$$\boldsymbol{B}=\begin{pmatrix} \boldsymbol{B}_1 & \boldsymbol{B}_1^2 & 0 & 0 & \cdots & 0 \\ \boldsymbol{B}_2^1 & \boldsymbol{B}_1 & \boldsymbol{B}_2^3 & 0 & \cdots & 0 \\ 0 & \boldsymbol{B}_3^2 & \boldsymbol{B}_1 & \boldsymbol{B}_3^4 & \cdots & 0 \\ \vdots & \vdots & \vdots & \vdots & \ddots & \vdots \\ 0 & 0 & 0 & \cdots & \boldsymbol{B}_n^{n-1} & \boldsymbol{B}_1 \end{pmatrix} \tag{A2.19}$$

where n represents the number of links of the manipulator. Therefore, the 2DOF manipulator matrices can be written as:

$$\boldsymbol{A}=\begin{pmatrix} \boldsymbol{A}_1 & \boldsymbol{A}_1^2 \\ \boldsymbol{A}_2^1 & \boldsymbol{A}_2 \end{pmatrix} \tag{A2.20}$$

$$\boldsymbol{B}=\begin{pmatrix} \boldsymbol{B}_1 & \boldsymbol{B}_1^2 \\ \boldsymbol{B}_2^1 & \boldsymbol{B}_2 \end{pmatrix} \tag{A2.21}$$